# The Development of the Cracked-Chevron-Notched Brazilian Disc Method for Rock Fracture Toughness Measurement and Tunnelling Machine Performance Prediction

by

**Jun Fang Chen**

**A Thesis submitted in partial fulfilment of the requirements for the degree of Doctor of Philosphy**

**Department of Mining Engineering**

**The University of Newcastle upon Tyne**

**1989**

## Abstract

This thesis consists of two parts:

Part I The Development of Cracked-Chevron-Notched Brazilian Disc Method for Rock Fracture Toughness Measurement.

Part II The Prediction of Tunnelling Machine Performance.

In part I, a new novel method–Cracked-Chevron-Notched Brazilain disc (CCNBD) specimen is developed for rock fracture toughness measurement based on three-dimensional numerical analysis and experimental validation.

A programme was undertaken to investigate the dependence of rock fracture toughness using CCNBD method on the dimensions of the specimen. A comparison with chevron-notched bending specimens and chevron-notched short rod specimens were performed. Mixed-mode rock fracture investigations and mode II rock fracture toughness measurement has been studied.

It is found that CCNBD method gives very comparable results with that of chevron-notched bending specimen and chevron-notched short-rod specimen recommended by the testing commission of the ISRM. The only requirements are that the diameter of specimen should be larger than 50 mm and a/R should be less than 0.85.

It is found that mode II rock fracture toughness testing results using the CSTBD method depends on its dimensionless crack length. The short crack length CSTBD specimen is recommended for further testing. Mode I rock fracture toughness testing using the CSTBD method also shows its dependence on dimensionless crack length $a/R$, short crack length could generate comparable results with that by the CCNBD, SR and CB methods.

The CCNBD method has the following advantages: (1) The loading and displacement measurement apparatus is very simple; (2) The magnitude of failure load is generally larger than 1 kN which is of considerable benefit to those loading machines with a preload of 1 kN; (3) can be used for mixed-mode rock fracture investigations and mode II rock fracture toughness measurements; (5) It needs only a small sample for testing; (6) It is convenient for measuring rock fracture toughness in different orientations; (7) Specimen preparation is very simple.

Author proposed that this method could be used for the third chevron-notched specimen for the measurement of mode I rock fracture toughness.

On the part II, the prediction of tunnelling machine performance was analysed based on comprehensive analysis of existing methods for the prediction of tunnelling machine performance and curvilinear regression analysis of intact rock cuttability using a large database including rock physical, mechanical, energy, textural and fracture properties. A full review of existing models for the drag tool rock cutting mechanisms is presented. A drag tool rock cutting mechanism based on rock fracture properties is presented. A new model based on mixed-mode rock fracture mechanism for drag tool rock cutting was recommended for future research.

The following conclusions were drawn: (1) the toughness index, moduli ratio are very important rock properties for the prediction of rock cuttability. (2)new prediction equations analysed by new statistical analysis give more accurate prediction than results analysed by McFeat Smith; (3) rock cuttability prediction has strong dependence on rock lithology determination; (4) the most important variables for the prediction of rock specific energy are: cone indenter, toughness index, moduli ratio. For the sandstone group, the most important prediction variables are: cone indenter, moduli ratio and toughness index; (5) the most important variables for the prediction of rock cutter wear are: grain roundness and lathe abrasivity index. For the sandstone group, the most important prediction variables are: cone indenter and lathe abrasivity index; (6) the most important prediction variables for coarseness index are: impact strength index, lathe abrasivity index and toughness index. For the sandstone group, the most important

prediction variables are: toughness index and grain density; (7) rock fracture toughness has strong correlation with rock specific energy.

## Acknowledgements

The research scholarship is sponsored jointly by the British Council and the Chinese government for three years on the basis of official Sino-British technical cooperation programme.

The author would like to express his sincere gratitude to the following people without whose helps, much of this research work would not have been possible:

Professor J. F. Tunnicliff, for providing facilities to carry out the research.

Dr. R. J. Fowell, supervisor and Reader in Excavation Engineering for his invaluable assistance, advice whilst supervising the work.

Mr. A. Szeki, lecturer (now retired) in rock mechanics for his invaluable assistance, discussion and encouragement while supervising the work.

Mrs. Mary Morris, Dr. Chris Woodford, Mr. Quentin Campbell and Mr. F. T. Greenwood, Computer Duty Advisers, give me valuable help in computing during whole research period.

Thanks are also due to a lecturer Dr. P. Mottahead for his guidance and discussion.

Thanks are also extended to Mr. M. McKenna, the chief technican and his staff, Mr. R. Jensen, Mr. V. Willey, Mr. R. Liddell, Mr. J. Williams, for their excellent cooperation.

Thanks are also due to Mrs. A. Schouw and Mrs. B. Leggatt, the secretaries in the Department of Mining Engineering for their help.

Thanks are also extended to Dr. J. T. Evans and Dr. S. E. Chandler in the Department of Mechanical, Materials and Manufacturing in the University of Newcastle upon Tyne in allowing access to the testing equipment and guidance during the testing.

Thanks are also extended to Professor F. Ouchterlony in Sweden and Dr. K. Hurt in MRDE, England, for their valuable information.

Thanks are also extended to Professor Ove Stephansson in Lulea University of Technology; Professor Finn Ouchterlony in SveDeFo, Sweden; Professor Y. Nishimatsu in Japan, Professor I. Farmer in USA etc. for their interest in my research project and encouragement.

Grateful acknowledgement to C.M. Beasy Limited for its excellent software for the Boundary Element Method Calibration of CCNBD Specimen.

Finally, the following colleages are acknowledged for their assistance: Mr. John Martin, Mr. Martin Beasley, Dr. G. Xiao, Mr. L. Zheng, Dr. D. Jiao and other fellow students who have given help and companionship during my research.

## Notations Used in Part I

| Symbols | Meaning of Symbols |
|---|---|
| a, A | Crack Length |
| A/R, a/R | Dimensionless Crack Length |
| $A_0$, $a_0$ | Initial Crack Length |
| $a_0/R$, | Dimensionless Initial Crack Length |
| $a_c$ | Critical Crack Length |
| $a_c/R$ | Critical Dimensionless Crack Length |
| b | Width of Crack Front |
| B | Thickness of Disc Specimen |
| BEASY | Boundary Element Analysis System |
| BEM | Boundary Element Method |
| $B/R$ | Dimensionless thickness |
| C | Cutting Depth for CCNBD Machining |
| $C_1$ | Point-Loading Compliance |
| $C_1EB$ | Dimensionless Point-Loading Compliance |
| $C_2$ | Crack Opening Compliance |
| $C_2EB$ | Dimensionless Crack Opening Compliance |
| CB | Chevron Bending Specimen |
| CCNBD | Cracked-Chevron-Notched Brazilian Disc |
| CSTBD | Cracked-Straight-through Brazilian Disc |
| $\lambda_{CMOD}$ | Crack Mouth Opening Displacement |
| D | Diameter of Disc Specimen |
| $D_1$ | Diameter of Diamond Saw Used for Curve Slot Cutting |
| E | Young's Modulus of Rock |

Continue

| | |
|---|---|
| F | Dimensionless Stress Intensity Factors |
| $F_0$ | Dimensionless Stress Intensity Factors at $x = 0$ of the Crack Front |
| $F_{ave}$ | Dimensionless Average Stress Intensity Factors |
| $F_1$, $F_C$,$F_{1C}$ | Critical Dimensionless Stress Intensity Factors |
| FEM | Finite Element Method |
| $K_I$ | Mode I Stress Intensity Factors |
| $K_{II}$ | Mode II Stress Intensity Factors |
| $K_{IC}$ | Mode I Critical Stress Intensity Factors |
| $K_{IIC}$ | Mode II Critical Stress Intensity Factors |
| LEFM | Linear Elastic Fracture Mechanics |
| $\lambda_{LPD}$ | Loading Point Displacement |
| LVDTs | Linear Variable Differential Transducers |
| P | Applied Load |
| PAFEC | Finite Element Software Package roduced by (PAFEC Ltd.) |
| $P_{max}$ | Failed Load |
| $S_t$ | Tensile Strength of Rock |
| SR | Short Rod Specimen |
| R | Radius of Curve Slot in CCNBD Specimen |
| UCS | Uniaxial Compressive Strength of Rock |
| $2x/b$ | Dimensionless Crack Front Width |
| X | X Axis Coordinate |
| Y | Y Axis Coordinate |
| Z | Z Axis Coordinate |
| 3D | Three Dimensional |
| 2D | Two Dimensional |

## Notations Used in Part II

| | |
|---|---|
| SE | Rock Specific Energy by Instrumented Cutting |
| CW | Rock Cutting Tool Wear by Instrumented Cutting |
| CoI | Rock Cutting Coarseness Index by Instrumented Cutting |
| CS | Rock Compressive Strength |
| TS | Rock Tensile Strength |
| $E_s$ | Secant Young's Modulus of Rock |
| ED | Dynamic Young's Modulus by wave velocity test |
| ET | Tangential Young's Modulus of Rock |
| WV | Wave Velocity |
| BD | Bulk Density |
| GD | Grain Density |
| P. | Porosity |
| SH | Shore Scleroscope Test |
| CI | Cone Indenter Index by NCB Cone Indenter |
| GS | Grain Size |
| GR | Rock Grain Roundness |
| CC | Cementation Coefficients |
| h | Cutting depth |
| $\theta$ | Internal friction angle of rock |
| Sst | The Content of Sandstone |
| Lst | The Content of Limestone |
| Mst | The Content of Mudstone |
| A | Lathe Abrasivity Index |
| ISI | Impact Strength Index |
| MI | Machinability Index |
| AI | Abrasivity Index |

| | |
|---|---|
| Ss | Shear Strength of Rock |
| SP | Saturated Porosity |
| ScH | Schmidt Rebound Hardness |
| IBI | Impact Blow Test |
| TI | Toughness Index of Rock |
| MR | Moduli Ratio of Rock |
| $K_{IC}$ | Mode I Rock Fracture Toughness |
| $K_{IIC}$ | Mode II Rock Fracture Toughness |
| $G_{IC}$ | Mode I Energy Release Rate |
| $G_{IIC}$ | Mode II Energy Release Rate |
| $G_C$ | Energy Release Rate |
| Y | Yield by Instrumented Cutting Testing |
| K | The Coefficient of Plasticity |

## Contents

## Appendicies

DEDICATED TO THE MEMORY OF MY GRANDMA

MRS PU-XIU ZHOU

# Part I

# Development of the Crack-Chevron-Notched Brazilian Disc Method for Rock Fracture Toughness Testing

# Chapter I

## Review and Introduction to Part I

### 1.1 Introduction

Many researchers have previously done work in rock fracture mechanics including developing ideal rock facture mechanics parameter; testing systems and applying rock fracture mechanics to rock engineering such as rock fragementation etc.

Barker L. M.; Schmidt R. A.; Rossmanith H. P.; Ingraffea A. R.; Fourney W. L.; Atkinson B.; Merdith P. G. (1983); Bubsey R. T.; Newman Jr J. C.(1984); Ouchterlony F.; Sun Z.; Mastsui K; etc. have contributed a lot to the development of Rock Facture Mechanics.

An understanding of the mechanics and mechanisms of rock fracture is a key element in solving a lot of engineering problems that involve geological structure.

The testing commission of the ISRM has recently recommended two standard specimens for mode I rock fracture toughness testing: Chevron-Notched Short Rod Specimen and Chevron-Notched Bending Specimen. In this research programe, another chevron-notched specimen – Cracked-Chevron-Notched Brazilian Disc specimen is developed for rock fracture toughness measurement. This specimen could be recommended to be the third **Chevron-Notched** specimen for rock fracture toughness testing by the testing commission of the ISRM.

### 1.2 The Application of Rock Fracture Mechanics

The application to rock fracture mechanics on mining can be divided into the following categories:

1 For the prediction tunnel boring machine performance;

2 For the analysis of rock cutting mechanisms;

3 To solve the difficulties which rock mechanics can not explain, such as rock internal crack, the poor reproduction of rock mechanics properties such as tensile strength, uniaxial compressive strength and their dependence on specimen size;

4 To develop new intact rock and rock mass classification index for engineering design, accident preventation, evaluation for all kinds of mining equipment (hydraulic supports, drilling machines, tunnelling machines, rockbolts);

5 To develop ideal testing methods for measuring the rock fracture mechanics parameters (rock fracture toughness, J-integer, crack extension resistance and so on).

## 1.3 The Development of Rock Fracture Mechanics

### 1.3.1 Introduction

At ambitent conditions, most rocks fracture when stress inside the rock exceeds the its critical level. Usually this level is called as the critical applied stress or fracture strength.

The rock strength criterion such as Mohr strength criterion, tensile strength etc. did not account for structural flaws (microcracks and pores). It was found that the fracture strength of many brittle materials like rock was, in general, not only poorly reproducible under apparently indentical testing conditions but it also rate, size and environment dependent. The inadequancy of the critical applied stress approach to failure lay in its entirely empirical character. Its lack of complete success in engineering applications led to a serious reconsideration of the conditions for rock fracture. Rock fracture mechanics was developed under this situation.

### 1.3.2 The Strength Criterion in Rock Mechanics

An important problem in rock mechanics and rock engineering is to ascertain the mechanical conditions which cause rock to deform permanently, or to facture. The best known failure criterion consist of the following:

1 The maximum tensile stress;

2 The maximum shear stress;

3 Coulomb's criterion of failure;

4 Mohr's criterion;

5 Griffith's criterion of brittle failure in tension.

The Griffith's theory of fracture has been applied in many variations to rock engineering with some success. Basically, the theory is one of equating the release of strain energy required to creat the new surfaces, i.e. surface energy. Griffith applied his theory to the fracture of glass and obtained crude agreement. Since the theory neglected all forms of energy dissipation other than surface energy, Orowan modified the theory slightly to account for small-scale plastic flow at the crack tip. Irwin later introduced the concept, K, which is basically the strength of the stress singularity at a crack tip and is directly related to the strain-energy rate, G.

Linear elastic fracture mechanics, as it is well known, is primarily based on the stress-intensity factor and has been applied with little or no modification to the study of the fracture of metals with outstanding success.

In contrast, in the field of rock engineering investigations, these have primarily focused on individual modifications to the original Griffith's theory for each application. As a result, a large number of theories exist such as the modified Griffith's criterion, generalized fracture criterion, energy balance theory etc. have been proposed.

Recently, fracture mechanics has been applied widely in the solution of rock engineering problems especially for competent brittle rocks under high stress state or dynamic loading. Fracture toughness of rock is one of the basic parameters in fracture mechanics indicating the ability of rock to resist fracturing, i.e. the initiation and propagation of cracks.

The application of fracture mechanics to rock requires the understanding that LEFM principles were not developed with rock material and geological structures

in mind. While certain basic theories of fracture mechanics will apply, large differences in basic material response and engineering application between rock and metallic materials must be considered.

## 1.4 The Basic Theories of Rock Fracture Mechanics

### 1.4.1 Introduction

Rock fracture mechanics is the study of the behaviour of cracks and their behaviour of cracks and their modes of propagation. During cracking, energy is consumed in creating new surface area. The more energy a rock absorbs, the higher is its fracture resistance. Just because of this principles, fracture mechanics parameters have been used as an indices for evaluating the performance of tunnelling machines, though the energy consumed in the process of crack propagation only accounts for about 1 to 2 percent or even less. The fracture energy is provided either by work done externally, by the release of elastic strain energy within the cracked body, or by a combination of these two effects. The following will discuss the basic principle and development of fracture mechanics briefly.

### 1.4.2 Stress Concentration

Pre-existing cracks had been long been supposed as percursors of failure. Inglis (1913) confirmed this by analysising the stress distribution around on elliptical hole in a plate subjected to a uniform tensile stress. The importance of this analysis lay in the discovery that the local stresses about a sharp notch or tip could produce much higher stress than the applied stress. Inglis showed that for an ellipitical notch, the point of maximum stress corresponds to the point of minimum radius of curvature, i.e. the 'tip 'of the ellipse. The local stress magnification was related to the magnitude of the remote applied stress through

$$S_{max}/S_t = 2(a/\rho)^{0.5}, \quad for \quad a \gg \rho \tag{1.1}$$

where

$S_{max}$: the maximum tensile stress at the crack tip;

$S_t$: the applied tensile stress normal to the major axis of the ellipse;

a: the semi-major axis of the ellipse;

$\rho$: the minimum radius of curvature.

The right hand side of equation (1.1) is known as the 'stress intensity factor' and shows that stress concentration only depends on the shape of crack tip not its size. The major breakthrough of Inglis's analysis was that it offered the first clue to the mechanism of fracture of a crack, because the limiting case of an ellipse with an infinitesimally small radius of curvature could be considered to represent a crack. Equation (1.1) shows that in the case of a crack-like ellipse, the local crack-tip stress would be several times the applied tensile stress. It did not analysis the condition of crack propagation.

### 1.4.3 Griffith Energy Balance Theory

On the basis of Inglis (1913) analysis of stress distribution around the crack tip, Griffith (1920) postulated that brittle materials contained submicroscopic defects (called Griffith's flaws later) which provide nucleation sites from which cracks could propagate as the ideal fracture stress had been exceeded locally. The major breakthrough of Griffith (1920) to the theoretical understanding of fracture was his formulation of a criterion for the propagation of an isolated plane crack in a stressed solid in terms of mechanical energy and thermodynamics. He modelled this system as a reversible thermodynamic process in which the crack would be in a state of equilbrium when the total free energy of the system was a minimum. For a static crack in an elastic-brittle solid, the total energy (U) is given by

$$U = (-W_l + U_e) + G' \tag{1.2}$$

Where:

$W_l$: the work done by the applied load;

$U_e$: the strain energy stored in the elastic solid;

$G'$: the thermodynamic surface energy.

The sum in the brackets is the total mechanical energy of the system, which favours crack extension. The surface term opposes crack propagation since cohesive molecular forces must be overcome in creating new crack surfaces. Equilbrium is achieved by balancing the mechanical and surface energy terms in Equation (1.2).

The value of this energy-balance approach is that by considering energy changes in the whole system, it is possible to de-focus attention from the highly concentrated local crack-tip stress field and derive a useful expression for the fracture stress. By combining the stress concentration analysis with the energy-balance criterion, Lange (1974) concluded the fracture equation, which defines the critical applied stress $P_t$ for crack extension as (Lange, 1974):

$$S_c > A\frac{G'E}{a(1-\nu^2)^{1/2}} \tag{1.3}$$

Where:

$S_c$: The critical applied stress;

A: a numerical constant which depends on the mode of loading and crack geometry;

a: the crack half-length;

$\nu$: Poisson's ratio.

The expression represents a major breakthrough in the understanding of fracture processes because not only does it show that pre-existing cracks are percursors to fracture, as indicated by Inglis's (1913) analysis, but also that, for a given configuration, the fracture stress depends only on the crack length and three material properties. The drawbacks of Griffith's energy balance theory negleted all forms of energy dissipation other than surface energy.

### 1.4.4 Linear Elastic Fracture Mechanics

Irwin (1958) modified and extended Griffith (1920, 1924) Energy-Balance theory, by means of the analysis of the stress field around a sharp, plane crack-tip in an isotropic, linear elastic continuum, which laid the foundation of modern fracture mechanics.

### 1.4.5 Modes of Crack Propagation

There are three basic modes of crack-propagation: mode I (tensile mode); mode II (in-plane shear); mode III (anti-plane shear). they are shown in Figure 1.1.

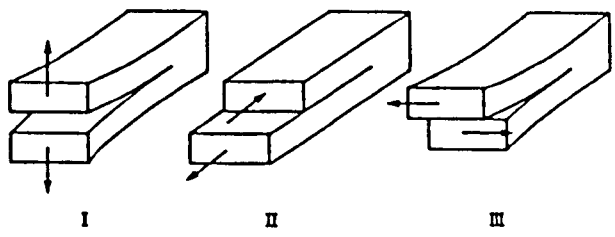


**Figure 1.1 — Three Basic Modes for Crack Propagation**

Of the three modes of crack tip propagation, Mode I is by far the most pertinent to crack propagation in brittle materials (Lawn and Willshaw, 1975). Most attention in the literature has been devoted to the opening or tensile mode because of its great importance in crack propagation through brittle rocks (brittle cracks tend to seek an orientation which minimised the shear component), that is why only the recommended standards for the measurement of mode I rock fracture toughness measurement were proposed. The author thought that Mode II fracture is also very important in studying mixed-mode rock fracture such as drag tool rock cutting mechanism and the movement of fault for the prediction of earthquakes. The detailed analysis will be reported later.

### 1.4.6 Stress Intensity Factors

In general, the near field stress distribution in a linear elastic solid modified by the introduction of a 'sharp' plane crack with traction-free walls may be expressed in polar coordinates as

$$S_{ij} = K/2\pi r^{1/2} \times f_{ij}(\Omega) + \Delta \tag{1.4}$$

Where

i, j: define the components of the stress tensor;

r: the distance from the crack tip or crack front;

$\Omega$: the angle measured from the plane of the crack;

$f_{ij}(\Omega)$): a well-defined function of $\Omega$ which depends only the mode of loading;

$\Delta$: incorporates the boundary condition at the crack tip.

Therefore, all details of the loading geometry and crack configuration are embodied in K, which consequently determines the intensity of the local stress field (Lawn and Willshaw, 1975). This stress intensity factors is the key index in the fracture mechanics method, because it relates directly to the energy flux in crack extension. For a two-dimensional plane crack of any mode it is given by

$$\mathrm{K1} = Y \times S_a \times a^{1/2} \tag{1.5}$$

Where:

Y: a geometrical constant;

$S_a$: the magnitude of the remotely applied stress;

a: a characteristic crack length.

The $K_I$ parameter reflects the level of loading near the crack tip; and has units of $MPa \times \sqrt{M}$. Therefore we define a critical stress intensity factor $K_{Ic}$,

sometimes called the 'fracture toughness ', which is a sufficient description of the conditions under which crack propagation will happen. The fracture toughness is a material constant which can be applied on all scales, in a similar way to the elastic constants. The advantages of this method is that from only the size of the most deleterious flaw and knowledge of the fracture toughness, the fracture strength of a body can be predicted.

### 1.4.7 Fracture Energy

Irwin (1958) derived a general expression for the crack extension force with the energetics of fracture.

$$G = -d(-W_l + U_e)/da \tag{1.6}$$

Where $W_l$ and $U_e$ are as previously defined. He reasoned that an equal amount of stored elastic energy must be released when a crack is allowed to extend, and so named the quantity G the 'strain energy release rate'. This parameter re-introduced the Griffith's criterion energy-balance concept as a crack extension criterion. Applied simply to the critical condition this produces

$$G_c = 2G' \tag{1.7}$$

in the absence of other dissipative processes, i.e. the critical crack extension force is exactly balanced by the maximum crack resistance force. Irwin (1958) and Orowan (1955), however, independently proposed that the thermodynamic surface energy was not the only mode of energy dissipation. Other process such as microplasticity, acoustic emission, heat generation and microcracking out of the plane of the main crack operate close to the propagation crack tip; so that a more realistic description is

$$G_c = 2G^* \tag{1.8}$$

$G^*$ is the 'Fracture Surface Energy'; $G^* > G'$ and; therefore, $G_c$ is the total 'Fracture Energy'.

The strain energy release rate G and stress intensity factor can be shown to be essentially equivalent. For example, in the important case of plane strain conditions and mode I

$$G = K_I^2(1-\nu^2)/E \tag{1.9}$$

### 1.4.8 Non-linear Elastic Fracture Mechanics

Although LEFM (Linear Elastic Fracture Mechanics) is directly related with the Griffith's theory, plastic flow and the other nonlinear behaviour can occur on a small scale without affecting its predictive success. The source of non-linear behaviour around the crack tip comes from the three aspects:

1 Microplasticity;

2 Microcracking;

3 Residual stresses.

Meredith (1983) and Ouchterlony (1981) stated that the micro-plasticity around the crack tip is not important compared to the microcracking. At ambient temperature, crack growth in silicate rocks is not accompanied by signficant plastic flow. Microcrack development in the process zone ahead of the crack tip, associated with macrocrack extension, is ubiquitous in polycrystalline ploy phase materials such as rocks (Buresch, 1978, 1979; Hoagland and et al., 1973; Kobayashi and Fourney, 1978). As known to us, the stress-strain behaviour of some rock in tension is known to be rather non-linear because of the microcracking development around the crack (pore or microcrack). Therefore, when the size of the process zone of non-linear behaviour at a crack tip can not be considered to be small compared to the crack length, recourse to other fracture theories such as J-integral method become necessary.

### 1.4.9 J-integral Resistance

The J-integral allows a certain extension of LEFM to non-linear material behavior. A basic feature of the J-integral is its path independence. This implies that J-integral is a characteristic scalar measure of the conditions at the crack tip, much as the stress intensity factor in LEFM.

For an elastic, but not necessary linear, material

$$J = G = -\left(\frac{\partial U}{\partial a_c}\right)_{\sigma_F} \tag{1.10}$$

Thus J is identical to the potential energy release rate.

### 1.4.10 Crack Extension Resistance Curves

A crack extension resistance curve (R-curve) is a plot of crack extension resistance as a function of crack length, in which the resistance to crack propagation is most commonly expressed in terms of a stress intensity factor, but could equally well be expressed as $J_r$ or $G_r$. The curves characterize the resistance of a material to the stable crack extension which results from growth of a non-linear process zone as the crack propagates from a 'sharp' notch.

Fracture mechanics theory is very complicated. It is not my attentation to give a detailed review. Only some basic fracture theories relating to my later work have been presented above.

Metal fracture mechanics measurement has developed over several decades The rock fracture mechanics parameters have been greatly influenced by these experiences and techniques. The testing of rock fracture mechanics parameters, however, involved some unique problems. Therefore some special measures including rock specimen preparation have to be considered in the measurement of rock fracture mechanics parameters.

## 1.5 Simple Review of Rock Fracture Toughness Testing Methods

### 1.5.1 Introduction

A lot of workers have used different geometry specimen for the measurement of rock fracture toughness, some of their results were not comparable with each other.

Specimens used by other worker are summarized in Figure 1.2.

### 1.5.2 Double Torsion Testing Method

The double torsion specimen as shown in Figure 1.2(10) can be considered as two elastic torsion bars of rectangular cross section.

Double torsion specimens are cut from single blocks of the appropriate starting material using a precision diamond saw. The top and bottom surfaces are ground flat and parallel to within 0.025 mm, as are the sides. A central, axial groove about 1 mm is cut along the length of each specimen with a diamond slot-cutting machine to a depth of approximately one third of the thickness. In addition, a notch about 1 cm long and 1 mm wide is cut in one end of each double torsion bar along the line of the axial groove. This is done so that on loading crack propagation occurred from the notch in a direction parallel to the specimen length. This is not considered further as it is too complicated to prepare the specimen.

### 1.5.3 The Burst Cylinder Specimen

This method was first introduced by Johnson et al. (1973) and later expanded by Abou-Sayed (1977). It is used for determining a rock's resistance to crack propagation, capable of simulating in situ conditions for blasting and hydrofracturing applications. The geometry of specimen is shown in Figure 1.2(14). The specimen is a pre-notched thick-walled cylinder subjected to internal pressure of the borehole wall only. Pressurisation of notch faces is prevented by internally jacketing the central hole. Its advantage lies its cylindrical shape and its disadvantages are listed as follows:

1 Crack length measurement is required;

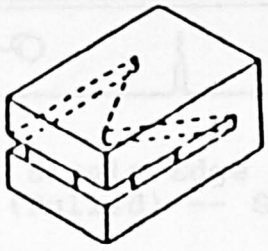

(1) Short Bar -- SB

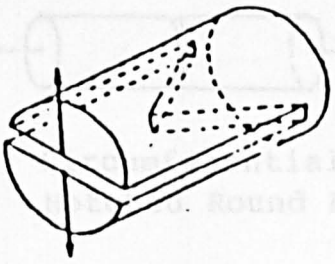

(2) Short Rod -- SR

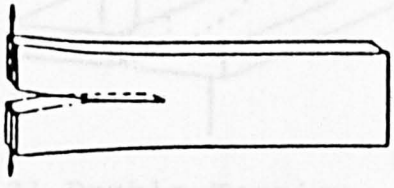

(3) Double Cantilever Beam (Pulled) -- DCBP

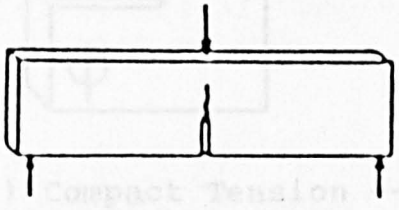

(4) Single Edge Notched Beam (Three Point Bending)

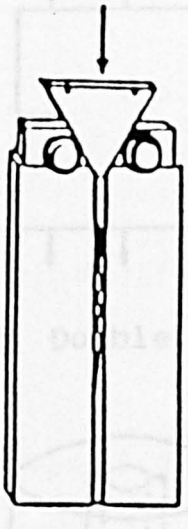

(5) Double Cantilever Beam (Wedge Loaded) -- DCBM

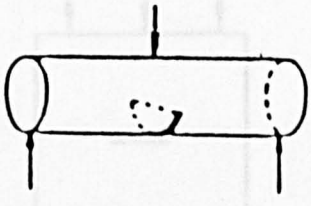

(6) Round Single Edge Notched Beam

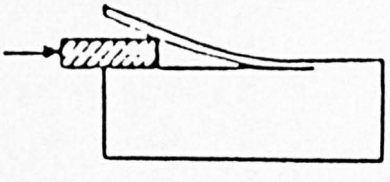

(7) Wedge Insert -- WI

**Figure 1.2 — Specimen Geometries Used for Rock Fracture Toughness Testing**

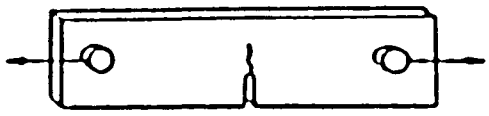

(8) Single Edge Notched Beam (Pulled) -- SENBP

(9) Circumferentially Notched Round Bar

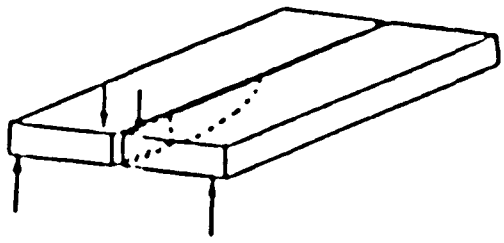

(10) Double Torsion -- DT

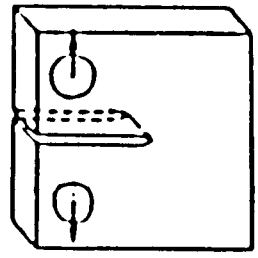

(11) Compact Tension -- CT

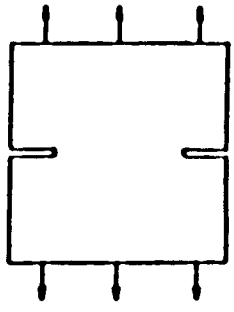

(12) Double Edge Notched Plate

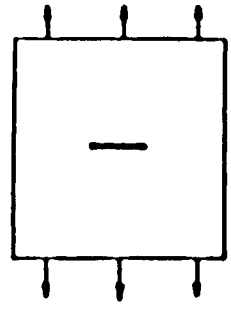

(13) Center Notched Plate

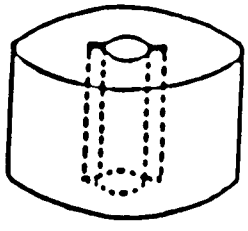

(14) Burst Test -- BT (Internally Notched)

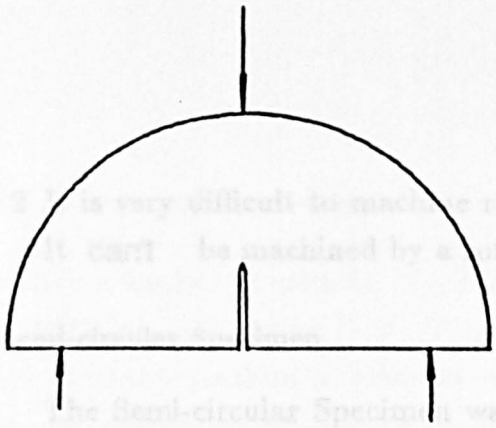

(15) Semi-Circular Plate

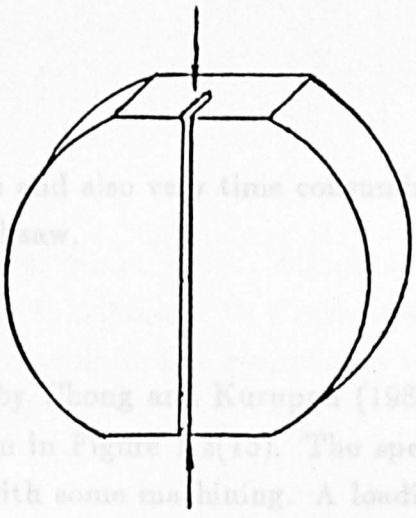

(16) Diametral Compression Disk -- DCD

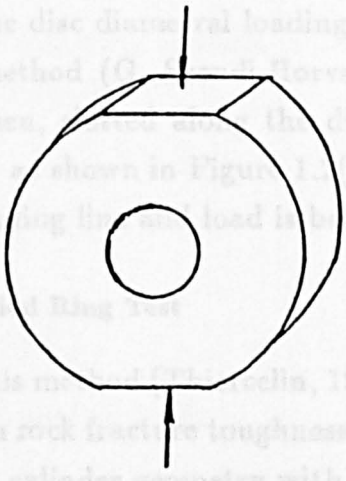

(17) Modified Ring

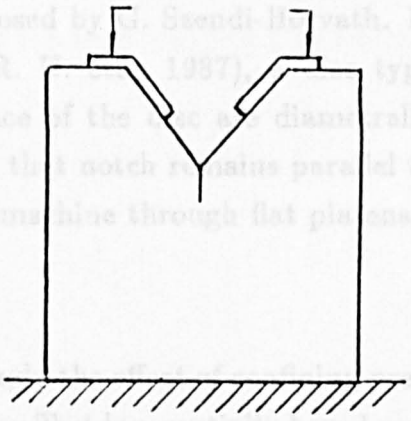

(18) Wedge Loaded Compact Tension

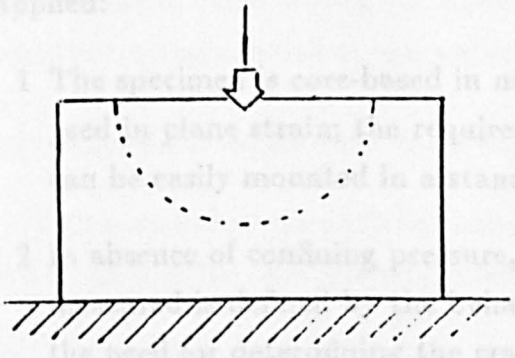

(19) Indentation Testing

2 It is very difficult to machine radial notches and also very time consuming. It can't be machined by a rotary diamond saw.

### 1.5.4 Semi-circular Specimen

The Semi-circular Specimen was proposed by Chong and Kuruppu (1984). The geometry and loading of specimen is shown in Figure 1.2(15). The specimen can be prepared from typical rock cores with some machining. A loading apparatus similar to three point bending testing is used.

### 1.5.5 Disc Diametral Loading Tests

The disc diametral loading method was proposed by G. Szendi-Horvath. In this method (G. Szendi-Horvath, 1982; Singh R. N. etc., 1987), a disc type specimen, slotted along the diameter, on one face of the disc are diametrally loaded as shown in Figure 1.2(16), in such a way that notch remains parallel to the loading line and load is being applied by the machine through flat platens.

### 1.5.6 Modified Ring Test

This method (Thiercelin, 1987) was used to study the effect of confining pressure on rock fracture toughness. The Modified Ring Test is essentially based on a hollow cylinder geometry with two, diametrically opposed, flat loading surfaces. The geometry of 'Modified Ring Test' is shown in Figure 1.2(17).

This test presents several advantages, especially when confining pressure is applied:

1 The specimen is core-based in nature, it is easy to prepare and can be analysed in plane strain; the required dimensions are small, hence the specimen can be easily mounted in a standard triaxial cell;

2 In absence of confining pressure, the load at which the fracture toughness is measured is defined by the behavior of the load-deformation curve, without the need for determining the crack length;

### 1.5.7 Direct Indentation Method

Some worker (Swain M. V., Lawn B. R., 1976; Swain M. V., Atkinson B. K., 1978; and Goodman D. J., Tabor D., 1978; B. K. Atkinson, V. Avdis, 1980) have used this method to measure rock fracture toughness. The geometry of the 'Direct Indentation Method' is shown in Figure 1.2(19).

The advantages using this method lies in:

1 Specimen preparation is very simple, only a single ground surface is required;

2 The loading apparatus is very simple; it is very fast to test;

The following formula is used to calculate rock fracture toughness by indentation method.

$$K_{IC} = \frac{P}{\pi C^{3/2}} \tan\psi \tag{1.11}$$

Where:

P = applied load;

$\psi$ = the half angle of point indenter;

2C = the magnitude of cracking.

The indentation testing methods ignore dynamic and kinetic effects and frictionless loading conditions are assumed.

### 1.5.8 Other Specimen Geometries Used for $K_{IC}$ Measurement

Other specimen geometries, as shown in Figure 1.2, have been used by different workers for rock fracture toughness measurement.

## 1.6 Requirements of ASTM standard E399

Even though standard E399 or BS 5447:1977 is not directly applicable to rocks and minerals, it forms a useful point of reference for establishing procedures

suited to rocks. It is pertinent, therefore, to consider the three major criteria of E399 before commencing a description of the various testing techniques.

### 1.6.1 Specimen Size

The purpose of this restriction is to make sure that the size of the plastic zone at the crack tip in a metallic specimen is insignificant compared to other specimen dimensions. Rocks, however, are more likely to exhibit microcracking as the main crack tip non-linearity (Hoagland et al., 1973). The shape of the microcrack zone is essentially similar to the plane stress conditions at the specimen surfaces (Ouchterlony, 1980a). As a result, K for rocks is expected to be almost independent of specimen thickness. Limited data on westerly granite by Schmidt and Lutz (1979) and on granite and sandstone by Rummel and Winter (1979) appear to confirm this. K is, however, influenced by the crack length if this is very short. Schmidt (1980) has suggested the following minimum crack length criterion:

$$a > 2.5K_{IC}/S_t \tag{1.13}$$

Where:

a: the crack length;

$K_{Ic}$: rock fracture toughness;

$S_t$: rock tensile strength.

This criterion is based on the uniaxial tensile strength ($S_t$) rather than the yield stress which is specified for metals in ASTM E399. This yields minimum crack lengths of from several millimeters to several centimetres for most rocks.

On accounting the influence of microstructure on the measurements of rock fracture mechanics parameters, the specimen dimensions and crack length must be considerably larger than the grain size. A ratio of 10:1 is usually deemed sufficient to ensure that measurements are representative of the bulk rock.

## 1.7 The Influence of Some Factors on Fracture Toughness

### 1.7.1 Introduction

Many factors (rock petrological factors such as rock internal-texture, porosity and mineralogical variations, enviromental factors such as water, temperature and confining pressure) affects the value of rock fracture mechanics parameters.

### 1.7.2 The Influence of Internal Texture

Singh et al. (1979), Rice et al. (1980), Meredith (1983), and Huang J. et al. (1985) have reported that the rock fracture mechanics parameters increases with increasing grain size. Huang J. et al. thought that the dependence of rock fracture mechanics parameters on the grain size is likely caused by the influence of grain boundary contact on the stress intensity factor at the tip of the pre-fabricated notch. The larger the grain size, then the larger are the grain boundary fissures, as well as the inter-granular cracks. From the point of view of fracture mechanics, the stress intensity factor is defined not only by stress but also by the size of fissures around the pre-fabricated notch. Since the low fracture toughness is caused to a great extent by the larger fissures, such rock may be of low mechanical strength due to a higher stress intensity factor developed at the tip of the fissures. Some authors concluded that the influence of grain size on rock fracture mechanics parameters is explained by the change from predominately transgranular fracture in coarse-grained materials to pre-dominantly intergranular fracture in fine-grained materials. This explanation has some similarity with the crack-pore interation extension in indentation testing under the observation using micro-scope video-camera in Sweden. Atkinson (1979) used scanning electron micrographs and found the fracture behaviour of Tennessee sandstone is strongly influenced by the failure of the matrix phyllo-silicates and quartz grains are often forced out of the phyllosilicate matrix as the crack propagates. Similar results have been reported by Sangha et al. and Friedman for other sandstones with weak matrices. Atkinson reported also that fracture in Carrara Marble involves both transgranular and intergranular and transgranular cracking is strongly affected by cleavage. The influence of crack propagation

direction (Intergranular or transgranular cracking) on rock mechanics was found to have similar results.

Fracture mechanics parameters related to crack propagation depends on a lot of factors:

1 Pore size and shape;

2 Grain size and shape;

3 Mineralogical composition;

4 Cementation force of grains;

5 The interaction of pore and crack.

### 1.7.3 The Influence of Porosity

Rice et al. (1978) have reviewed the influence of porosity on fracture propagation. Interpretation of data was complicated by both pore shape and pore distribution. Meredith (1983) concluded that the fracture toughness of rocks decreased with increasing porosity though a sustantial amount of scatter and variation existed.

### 1.7.4 The Influence of Mineralogy

Meredith (1983) reported that fracture toughness increases with decreasing quartz content and increasing content of ferromagnesian minerals and found the fracture toughness of rocks increase from the order of sandstones, through quartzites, granites and basic rocks to ultrabasic rocks. Norton and Atkinson (1981) reported that $K_{IC}$ for some types of very dry natural quartz is considerably higher than that for synthetic quartz. The low values for some sandstones suggested that the failure in these materials must be pre-dominantly intergranular, and is controlled by the weak matrix or cement between quartz grains.

### 1.7.5 Relation between $K_{IC}$ and Rock Properties

Huang and Wang (1980) studied the relation between $K_{IC}$ and rock properties such as grain size, acoustic wave velocity, uniaxial compressive strength,

tensile strength etc. The results is shown in Figure 1.3.

## 1.8 Introduction to the CCNBD Specimen

The chevron notched specimen has gained wide acceptance for fracture toughness testing since the invention of the chevron notch short rod specimen by Barker, Ouchterlony et al. They developed the chevron notched bending specimen for rock fracture toughness testing.

A summary of various chevron-notched fracture specimen configurations are shown in Figure 1.4.

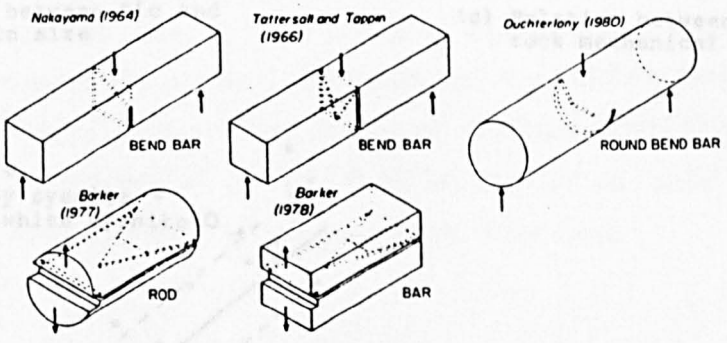


**Figure 1.4 — Various Chevron-Notched Fracture Specimen Geometries**

Newman (1984) presented a very comprehensive review on chevron-notched fracture specimens, including the history, development, specimen types, advantages and disadvantages, and possible applications for ductile materials. The chevron-notched bend bar specimen was first used by Nakayama (1964). Tattersall and Tappin (1966) proposed a symmetrical chevron-notched bend bar specimen.

There is a growing tendency in the use of chevron notched specimens for fracture toughness testing of rocks. Barker (1977) first introduced the chevron-notched short rod method to measure the fracture mechanics parameters of rocks like siltstone and limestone. He designed a very simple device which used a bucket of water to produce the breaking load. Later Costin used the chevron notched

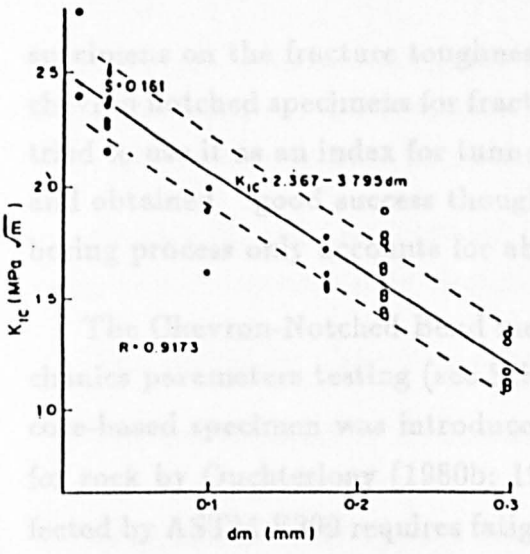


(a) Relation between Kic and rock grain size

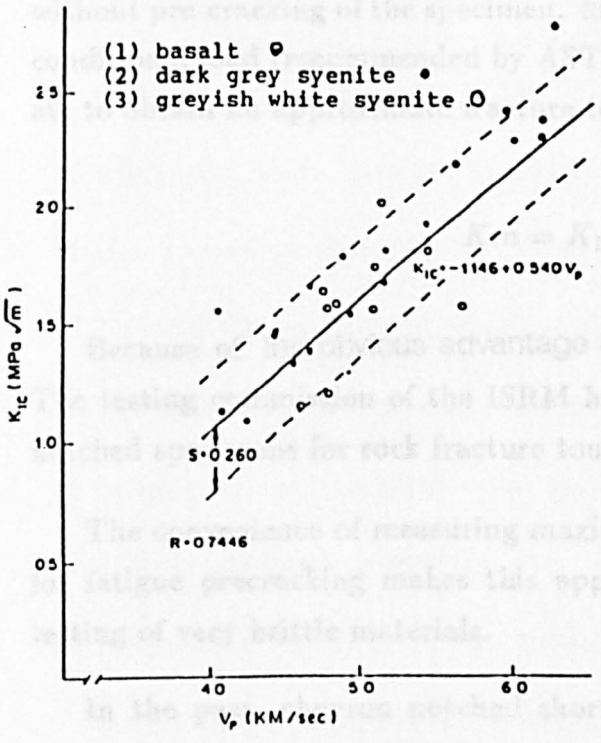


(b) Relation between Kic and acoustic wave velocity (Vp)

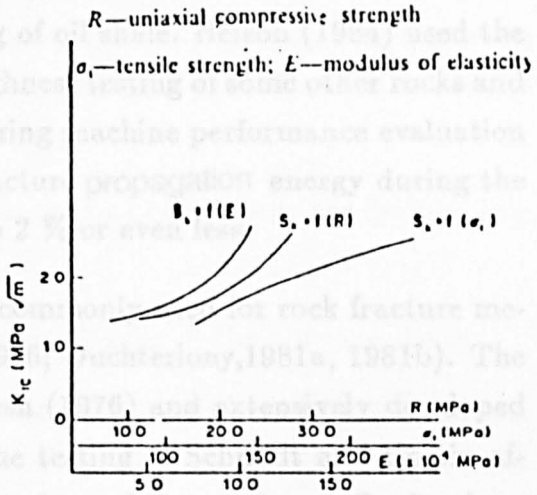


(c) Relation between Kic and rock mechanical properties

**Figure 1.3 — Relation between $K_{IC}$ and Rock Properties by Huang and Wang**

specimens on the fracture toughness testing of oil shale. Nelson (1984) used the chevron notched specimens for fracture toughness testing of some other rocks and tried to use it as an index for tunnelling boring machine performance evaluation and obtained good success though the fracture propagation energy during the boring process only accounts for about 1 to 2 % or even less.

The Chevron-Notched Bend method is commonly used for rock fracture mechanics parameters testing (see Schmidt, 1976; Ouchterlony,1981a, 1981b). The core-based specimen was introduced by Bush (1976) and extensively developed for rock by Ouchterlony (1980b; 1982). The testing of Schmidt and Costin affected by ASTM E399 requires fatigue pre-cracking of the specimen. Ouchterlony and Swan introduced the advantages of the chevron notch and single bending. They developed into the chevron bend specimen which gave high stress intensity factors at the vertex of the notch. They measured the fracture mechanics parameters without pre-cracking of the specimen, and used the failure load, Pmax, instead of the conditional load (recommended by ASTM E399),Pq, and an initial notch depth, a0, to obtain an approximate fracture toughness value from

$$Km = K_1(a_0, P_{max}) \tag{1.12}$$

Because of the obvious advantage of avoiding pre-cracking by fatigue loading. The testing commission of the ISRM has recommended two standard chevron-notched specimens for rock fracture toughness measurement.

The convenience of measuring maximum load ($P_{max}$) only without the need for fatigue precracking makes this approach attractive for fracture toughness testing of very brittle materials.

In the past, chevron notched short rod and short bar specimen for fracture toughness measurement has been well developed on the basis of numerical analysis and experimental calibration by Barker, Newman and Ingraffea et al. Chevron-notched bending specimen has been developed by Ouchterlony et al.

The present two methods, for rock fracture properties measurement, recommended by the testing commission of the ISRM, using two specimens that can

be machined directly from piece of rock Core, the short rod and the chevron bending specimen. Both specimens have the common characteristic which is they are chevron-notched specimens.

Compared with conventional fracture toughness specimen, the unique features of a chevron-notched specimen are:

1 The extremely high-stress concentration at the tip of the chevron notch;

2 The development of a minimum stress-intensity factor as the crack grows. The high-stress concentration at the tip of the chevron-notch causes a crack to initiate at a low applied load, eliminating the need to precrack a specimen, a costly and time consuming procedure (no fatigue precracked);

3 From the minimum stress-intensity factor, the fracture toughness can be evaluated from the maximum load. Therefore, a load-displacement record, as is currently required in the ASTM test method for plane-strain fracture toughness measurements (E399-83) is not needed;

4 Minimum crack "pop-in" at initiation of crack growth;

5 Good crack guidance by the slots;

6 Appreciable crack front width at the time of toughness measurement;

7 Crack near specimen center at the time of the toughness measurement;

8 Load at or near its peak value at the time of the toughness measurement;

9 Simple specimen geometry;

10 Economical use of specimen material.

In addition to the above advantages of chevron-notched specimens, the Cracked Chevron-Notched Brazilian Disc (CCNBD) specimen has the following unique features:

1 The loading and displacement measurement apparatus is very simple, it takes less time to setup the testing rig than the SR and CB methods, it does not require a machine with a preload of zero or expensive tensile testing machine.

2 The CCNBD specimen preparation does not require complicate machining equipment or auxillary devices;

3 Can be used for mixed-mode rock fracture investigations and mode II (shear mode) rock fracture toughness measurement when the CCNBD specimen is machined to CSTBD specimen by cutting off 'V' section of chevron-notch using a hand saw;

4 It needs only a small sample for testing, which gives an obvious advantage over the chevron-notched CB specimens;

5 It is very convenient when measuring rock fracture toughness in different orientations;

6 The magnitude of failure load is generally larger than 1kN which is essential when using a loading machines with a preload of at least 1 kN;

7 Experimental setup and displacement measurement are very simple.

### 1.8.1 Specimen Geometry

The geometry with basic notation of the CCNBD is shown in Figure 1.5.

As seen from Figure 1.5,

$$C = \sqrt{D^2/4 - a_0^2/4} \tag{1.14}$$

$$\alpha = \arctan \frac{\sqrt{D'^2/4 - a_0^2}}{a_0} \tag{1.15}$$

$$\begin{aligned} \beta &= \frac{\pi}{2} - \alpha \\ &= \frac{\pi}{2} - \arctan \frac{\sqrt{D'^2/4 - a_0^2}}{a_0} \end{aligned} \tag{1.16}$$

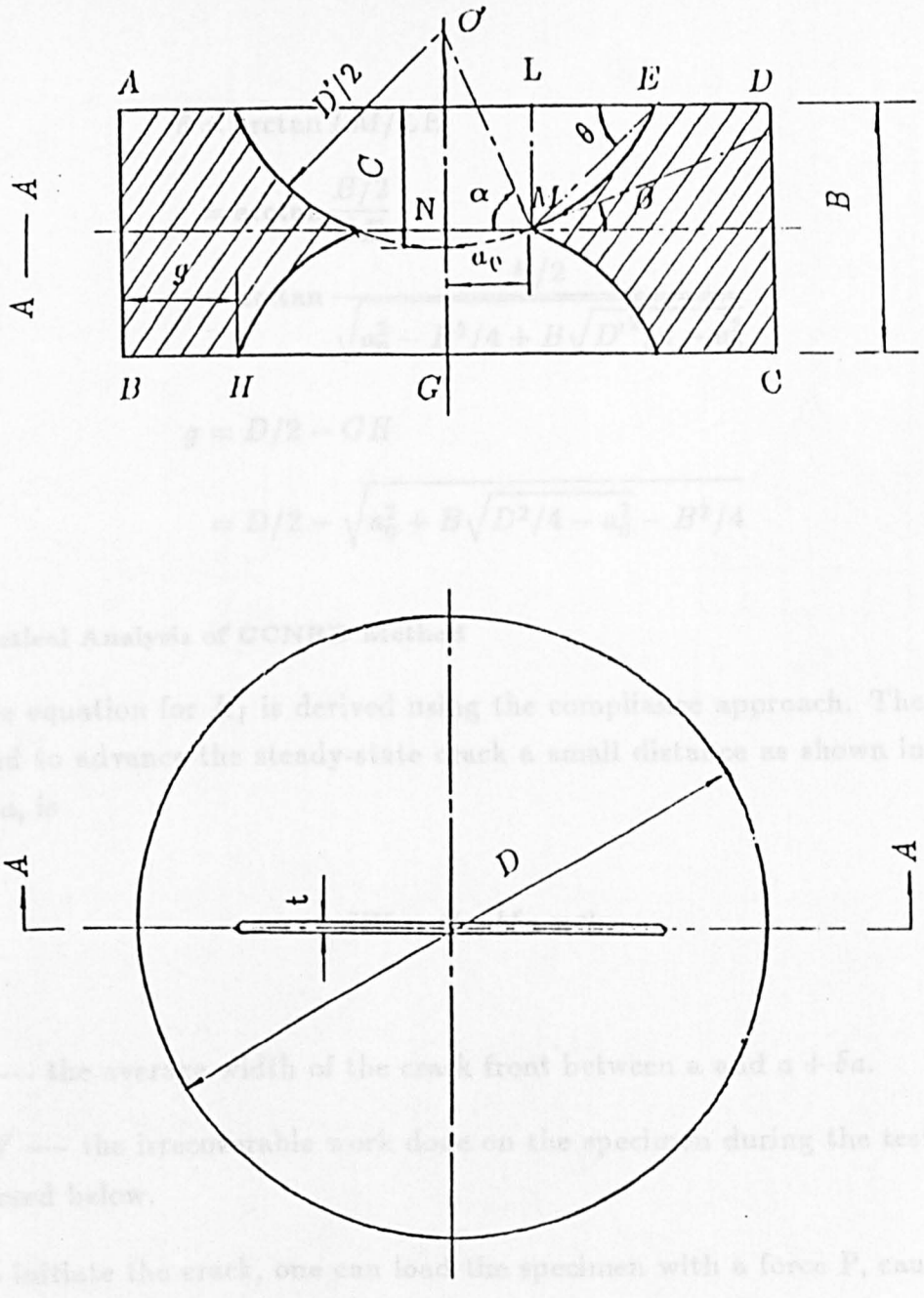


NOTATIONS:

B -- Specimen Thickness;
D -- Specimen Diameter;
D' -- Diameter of Diamond Saw;
a0 -- Initial Crack Length;
C -- Slot Cutting Depth;
t -- Slot Thickness;

**Figure 1.5 — The Geometry with Basic Notation of the CCNBD**

$$\begin{aligned}\theta &= \arctan LM/LE \\ &= \arctan \frac{B/2}{LE} \\ &= \arctan \frac{B/2}{\sqrt{a_0^2 - B^2/4 + B\sqrt{D'^2/4 - a_0^2}}}\end{aligned} \tag{1.17}$$

$$\begin{aligned}g &= D/2 - GH \\ &= D/2 - \sqrt{a_0^2 + B\sqrt{D^2/4 - a_0^2} - B^2/4}\end{aligned} \tag{1.18}$$

### 1.8.2 Theoretical Analysis of CCNBD Method

The equation for $K_I$ is derived using the compliance approach. The energy required to advance the steady-state crack a small distance as shown in Figure 1.6a, $\delta a$, is

$$\delta W = G_{IC} b \delta a \times 2 \tag{1.19}$$

where:

b — the average width of the crack front between a and $a + \delta a$.

$\delta W$ — the irrecoverable work done on the specimen during the test as discussed below.

To initiate the crack, one can load the specimen with a force P, causing the front of the specimen to open by an amount x (Figure 1.6b) proceeds up a steep linear elastic slope as depicted in Figure 1.6c. The onset of nonlinearty signifies the initiation of the crack point of the 'V'.

Suppose that specimen is loaded under the controlled conditions until the steady-state crack-tip configuration is attained and until the loading point opening, x, and the crack length, a, are as shown in Figure 1.6c.

The loading path is then assumed to be at A in Figure 1.6c. If specimen were unloaded from that point, and if no crack growth occurs on unloading, the

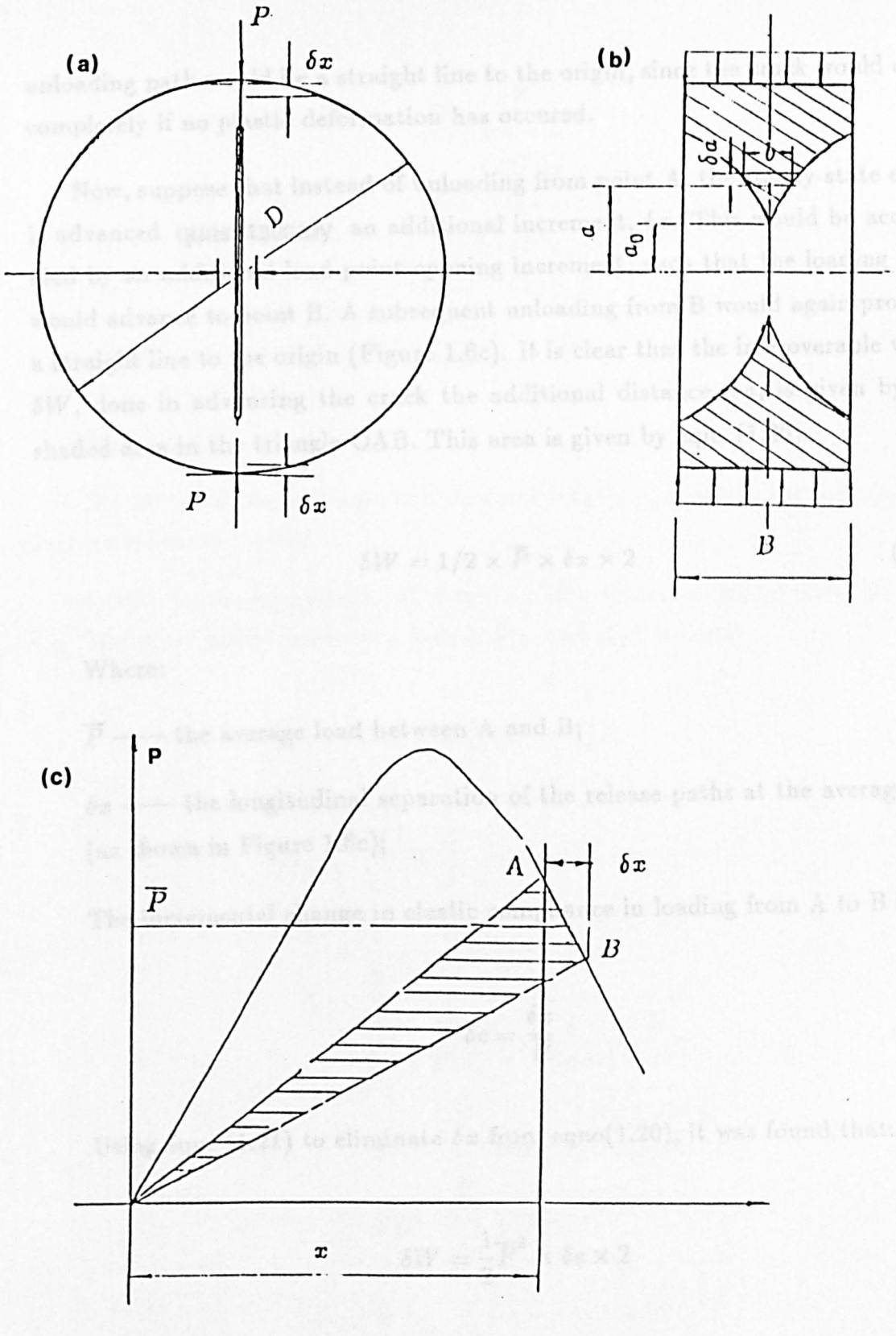


**Figure 1.6 — The Diagram Used for the Analysis of the CCNBD**

unloading path would be a straight line to the origin, since the crack would close completely if no plastic deformation has occured.

Now, suppose that instead of unloading from point A, the steady-state crack is advanced quasistatically an additional increment, $\delta a$. This would be accompanied by an additional load-point-opening increment, such that the loading path would advance to point B. A subsequent unloading from B would again produce a straight line to the origin (Figure 1.6c). It is clear that the irrecoverable work, $\delta W$, done in advancing the crack the additional distance, $\delta a$, is given by the shaded area in the triangle OAB. This area is given by eqn. (1.20).

$$\delta W = 1/2 \times \overline{P} \times \delta x \times 2 \tag{1.20}$$

Where:

$\overline{P}$ —— the average load between A and B;

$\delta x$ —— the longitudinal separation of the release paths at the average load (as shown in Figure 1.6c);

The incremental change in elastic compliance in loading from A to B is:

$$\delta c = \frac{\delta x}{\overline{P}} \tag{1.21}$$

Using eqn. (1.21) to eliminate $\delta x$ from eqno(1.20), it was found that:

$$\delta W = \frac{1}{2}\overline{P}^2 \times \delta c \times 2 \tag{1.22}$$

Eliminating $\delta W$ by use of eqn.(1.19) and taking the limit as $da$ and approach zero, the following equation is reached:

$$
\begin{aligned}
G_{IC} &= \lim_{\delta a \to 0} \frac{\delta W}{b\delta a \times 2} \\
&= \lim_{\delta a \to 0} \frac{1/2\overline{P}\delta x \times 2}{b\delta a \times 2} \\
&= \lim_{\delta a \to 0} \frac{1/2\overline{P}^2 \delta c \times 2}{b\delta a \times 2} \\
&= \frac{P^2 da}{2bdc}
\end{aligned}
\tag{1.23}
$$

Where:

b, P, and $dc/da$ are evaluated at the crack length, a, at which the incremental crack advance took place.

In order to cast equation(1.19) in terms of the critical stress intensity factors, $K_{IC}$, the plane strain equation relating $G_{IC}$ and $K_{IC}$ is used:

$$
G_{IC} = K_{IC}^2(1-\nu^2)/E \tag{1.24}
$$

So:

$$
\begin{aligned}
K_{IC} &= \sqrt{\frac{G_{IC}E}{1-\nu^2}} \\
&= \sqrt{\frac{P^2 dcE}{2bda(1-\nu^2)}} \\
&= \sqrt{\left(\frac{P}{BD^{0.5}}\right)^2 \times \frac{DB^2 dcE}{2bda(1-\nu^2)}} \\
&= \frac{P}{BD^{0.5}(1-\nu^2)^{0.5}} \sqrt{\frac{Bd(CBE)}{bd(a/R)}} \\
&= \frac{P}{BD^{0.5}(1-\nu^2)^{0.5}} f(a/R)
\end{aligned}
\tag{1.25}
$$

So:

$$
K_{IC} = \frac{P}{BD^{0.5}(1-\nu^2)^{0.5}} f(a/R) \tag{1.26}
$$

Where:

R: the radius of CCNBD disc; and

$f(a/R) = \sqrt{\frac{Bd(CBE)}{bd(a/R)}}$

The term in the brackets is a dimensionless function only of the ratio $a/R$. It is independent of the specimen material as long as the scaled specimen configuration remains constant.

Since the scaled crack position, $a_c/R$, at which the peak load is encounted is a constant (provided LFEM conditions prevail), the value of $f(a/R)$ in eqn(1.26) at the time of the maximum load, $F_c$, is a constant, $F_C = f(a_c/R)$.

Therefore,

$$K_{IC} = \frac{F_C P_{max}}{B D^{0.5}} \tag{1.27}$$

Where:

$K_{IC}$ – Mode I rock fracture toughness;

$F_C$ – Dimensionless critical stress intensity factors;

$P_{max}$ – Maximum failure load;

B – The thickness of CCNBD specimen;

D – The diameter of CCNBD specimen.

The dimensionless stress intensity factor $F_C$ for the chevron-notched specimen can be determined in three ways:

1 Experimental determination of $F_C$ based on a comparison with standard $K_{IC}$ values;

2 Analytical or semianalytical approach based on the compliance and the stress-intensity factor determined for specimens with straight cracks;

3 Full stress analysis, such as a three-dimensional finite element or three-dimensional boundary element analysis.

The first and third approaches should yield exact values of $F_C$, while the second approach is basically an approximation which need to be verified.

In this research programme the determination of the dimensionless stress intensity factor used the third method, i.e. a three-dimensional finite element and three-dimensional boundary element method.

## 1.9 Introduction to the Research Programme

This research programe for the development of the CCNBD specimen for mode I rock fracture toughness measurement consists of the following parts:

1 Three-dimensional finite-element calibration of the CCNBD specimen;

2 Three-dimensional boundary-element calibration of the CCNBD specimen;

3 Two-dimensional finite-element calibration of the CSTBD specimen;

4 Two-dimensional boundary-element calibration of the CSTBD specimen;

5 Comparison between FEM, BEM calibration of the Cracked Brazilian Disc specimen;

6 The size requirement study of mode I rock fracture toughness testing using the CCNBD method;

7 Experimental validation of the CCNBD method for rock fracture toughness measurement by comparison with the two ISRM recommended methods, i.e. the CB and SR methods.

# Chapter II

## Numerical Calibration of the Cracked Brazilian Disc Specimen

### 2.1 Introduction

Because of its many advantages over the conventional rock fracture toughness testing methods, the cracked-chevron-notched Brazilian disc method was developed for rock fracture toughness measurement in this research programme. The author proposed that this method could be recommended as the third chevron-notched rock fracture toughness testing method.

Maximum confidence in a rock fracture toughness testing method can only be achieved after careful study and calibration by numerical techniques, experimental validation testing and specimen size requirement investigations.

In this chapter, the three dimensional boundary element method and finite element method are used to calibrated the CCNBD specimen. Also the CSTBD specimen is calibrated by two-dimensional finite element and boundary element methods. The effect of Poisson's ratio, loading contact angle, element mesh number etc. on dimensionless stress intensity factors, dimensionless crack opening displacement compliance and dimensionless loading line displacement compliance are analysed. Short crack approximation for the CCNBD specimen is analysed. A comparison between FEM and BEM for the calibration of the Cracked Brazilian Disc specimen was performed.

### 2.2 The Application of Boundary Element Method on LEFM

#### 2.2.1 Introduction

The boundary element programme used for the solution of crack problems is based on the technique of 'stiching' two linear elastic regions together so that the crack occupies part of the interface between the two regions [Blandford et al,

1981]. At nodes on the interface between region I and II, we require continuity of the displacement u and equilibrium for the traction so that:

$$U_I = U_{II} \quad , \quad t_I = -t_{II} \tag{2.1}$$

Nodes on the crack surface are not 'stiched' and these surfaces may thus move independently. In order to model the known local crack tip behaviour [Williams, 1957], the usual isoparametric quadratic element where displacements U (and tractions t) are given by the expression of the form

$$U = a + b\xi + c\xi^2 \tag{2.2}$$

must be modified. Shifting the middle node to the quarter-point position leads to quarter-point elements [Henshell and Shaw, 1975], and these are shown with crack tip parameters in Figure 2.1.

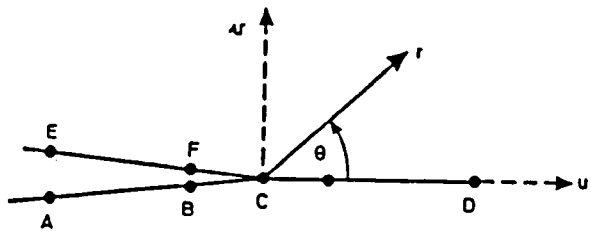


**Figure 2.1 — Crack Tip Parameters**

The displacements (and tractions) are now defined by the equation

$$U = a' + b'\sqrt{r} + c'r \tag{2.3}$$

However, the stress within the material adjacent to the crack tip vary with a leading term of order $r^{-1/2}$ and this may be modelled by multiplying the crack tip element coefficients by $\sqrt{1/r}$ (Cruse and Willison, 1977):

$$t = a' + b'\sqrt{r} + c'r = a''/\sqrt{r} + b'' + c''\sqrt{r} \tag{2.4}$$

This gives a traction-singular element. These modifications to the usual quadratic isoparametric elements ensure the correct behaviour on elements adjacent to the crack tip and give much improved stress intensity factors. Stress intensity factors may be calculated in a number of ways, the simplest using computed displacements adjacent to the crack tip.

A, B and C in Figure 2.1 are the nodes of the discontinuous boundary elements around the crack tip. The displacements at B and F can be directly related to a Williams series expansion to give the formulae for the stress intensity factors calculation.

$$K_I = \frac{2\mu}{k+1}\sqrt{\frac{\pi}{2r}}(V_F - V_B) \tag{2.5}$$

$$K_{II} = \frac{2\mu}{k+1}\sqrt{\frac{\pi}{2r}}(U_F - U_B) \tag{2.6}$$

Where:

$\mu$: $\frac{E}{2(1+\nu)}$;

E: Young's modulus;

$\nu$: Poisson's ratio;

$k$ : $3 - 4\nu$ for plane strain and; $\frac{3-\nu}{1+\nu}$ for plane stress;

r: the distance from the crack tip to the nearest node with zero traction;

U: the x-displacement;

V: the y-displacement;

Using the first two terms in the expansion and equating coefficients of $\sqrt{r}$ leads to a two point formulae. The use of such formulae is considered by Smith and Manson (1983) who showed the one-point form is much less sensitive to element length.

In the modelling of the CCNBD specimen, the $V_B - V_C$ term in Eqn.(2.5) for $K_I$ is replaced by a $2 \times V_B$ because of the symmetry of both loading and geometry.

The stresses near the tip of a traction-free crack for values of r which are much smaller than the crack length are given by (Irwin 1958) as:

$$\sigma_{XX} = \frac{K_I}{\sqrt{2\pi r}} \cos\frac{\theta}{2}(1 - \sin\frac{\theta}{2}\sin\frac{3\theta}{2}) - \frac{K_{II}}{\sqrt{2\pi r}} \sin\frac{\theta}{2}(2 + \cos\frac{\theta}{2}\cos\frac{3\theta}{2}) + O(1) \quad (2.7)$$

$$\sigma_{YY} = \frac{K_I}{\sqrt{2\pi r}} \cos\frac{\theta}{2}(1 + \sin\frac{\theta}{2}\sin\frac{3\theta}{2}) + \frac{K_{II}}{2\pi r} \cos\frac{\theta}{2}\sin\frac{\theta}{2}\cos\frac{3\theta}{2} + O(1) \quad (2.8)$$

$$\sigma_{XY} = \frac{K_I}{\sqrt{2\pi r}} \sin\frac{\theta}{2}\cos\frac{\theta}{2}\cos\frac{3\theta}{2} + \frac{K_{II}}{\sqrt{2\pi r}} \cos\frac{\theta}{2}(1 - \sin\frac{\theta}{2}\sin\frac{3\theta}{2}) + O(1) \quad (2.9)$$

If we restrict ourselves to problems with no crack sliding and for which the only stresses required are along the line of crack the relevant equations are:

$$K_I = \frac{2\mu}{K+1}\sqrt{\frac{\pi}{2r}}(V_B - V_C) \quad (2.10)$$

$$\sigma_{YY} = \frac{K_I}{\sqrt{2\pi r}} \quad (2.11)$$

### 2.2.2 Continuous Element and Discontinuous Element

If the nodes are placed at the extremeties of the elements, and if adjacent elements are such that one or more of their nodal positions are the same, then the values of the problem variables will be continuous over the surface of the object. Such elements will be henceforth known as 'Continuous'. Continuous elements can not be used in completely general fashion at all positions on the surface of an object, and these drawbacks with others led to the development of discontinuous elements. Here the nodes are placed not at the extremetries of the elements but at other positions of the elements. The geometry is modelled by the mesh points so that boundary is still continuous. Using this type of element each nodal position of each element has associated with a set of problem unknowns.

Because no nodes are common to more than one element, the values of problem variables may be discontinuous at element edges. This is a positive advantage because traction is frequently discontnuous, as in the case of a load on Brazilian disc surface for example. This discontinuity also allows stress concentrations to be modelled very accurately. This is very important in the modelling of fracture mechanics problems.

The stress intensity factors calculations in this research programme were carried out using the BEASY programme. The BEASY programme uses discontinuous elements to model the stress concentration at the crack tip.

## 2.3 Two-dimensional BEM Calibration of the CSTBD Specimen

### 2.3.1 Element Mesh Idealization

The problem analysed here is a CSTBD (Cracked Straight-Through Brazilian Disc) specimen which is subjected to a diametral loading along the slot direction, and in which a crack has been allowed to develop.

Because of the symmetry along $X = 0$ plane, only half of the disc is considered for modelling. It is shown in Figure 2.2.

The disc can be analysed using three possible types of boundary element mesh:

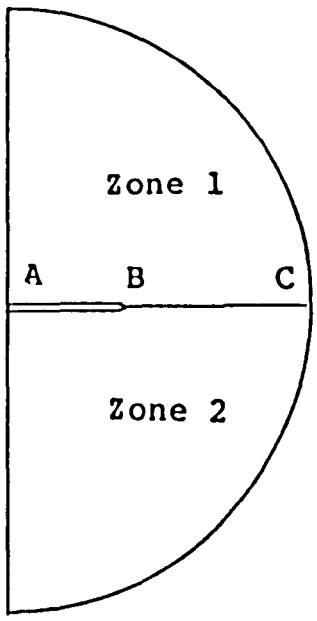


(a) Two Zone Mesh with Discontinuity for Crack

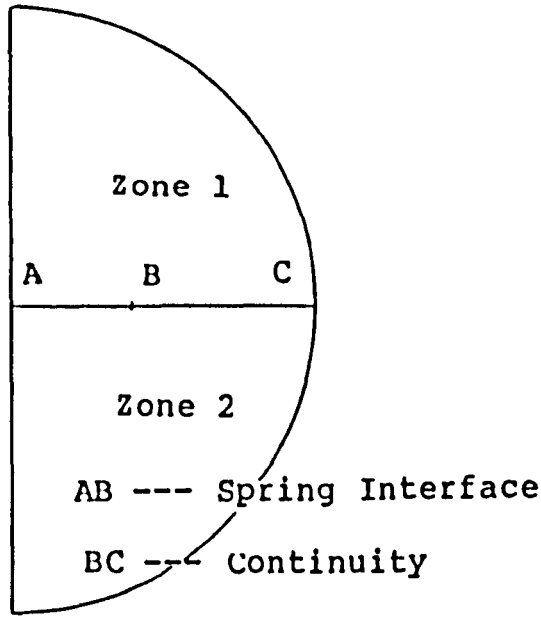


(b) Two Zone Mesh with Spring Interface for Crack

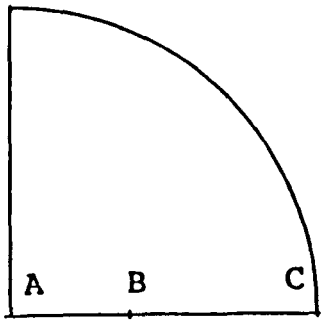


(c) Single Zone Mesh with Zero Displacemnt for BC in Y-Direction

Figure 2.2 — Three Possible Types of Boundary Element Mesh

1 The whole disc can be modelled as a two zone problem, the line AB being represented by two sets of boundary elements which are given zero traction (free surface) boundary conditions. It is shown in Figure 2.2(a);

2 The whole plate, i.e. disc, can be modelled as a two zone problem, the line AC being represented by a single set of interface elements. Over the portion BC of the interface, the (default) continuity condition is applied. Over the portion AB of the interface an internal spring of very low stiffness may be used to model the crack behaviour. This is shown in Figure 2.2(b);

3 The third method is: only the top half of the disc is modelled, and symmetry is enforced by having line BC zero displacement in y direction. Therefore the crack is modelled by a free surface, boundary elements must be used to model the line AB. This is the simplest compared with the former two methods. Therefore this method is used in this research throughout. It is shown in Figure 2.2(c).

In modelling the crack tip behavior with high stress concentration, the elements near the crack tip must be very small. In BEASY, this can be done by using element grading facility in BEASYG. Figure 2.3(a) shows the element mesh idealization with larger elements for the far crack tip domain than crack tip domains, using patch BL and BC to model the 2D geometry of the CSTBD specimen.

Elements should be graded such that large elements do not appear close to small elements. Poor grading can cause numerical problems to arise, resulting in a possible loss of accuracy. In BEASY, a data check can be carried out before the full analysis is attempted, in order to ensure that computer time is not wasted.

### 2.3.2 Boundary Conditions and Interface Information

As shown in Figure 2.3(a), the symmetry boundary condition were applied on the $X = 0$ plane. On the $y = 0$ plane, all nodes were free except those that lie in the shaded region. The symmetry interface condition for $y = 0$ plane. In this plane, the displacements in x direction for the shaded area is zero. The load is appled along the slot direction.

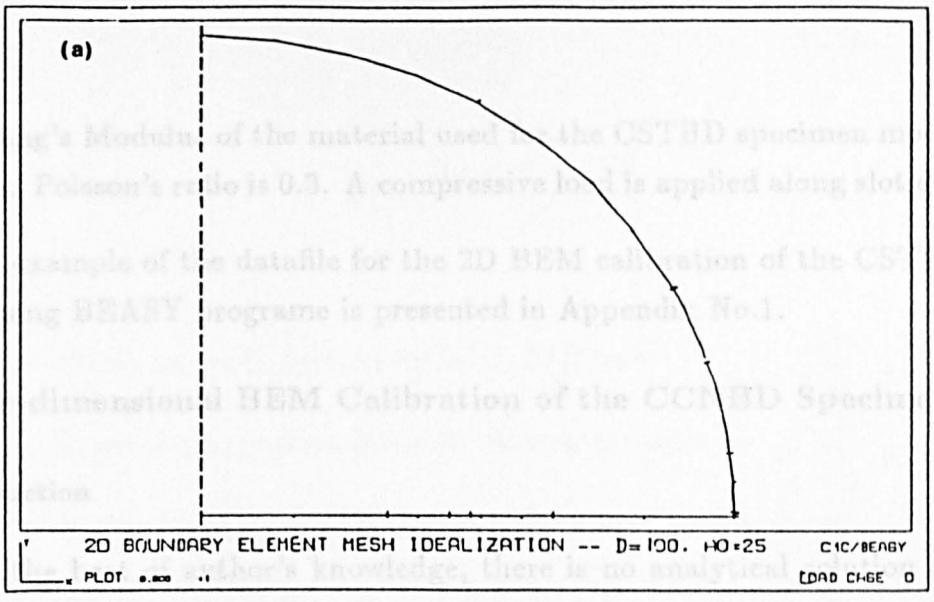


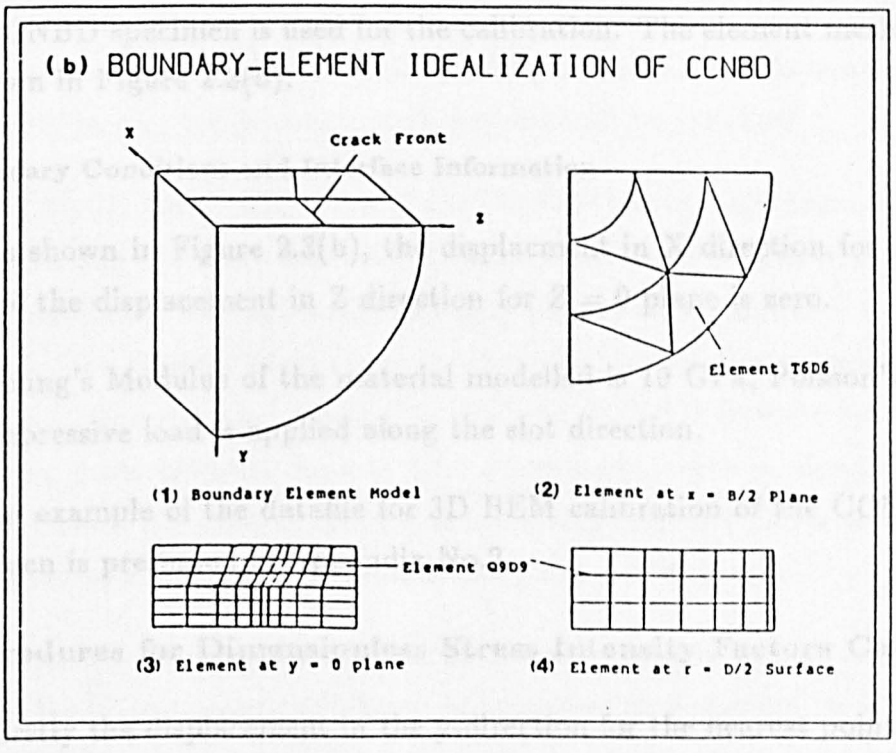


**Figure 2.3 — Boundary Element Mesh Idealization for the Cracked Brazilian Disc**

Young's Modulus of the material used for the CSTBD specimen modelling is 10 GPa. Poisson's ratio is 0.3. A compressive load is applied along slot direction.

An example of the datafile for the 2D BEM calibration of the CSTBD specimen using BEASY programe is presented in Appendix No.1.

## 2.4 Three-dimensional BEM Calibration of the CCNBD Specimen

### 2.4.1 Introduction

To the best of author's knowledge, there is no analytical solution available for the CCNBD specimen. No numerical calibration has been found so far for the calibration of the CCNBD specimen.

### 2.4.2 Element Mesh Idealization

Because of the symmetry of both loading and geometry, only one eighth of the CCNBD specimen is used for the calibration. The element mesh idealization is shown in Figure 2.3(b).

### 2.4.3 Boundary Conditions and Interface Information

As shown in Figure 2.3(b), the displacment in X direction for $X = 0$ plane is zero, the displacement in Z direction for $Z = 0$ plane is zero.

Young's Modulus of the material modelled is 10 GPa, Poisson's ratio is 0.3. A compressive load is applied along the slot direction.

An example of the datafile for 3D BEM calibration of the CCNBD fracture specimen is presented in Appendix No.2.

## 2.5 Procedures for Dimensionless Stress Intensity Factors Calculation

Firstly the displacement in the y-direction for the nearest point to the crack tip is obtained directly from BEM calculation by BEASY program; then the stress intensity factors for dimensionless crack length $a/R$ can be computed using eqn.(2.5). Dimensionless stress intensity factors could be calculated by the following formulae.

$$F_1 = \frac{K_I \times B \times D^{0.5}}{P} \tag{2.12}$$

Where:

$K_I$ – Stress intensity factors for $a/R$, $MN/m^{1.5}$;

$F_I$ – Dimensionless stress intensity factors for $a/R$;

B – The thickness of the cracked Brazilian disc specimen, m;

D – The diameter of the cracked Brazilian disc specimen, m;

P – The load applied on the specimen.

For the two dimensional BEM calibration of the CSTBD specimen, stress intensity factors is calculated using eqn.(2.5). Then dimensionless stress intensity factor is calculated using eqn.(2.12). The boundary element mesh is generated for another crack length, the same procedure is repeated. So dimensionless stress intensity factors for different crack lengths can be obtained.

In the 3D BEM calibration of the CCNBD fracture specimen, stress intensity factors along the crack front for dimensionless crack length $a/R$ are calculated using eqn.(2.5). Average stress intensity factors along the crack front can be obtained, then dimensionless stress intensity factors for dimensionless crack length is calculated using the eqn.(2.12). For one CCNBD fracture specimen, dimensionless stress intensity factors were computed pointwise along each of 5 to 7 crack fronts. The critical dimensionless stress intensity factor is the minimum dimensionless stress intensity factors along the slot direction.

A datafile for dimensionless stress intensity factors and critical dimensionless stress intensity factors calculation is presented in Appendix No.3.

## 2.6 Comparison of Stresses Results Obtained from BEM or the SIFs

If we take the stress intensity factor $K_I$, then the indirectly derived stress can be obtained from the following formulae:

$$\sigma_{yy} = \frac{K_I}{\sqrt{2\pi r}} \tag{2.13}$$

Where:

$\sigma_{yy}$: the stress in y direction;

r – the distance between the crack tip and the nearest points to the crack tip.

A comparison between the stress results calculated using eqn.(2.13) or directly from the BEASY calculation results is performed, it is shown in Figure 2.4.

As seen in Figure 2.4(a), it shows that the element mesh used is fine enough to obtain satisfactory stress and stress intensity factors results.

## 2.7 Variation of F along the Crack Front

The distribution of the dimensionless stress intensity factors along the crack front is shown in Figure 2.5. It showed nearly constant dimensionless stress intensity factors for $2x/b \leq 0.5$. The dimensionless stress intensity factors increased rapidly as $2x/b$ approached unity. Ingraffea and Newman et al. have reported the same conclusions for the normalized stress intensity factors distribution alone the crack front for the chevron-notched short rod specimen.

## 2.8 Effect of Element Mesh Refinement

In order to study the effect of the element mesh on the calibration results of cracked Brazilian disc specimen, the element mesh varies from coarse to fine, the element number varies from 42 to 301 in the 2D BEM calibration of the CSTBD specimen, the element number varies from 64 to 168 in the 3D BEM calibration of the CCNBD specimen. The dimensionless stress intensity factors vs the number of mesh elements used in the 2D BEM calibration of the CSTBD specimen or the 3D BEM calibration of the CCNBD specimen are shown in Figure 2.6(a) and Figure 2.6(b).

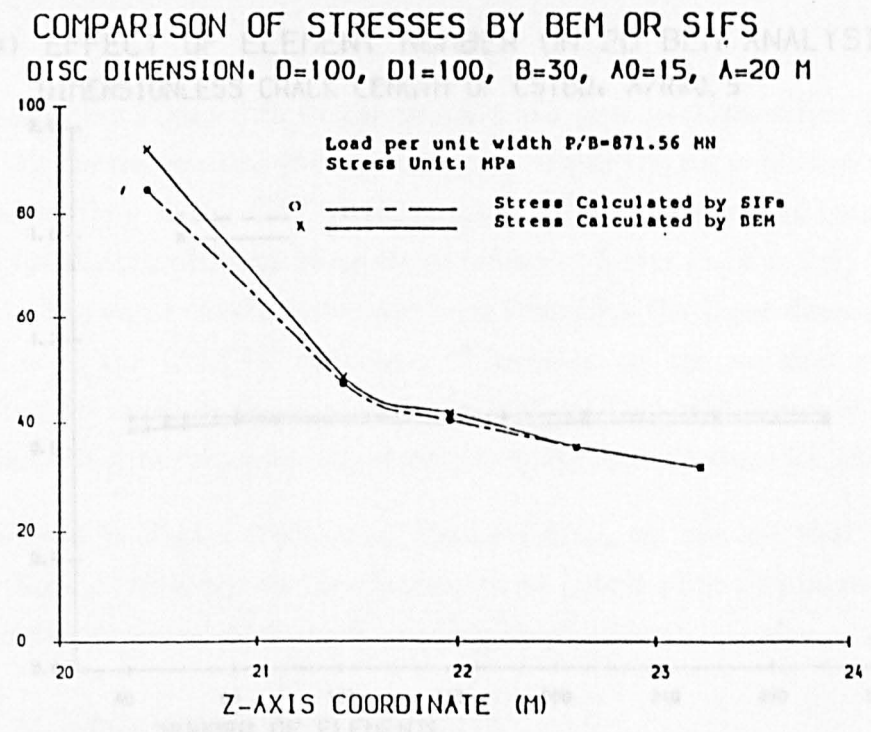


**Figure 2.4 — Comparison of Stress Calculation Results by BEM and SIFs**

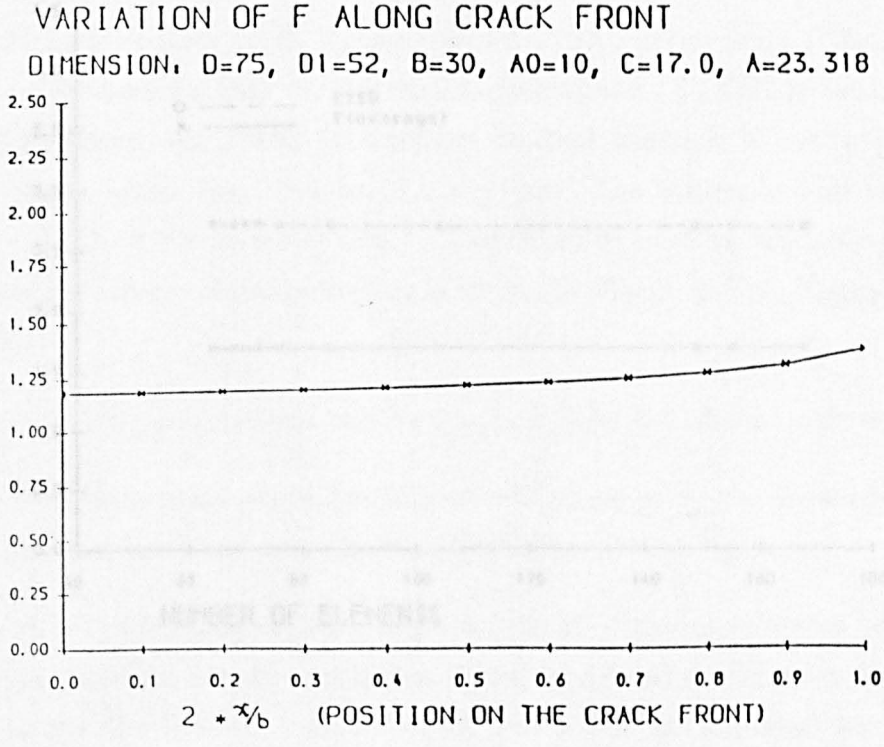


**Figure 2.5 — Variation of $F_1$ along the Crack Front**

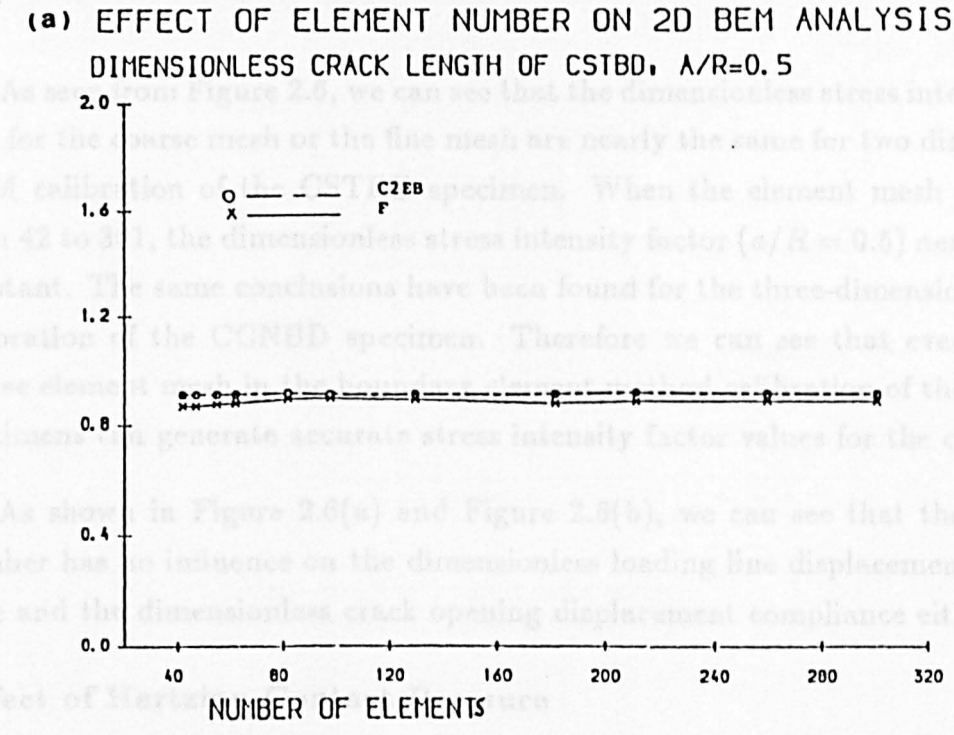


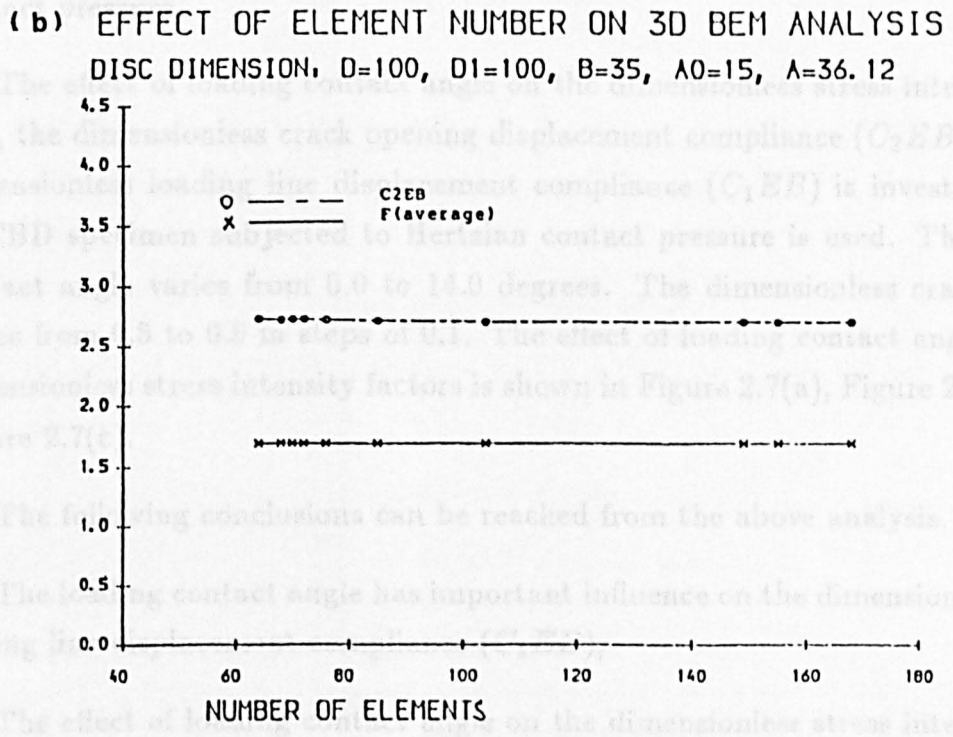


**Figure 2.6 — Effect of Mesh Idealization on the BEM Calibration Results**

As seen from Figure 2.6, we can see that the dimensionless stress intensity factors for the coarse mesh or the fine mesh are nearly the same for two dimensional BEM calibration of the CSTBD specimen. When the element mesh is refined from 42 to 301, the dimensionless stress intensity factor ($a/R = 0.5$) nearly keeps constant. The same conclusions have been found for the three-dimensional BEM calibration of the CCNBD specimen. Therefore we can see that even relative coarse element mesh in the boundary element method calibration of the fracture specimens can generate accurate stress intensity factor values for the crack tip.

As shown in Figure 2.6(a) and Figure 2.6(b), we can see that the element number has no influence on the dimensionless loading line displacement compliance and the dimensionless crack opening displacement compliance either.

## 2.9 Effect of Hertzian Contact Pressure

When the disc is loaded by circular anvils, the disc is subjected a Hertzian contact pressure.

The effect of loading contact angle on the dimensionless stress intensity factors, the dimensionless crack opening displacement compliance ($C_2EB$) and the dimensionless loading line displacement compliance ($C_1EB$) is investgated. A CSTBD specimen subjected to Hertzian contact pressure is used. The loading contact angle varies from 0.0 to 14.0 degrees. The dimensionless crack length varies from 0.5 to 0.9 in steps of 0.1. The effect of loading contact angle on the dimensionless stress intensity factors is shown in Figure 2.7(a), Figure 2.7(b) and Figure 2.7(c).

The following conclusions can be reached from the above analysis.

1 The loading contact angle has important influence on the dimensionless loading line displacement compliance ($C_1EB$);

2 The effect of loading contact angle on the dimensionless stress intensity factors depends on its dimensionless crack length $a/R$. The smaller the $a/R$, the larger the loading contact angle which has no influence on the dimensionless stress intensity factors. For example, when $a/R = 0.5$, the loading contact angle which has no influence on the dimensionless stress intensity

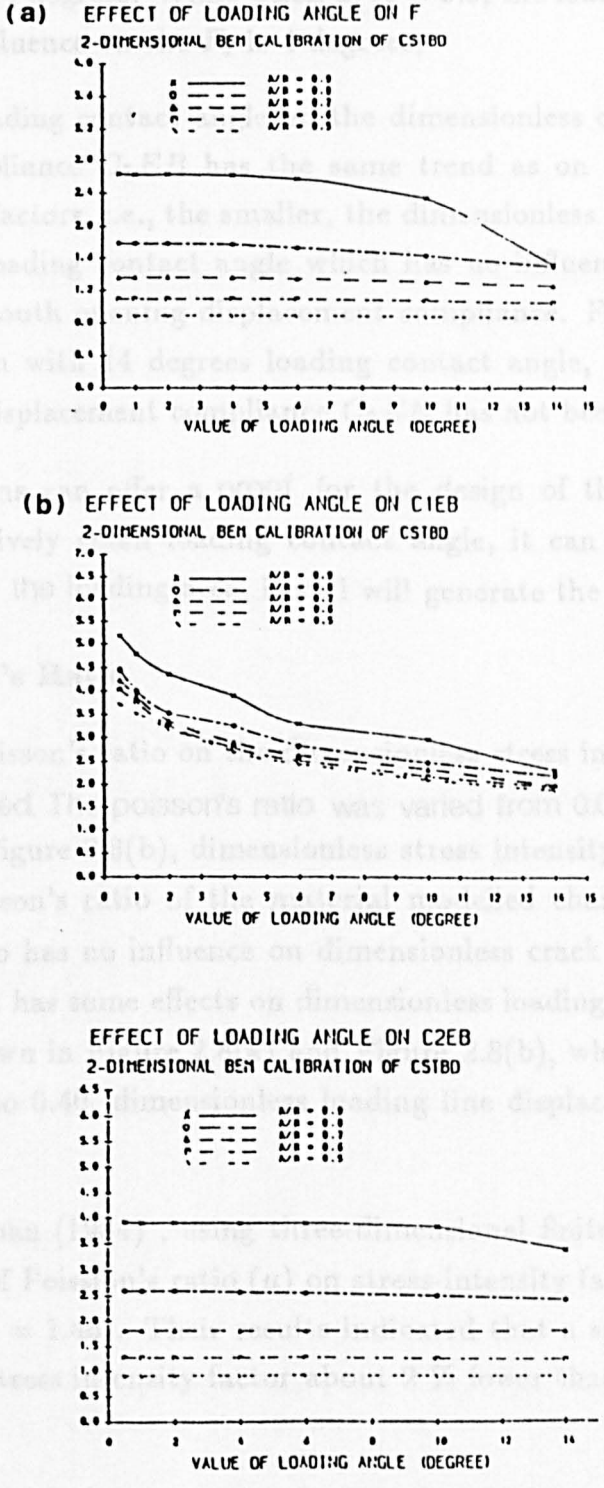


**Figure 2.7 — Effect of Loading Contact Angle on the BEM Calibration Results**

factors value is 14 degrees. While when $a/R = 0.9$, the loading contact angle which has no influence on the $F_1$ is 4 degrees;

3 The effect of loading contact angle on the dimensionless crack opening displacement compliance $C_2EB$ has the same trend as on the dimensionless stress intensity factors, i.e., the smaller, the dimensionless crack length $a/R$, the larger the loading contact angle which has no influence on the dimensionless crack mouth opening displacement compliance. For example, when $a/R = 0.5$, even with 14 degrees loading contact angle, the dimensionless crack opening displacement compliance $C_2EB$ has not been changed.

4 These conclusions can offer a proof for the design of the curved loading rig. With relatively small loading contact angle, it can avoid high stress concentration in the loading area, it still will generate the same test results.

## 2.10 Effect of Poisson's Ratio

The effect of Poisson's ratio on the dimensionless stress intensity factors results was investigated. The poisson's ratio was varied from 0.0 to 0.4. As shown in Figure 2.8(a) and Figure 2.8(b), dimensionless stress intensity factors increases 5 % when the Poisson's ratio of the material modelled changes from 0.17 to 0.40. Poisson's ratio has no influence on dimensionless crack opening displacement compliance. It has some effects on dimensionless loading line displacement compliance. As shown in Figure 2.8(a) and Figure 2.8(b), when Poisson's ratio changes from 0.00 to 0.40, dimensionless loading line displacement compliance increases about 4%.

Raju and Newman (1984) , using three-dimensional finite-element method, studied the effects of Poission's ratio ($\mu$) on stress-intensity factors for the short rod specimen ($w/B = 1.45$). Their results indicated that a specimen with $\mu = 0.17$ would have a stress intensity factor about 2 % lower than a specimen with $\mu = 0.3$.

## 2.11 Presentation of the 2D BEM Calibration Results of the CSTBD

The results for the calibration of the CSTBD specimen using 2D BEM is presented in Appendix No.4.

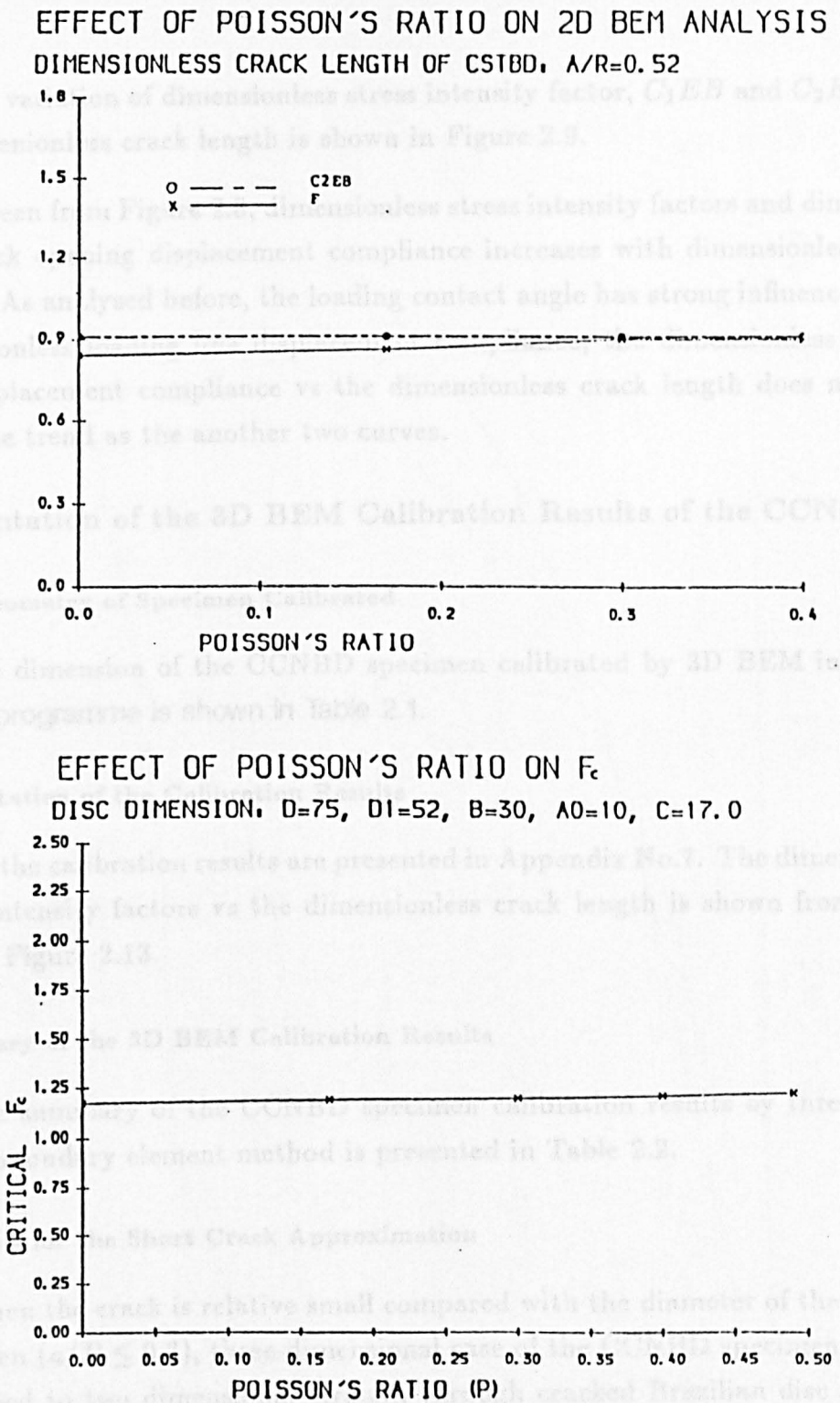


**Figure 2.8 — Effect of Poisson's Ratio on the BEM Calibration Results**

The variation of dimensionless stress intensity factor, $C_1EB$ and $C_2EB$ with the dimenionless crack length is shown in Figure 2.9.

As seen from Figure 2.8, dimensionless stress intensity factors and dimensionless crack opening displacement compliance increases with dimensionless crack length. As analysed before, the loading contact angle has strong influence on the dimensionless loading line displacement compliance, the dimensionless loading line displacement compliance vs the dimensionless crack length does not obey the same trend as the another two curves.

## 2.12 Presentation of the 3D BEM Calibration Results of the CCNBD

### 2.12.1 The Geometry of Specimen Calibrated

The dimension of the CCNBD specimen calibrated by 3D BEM in this research programme is shown in Table 2.1.

### 2.12.2 Presentation of the Calibration Results

All the calibration results are presented in Appendix No.7. The dimensionless stress intensity factors vs the dimensionless crack length is shown from Figure 2.10 to Figure 2.13.

### 2.12.3 Summary of the 3D BEM Calibration Results

The summary of the CCNBD specimen calibration results by three dimensional boundary element method is presented in Table 2.2.

### 2.12.4 Analysis for the Short Crack Approximation

When the crack is relative small compared with the diameter of the CCNBD specimen ($a/R \leq 0.3$), three-dimensional case of the CCNBD specimen could be simplified to two dimensional straight through cracked Brazilian disc specimen without lost its accuracy.

Shetty D. K. (1985) has employed the straight-through-crack assumption for the chevron-notched specimen. He obtained the following equations for the chevron notched diametral compression specimen when the $a_1/R$ is quite small.

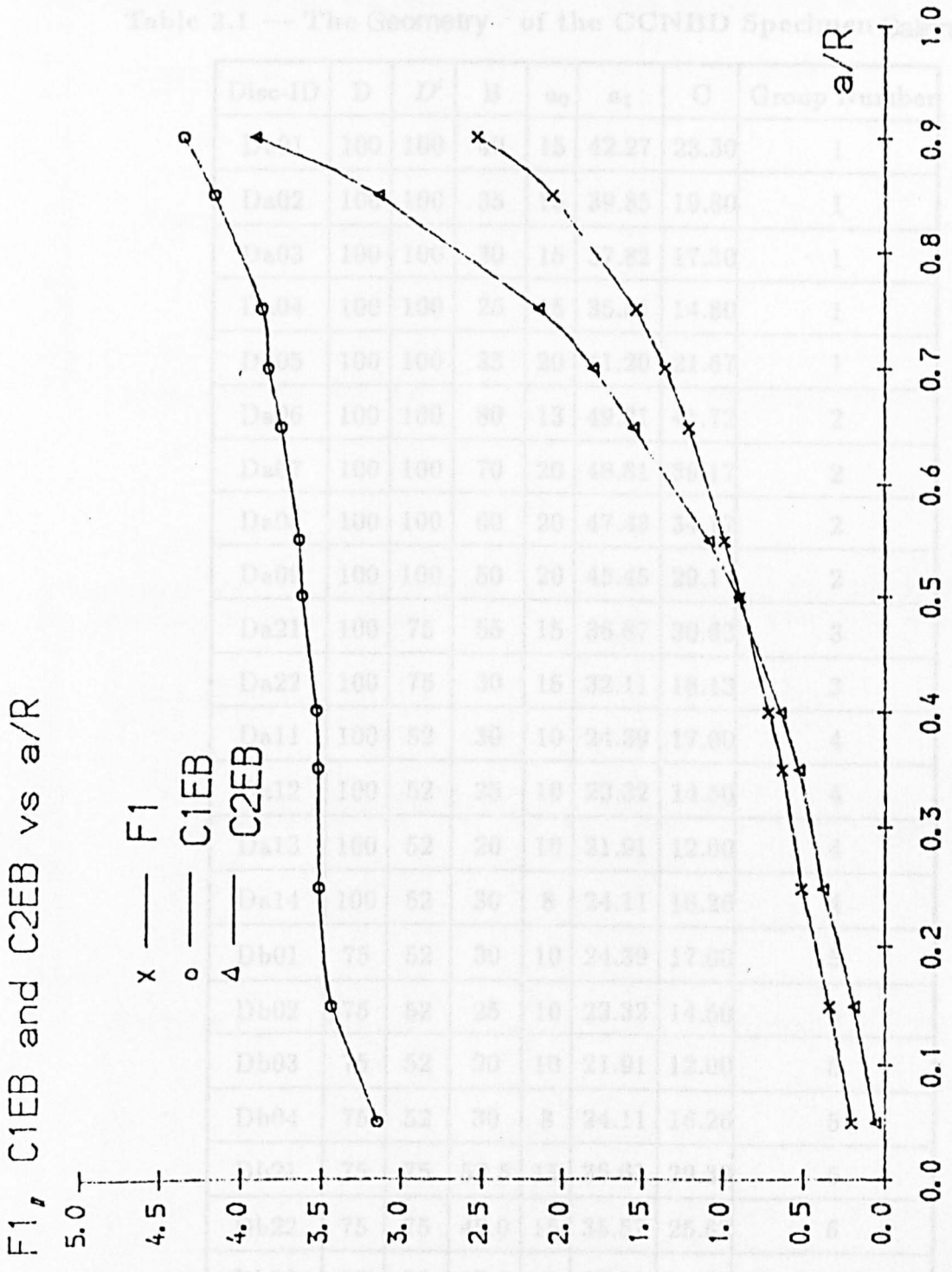


**Figure 2.9 — Two-dimensional BEM Calibration Results for the CSTBD**

Table 2.1 — The Geometry of the CCNBD Specimen Calibration

| Disc-ID | D | $D'$ | B | $a_0$ | $a_1$ | C | Group Number |
|---|---|---|---|---|---|---|---|
| Da01 | 100 | 100 | 40 | 15 | 42.27 | 23.30 | 1 |
| Da02 | 100 | 100 | 35 | 15 | 39.85 | 19.80 | 1 |
| Da03 | 100 | 100 | 30 | 15 | 37.82 | 17.30 | 1 |
| Da04 | 100 | 100 | 25 | 15 | 35.51 | 14.80 | 1 |
| Da05 | 100 | 100 | 35 | 20 | 41.20 | 21.67 | 1 |
| Da06 | 100 | 100 | 80 | 13 | 49.31 | 41.72 | 2 |
| Da07 | 100 | 100 | 70 | 20 | 48.81 | 39.17 | 2 |
| Da08 | 100 | 100 | 60 | 20 | 47.43 | 34.17 | 2 |
| Da09 | 100 | 100 | 50 | 20 | 45.45 | 29.17 | 2 |
| Da21 | 100 | 75 | 55 | 15 | 36.87 | 30.63 | 3 |
| Da22 | 100 | 75 | 30 | 15 | 32.11 | 18.13 | 3 |
| Da11 | 100 | 52 | 30 | 10 | 24.39 | 17.00 | 4 |
| Da12 | 100 | 52 | 25 | 10 | 23.32 | 14.50 | 4 |
| Da13 | 100 | 52 | 20 | 10 | 21.91 | 12.00 | 4 |
| Da14 | 100 | 52 | 30 | 8 | 24.11 | 16.26 | 4 |
| Db01 | 75 | 52 | 30 | 10 | 24.39 | 17.00 | 5 |
| Db02 | 75 | 52 | 25 | 10 | 23.32 | 14.50 | 5 |
| Db03 | 75 | 52 | 20 | 10 | 21.91 | 12.00 | 5 |
| Db04 | 75 | 52 | 30 | 8 | 24.11 | 16.26 | 5 |
| Db21 | 75 | 75 | 52.5 | 15 | 36.61 | 29.38 | 6 |
| Db22 | 75 | 75 | 45.0 | 15 | 35.57 | 25.63 | 6 |
| Db23 | 75 | 75 | 37.5 | 15 | 34.09 | 21.88 | 6 |
| Dc01 | 50 | 52 | 20 | 10 | 21.91 | 12.00 | 7 |
| Dc02 | 50 | 52 | 15 | 10 | 20.09 | 9.50 | 7 |

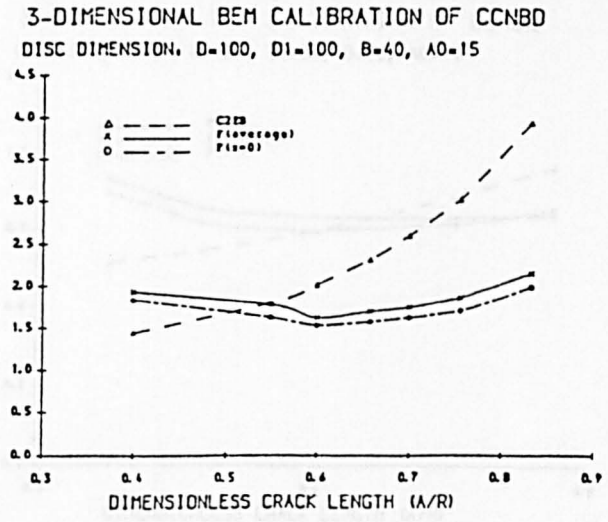


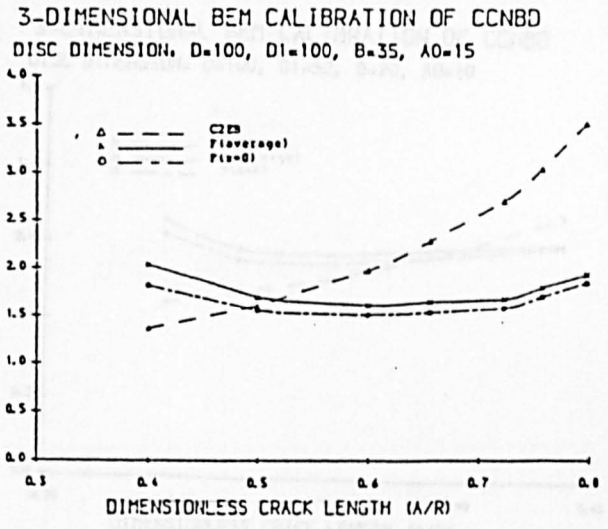


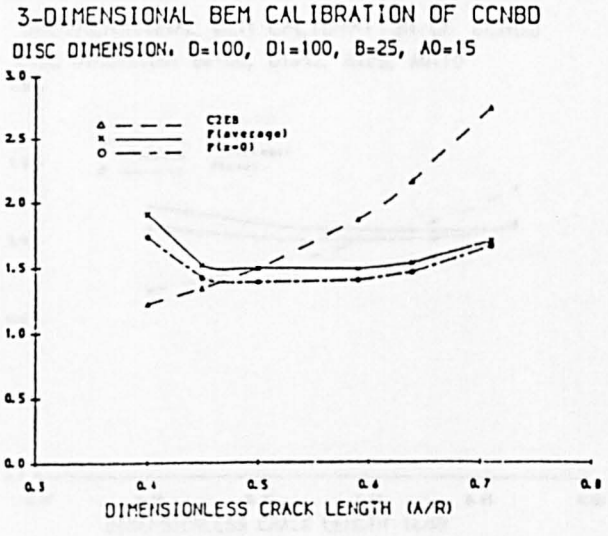


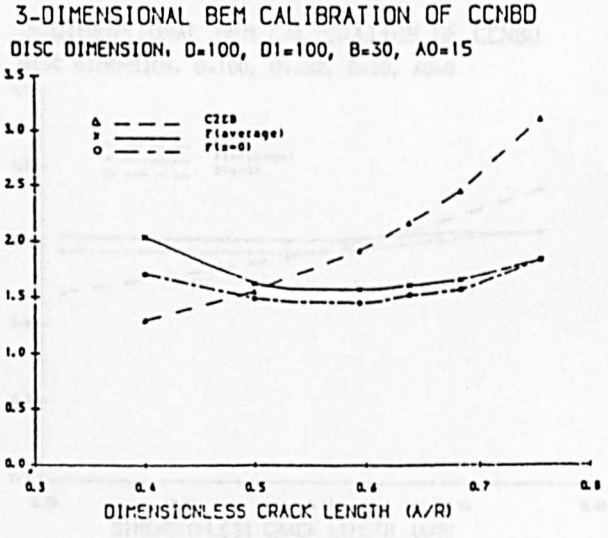


**Figure 2.10 — 3D BEM Calibration Results for Da01, Da02, Da03 and Da04**

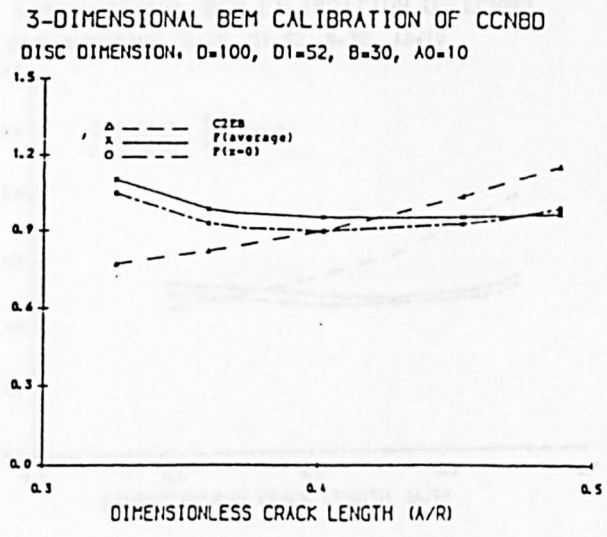


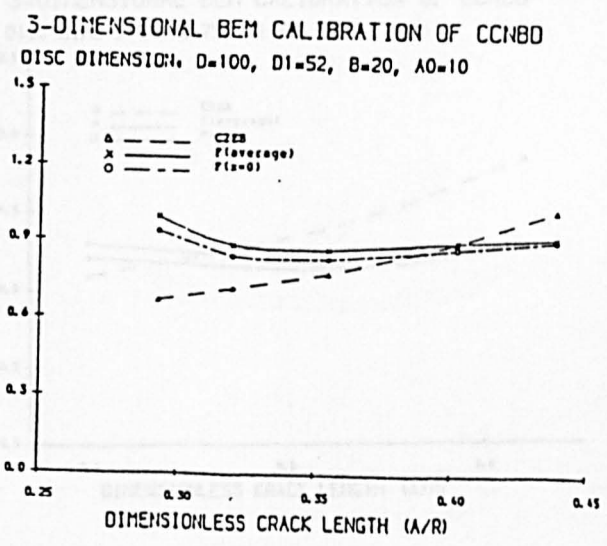


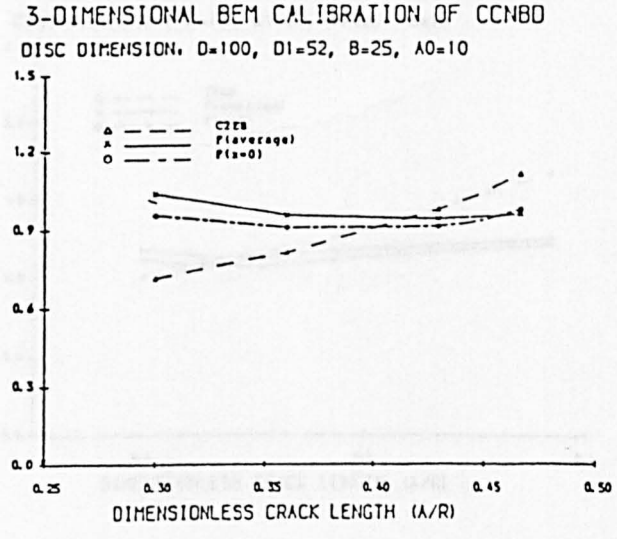


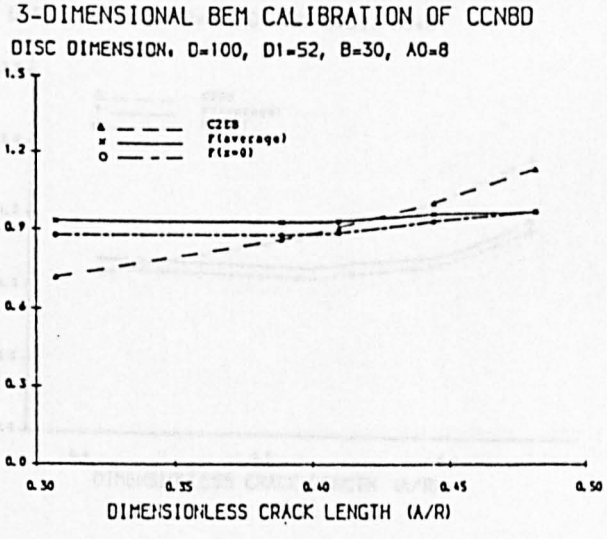


**Figure 2.11 — 3D BEM Calibration Results for Da11, Da12, Da13 and Da14**

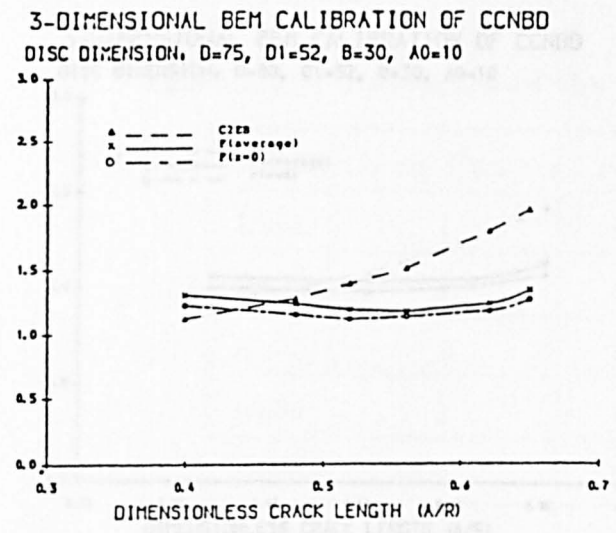


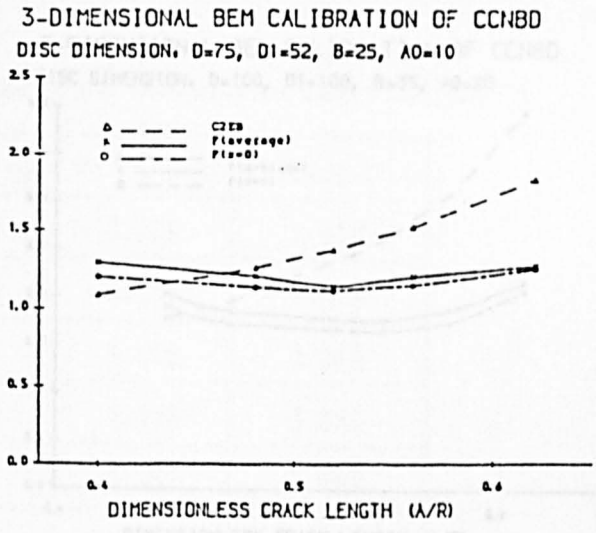


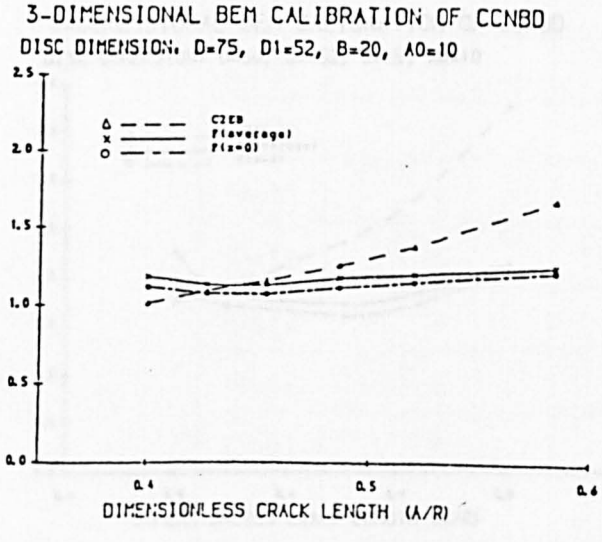


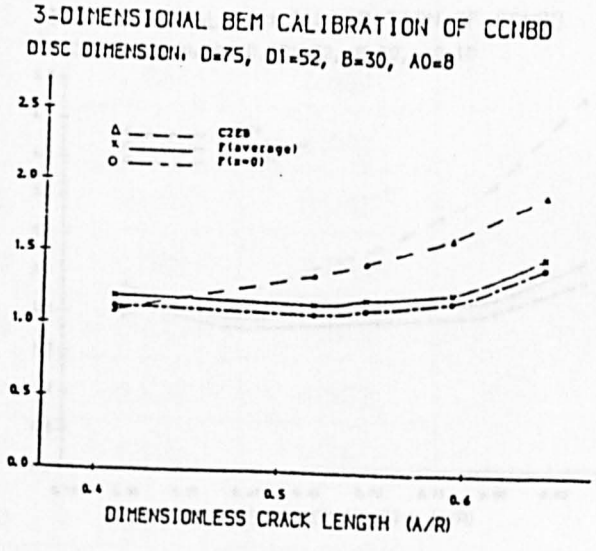


**Figure 2.12 — 3D BEM Calibration Results for Db01, Db02, Db03 and Db04**

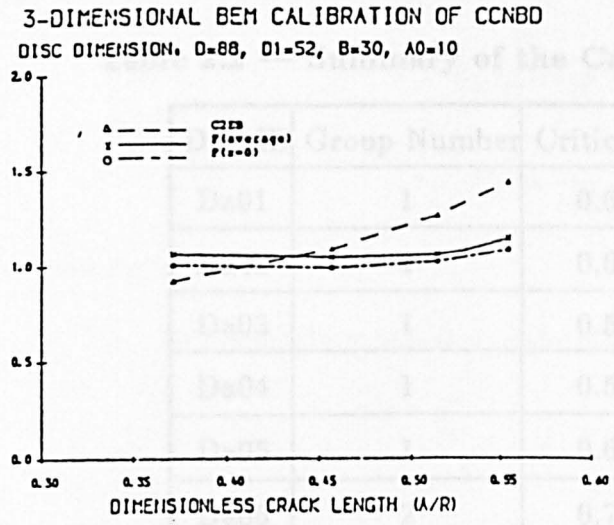


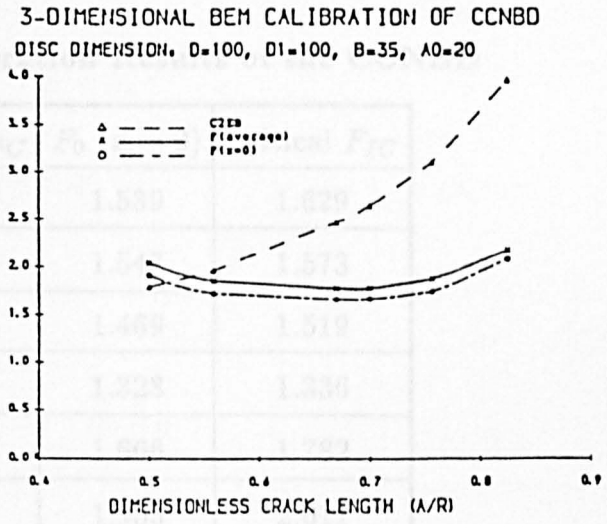


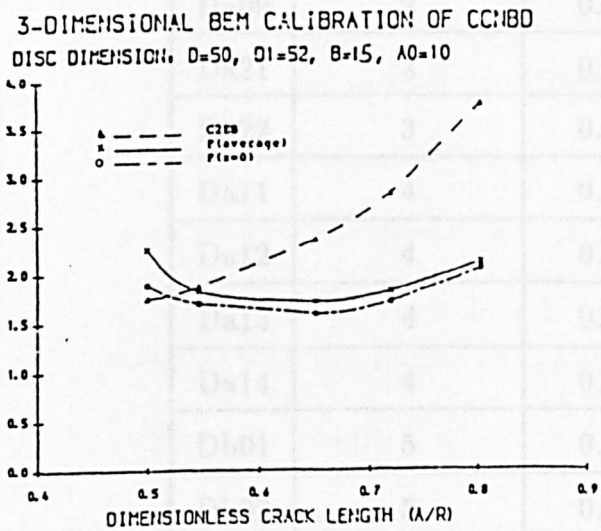


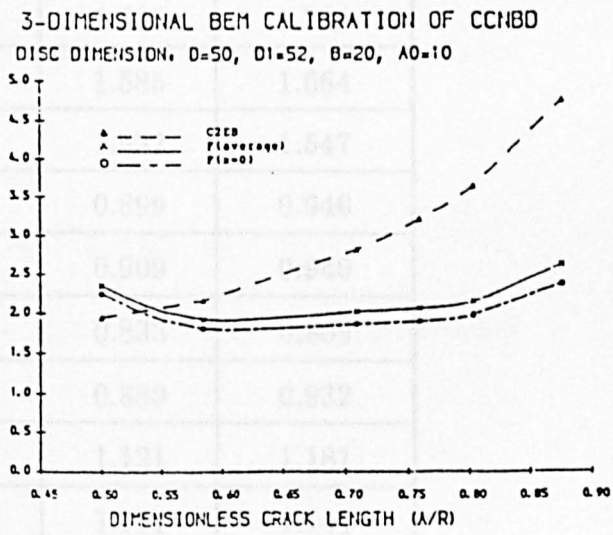


**Figure 2.13 — 3D BEM Calibration Results for Da05, Dc01, Dc02 and Db11**

**Table 2.2 — Summary of the Calibration Results of the CCNBD**

| Disc-ID | Group Number | Critical $a_C$ | $F_0$ $(x = 0)$ | Critical $F_{IC}$ |
|---|---|---|---|---|
| Da01 | 1 | 0.657 | 1.539 | 1.629 |
| Da02 | 1 | 0.600 | 1.547 | 1.573 |
| Da03 | 1 | 0.595 | 1.469 | 1.519 |
| Da04 | 1 | 0.590 | 1.328 | 1.336 |
| Da05 | 1 | 0.671 | 1.666 | 1.782 |
| Da06 | 2 | 0.728 | 1.955 | 2.011 |
| Da07 | 2 | 0.734 | 2.067 | 2.156 |
| Da08 | 2 | 0.687 | 1.735 | 1.823 |
| Da09 | 2 | 0.634 | 1.663 | 1.734 |
| Da21 | 3 | 0.545 | 1.585 | 1.664 |
| Da22 | 3 | 0.521 | 1.532 | 1.547 |
| Da11 | 4 | 0.402 | 0.899 | 0.946 |
| Da12 | 4 | 0.360 | 0.909 | 0.940 |
| Da13 | 4 | 0.355 | 0.833 | 0.869 |
| Da14 | 4 | 0.389 | 0.889 | 0.932 |
| Db01 | 5 | 0.520 | 1.121 | 1.181 |
| Db02 | 5 | 0.520 | 1.111 | 1.141 |
| Db03 | 5 | 0.453 | 1.074 | 1.134 |
| Db04 | 5 | 0.519 | 1.092 | 1.156 |
| Db21 | 6 | 0.734 | 2.067 | 2.156 |
| Db22 | 6 | 0.687 | 1.735 | 1.823 |
| Db23 | 6 | 0.634 | 1.663 | 1.733 |
| Dc01 | 7 | 0.585 | 1.814 | 1.926 |
| Dc02 | 7 | 0.546 | 1.592 | 1.716 |

$$K_I = \frac{P}{(\pi R)^{1/2} B} N_I(\alpha)(\frac{\alpha_1 - \alpha_0}{\alpha - \alpha_0})^{1/2} \tag{2.14}$$

or

$$K_I = \frac{P}{(\pi R)^{1/2} B} \times Y \tag{2.15}$$

Where:

Y – Dimensionless parameter defined by

$$Y = \alpha^{1/2} N_I(\alpha)(\frac{\alpha_1 - \alpha_0}{\alpha - \alpha_0})^{1/2} \tag{2.16}$$

R – The radius of the disc;

P – The load applied on the disc;

$N_I$ – Dimensionless stress intensity factor for the CSTBD specimen analysed by Atkinson and co-workers (1980);

$\alpha$ – Dimensionless crack length ($\alpha = a/R$);

$\alpha_0$ – Initial dimensionless crack length ($\alpha_0 = a_0/R$);

$\alpha_1$ – Dimenionless crack length for the points where the chevron-notches intersects with the surface of the disc;

a – The crack length;

B – The thickness of disc.

As analysed by Atkinson and co-workers, for a central through-crack of length 2a in the CSTBD specimen the stress intensity factor can be writen as

$$K_I = \frac{P}{\pi R B} (\pi a)^{0.5} N_I \tag{2.17}$$

Shetty D. K. et al. ploted the equation (2.14) and equation (2.17), the plots is shown in Figure 2.14(a). The chevron-notch geometry used: $\alpha_0 = 0.25$, $\alpha_I = 0.4$, $R = 16mm$, $B = 2.5mm$ and the radius of the curves ($R_I$) is 11

mm. He used a short crack chevron notched disc specimen to measure Ceramic fracture toughness.

The 3D numerical calibration for the short crack length specimen such as Dal1, Dal2, Dal3 and Dal4 proves this assumption is reasonably accurate. In these specimens, the stress intensity factor at the points which the chevron notches intersect with the surfaces of the disc specimen reach its minimum value or close to it. As shown in Figure 2.14(b), the dashed curve shows the dimensionless stress intensity factors for the CSTBD specimen as a function of $a/R$. This curve is a monotonically increasing function with crack length. The solid curve shows the solution for the CCNBD specimen. For $a = a_0$, the stress-intensity factor is very large, but it rapidly drops as the crack length increases. There is little change for the dimensionless stress intensity factors until $a_1$. The minimum dimensionless stress intensity factors is approximately equal to the dimensionless stress intensity factors value for $a_1$. Therefore, it is quite reasonable to assume the short chevron crack as the straight-through crack.

For the long crack case, as shown in Figure 2.14(c), the chevron-notched specimen can not be assumed to a straight-through specimen for the calculation of stress intensity factors. The dimensionless stress intensity factor will reach its minimum value before the points which the chevron-notch intersects with the surface of the CCNBD specimen. The dashed curve shows the dimensionless stress-intensity factors for the CSTBD (cracked straight-through Brazilian disc) specimen as a function of $a/R$. This curve is a monotonically increasing function with the dimensionless crack length. The solid curve shows that the solution for the CCNBD specimen. For $a = a_0$, the stress intensity factor is very large, but it rapidly drops as the dimensionless crack length increases. A minimum value is reached when the crack length is between $a_0/R$ and $a_1/R$. For $a/R \geq a_1/R$, the stress-intensity factors for the chevron-notched specimen and for the straight-through crack specimen are identical because the configurations are identical.

Because of the large grain size of rock and the relative large size of the diamond saw used for rock specimen preparation, only relative long crack Brazilian discs could be prepared. Even Disc DA11 and Dal2 which were prepared using the smallest diamond saw available for rock machining can not be treated as (two

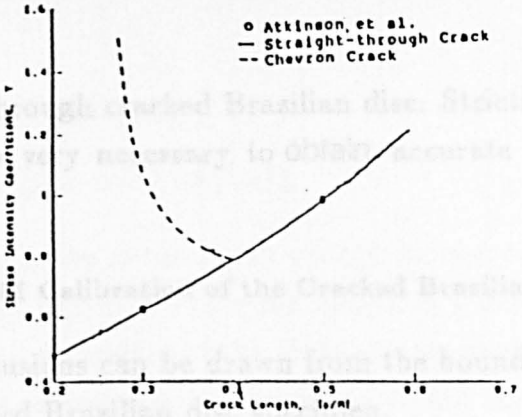


Stress Intensity Coefficients for Straight-through and Chevron Cracks in Diametral-compression Specimens (from Shetty, 1985) (Note: for small crack case, Chen)

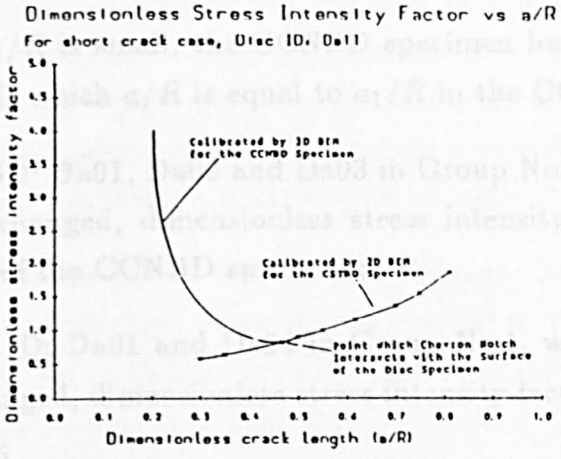


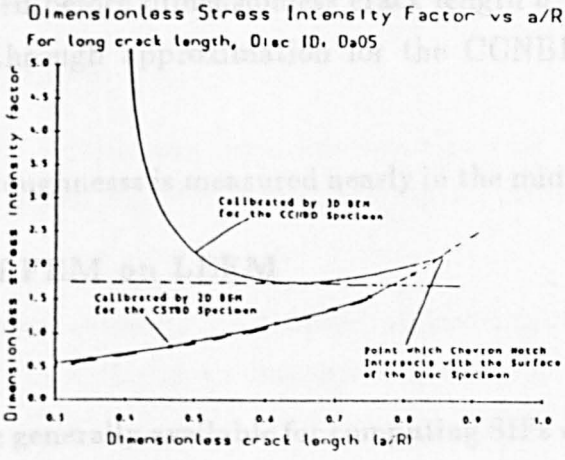


**Figure 2.14 — Dimensionless SIFs vs $a/R$ in Different Case**

dimensional) straight through cracked Brazilian disc. Strictly three dimensional numerical calibration is very necessary to obtain accurate dimensionless stress intensity factors.

### 2.12.5 Conclusions for the BEM Calibration of the Cracked Brazilian Disc

The following conclusions can be drawn from the boundary element method calibration of the cracked Brazilian disc specimen.

1 When the $a/R$ is small, after the peak value of the crack tip, the stress intensity factor tends to change very little until the crack length $a_1$. It can be seen from disc DA11, DA12, DA13, DA14 and DB12 etc.;

2 When $a_0/R$ and $a_1/R$ is small, the CCNBD specimen has nearly the same $F_1$ with the CSTBD which $a/R$ is equal to $a_1/R$ in the CCNBD specimen;

3 As seen from Disc ID: Da01, Da02 and Da03 in Group No.1, when the other parameters are unchanged, dimensionless stress intensity factors increases with the thickness of the CCNBD specimen;

4 As seen from Disc ID: Da01 and Da04 in Group No.1, when the other parameters are unchanged, dimensionless stress intensity factors increases with initial crack length;

5 But when dimensionless crack length is large enough, minimum stress intensity factor is reached before dimensionless crack length $a/R = a_1/R$. Therefore the straight through approximation for the CCNBD specimen is not accurate.

6 The rock fracture toughnesss is measured nearly in the middle of $a_1/R - a_0/R$.

## 2.13 The Application of FEM on LEFM

### 2.13.1 Introduction

Three methods are generally available for computing SIFs using finite element method. These techniques can be labled:

1 Global energy release method (GER);

2 Hybrid-direct method (HD);

3 Displacement correlation method (DC).

In the GER method, the total strain energy in the structure is computed before and after a small increment of crack length is given to a crack. Since it has been shown that the derivative of the global strain energy can be released to the SIFs these can be theoretically be computed at the tip of the original crack by using small increments. There are, however, numerous disadvantages to this technique. At least two computer runs are required to compute the SIF for pure mode I loading.

The HD method takes its name from the fact it computes SIFs directly by making them nodal variables, along with displacements, in a hybrid FEM technique. Although it is possibly the most accurate and efficient of the three methods, its main disadvantages is that it involves a special element stiffness formulation and it is not available in most general purpose FEM programmes.

The DC technique is the most versatile and popular. In this method, displacements obtained at nodes near crack tip are correlated with the theoretical values. The success of this technique depends on an accurate modelling of the $r^{1/2}$ displacement variation near the crack tip.

PAFEC uses the GER techniqe for the computation of stress intensity factors at the crack tip.

### 2.13.2 The Use of PAFEC on LEFM

The PAFEC program adapts any isoparametric elements (restricted to 37210 triangular elements) in the region of the crack tip to produce an appropriate singularity.

For three-dimensional elements, all elements containing crack tip nodes must be the wedge type 37210 with crack running along the edges of the rectangular face.

### 2.13.3 Introduction to Research Programme

On account of the complexity of using FEM for three dimensional fracture mechanics problems such as data preparation, FEM calibration here is used only for comparison with the results calibrated by the BEM. Therefore only one CC-NBD specimen and one CSTBD specimen were calibrated by FEM.

## 2.14 2D FEM Calibration of the CSTBD Specimen

Only half of the specimen is modelled because of the symmetry of geometry and loading of the CSTBD specimen. A typical finite element mesh is shown in Figure 2.15(a). The 4-noded isoparametric solid elements are used everywhere except around the crack tip. The element around the crack tip is modelled by type 9 pafblock. All elements around the crack tip are 36110 to represent the crack tip elastic singularity. The mesh close to the crack tip is made finer than the rest of the body to cater for the high stress gradient close to the crack tip. The thickness of the slot is modelled as 0.01, it is very small compared with the disc size.

### 2.14.1 3D FEM Calibration of the CCNBD Specimen

The coordinate system used to define the cracked chevron-notched Brazilian disc specimen is shown in Figure 2.15(b).

According to the literature by Barker L. M. et al, there is no influence on the stress intensity factors if the slot thickness is reasonably small compared with specimen size. In this analysis, the slot thickness is modelled as zero.

Two types of elements (isoparametric and singular) were used in combination to model the specimens. Figure 2.15(b) shows a typical finite element model for the cracked chevron-notched Brazilian disc specimen.

The model idealized one eighth of the specimen. The isoparametric eight-noded or 6-noded element are used everywhere except at the crack tip, where singularity elements are composed of 8 triangular wedge element 37210. The singularity elements produced a square-foot singularity in stress and strain at the crack front.

**a** Finite Element Idealization of the CSTBD under Open-mode

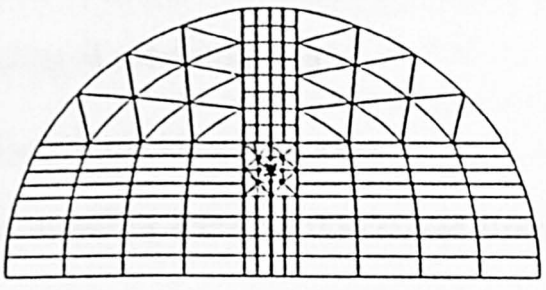

**b** Finite Element Idealization of the CCNBD

Only surface traces of elements shown for clarity

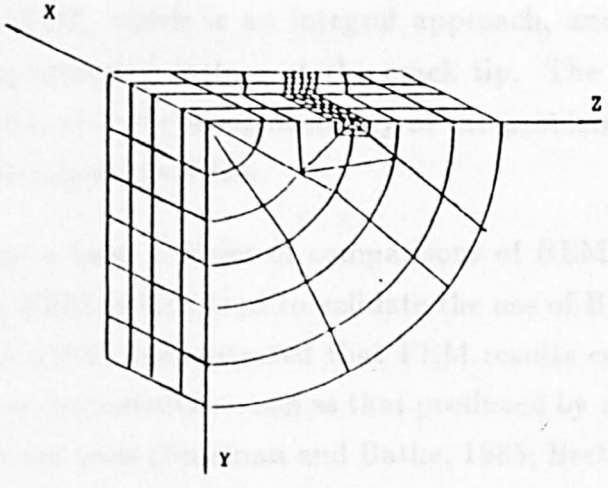


**Figure 2.15 — FEM Mesh Idealization for the Cracked Brazilian Disc**

### 2.14.2 Boundary Conditions and Applied Loading

The following boundary and loading conditions are applied:

1 Symmetry boundary conditions were applied on the $Y = 0$ plane;

2 Symmetry boundary conditions were applied on the $X = 0$ plane;

3 Load is applied along the slot direction.

### 2.14.3 Presentation of the Calibration Results by FEM

All the results calibrated by FEM for the cracked Brazilian disc is presented in Appendix No.9.

## 2.15 Comparison of Calibration Results by FEM and BEM

### 2.15.1 Introduction

There are basically three numerical approaches to obtaining the solutions of linear elastic fracture mechanics problems: the finite element method, the finite difference method and the integral method. This study is concerned with comparison of the BEM, which is an integral approach, and the FEM for the calculation of stress intensity factors at the crack tip. The motivation behind the integral method is that the dimensionality of the problem is reduced by one through the use of integral identities.

There has recently been a series of comparisons of BEM results with other solutions, including FEM, which tend to validate the use of BEM for engineering applications. Floyd, 1984, demonstrated that FEM results can be inaccurate in the presence of stress concentration such as that produced by reentry corners. His results led to a series of tests (Sussman and Bathe, 1985; Brebbia and Trevelyan, 1986) which confirmed that BEM results were highly accurate in engineering practice.

For FEM, the problem is much more pronounced in 3D analysis with complex geometry, where refinement of mesh around stress critical areas demands a large amount of engineering resources. Yet analysts are often frustrated with the

result which fluctuates considerably from one analysis to the other. On the other hand, BEM requires only discretization of the domain boundary, which is a big advantage over FEM, for it provides us with greater flexibility in modelling 3D geometry and should amount to a considerable time saving. The advantage over FEM becomes clear in the application to Linear-Elastic-Fracture-Mechanics (LEFM), where an extremely fine grid is needed around the crack tip to model the crack growth, and accurate stress values ahead of the crack tip are essential for reliable analysis in LEFM. The fact that BEM generates accurate results with a relatively coarse grid, and the fact that, once the boundary problem is solved, stresses can be readily computed at any point inside the domain makes BEM a very attractive tool for LEFM (Cruse and Wilson, 1977; Peruccio and Ingraffea, 1985).

In summary, the main advantages of the BEM can be listed as following:

1 Ease of data preparation, since only the boundary of the region under study needs to be defined;

2 High accuracy for problems involving singularities and or larger gradient such as in LEFM;

3 Internal results obtained only at points requested by the user.

The primary purpose of this investigation is to compare the accuracy and efficiency with a finite element method for the calibration of the CCNBD specimen, i.e., computer time, accuracy of the solution, and the simplicity of data structure. It is found that the calibration of the CCNBD by BEM takes about two thirds of CPU time used by FEM. Especially important, it is very convenient to model the change of geometry. It takes much less time for the data preparation. As analysed later, both methods can generate comparable results.

### 2.15.2 Comparison of the CSTBD Calibration by FEM and BEM

The comparison between the dimensionless stress intensity factors results by both two dimensional FEM and BEM for the CSTBD specimen is shown in Figure 2.16(a). It can be seen that both methods can generate comparable results.

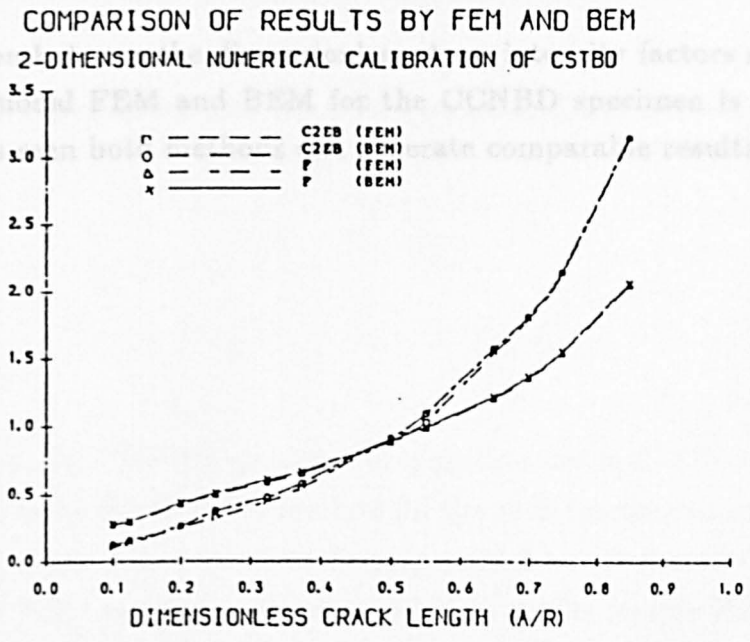


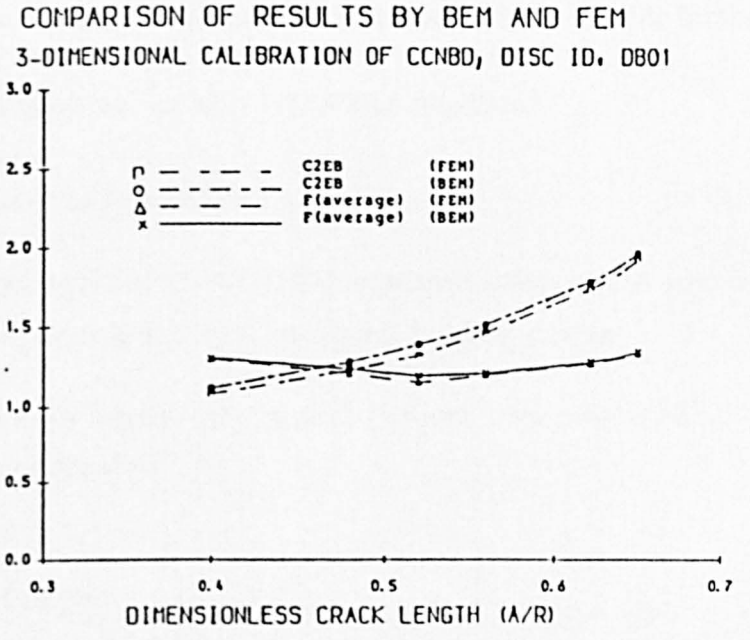


**Figure 2.16 — Comparison of the Calibration Results by FEM and BEM**

### 2.15.3 Comparison of the CCNBD Calibration by FEM and BEM

The comparison between the dimensionless stress intensity factors results by both three dimensional FEM and BEM for the CCNBD specimen is shown in Figure 2.16(b). As seen both methods can generate comparable results.

# Chapter III

# Specimen Preparation and Size Requirements of the CCNBD Method

## 3.1 Introduction

In this chapter, the CCNBD specimen preparation method is described. The size requirements using the CCNBD method for the rock fracture toughness measurement were studied. The curved loading rig used for rock fracture toughness testing by the CCNBD method was designed based on the former BEM calibration of the cracked Brazilian disc specimen. A detailed comparison between the rock tensile strength and rock fracture toughness testing methods was made. A set of semi-circular rock fracture specimens are recommended for further research.

## 3.2 Specimen Preparation of the CCNBD Method

### 3.2.1 The CCNBD Specimen Preparation Apparatus

The equipment used for the CCNBD specimen preparation consists of a vice, milling machine, diamond saw and specimen holding device.

The diamond saws used in this reseach project were produced by ADAMAS UK Ltd., whose address is:

Winchester Avenue
Blaby Industrial Park
Blaby, Leicester LE8 3GZ
Tel: 0533-779894, Fax No.: 0533 477614

The diamond saws (thickness 1 mm, diameter is not less than 50 mm) can be manufactured by this company.

A set of diamond saws with the required diameter used are shown in Photo 3.1.

The chevron notches of the CCNBD specimen are formed by two cuts from both front and back. The specification of the diamond saw used for the cutting of the curved slot of the CCNBD specimens are listed in Table 3.1.

Table 3.1 — The Specification of the Diamond Saw Used

| | |
|---|---|
| The diameter of the diamond saw | 52, 75 or 100 mm |
| The thickness of the diamond saw | 1.0 mm |
| The central hole diameter of the diamond saw | 10 mm |
| The diameter of the rotating axis | 15 mm |

The geometry with basic notation of the diamond saws used for the CCNBD specimen preparation is shown in Figure 3.1.

### 3.2.2 The CCNBD Specimen Preparation Procedures

A practical testing system should not involve time-consuming, expensive specimen preparation procedures and complex apparatus.

The CCNBD specimen holding apparatus is shown in Figure 3.2. The process of the CCNBD specimen preparation is shown in Figure 3.3 and Photo 3.2.

Five simple operations are used to prepare a cracked-chevron-notched Brazilian disc specimen.

1 The disc shaped specimen is obtained directly from rock core or a rock block. The slot direction on the core specimen is marked using a water-proof pen as shown in Figure 3.2. The slot direction for all the samples used for the size requirements investigation is the same;

2 Both the top and bottom surfaces of the disc shaped specimen were ground to the required thickness. The specimen machining is accurate to 0.01 mm.

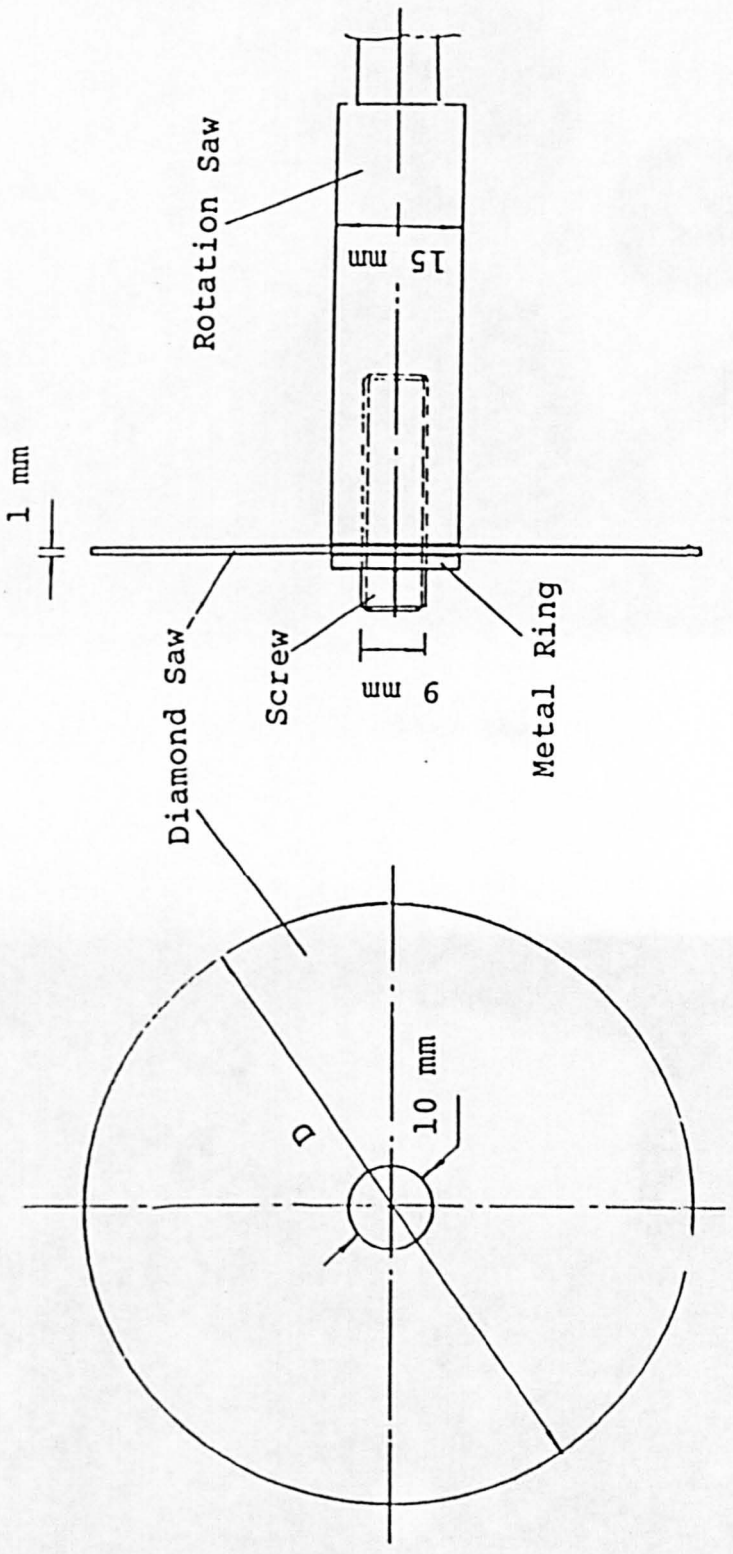


**Figure 3.1 — The Geometry with Basic Notation of the Diamond Saw**

Photo 3.1 - A Set of the Diamond Saws

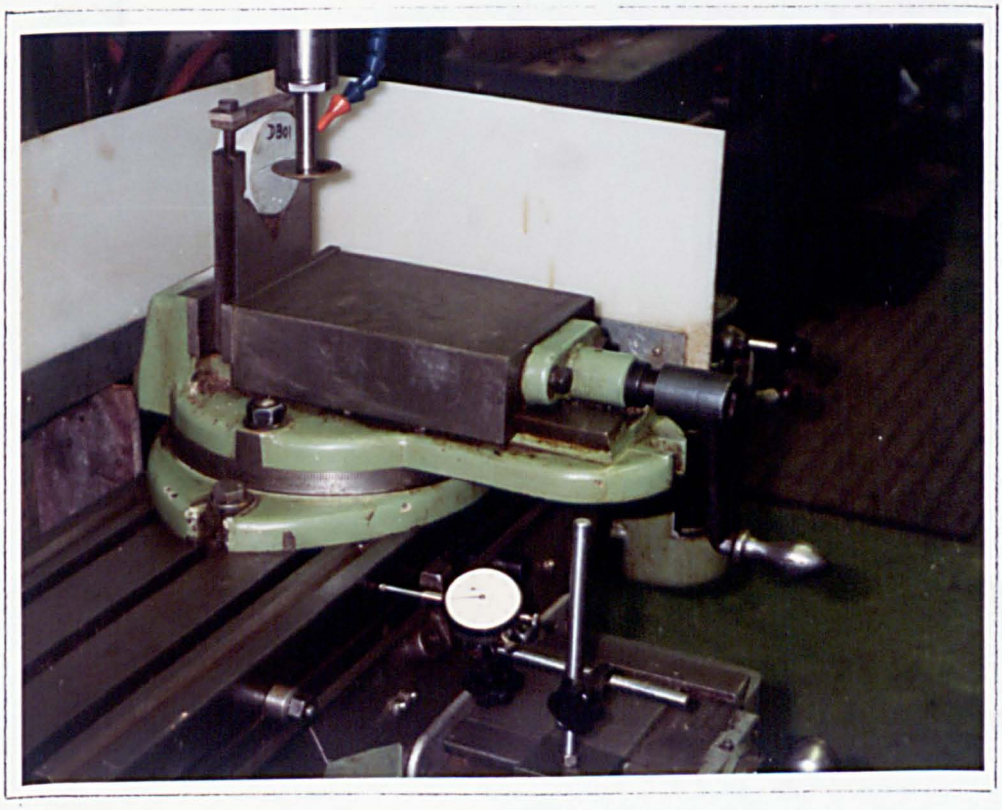

Photo 3.2 - The CCNBD Specimen Preparation

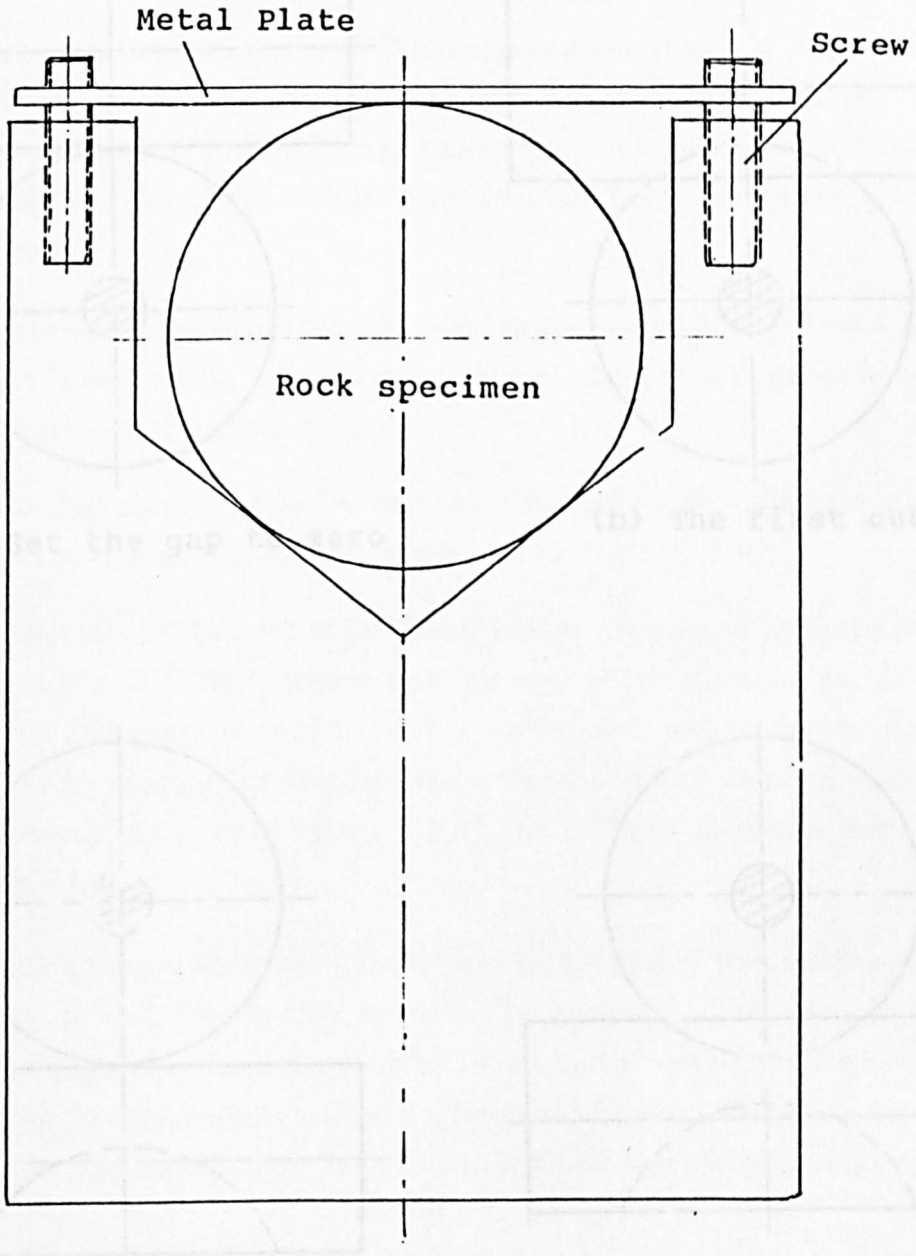


**Figure 3.2 — The Diagram of the CCNBD Specimen Holding Device**

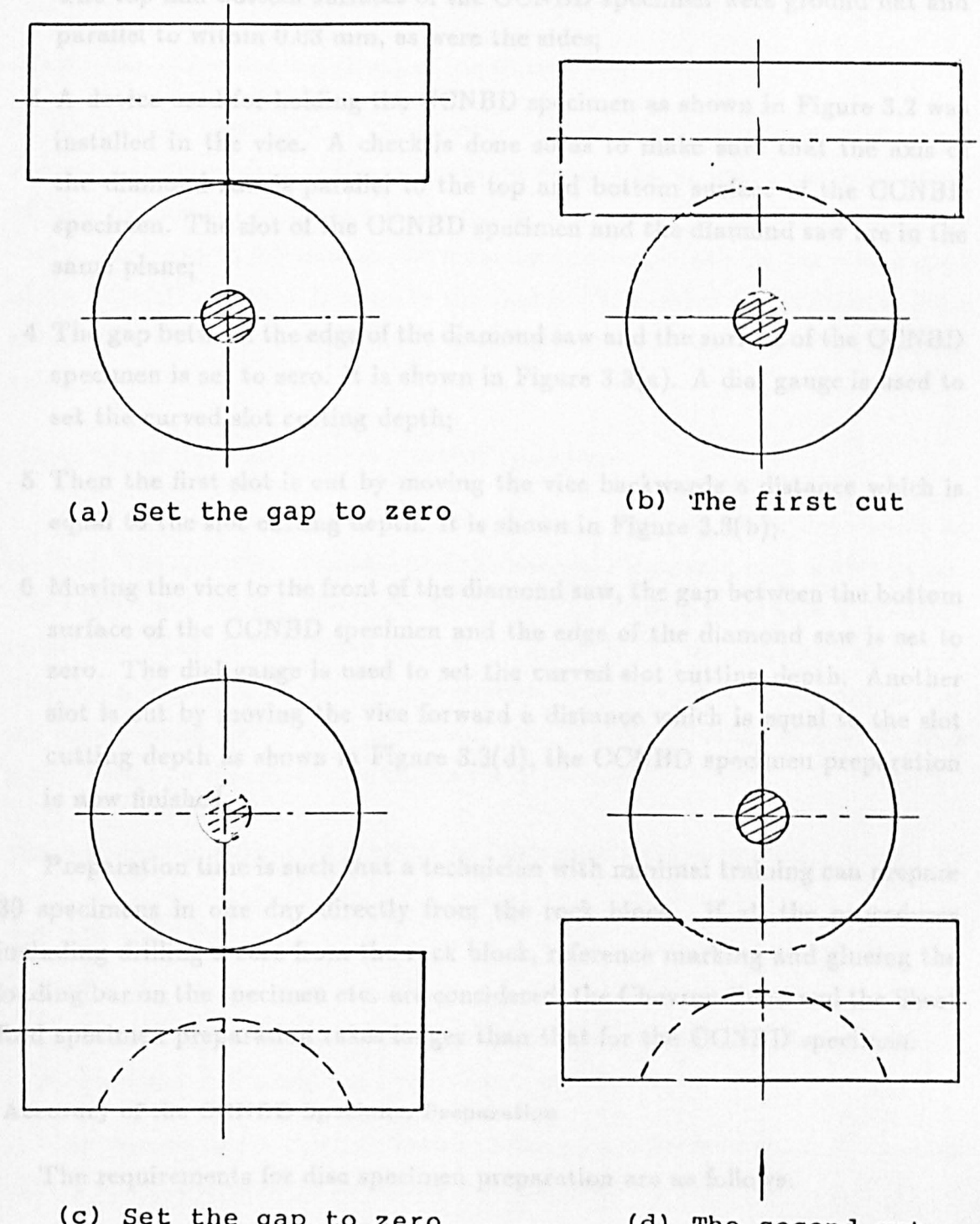


**Figure 3.3 — The Diagram of the CCNBD Specimen Preparation**

The top and bottom surfaces of the CCNBD specimen were ground flat and parallel to within 0.03 mm, as were the sides;

3 A device used for holding the CCNBD specimen as shown in Figure 3.2 was installed in the vice. A check is done so as to make sure that the axis of the diamond saw is parallel to the top and bottom surface of the CCNBD specimen. The slot of the CCNBD specimen and the diamond saw are in the same plane;

4 The gap between the edge of the diamond saw and the surface of the CCNBD specimen is set to zero. It is shown in Figure 3.3(a). A dial gauge is used to set the curved slot cutting depth;

5 Then the first slot is cut by moving the vice backwards a distance which is equal to the slot cutting depth. It is shown in Figure 3.3(b);

6 Moving the vice to the front of the diamond saw, the gap between the bottom surface of the CCNBD specimen and the edge of the diamond saw is set to zero. The dial gauge is used to set the curved slot cutting depth. Another slot is cut by moving the vice forward a distance which is equal to the slot cutting depth as shown in Figure 3.3(d), the CCNBD specimen preparation is now finished.

Preparation time is such that a technician with minimal training can prepare 30 specimens in one day directly from the rock block. If all the procedures including drilling a core from the rock block, reference marking and glueing the loading bar on the specimen etc. are considered, the Chevron Bend and the Short Rod specimen preparation takes longer than that for the CCNBD specimen.

### 3.2.3 Accuracy of the CCNBD Specimen Preparation

The requirements for disc specimen preparation are as follows:

1 The disc thickness is machined accurate to 0.01 mm;

2 The curved slot should be cut so that both sides have equal traces;

3 The curved slot cutting depth should be accurate to 0.01 mm;

4 The top and bottom surfaces are ground flat and parallel to within 0.03 mm.

#### 3.2.4 Restriction of the Cutting Depth of the Curved Slot

Due to the dimension of the rotating axis for the diamond saw, the curved slot can't be cut as deep as the radius of the diamond saw. In the workshop of the Mining Engineering Department the radius of the rotating axis for the diamond saw is machined to 4.5 mm, so the maximum cutting depth for the preparation of the CCNBD specimen is equal to the diamond saw radius minus 5.0 mm, if 0.5 mm is used for the safety gap between the specimen and the edge of the rotation axis.

#### 3.2.5 Check of the Dimensions of the CCNBD Specimens

After the preparation, the dimensions of the CCNBD specimens should be checked. The specimen diameter and thickness are measured by a venier gauge. The curved slot cutting depth can be checked by a circle plate with a thickness of 0.8 mm. The circular plate diameter is equal to the diamond saw diameter. The slot geometry on both top and bottom surfaces should be symmetrical to the central points of the disc specimen. Also the slot direction relative to rock fabric, core axis etc. should be checked and recorded.

### 3.3 Experimental Apparatus and the Instrumentation System

#### 3.3.1 Loading Apparatus

Either the RDP or Instron testing machine with controlled displacement rate, with a + 20 kN dynamic load capacity in Metallurgy and Material Science section of the Mechanical Engineering Department was used.

The tests using the RDP or Instron testing machine were run in a constant loading line displacement rate of 0.08 mm/minute.

#### 3.3.2 Displacement Measurement Apparatus

The LVDT with linear ball bearings, with ± 1.0 mm linear range and a measurement reproduction of 0.1 $\mu m$ is used for measuring the loading line dis-

placement (parallel to the slot direction). Another AC-operated LVDT with the same specification is used for measuring the crack opening displacement, it is installed across the two blocks along the diametral line which is vertical to the slot direction. The gap between the two blocks is 10 mm.

The apparatus for measuring the loading line displacement and crack opening displacement is shown in Figure 3.4.

After the careful calibration, the technical characteristics of the AC-operated LVDTs are listed in Table 3.2.

Table 3.2 — Technical Characteristics of the LVDTs

| | |
|---|---|
| Linear range | ± 1.00 mm |
| Sensitivity | 1000 $\mu m/Volt$ |
| Reproduction of LVDTs | 0.1 $\mu$m |

### 3.3.3 Data Recording Equipment

The signals from load transducer and LVDTs are recorded by the datalogger. Load transducer signal is input into the datalogger directly. The AC-operated LVDTs signal is input into the AC-DC converter firstly, then the output (DC voltage signal) from the AC-DC converter is input into the datalogger. The data can be stored either by built-in printer or tape. The speed of recording is 2 times/second or more. By a program, the magnitude of DC voltage is transfered to kN or $\mu m$ unit as required. All the data recorded by the datalogger is analysed by MTS on the University's main frame computer.

The instrumentation system used is shown in Figure 3.5 and Photo 3.3.

Three channels are used to record the load and displacements signals.

### 3.3.4 Loading Rig Design

The experimental rig for rock fracture toughness measurement by the cracked chevron-notched Brazilian disc specimen is shown in Figure 3.4 and Photo 3.3.

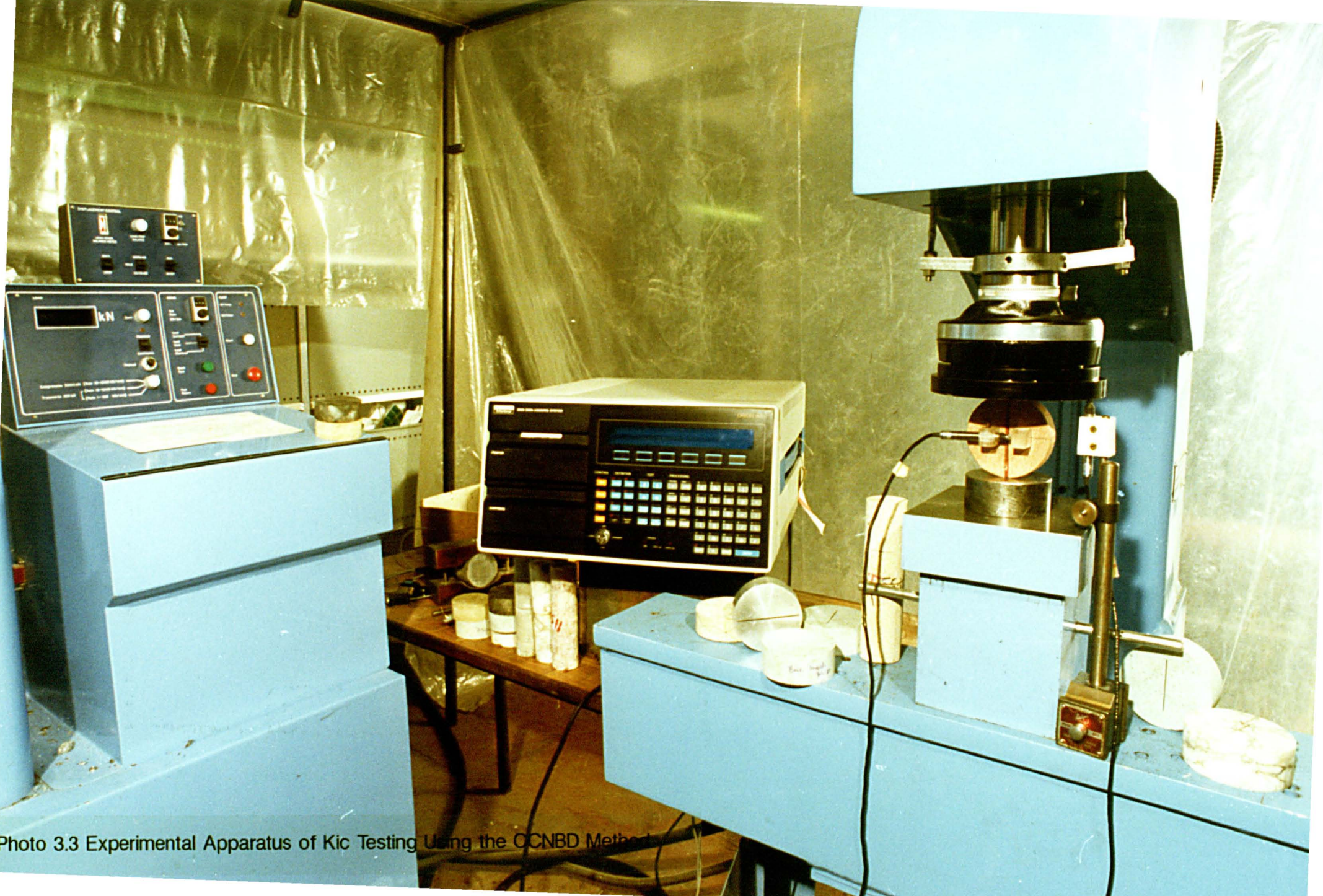


Photo 3.3 Experimental Apparatus of Kic Testing Using the CCNBD Method

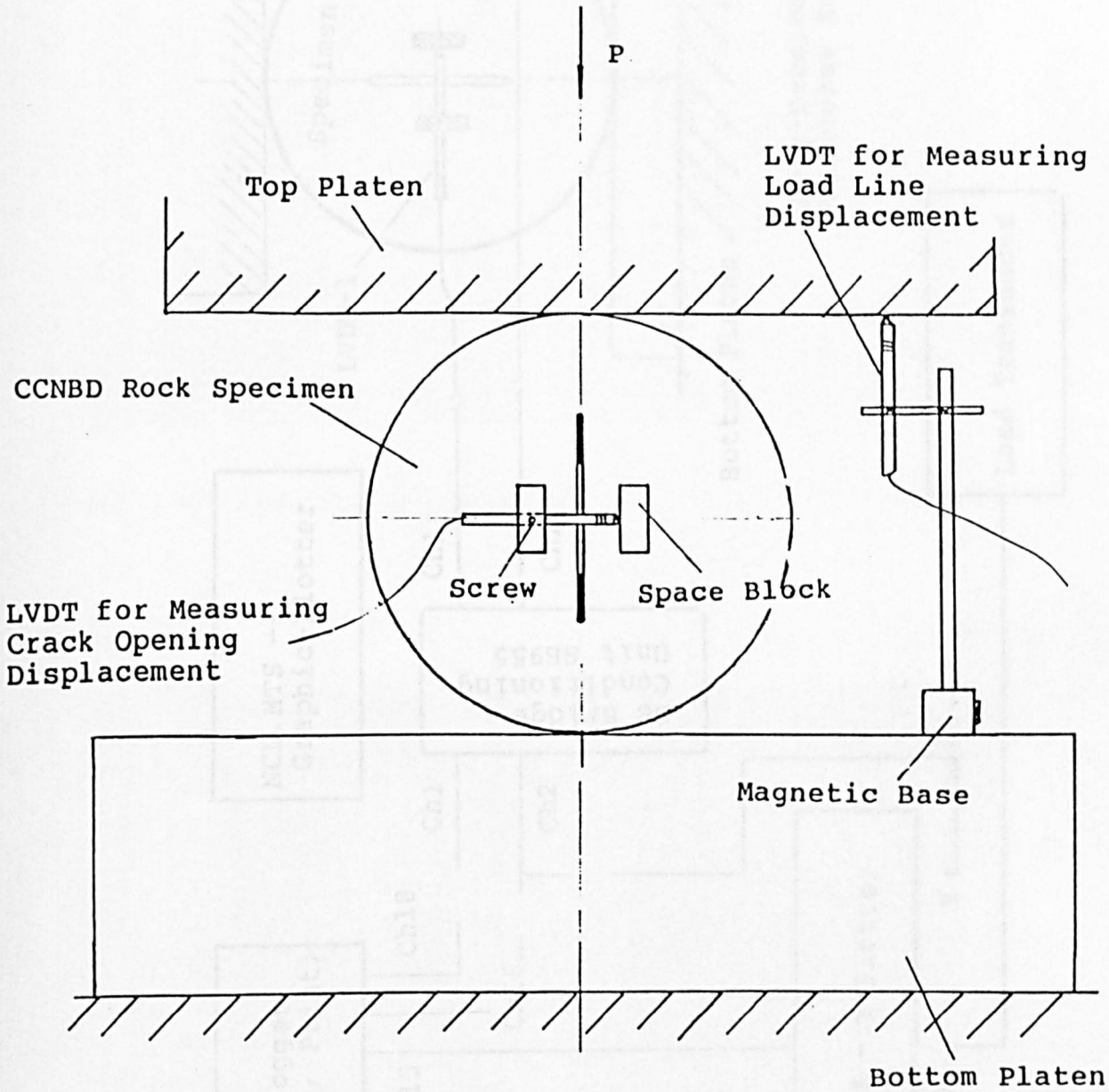


**Figure 3.4 — The Displacement Measurement Apparatus**

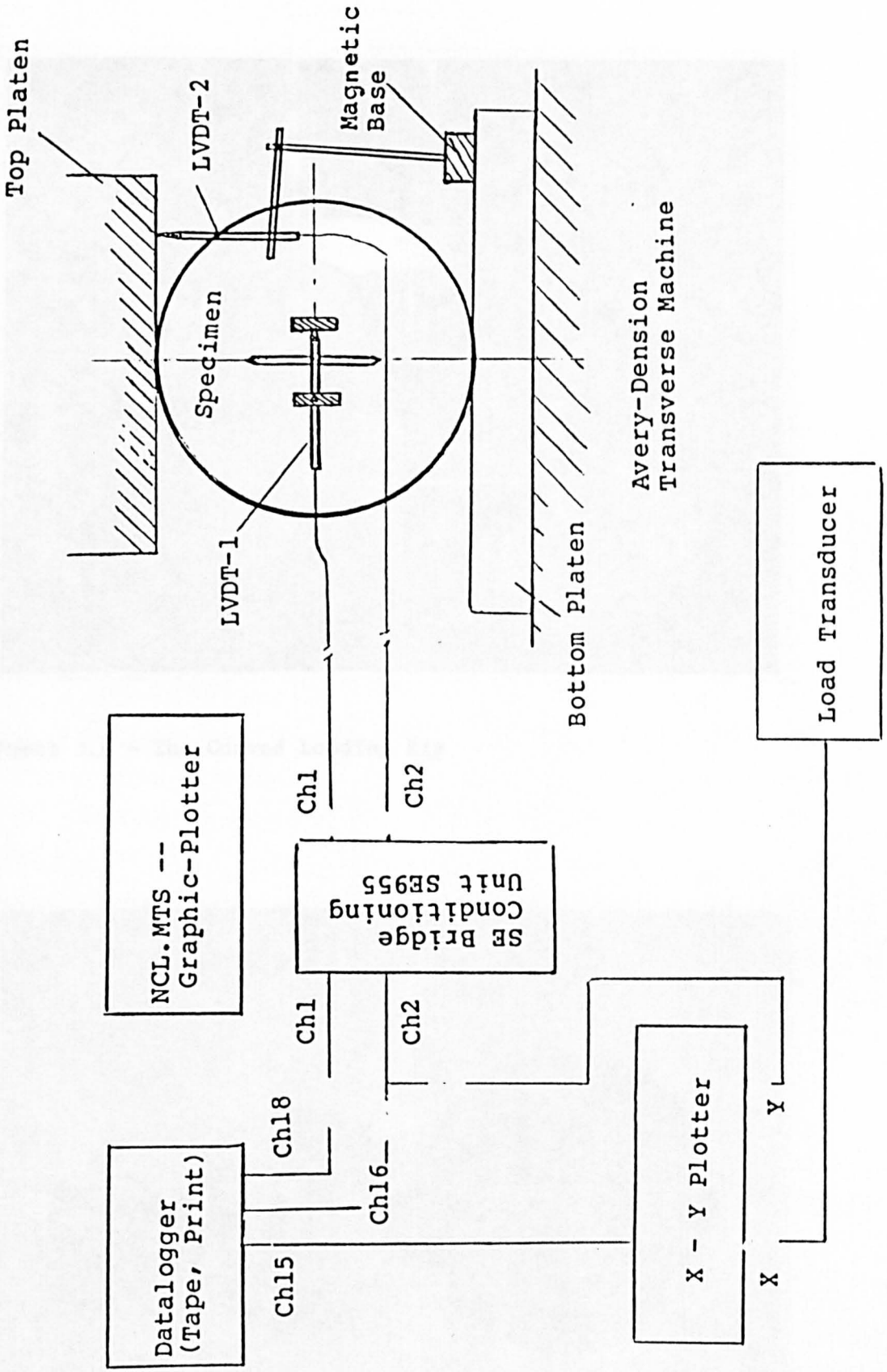


**Figure 3.5 — The Instrumentation System Used in this Research**

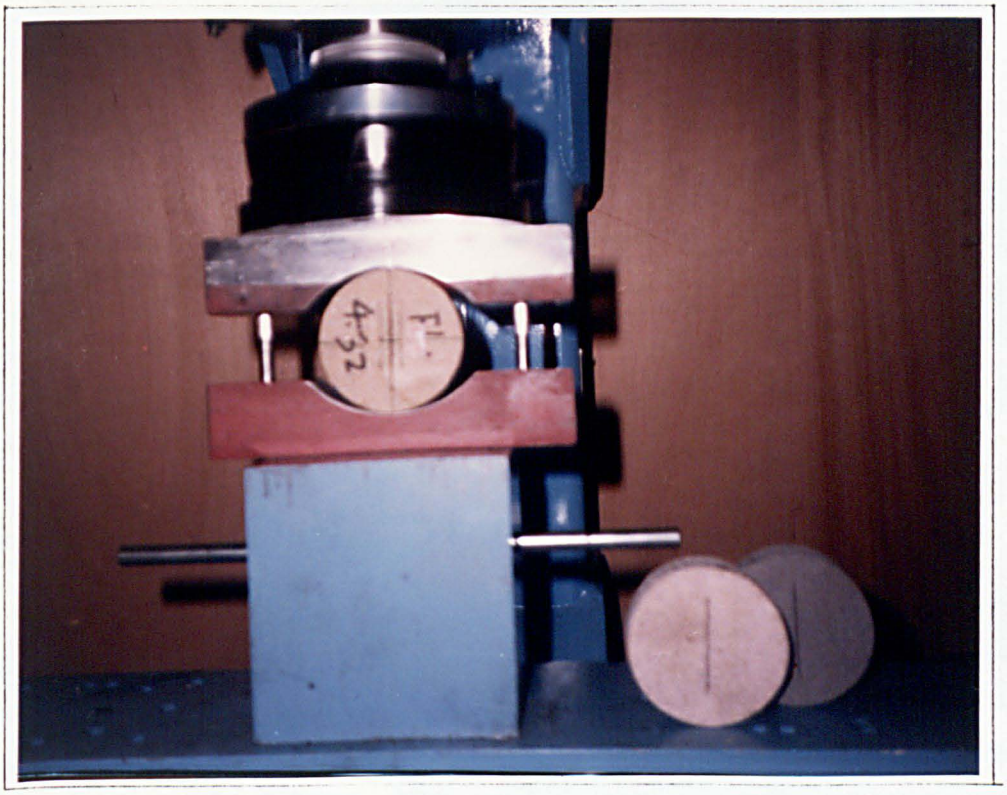

Photo 3.4 - The Curved Loading Rig


Photo 3.5 - Three CCNBD Specimens with Diameter 50, 75 and 100 mm

Some measures are taken in order to keep the slot in the vertical direction. As shown in Figure 3.6, two plates are used for this purpose. The thickness of the plate used for inserting the slot of the CCNBD specimen should be less than 1 mm, its width should be less than the initial crack length of the CCNBD specimen, its length should be larger than the half of the thickness of the CCNBD specimen. The plate used for connetcing metal blade should be heavy enough to stabilize the CCNBD specimen.

### 3.3.5 The Curved Loading Rig

In order to avoid the highly-localized compressive stresses under the load, a device as that used in the indirect tensile strength testing by Brazilian disc is used for rock fracture toughness measurement by the CCNBD method. The curved load rig is quite heavy, the preload which is brought by the weight of the upper jaw must be deleted. This could be done by connecting the upper jaw with the crosshead of the top platen of the loading machine as shown in Figure 3.8. The load applied on the specimen comes from the pressure of the hydraulic system. Therefore the weight of the upper jaw are not used for preload during the testing.

As analysed in chapter 2, the degrees of the loading contact angles has no influence if the angle is less than 10 degrees for $\frac{a_1}{R} \leq 0.8$. Therefore, the curved loading rig with 10 degrees loading contact angles will not affect the rock fracture toughness testing results.

The curved loading rig is shown in Figure 3.7 and Photo 3.4.

The curved diameter of the loading rig is 1.5 times the CCNBD specimen diameter, the thickness is 8 mm wider than the CCNBD specimen thickness. Two pins are used as guides during loading.

### 3.3.6 $K_{IC}$ Testing by a Curved Loading Rig

If a curved loading rig is used, care must be taken in the determination of maximum failure load. Load will increase again after a short stop when the specimen fails, the increasing load can still be substained by the half disc. The magnitude of the failure load is better determined by the load vs loading line

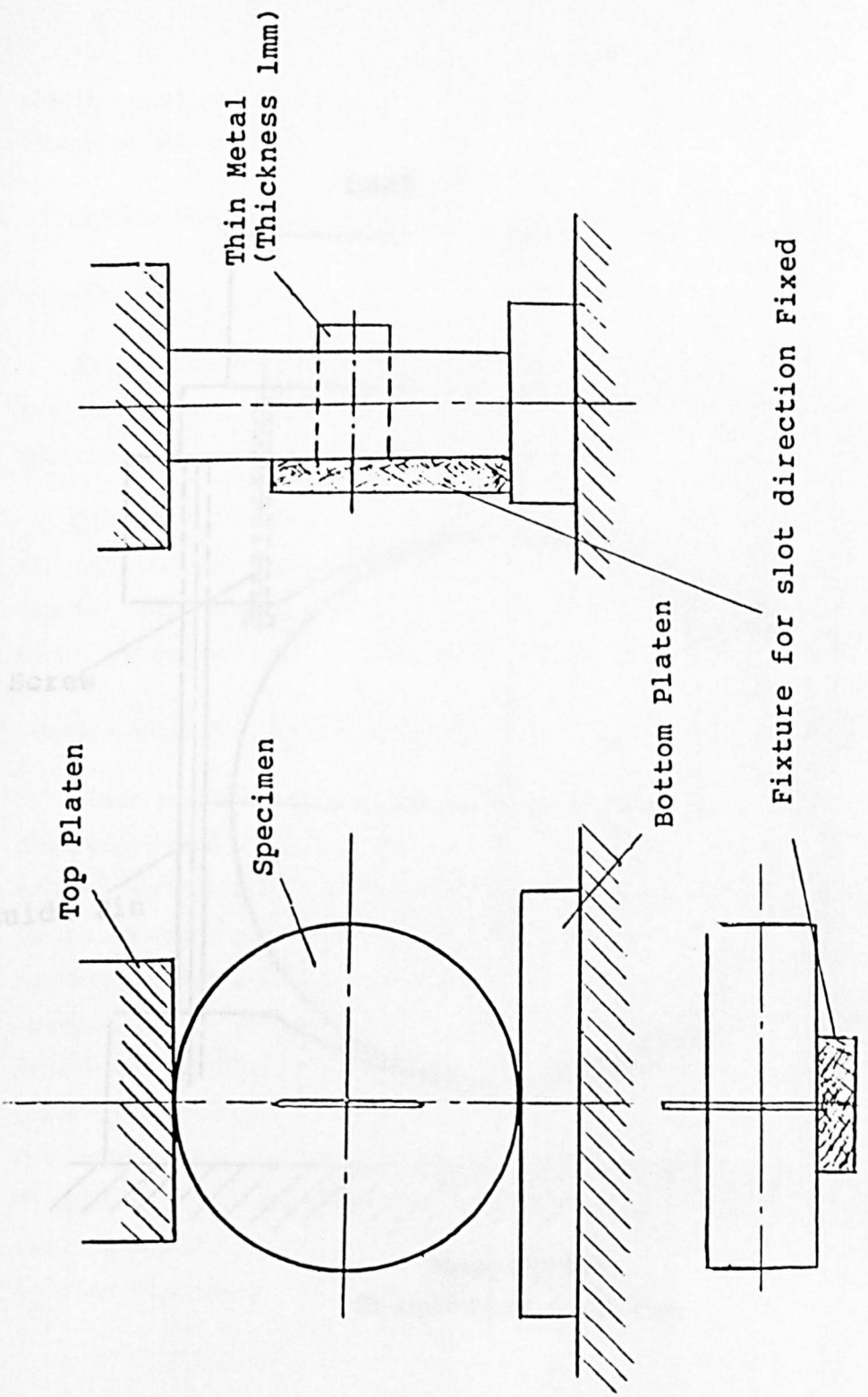


**Figure 3.6 — The Fixture for Arranging Vertical Slot Direction**

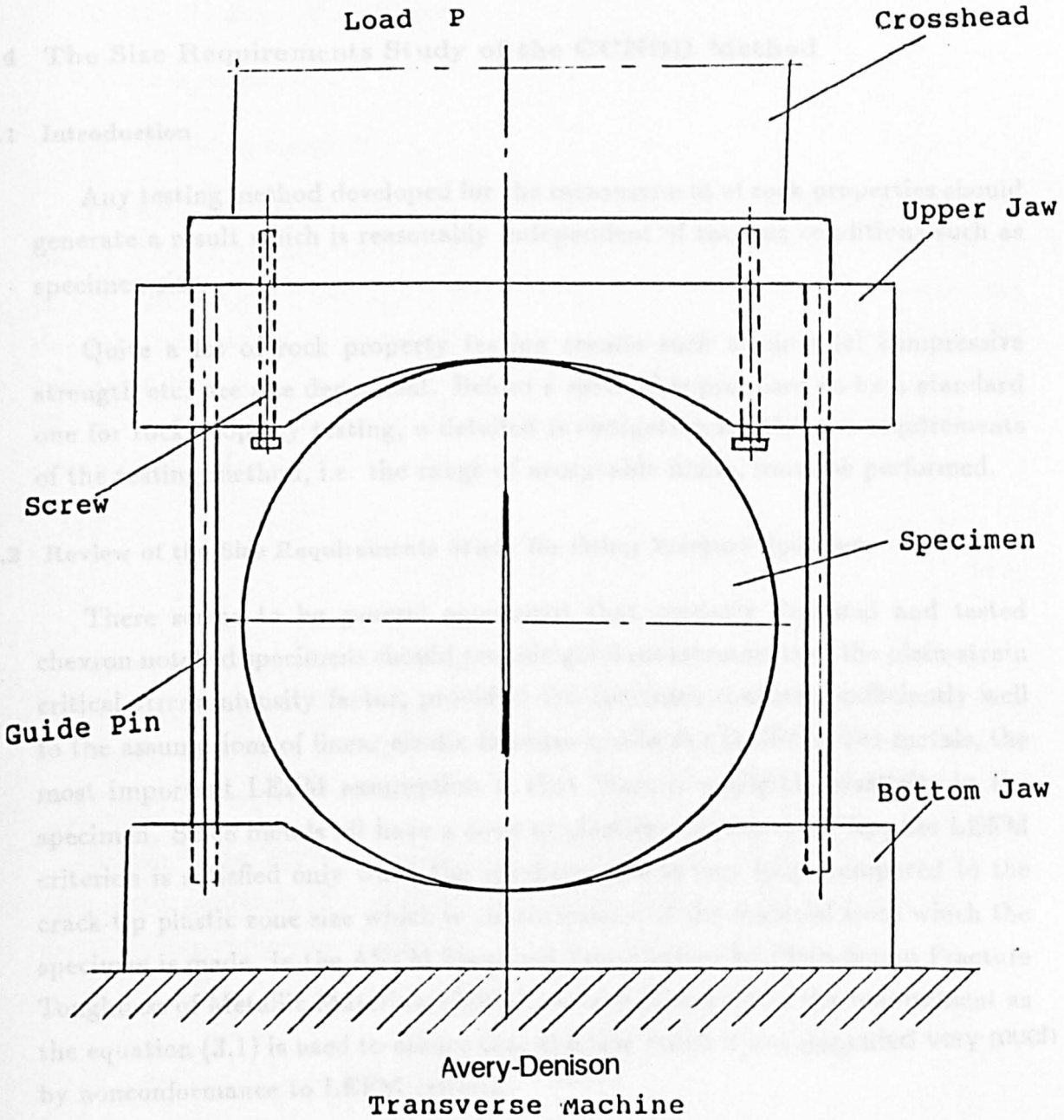


**Figure 3.7 — The Curved Loading Rig for $K_{IC}$ Testing Using the CCNBD Method**

displacement curve. It is similar to indirect rock tensile strength testing by the Brazilian disc method.

## 3.4 The Size Requirements Study of the CCNBD Method

### 3.4.1 Introduction

Any testing method developed for the measurement of rock properties should generate a result which is reasonably independent of the test conditions such as specimen size.

Quite a lot of rock property testing results such as uniaxial compressive strength etc. are size dependent. Before a method is proposed to be a standard one for rock property testing, a detailed investigation for the size requirements of the testing method, i.e. the range of acceptable limits, must be performed.

### 3.4.2 Review of the Size Requirements Study for Other Fracture Specimen

There seems to be general agreement that properly designed and tested chevron notched specimens should provide good measurements of the plain-strain critical stress-intensity factor, provided the specimen conforms sufficiently well to the assumptions of linear elastic fracture mechanics (LEFM). For metals, the most important LEFM assumption is that there is negligible plasticity in the specimen. Since metals all have a zone of plasticity at the crack tip, the LEFM criterion is satisfied only when the specimen size is very large compared to the crack-tip plastic zone size which is characteristic of the material from which the specimen is made. In the ASTM Standard Test Method for Plain-Strain Fracture Toughness of Metallic Materials (E399), certain rules such as the requirement as the equation (3.1) is used to assure that the test result is not degraded very much by nonconformance to LEFM criteria.

$$a,\ B,\ (W-a) \geq 2.5(\frac{K_{IC}}{\sigma_y})^2 \tag{3.1}$$

Where:

$K_{IC}$ – a material fracture toughness value and

$\sigma_y$ – the yield stress. For rock, $\sigma_y$ can be replaced by $\sigma_t$, the rock tensile strength (Schmidt, 1980).

B – the thickness of specimen;

a – crack length;

W – specimen diameter;

The inequality above then gives a required minimum specimen size ($D_{min} = 2a_{min}$) of about 230 mm for three point bending specimen, if Sandstone results of $K_{IC} = 0.62MN/m^{1.5}$ and $\sigma_t = 2.88MPa$ are used. Munz (1979) reported that size requirements for thickness may be less stringent however. Schmidt (1980) concluded that $K_{IC}$ for Westerly granite is insensitive to thickness in the range 13 -103 mm. Based on the work of others, Munz (1979) found that for metals the factor 2.5 above could be replaced by

$$\beta = \alpha(1 - \mu^2)\sigma_y/E \tag{3.2}$$

where $\alpha = 25 - -50$. Inserting values for Westerly granite, Indian limestone, or Ekeberg marble into the above equation with $\sigma_y$ replaced by $\sigma_t$ and using inequality (3.1), gives $B_{min}$ less than 0.5 mm (Ouchterlony, 1986). This tends to confirm that fracture toughness is insensitive to specimen thickness.

Barker L. M. (1984) studied the size effect of the short rod specimen, he proposed a minimum short-rod specimen size criterion as the equation (3.3). for metal fracture toughness testing.

$$B \geq 1.25(\frac{K_{IC}}{\sigma_y})^2 \tag{3.3}$$

The specimen size effect studies here should help to establish a minimum size criterion for rock fracture toughness testing using the CCNBD method.

A fine grained sandstone was used for the size requirements study for the CCNBD method.

### 3.4.3 Rock Mechanical Properties

Uniaxial compressive strength, tensile strength, Poisson's ratio, rock fracture toughness by both the CB and SR methods, rock specific energy by the instrumented cutting testing, NCB cone indenter index and Young's modulus of the Sandstone were tested.

The results are presented in Table 3.3.

Table 3.3 — Rock Properties Tested

| | |
|---|---|
| Rock uniaxial compressive strength (MPa) | $47.25 \pm 0.87$ |
| Rock tensile strength by Brazilian disc testing (MPa) | $2.87 \pm 0.05$ |
| Secant Young Modulus (GPa) | $11.26 \pm 0.56$ |
| Poisson's ratio | 0.23 |
| Density ($g/cm^3$) | 2.32 |
| NCB cone indenter index | $1.54 \pm 0.21$ |
| Rock specific energy ($MJ/m^3$) | $11.25 \pm 0.76$ |
| $K_{IC}$ tested by short rod method ($MN/m^{1.5}$) | $0.63 \pm 0.09$ |
| $K_{IC}$ tested by chevron bend method ($MN/m^{1.5}$) | $0.62 \pm 0.07$ |

From Table 3.3, we can see the repeatability of the rock property testing results is excellent. This rock is highly homogeneous on the macroscopic scale.

### 3.4.4 The Geometry of the CCNBD Specimens Tested

The specimen dimensions used for the investigation of the size requirements of rock fracture toughness measurement by the CCNBD method are listed in Table 3.4.

In Table 3.4, GN represents "Group Number", SpN represents "Specimen Number Tested".

**Table 3.4 — The Dimensions of the CCNBD Specimen**

| Disc-ID | D, mm | $D'$, mm | B, mm | $a_0$, mm | C | $a_1/R$ | GN | SpN |
|---|---|---|---|---|---|---|---|---|
| Da01 | 100 | 100 | 40.0 | 15 | 23.30 | 0.846 | 1 | 4 |
| Da02 | 100 | 100 | 35.0 | 15 | 19.80 | 0.797 | 1 | 4 |
| Da03 | 100 | 100 | 30.0 | 15 | 17.30 | 0.757 | 1 | 4 |
| Da04 | 100 | 100 | 25.0 | 15 | 14.80 | 0.710 | 1 | 4 |
| Da05 | 100 | 100 | 35.0 | 20 | 21.67 | 0.824 | 1 | 4 |
| Da06 | 100 | 100 | 80.0 | 13 | 41.72 | 0.986 | 1 | 4 |
| Da07 | 100 | 100 | 70.0 | 20 | 39.17 | 0.976 | 2 | 4 |
| Da08 | 100 | 100 | 60.0 | 20 | 34.17 | 0.949 | 2 | 4 |
| Da09 | 100 | 100 | 50.0 | 20 | 29.17 | 0.909 | 2 | 4 |
| Da21 | 100 | 75 | 55.0 | 15 | 30.63 | 0.737 | 3 | 4 |
| Da22 | 100 | 75 | 30.0 | 15 | 18.13 | 0.642 | 3 | 4 |
| Da11 | 100 | 52 | 30.0 | 10 | 17.00 | 0.488 | 4 | 4 |
| Da12 | 100 | 52 | 25.0 | 10 | 14.50 | 0.466 | 4 | 4 |
| Da13 | 100 | 52 | 20.0 | 10 | 12.00 | 0.438 | 4 | 4 |
| Da14 | 100 | 52 | 30.0 | 8 | 16.26 | 0.482 | 4 | 4 |
| Db01 | 75 | 52 | 30.0 | 10 | 17.00 | 0.651 | 5 | 20 |
| Db02 | 75 | 52 | 25.0 | 10 | 14.50 | 0.622 | 5 | 4 |
| Db03 | 75 | 52 | 20.0 | 10 | 12.00 | 0.584 | 5 | 4 |
| Db04 | 75 | 52 | 30.0 | 8 | 16.26 | 0.643 | 5 | 4 |
| Db21 | 75 | 75 | 52.5 | 15 | 29.38 | 0.976 | 6 | 4 |
| Db22 | 75 | 75 | 45.0 | 15 | 25.63 | 0.949 | 6 | 4 |
| Db23 | 75 | 75 | 37.5 | 15 | 21.88 | 0.909 | 6 | 4 |
| Dc01 | 50 | 52 | 20.0 | 10 | 12.00 | 0.876 | 7 | 4 |
| Dc02 | 50 | 52 | 15.0 | 10 | 9.50 | 0.804 | 7 | 4 |

As seen from Table 3.4, the following parameters are studied to investigate the effect of the specimen geometry on the rock fracture toughness:

1 The specimen diameter;

2 The curved slot diameter, or the diamond saw diameter;

3 The specimen thickness;

4 The specimen initial crack length.

The thickness of the curved slot is machined about 1 mm. The effect of slot thickness on $K_{IC}$ testing has been studied by some workers (Barker et al.) and shows that there is no influence if the thickness of the slot is relatively thin.

As shown in Table 3.4, the CCNBD specimen diameter is 50, 75 and 100 mm; the thickness varies from 15 to 80 mm; the initial crack length varies from 8 to 20 mm; the diameter of the curved slot is 52, 75 and 100 mm. A total of 24 different geometries for the CCNBD specimens were used.

The largest sample is Da06, the smallest sample is Dc02.

Three CCNBD specimens with 50, 75 and 100 mm diameter are shown in Photo 3.5.

As shown in Table 3.4, seven groups of the CCNBD specimens were used for the study of the effect of the specimen size on the rock fracture toughness value. It can be summarized as following:

Group No.1: in this group, specimen diameter was 100 mm, curved slot diameter was 100 mm. It was used for the investigation of specimen thickness on $K_{IC}$ value. Also Disc Da01 and Da05 had the same diameter, thickness and curved slot radius, they were used for the study of the effect of initial crack length on the rock fracture toughness;

Group No.2: in this group, specimen diameter was 100 mm, curved slot diameter was 100 mm. Specimen thicknesses was 70, 60 and 50 mm. On the one hand, it was used for the study of the effect of specimen thickness on the $K_{IC}$ value; on the other hand, it was used for the study of the requirements

of $a_1/R$ for the CCNBD methods. Also this group was used for comparison with Group No.6;

Group No.3: in this group, specimen diameter was 100 mm, curved slot diameter was 75 mm. It was used for comparison with Group No.1 and Group No.2 to study the effect of curved slot diameter on the rock fracture toughness. Inside this group, it was used for investigating the effect of specimen thickness on the rock fracture toughness;

Group No.4: in this group, specimen diameter was 100 mm, curved slot diameter was 52 mm. On the one hand, it was used to study the effect of curved slot diameter on the rock fracture toughness by comparison with Group No.1 and Group No.3; on the other hand, it was used to study the effect of specimen diameter on the rock fracture toughness by comparison with Group No.5. Inside the group, it was used for the study of the effect of specimen thickness and initial crack length on the rock fracture toughness. The $a_0/R$ and $a_1/R$ of the specimen inside this group were the lowest among all the CCNBD specimens tested;

Group No.5: in this group, specimen diameter was 75 mm, curved slot diameter was 52 mm. On the one hand, it was used to study the effect of specimen diameter on the rock fracture toughness value by comparison with Group No.4 and Group No.7; on the other hand, it was used to study the effect of curved slot diameter on the rock fracture toughness value by comparison with Group No.6. Inside the group, it was used to study the effect of specimen thickness and initial crack length on the rock fracture toughness value;

Group No.6: in this group, the specimen diameter was 75 mm, the curved slot diameter was 75 mm. On the one hand, it was used to study the effect of curved slot diameter on the rock fracture toughness value by comparison with Group No.5; on the other hand, it was used to study the effect of specimen thickness on the rock fracture toughness value. The dimension of Disc Db21, Db22 and Db23 were proportional to that of Disc Da07, Da08 and Da09 individually. It was also used to study the requirements of $a_1/R$ in the CCNBD method;

Group No.7: in this group, specimen diameter was 50 mm, curved slot diameter was 52 mm. It was used to study the requirement of specimen diameter.

### 3.4.5 Experimental Procedure

All the CCNBD specimens from Sandstone were tested using the RDP or Instron testing machine.

All the tests were run under the constant loading line displacement rate of 0.08 mm/min. All tests were run until the specimen fails. The loading rig and the instrumentation system used have been described in the earlier part of this chapter. The maximum failure load was recorded. Sometimes the load vs load line displacment and crack opening displacement were recorded.

### 3.4.6 Calculation of $K_{IC}$

The following formulae is used for the critical stress intensity factors calculation (Mode I) using the CCNBD method:

$$K_{IC} = F_{IC} \times \frac{P_{max}}{BD^{0.5}} \tag{3.4}$$

Where:

$K_{IC}$ – Critical Stress Intensity Factors, $MN/m^{1.5}$;

$F_{IC}$ – Dimensionless critical stress intensity factors, as presented in Table 3.1 for different geometry of the CCNBD specimens;

$P_{max}$ – The maximum failure load, kN;

B – The thickness of the cracked Brazilian disc, cm;

D – The diameter of the cracked Brazilian disc, cm.

### 3.4.7 Presentation of Results

The experimental results for the size requirements study of the CCNBD method are presented in Table 3.5. "GN" represents "Group Number".

**Table 3.5 — Experimental Results for the Size Requirements Study**

| Disc-ID | GN | $a/R$ | $F_{IC}$ | $K_{IC}$, $MN/m^{1.5}$ | *Average* $\pm$ *Sted.* |
|---|---|---|---|---|---|
| Da01 | 1 | 0.846 | 1.629 | 0.605, 0.607, 0.577, 0.604 | 0.598 $\pm$ 0.012 |
| Da02 | 1 | 0.797 | 1.573 | 0.616, 0.624, 0.614, 0.608 | 0.615 $\pm$ 0.006 |
| Da03 | 1 | 0.757 | 1.519 | 0.610, 0.603, 0.615, 0.612 | 0.610 $\pm$ 0.004 |
| Da04 | 1 | 0.710 | 1.336 | 0.624, 0.616, 0.625, 0.613 | 0.619 $\pm$ 0.005 |
| Da05 | 1 | 0.824 | 1.782 | 0.628, 0.597, 0.618, 0.620 | 0.616 $\pm$ 0.012 |
| Da06 | 2 | 0.986 | 2.011 | 0.443, 0.456, 0.449, 0.455 | 0.451 $\pm$ 0.005 |
| Da07 | 2 | 0.976 | 2.156 | 0.484, 0.428, 0.466, 0.469 | 0.462 $\pm$ 0.021 |
| Da08 | 2 | 0.949 | 1.823 | 0.442, 0.426, 0.434, 0.440 | 0.436 $\pm$ 0.006 |
| Da09 | 2 | 0.909 | 1.734 | 0.427, 0.430, 0.432, 0.433 | 0.430 $\pm$ 0.002 |
| Da21 | 3 | 0.737 | 1.664 | 0.621, 0.619, 0.625, 0.616 | 0.620 $\pm$ 0.003 |
| Da22 | 3 | 0.642 | 1.547 | 0.619, 0.603, 0.623, 0.621 | 0.617 $\pm$ 0.008 |
| Da11 | 4 | 0.488 | 0.946 | 0.589, 0.599, 0.606, 0.600 | 0.599 $\pm$ 0.006 |
| Da12 | 4 | 0.464 | 0.940 | 0.629, 0.637, 0.610, 0.623 | 0.625 $\pm$ 0.010 |
| Da13 | 4 | 0.438 | 0.869 | 0.583, 0.588, 0.587, 0.589 | 0.587 $\pm$ 0.002 |
| Da14 | 4 | 0.482 | 0.932 | 0.591, 0.619 0.610, 0.611 | 0.608 $\pm$ 0.010 |
| Db01 | 5 | 0.651 | 1.181 | 0.599, 0.593, 0.617, 0.609 | 0.605 $\pm$ 0.010 |
| Db02 | 5 | 0.622 | 1.141 | 0.597, 0.627, 0.628, 0.612 | 0.616 $\pm$ 0.013 |
| Db03 | 5 | 0.584 | 1.134 | 0.623, 0.617, 0.625, 0.608 | 0.618 $\pm$ 0.007 |
| Db04 | 5 | 0.643 | 1.156 | 0.598, 0.608, 0.598, 0.599 | 0.600 $\pm$ 0.004 |
| Db21 | 6 | 0.976 | 2.156 | 0.395, 0.433, 0.432, 0.421 | 0.420 $\pm$ 0.015 |
| Db22 | 6 | 0.949 | 1.823 | 0.312, 0.312, 0.342, 0.332 | 0.325 $\pm$ 0.013 |
| Db23 | 6 | 0.909 | 1.734 | 0.339, 0.368, 0.367, 0.357 | 0.358 $\pm$ 0.012 |
| Dc01 | 7 | 0.876 | 1.926 | 0.530, 0.586, 0.534, 0.581 | 0.558 $\pm$ 0.026 |
| Dc02 | 7 | 0.804 | 1.716 | 0.501, 0.537, 0.527, 0.537 | 0.526 $\pm$ 0.015 |

## 3.5 Conclusions

From Table 3.5, the following statements can be reached:

1 The rock fracture toughness testing results using the CCNBD method are size independent once the specimen diameter is larger than 50 mm and $a_1/R$ is less than 0.85;

2 Group No.1: it showed that specimen thickness has no influence on rock fracture toughness testing results when the thickness varies from 25 to 40mm. Also the testing results by Da01 and Da05 shows that $K_{IC}$ does not change when the initial crack length varies from 15 to 20 mm;

3 Group No.2: it showed that the CCNBD specimen with long crack is not suitable for rock fracture toughness value. The lower critical stress intensity factors results generated comes from the reduced load substaining thickness because of the stress concentration of the crossing area of the loading line and chevron notches. This is also proved by the testing results in Group No.6. The critical stress intensity factors tested by this group of specimens are generally 30 % less than by the Group No.1 or other group. Therefore it is strongly suggested that the dimensionless crack length $a_1/R$ should be less than 0.85;

4 Group No.3: it showed that curved slot diameter does not affect the $K_{IC}$ testing results by comparison with Group No.1 and Group No.4. Inside the group, when the specimen thickness varies from 30 to 55 mm, the $K_{IC}$ remains unchanged;

5 Group No.4: the relatively short crack specimens are tested. It showed that specimen thickness does not affect the $K_{IC}$ value when the thickness varies from 20 to 30 mm. The testing results by Disc Da11 and Da14 showed again that initial crack length does not change the $K_{IC}$ value when the initial crack length changes from 15 to 20 mm. By comparison with Group No.1 and No.4, it showed that the curved slot diameter does not affect the $K_{IC}$ value once the specimen diameter is not less than 75 mm;

6 Group No.5: inside the group, it showed that specimen thickness does not

affect the $K_{IC}$ value when the thickness varies from 20 to 30 mm. It also proved that initial crack length does not affect the value of the $K_{IC}$. By comparison with Group No.4, it showed that specimen diameter has no influence on the $K_{IC}$ when the diameter is not less than 75 mm.

7 Group No.6: The relatively long crack specimens are tested. The results obtained are generally 40 % less than by the Group No.1 or the chevron bend specimen. It proved again that the $a_1/R$ should not be machined larger than 0.85. By comparison with the testing results by Group No.2 specimens, it showed that their results are not comparable;

8 Group No.7: It showed that the CCNBD specimen with smaller diameter is not suitable for rock fracture toughness testing. It is suggested that the specimen diameter should be larger than 50 mm;

9 If a geometry correction factor $k = 1.2$ is used, the rock fracture toughness measurement using the CCNBD method can be used for a diameter of 50 mm or less. It offers great advantages over the other two methods. In other words, the rock fracture toughness can be tested once the dimension of the rock block are larger than $60mm \times 60mm \times 30mm$.

10 The rock fracture toughness testing by Disc Da01, Da02, Da03, Da04, Da05, Da21, Da22, Da11, Da12, Da13, Da14, Db01, Db02, Db03 and Db04 showed that the testing results are quite comparable with that by the Chevron-Notched Bend method or the Chevron-Notched Short Rod method;

11 The variation coefficients of rock fracture toughness values for sandstone using the same disc are generally less than 3%.

12 The testing results by disc Db01 are quite comparable with that by Da01 etc. Also the results are quite comparable with that by the CB and SR method. Therefore disc Db01 will be used for the experimental validation of the CCNBD method for mode I rock fracture toughness measurement in Chapter 4.

## 3.6 $K_{IC}$ of Sandstone Tested by the CSTBD Specimen

For comparison with the chevron-notch specimens, the straight-through notch specimens with thickness and diameter matching those of the chevron notched Brazilian disc specimen were tested.

The procedure and the results analysis will be presented in Chapter 5. Here only some of the results are cited. It showed that the $K_{IC}$ testing when using CSTBD specimens are generally 10 percent less than that by the CCNBD method or the CB and SR methods. It also showed that the testing results by the CSTBD method are strongly dependent on the dimensionless crack length. Because only large $a/R$ samples have been used. The short crack CSTBD specimen may generate comparable results with that by the CCNBD specimen and the Chevron-Notched Bend specimen. Further research is recommended.

## 3.7 Transverse Tensile Failure

The relative compactness of the cantilever arms of the Chevron Bend Specimen will seldom induce tensile stresses of sufficient magnitude to cause transverse failure of the arms before the evaluation of fracture toughness can be made. The relative slenderness of the Short Rod arms may be satisfactory however (Ouchterlony, 1989). This phonomena has been observed during the rock fracture toughness testing using the SR method in the later experiments.

The relative compactness of the semi-disc of the CCNBD specimen makes it impossible to induce sufficient magnitude tensile stresses to cause transverse failure of the semi-disc of the CCNBD specimen. The $K_{IC}$ testing using the CCNBD method confirms this statement.

## 3.8 Comparison of Tensile Strength and $K_{IC}$ Testing Methods

If we examine the geometry of the testing specimens for rock tensile strength and mode I rock fracture toughness measurement as shown in Figure 3.8, there is quite a lot of similarity. The rock tensile strength can be tested by three-point bending method and Brazilian disc method. The rock fracture toughness measurement can be tested by the chevron-notched three-point bend method and the cracked and the cracked chevron-notched Brazilian disc method. The only

difference between these two rock property testing methods lies in that there is a slot in the center of the rock fracture toughness testing specimen. The size requirement suggested by the testing commission of the ISRM for rock tensile strength testing is that the diameter of the Brazilian disc should be larger than 55 mm and its thickness is the half of the diameter of the disc. Therefore both methods have the same requiremens for specimen diameter.

The stress distribution along the loading direction and the proposed failed sequence for both methods are presented in Figure 3.9 and Figure 3.10. In Brazilian disc testing for indirect rock tensile strength, the tensile stress distribution is uniform around the center of the disc along the loading direction. For the CCNBD specimen, the stress of the crack tip is theoretically infinite, crack propagates initially from the tip.

## 3.9 A Set of Rock Fracture Specimens Based on Disc

If a CCNBD specimen is cut into half along the diameter perpendicular to the slot direction of the CCNBD specimen, as shown in Figure 3.11, two semi-circular chevron-notched specimens are formed. Both semi-circular specimens could be used for semi-circular chevron bend and semi-circular chevron notched compact tension testing for rock fracture toughness testing. It is suggested that both the chevron bend and chevron notched compact tension methods using semi-circular specimens should be studied for rock fracture toughness testing in later research.

If a Brazilian disc and a CCNBD specimen are all cut into halves, a set of semi-circular fracture specimens can be formed, as shown in Figure 3.12. In fact semi-circular bend (straight notch) has been used by Cheng (1986) for rock fracture toughness (mode I) testing and mixed-mode rock fracture investigation.

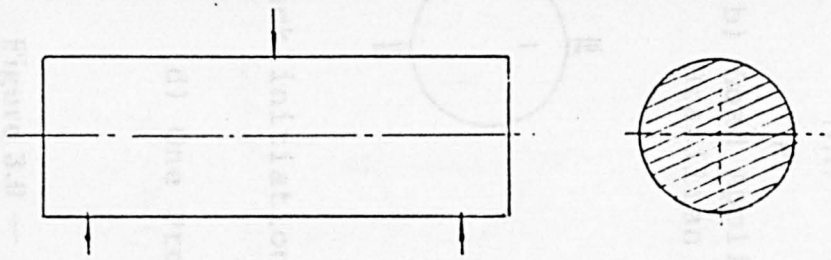

(a) Three Point Bending Specimen for Rock Tensile Strength Testing

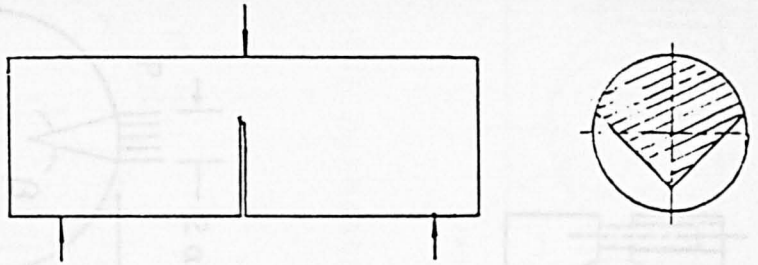

(b) Chevron-Notched Bending Specimen for Rock Fracture Toughness Testing

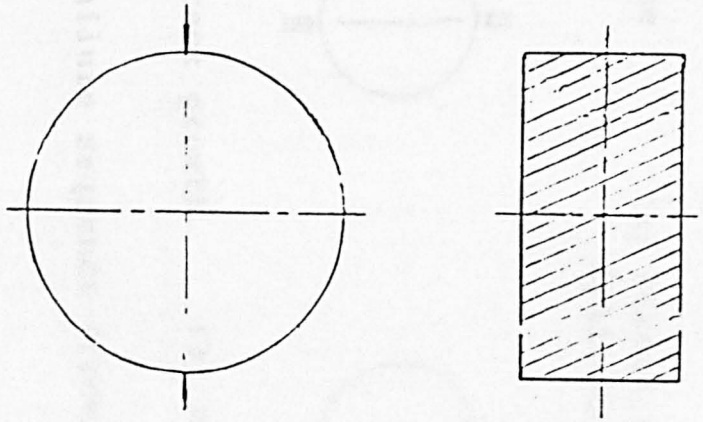

(c) Brazilian Disc for Indirect Rock Tensile Strength Testing

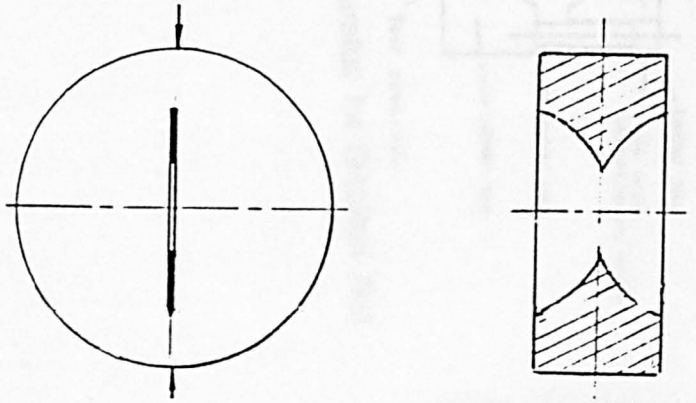

(d) Cracked-Chevron-Notched Brazilian Disc for Rock Fracture Toughness Testing

**Figure 3.8 — The Development from Rock Tensile Strength Testing to Rock Fracture Toughness Testing**

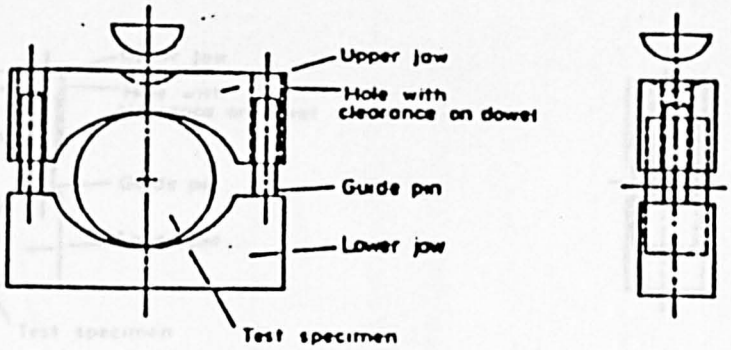


(a) Apparatus for Brazilian Test

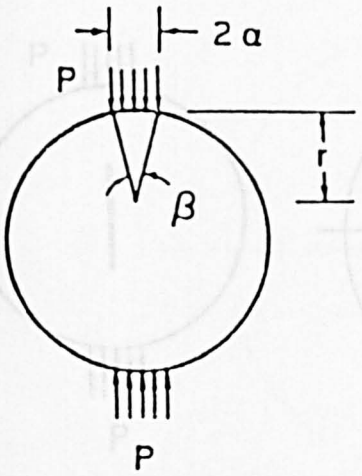


(b) Load Applied on the Brazilian Disc

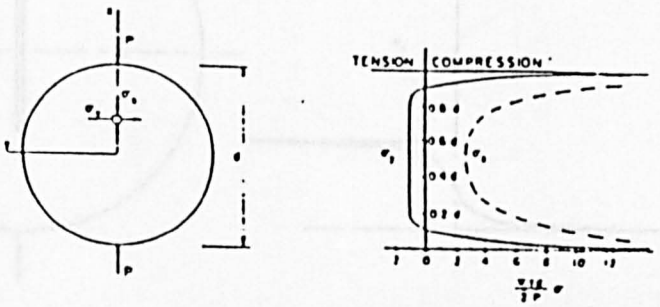


(c) Stress across Diameter of Cylinder Loaded as in (b)

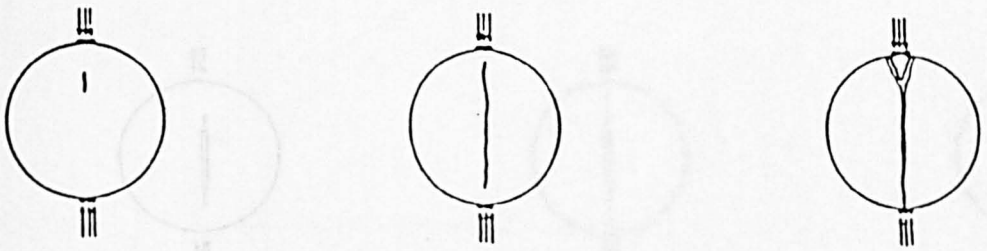

(1) Crack initiation (2) Crack growth (3) Failure

(d) One Proposed Failure Sequence (from Hannant, 1973)

**Figure 3.9 — Rock Tensile Strength Testing Using Brazilian Disc**

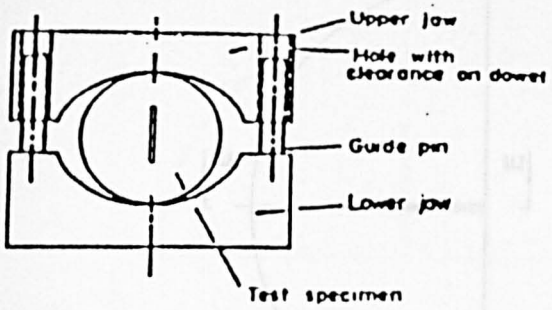


(a) Apparatus for Kic Testing Using the CCNBD Method

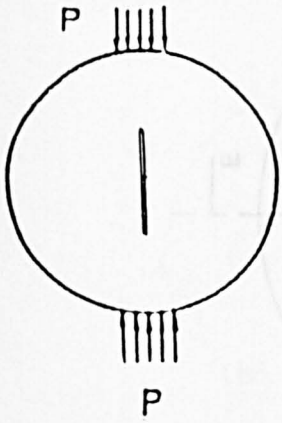


(b) Load Applied on the CCNBD Specimen

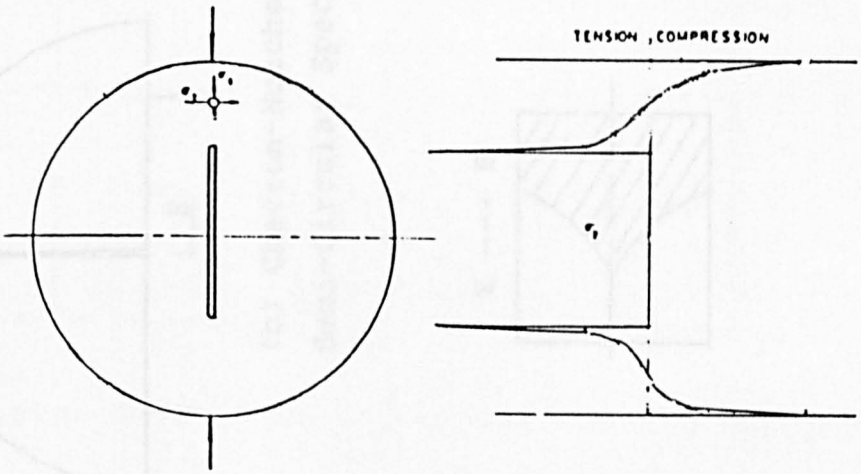


(c) Stress across Diameter of Cylinder Loaded as in (b)

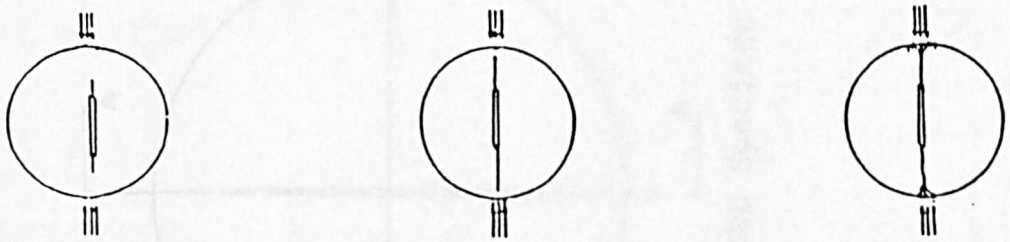

(1) Crack initiation (2) Crack growth (3) Failure

(d) One Proposed Failure Sequence

Figure 3.10 — Rock Fracture Toughness Testing Using the CCNBD Method

**Figure 3.11 — A Set of the Chevron-notched Semi-circular Specimens**

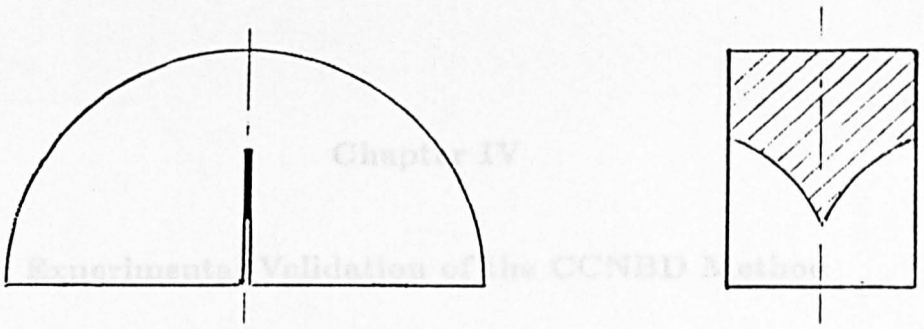

(a) Chevron-Notched Compact Tension Specimen

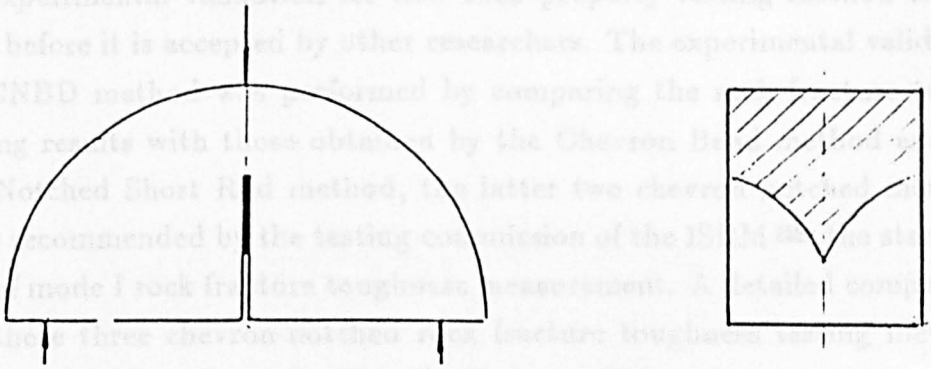

(b) Chevron-Notched Semi-Circular Bending Specimen

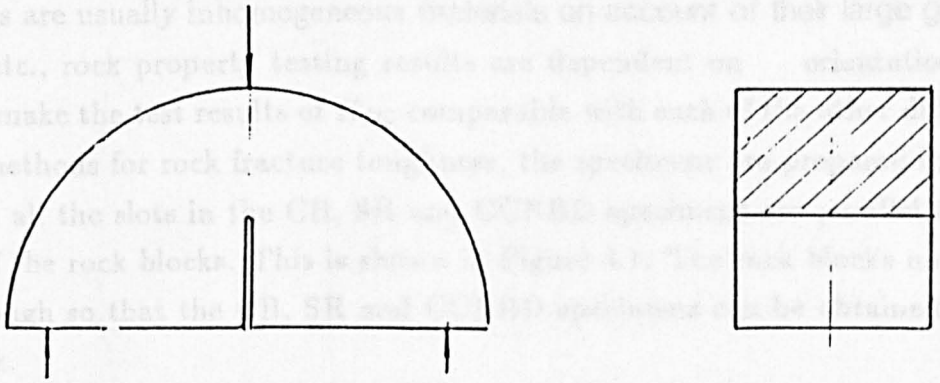

(c) Semi-Circular Bending Specimen

**Figure 3.12 — A Set of Semi-circular Fracture Specimens**

# Chapter IV

## Experimental Validation of the CCNBD Method

### 4.1 Introduction

The experimental validation for new rock property testing method is very necessary before it is accepted by other researchers. The experimental validation of the CCNBD method was performed by comparing the rock fracture toughness testing results with those obtained by the Chevron Bend method and the Chevron-Notched Short Rod method, the latter two chevron notched methods have been recommended by the testing commission of the ISRM as the standard methods of mode I rock fracture toughness measurement. A detailed comparison between these three chevron-notched rock fracture toughness testing methods was performed. The effect of rock anisotropy on the rock fracture toughness testing results was studied.

### 4.2 Specimen Selection

Rocks are usually inhomogeneous materials on account of their large grain size, fissures etc., rock property testing results are dependent on orientation. In order to make the test results of $K_{IC}$ comparable with each of the other different testing methods for rock fracture toughness, the specimens are prepared in such way that all the slots in the CB, SR and CCNBD specimens are parallel to the X-axis of the rock blocks. This is shown in Figure 4.1. The rock blocks must be large enough so that the CB, SR and CCNBD specimens can be obtained from one block.

All core based specimens should be marked with a reference using a waterproof pen before the specimens are prepared so that the core axis and the slot directions relative to rock fabric, block sample faces, core log etc. are known. All samples are preserved in the air-dried state.

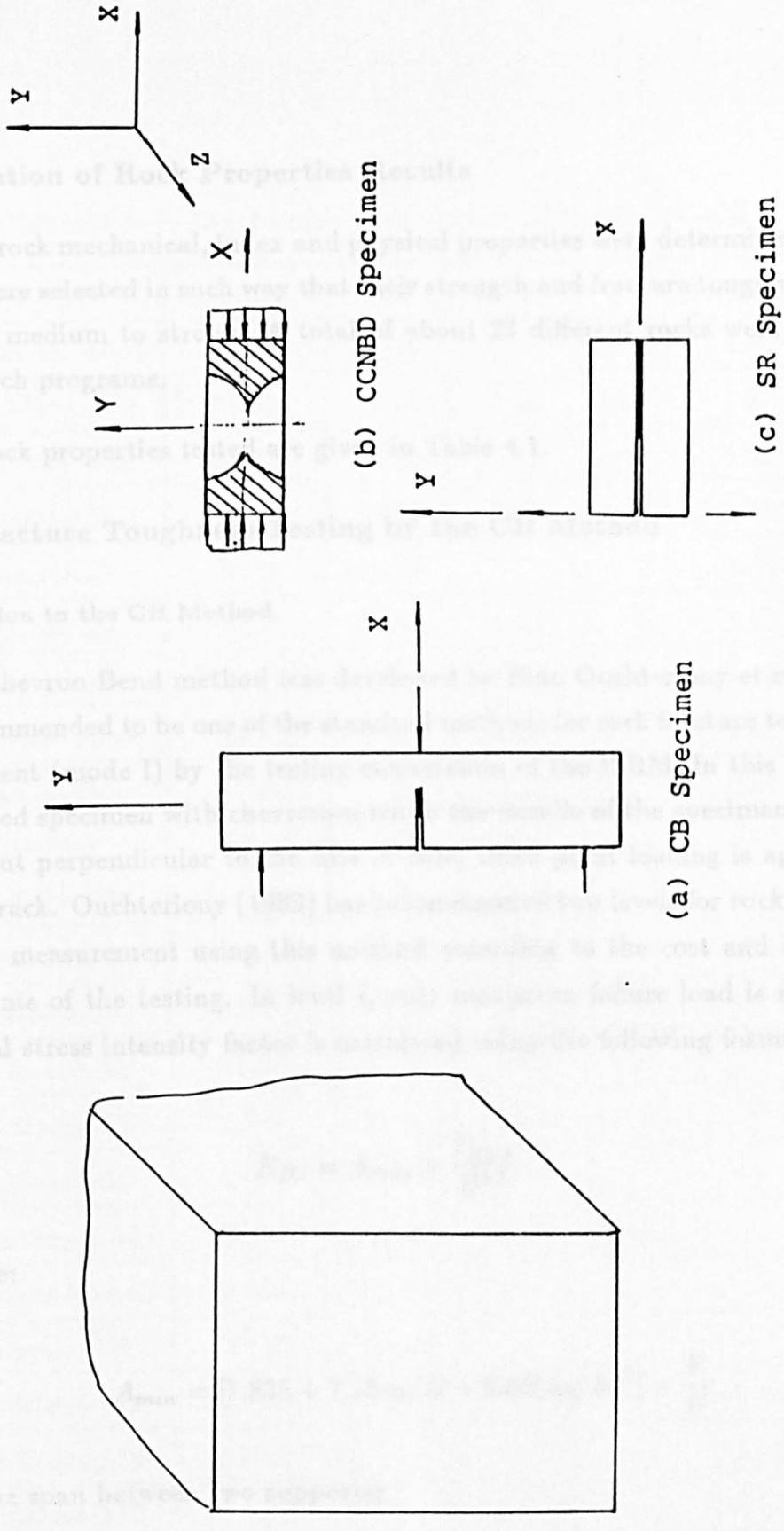


**Figure 4.1 — The Slot Orientation for the CB, SR and CCNBD Specimen Preparation**

## 4.3 Presentation of Rock Properties Results

Many rock mechanical, index and physical properties were determined. Rock samples were selected in such way that their strength and fracture toughness vary from soft, medium to strong. A total of about 23 different rocks were used in this research programe.

The rock properties tested are given in Table 4.1.

## 4.4 Rock Fracture Toughness Testing by the CB Method

### 4.4.1 Introduction to the CB Method

The Chevron Bend method was developed by Finn Ouchterlony et al. It has been recommended to be one of the standard methods for rock fracture toughness measurement (mode I) by the testing commission of the ISRM. In this method, a core based specimen with chevron-notch in the middle of the specimen is used, a slot is cut perpendicular to the axis of core, three point loading is applied to part the crack. Ouchterlony (1989) has recommended two levels for rock fracture toughness measurement using this method according to the cost and accuracy requirements of the testing. In level I, only maximum failure load is recorded, the critical stress intensity factor is calculated using the following formulae:

$$K_{IC} = A_{min} \times \frac{P_{max}}{D^{1.5}} \tag{4.1}$$

Where:

$$A_{min} = [1.835 + 7.15a_0/D + 9.85(a_0/D)^2] \times \frac{S}{D} \tag{4.2}$$

S – the span between two supports;

D – the diameter of the core specimen;

$a_0/D$ – the dimensionless initial crack length.

**Table 4.1 — Mechanical Properties of Rocks Tested**

| Rock Type | UCS,(MPa) | E (GPa) | $\sigma_t$, (MPa) | $\mu$ | Cone Indenter |
|---|---|---|---|---|---|
| Pennant Sandstone | 197.17 | 17.86 | 11.22 | 0.23 | 2.68 |
| Sandstone-Dos | 69.35 | 13.58 | 2.58 | 0.24 | 1.67 |
| Sandstone-Disc | 47.03 | 11.26 | 2.87 | 0.23 | 1.54 |
| Limestone-Eim | 62.91 | 32.68 | 2.72 | | 1.78 |
| Limestone-2 | 58.21 | 10.28 | | | 1.53 |
| Limestone-Hard | 134.32 | 31.23 | 6.62 | | 2.02 |
| Gneiss-Eim5 | 292.66 | | 12.40 | | 2.99 |
| Rhyolite-Eim4 | 126.42 | 30.74 | 8.81 | | 2.01 |
| Gypsum-Dos | 34.47 | | 2.30 | | 0.54 |
| Ore-Eim | 133.38 | | 3.82 | | 1.78 |
| Sandstone-Fai | 47.21 | 9.26 | | | 1.04 |
| Sandstone-7 | 58.71 | 9.73 | | | 0.78 |
| Sandstone-9 | 63.21 | 11.28 | | | |
| Sandstone-31 | 71.34 | 12.86 | 4.58 | | |
| Sandstone-33 | 27.46 | 11.76 | 2.54 | | |
| Sandstone-34 | 68.21 | 12.13 | | | |
| Sandstone-Spr41 | 38.30 | 11.90 | 3.02 | 0.28 | |
| Gypsum-Pink48 | 63.31 | 13.19 | | | |
| Limestone-54 | 121.27 | 19.26 | | | |
| Sandstone-S15 | 33.53 | | | | 1.84 |
| Sandstone-S18 | 37.85 | | | | 1.75 |
| Sandstone-S19 | 45.23 | | | | 2.07 |
| Sandstone-S25 | 29.34 | | | | 1.84 |
| Sandstone-S26 | 21.23 | | | | 1.91 |

Level II rock fracture toughness testing is quite complicated. It involves plasticity correction for the rock material. Testing is performed under constant loading point displacement rate. Load vs loading point displacement is recorded. The calculation of stress intensity factors stated as in eqn(4.1). Then a non-linearity correction factor shall be evaluated in the load vs LPD record using the graphical construction methods suggested by Ouchterlony (1988).

In this research, the procedures for level I testing were used.

### 4.4.2 The Geometry of the Chevron Bend Specimen

The geometry with basic notation of the chevron bend specimen is shown in Figure 4.2. The standard geometry of the CB specimen suggested by Ouchterlony (1988) is used. The standard geometry specimen dimensions are listed in Table 4.2.

Table 4.2 — The Dimensions of the CB Specimen

| Geometry parameter | Value | Tolerance |
|---|---|---|
| Specimen diameter | D | $\geq 10 \times$ *grain size* |
| Specimen length | $4 \times D$ | $\geq 3.5 \times D$ |
| Support span, S | $3.33 \times D$ | $\pm 0.02 \times D$ |
| Subtended chevron, angle $\theta$ | $90.0^o$ | $\pm 1.0^o$ |
| Chevron V tip position, $a_0$ | $0.15 \times D$ | $\pm 0.10 \times D$ |
| Notch width, t | 1.2 mm | or less |

### 4.4.3 The Chevron Bend Specimen Preparation

The cores specimen from the rock blocks shall be obtained as instructed in Figure 4.1. The machining of the Chevron-Notched Bending Specimen is shown in Photo 4.1 and Figure 4.3. The reference points used for the guide of specimen preparation and loading were marked using water-proof pen. A diamond saw, a milling machine and specimen holding specimen were used to cut a notch.

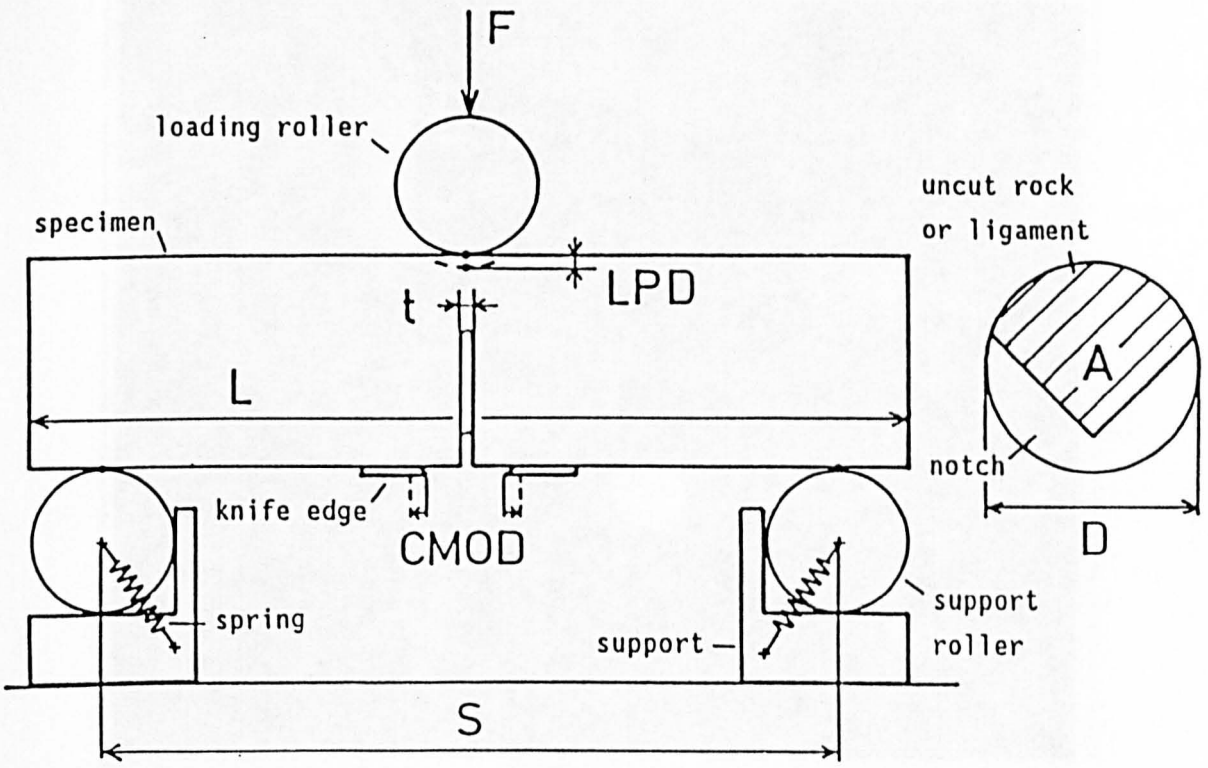


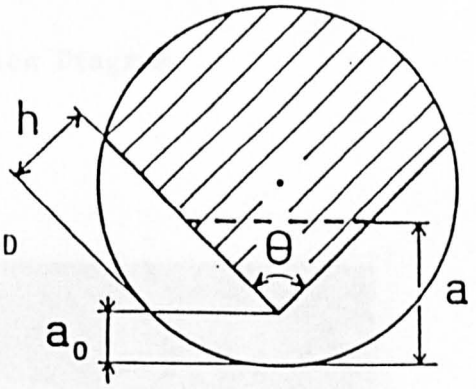


Basic notation:

D = diameter of chevron bend specimen
S = distance between support points, 3.33·D
$\theta$ = chevron angle, 90°
$a_0$ = chevron tip distance from specimen surface, 0.15·D.
a = crack length
t = notch width
h = depth of cut in notch flank
L = specimen length
A = projected ligament area
F = load on specimen
LPD = deflection of load point relative to support points
CMOD = relative opening of knife edges

**Figure 4.2 — The Geometry with Basic Notation of the CB Specimen, From Ouchterlony, (1988)**

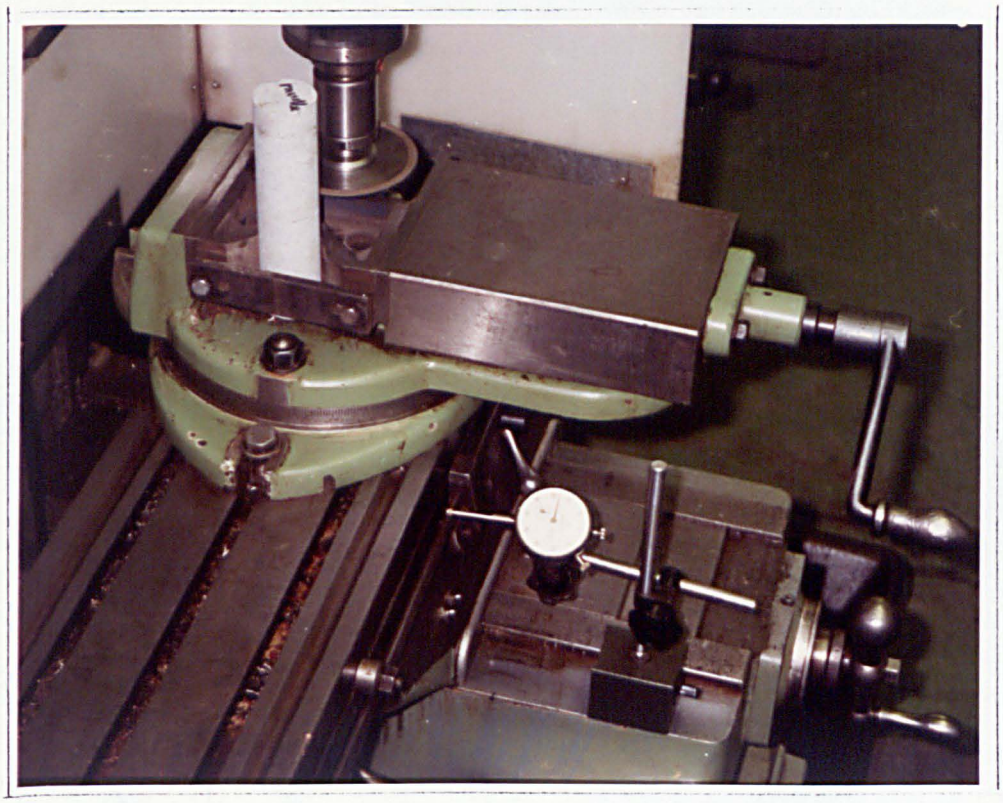

Photo 4.1 - The CB Specimen Preparation Diagram

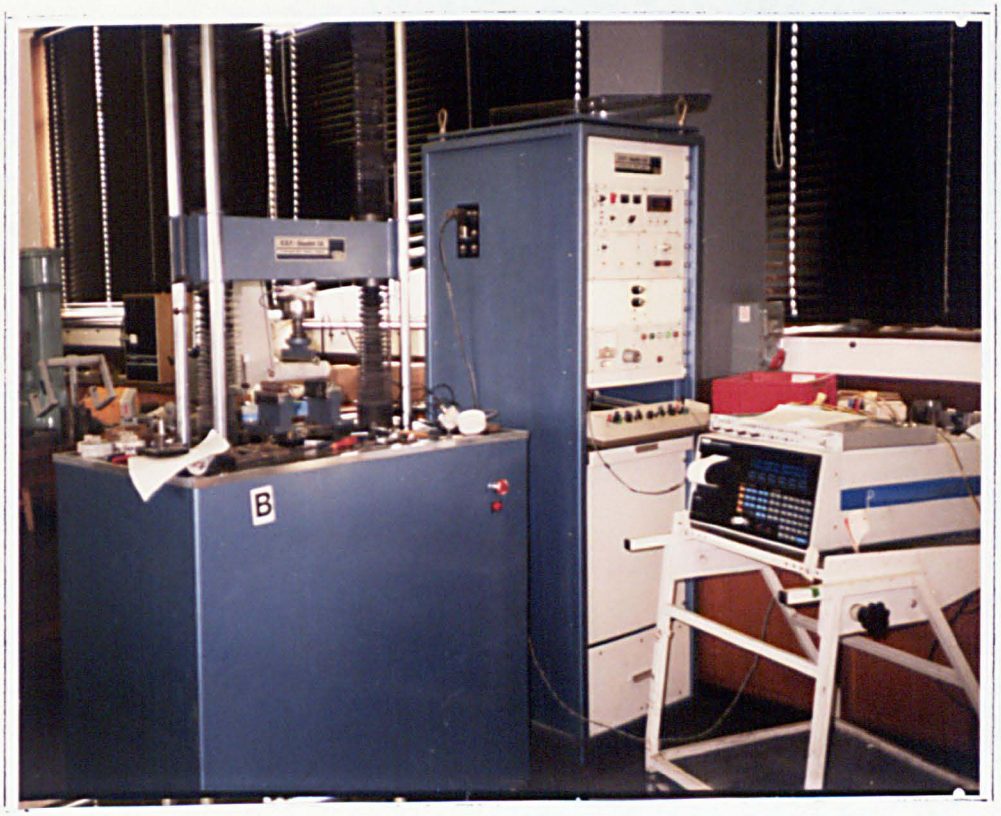


Photo 4.2 - Experimental Rig of Rock Testing Using the CB Method

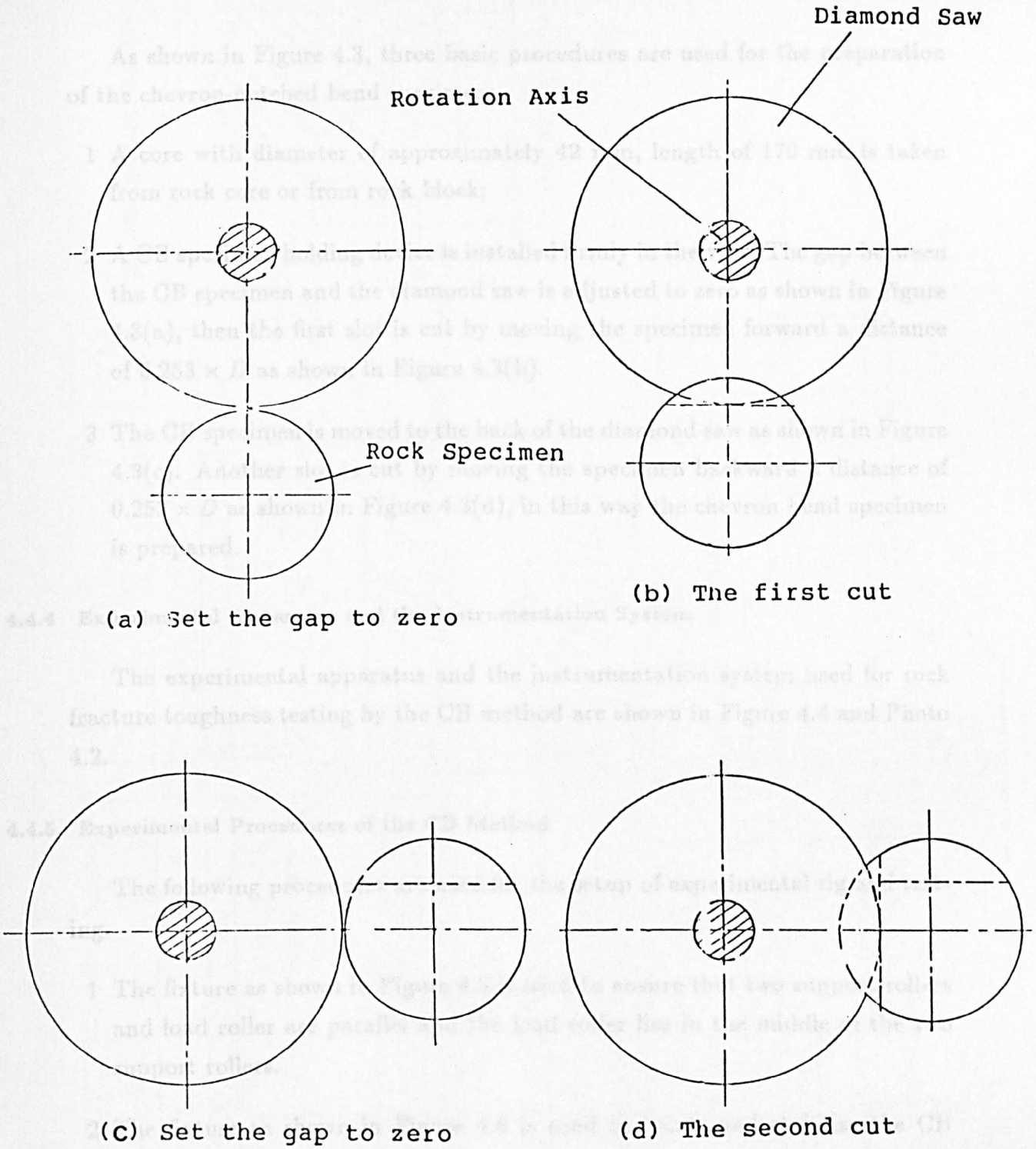


**Figure 4.3 — The Diagram of the CB Specimen Preparation**

As shown in Figure 4.3, three basic procedures are used for the preparation of the chevron-notched bend specimen:

1 A core with diameter of approximately 42 mm, length of 170 mm is taken from rock core or from rock block;

2 A CB specimen holding device is installed firmly in the vice. The gap between the CB specimen and the diamond saw is adjusted to zero as shown in Figure 4.3(a), then the first slot is cut by moving the specimen forward a distance of $0.253 \times D$ as shown in Figure 4.3(b).

3 The CB specimen is moved to the back of the diamond saw as shown in Figure 4.3(c). Another slot is cut by moving the specimen backward a distance of $0.253 \times D$ as shown in Figure 4.3(d), in this way the chevron bend specimen is prepared.

#### 4.4.4 Experimental Apparatus and the Instrumentation System

The experimental apparatus and the instrumentation system used for rock fracture toughness testing by the CB method are shown in Figure 4.4 and Photo 4.2.

#### 4.4.5 Experimental Procedures of the CB Method

The following procedures are used for the setup of experimental rig and testing.

1 The fixture as shown in Figure 4.5 is used to ensure that two support rollers and load roller are parallel and the load roller lies in the middle of the two support rollers.

2 The fixture as shown in Figure 4.6 is used to locate and stabilize the CB specimen. It is located directly under the load roller, parallel to the two support roller and lies in the middle of the two support rollers. The tip of the chevron section of the metal blade should lie in the axis line of the load cell. The level is used to make sure that the both sides of the chevron section of the metal blade are symmetrcall to the axis of the load cell.

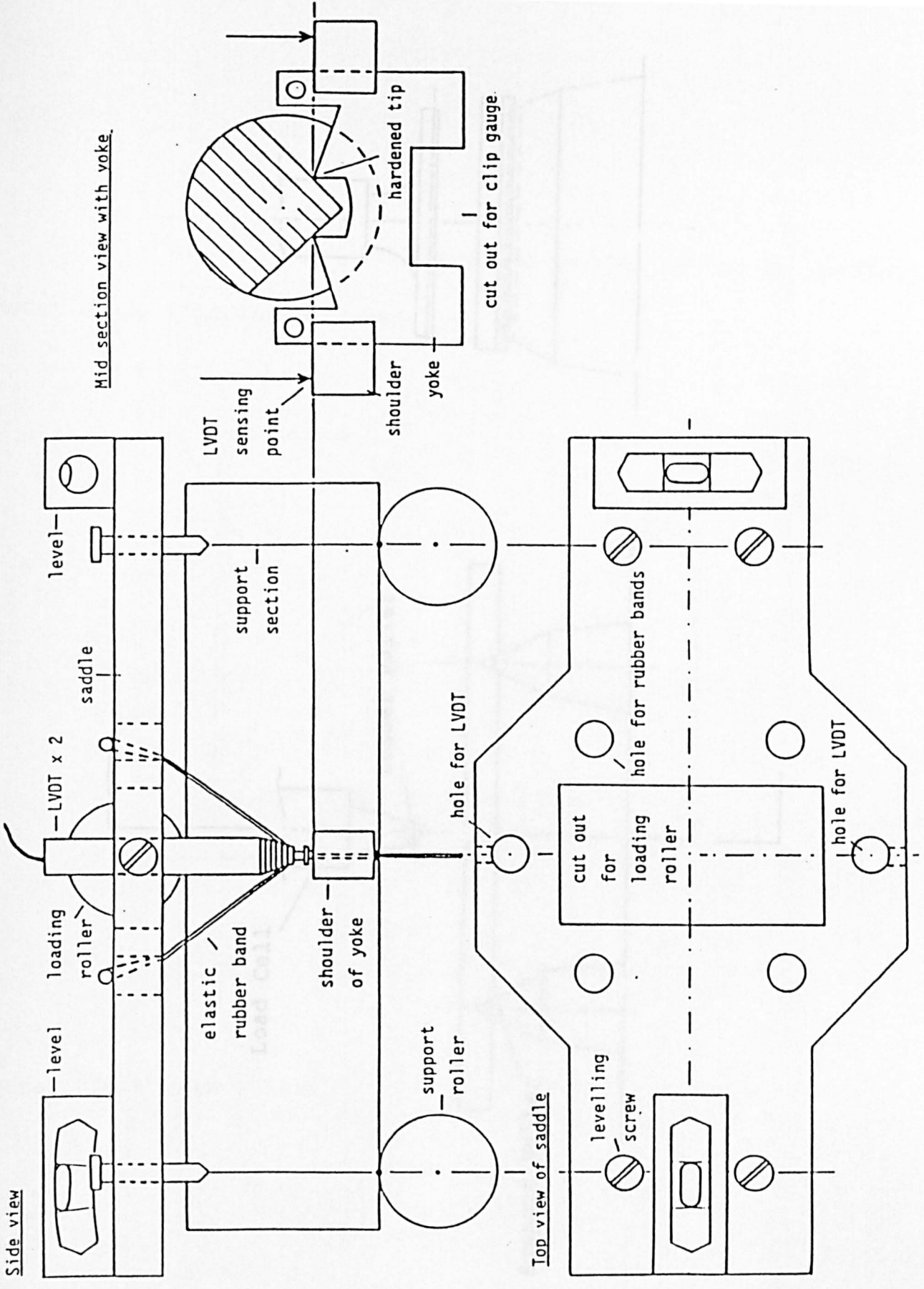


**Figure 4.4 — Experimental Diagram for $K_{IC}$ Testing Using the CB Method**

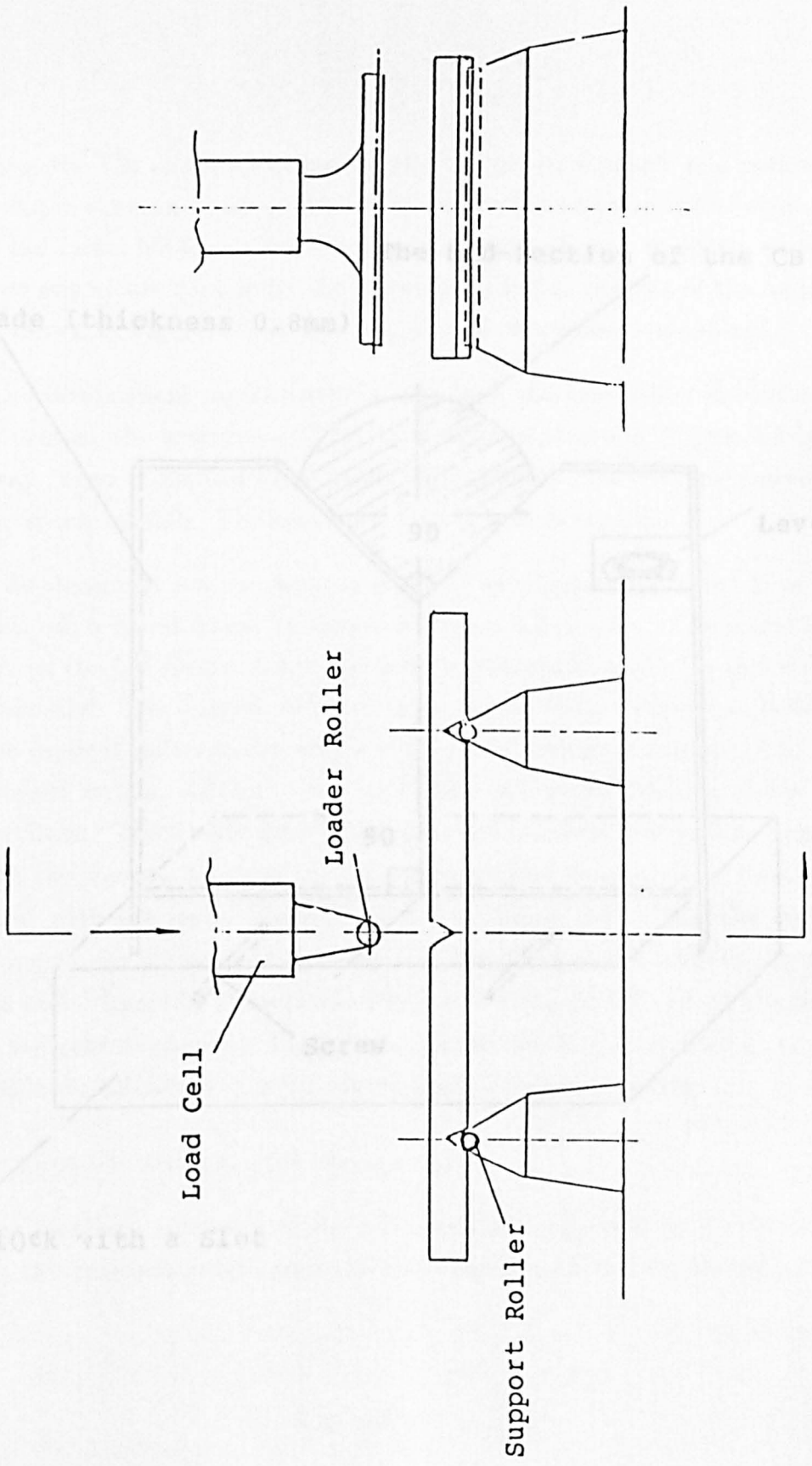


**Figure 4.5 — Diagram of the Device for the CB Specimen Setup**

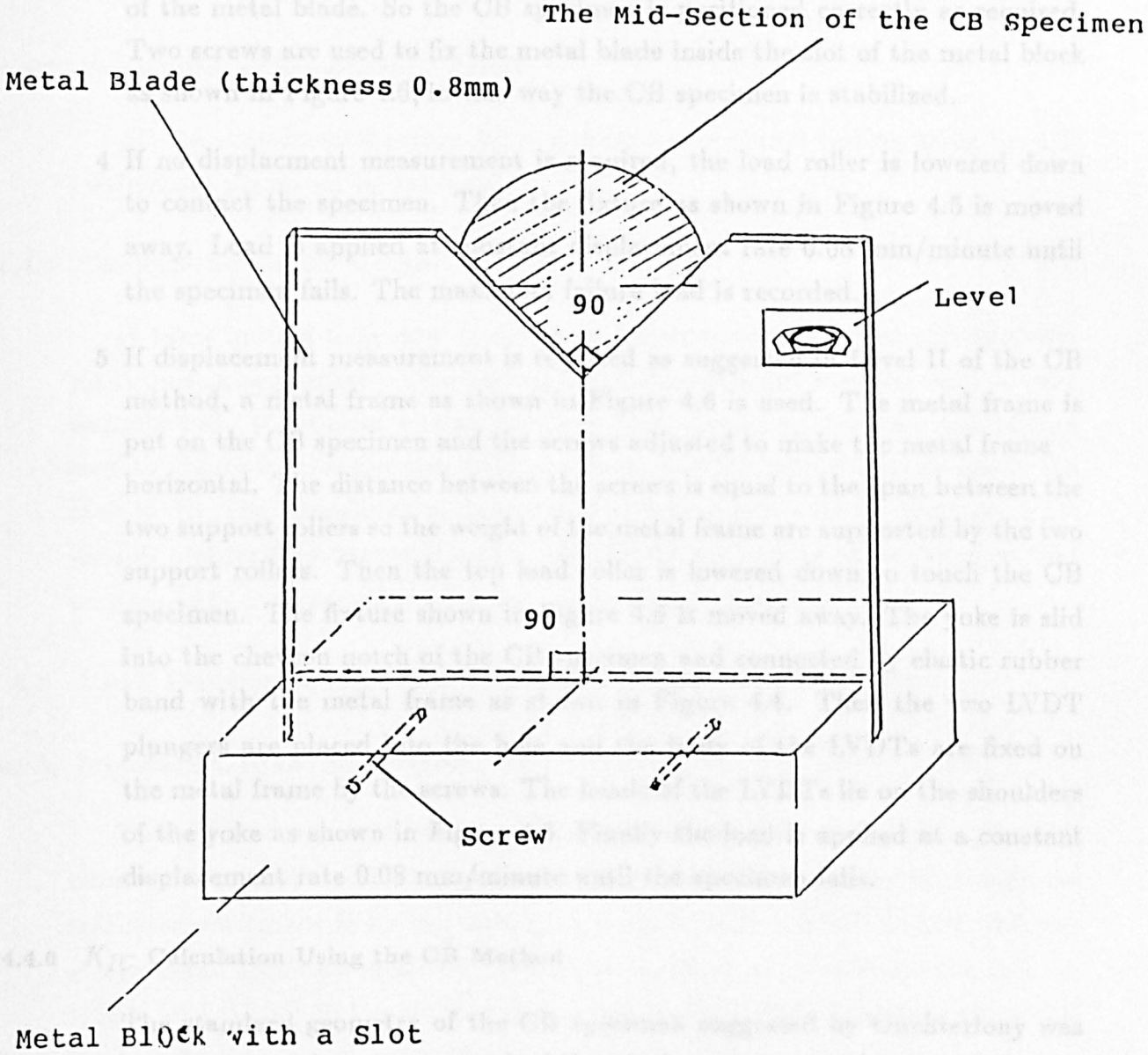


**Figure 4.6 — The Diagram of the CB Specimen Rotation Alignment Fixture**

3 Then the CB specimen is put on the two support rollers and makinge sure that the chevron notch of the CB specimen lies right on the chevron section of the metal blade. So the CB specimen is positioned correctly as required. Two screws are used to fix the metal blade inside the slot of the metal block as shown in Figure 4.6, in this way the CB specimen is stabilized.

4 If no displacment measurement is required, the load roller is lowered down to contact the specimen. Then the fixture as shown in Figure 4.5 is moved away. Load is applied at constant displacement rate 0.08 mm/minute until the specimen fails. The maximum failure load is recorded.

5 If displacement measurement is required as suggested in Level II of the CB method, a metal frame as shown in Figure 4.6 is used. The metal frame is put on the CB specimen and the screws adjusted to make the metal frame horizontal. The distance between the screws is equal to the span between the two support rollers so the weight of the metal frame are supported by the two support rollers. Then the top load roller is lowered down to touch the CB specimen. The fixture shown in Figure 4.6 is moved away. The yoke is slid into the chevron notch of the CB specimen and connected by elastic rubber band with the metal frame as shown in Figure 4.4. Then the two LVDT plungers are placed into the hole and the body of the LVDTs are fixed on the metal frame by the screws. The heads of the LVDTs lie on the shoulders of the yoke as shown in Figure 4.6. Finally the load is applied at a constant displacement rate 0.08 mm/minute until the specimen fails.

### 4.4.6 $K_{IC}$ Calculation Using the CB Method

The standard geometry of the CB specimen suggested by Ouchterlony was used in this research programme, the following formula is used for the calculation of $K_{IC}$.

$$K_{IC} = 10.42 \times \frac{P_{max}}{D^{1.5}} \tag{4.3}$$

Where:

$K_{IC}$ – Mode I rock fracture toughness ($MN/m^{1.5}$);

$P_{max}$ – Maximum failure load (kN);

D – The CB specimen diameter (cm).

### 4.4.7 Presentation of Experimental Results

All the experimental results for rock fracture toughness testing using the CB method are presented in Table 4.5.

### 4.4.8 Comment for the CB Methods

It takes quite a long time to setup the experimental rig. The experimental rig is quite complicated. The loading point displacement measurement is very compliacted. It requires a relatively long core specimen, these are not always easy to obtain from rock cores or blocks because of the discontinuities inside the rock body. The magnitude of failure load is very small (usually less than 1 kN for soft and medium strength rocks), therefore great care must be taken so that no preload is used even for the setup of the experimental rig.

## 4.5 Rock Fracture Toughness Measurement by the SR Method

### 4.5.1 Introduction to the SR Method

This method was developed by Barker and Ouchterlony et al. It has been recommended to be the second chevron-notched method for rock fracture toughness measurement (mode I) by the testing commission of the ISRM. In this method, a core based specimen is used. The chevron notch is cut parallel to the axis. A tensile load is applied to part the crack. Ouchterlony (1988) suggested two levels for rock fracture toughness testing according the testing accuracy and costs.

In this research programme, the testing results are for the experimental validation of the CCNBD method. Level I testing procedures are used.

### 4.5.2 The Geometry of the SR Specimen

The geometry with basic notation of the short rod specimen is shown in Figure 4.7.

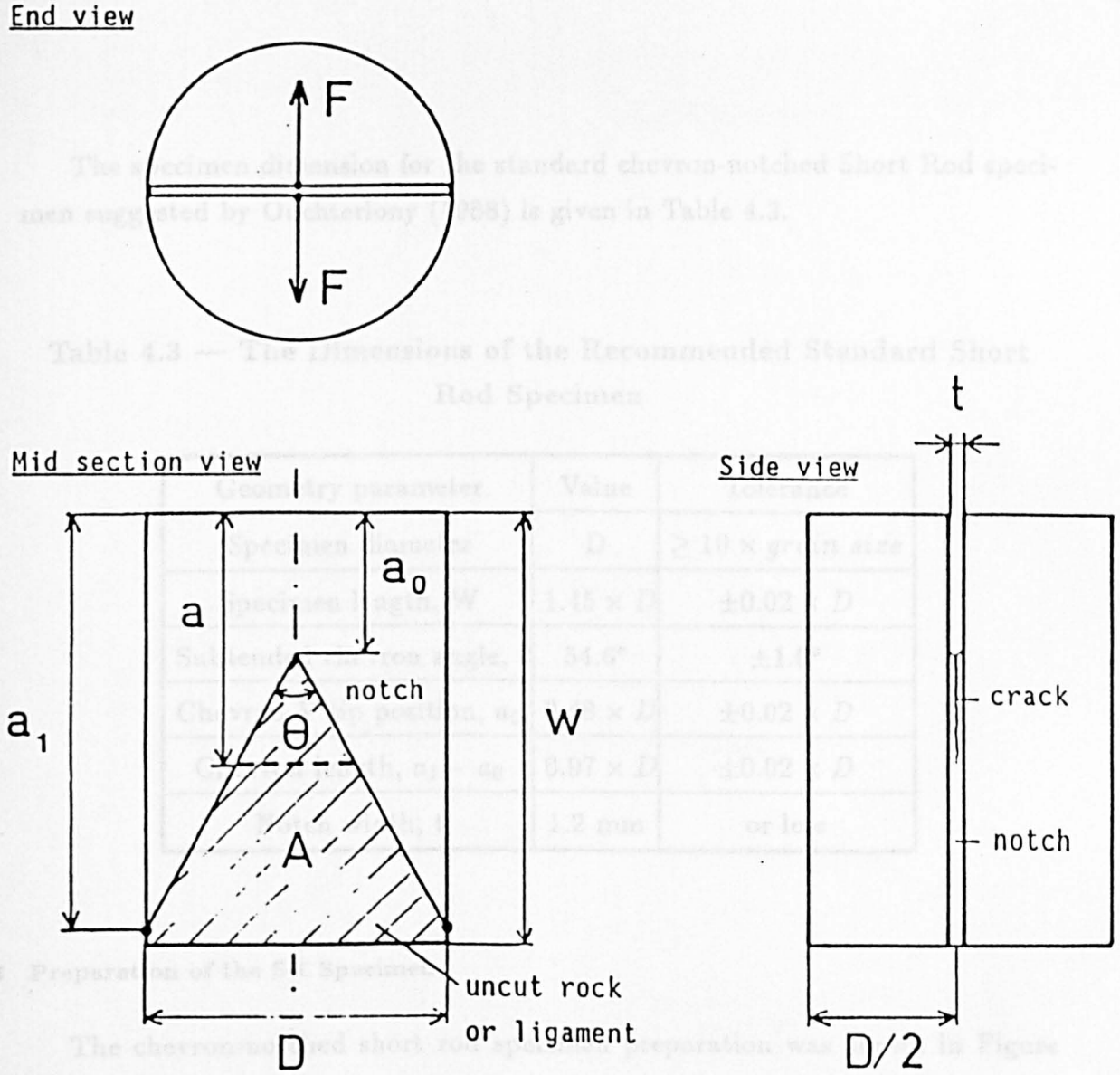


Basic notation:

D = diameter of short rod specimen
w = length of specimen, 1.45D
$\theta$ = chevron angle, 54.6°
$a_0$ = chevron tip distance from loaded end, 0.48·D
a = crack length
$a_1$ = maximum depth of chevron flanks
t = notch width
A = projected ligament area
F = load on specimen

**Figure 4.7 — The Geometry with Basic Notation of the SR Specimen, From Ouchterlony, (1988)**

The specimen dimension for the standard chevron-notched Short Rod specimen suggested by Ouchterlony (1988) is given in Table 4.3.

Table 4.3 — The Dimensions of the Recommended Standard Short Rod Specimen

| Geometry parameter | Value | Tolerance |
|---|---|---|
| Specimen diameter | D | $\geq 10 \times$ *grain size* |
| Specimen length, W | $1.45 \times D$ | $\pm 0.02 \times D$ |
| Subtended chevron angle, $\theta$ | $54.6^{o}$ | $\pm 1.0^{o}$ |
| Chevron V tip position, $a_0$ | $0.48 \times D$ | $\pm 0.02 \times D$ |
| Chevron length, $a_1 - a_0$ | $0.97 \times D$ | $\pm 0.02 \times D$ |
| Notch width, t | 1.2 mm | or less |

#### 4.5.3 Preparation of the SR Specimen

The chevron-notched short rod specimen preparation was shown in Figure 4.8 and Photo 4.3. A diamond saw, a specimen holding device and a milling machine are used to cut a notch.

As shown in Photo 4.3 and Figure 4.8, four basic procedures are used for the short rod specimen preparation:

1 The short rod specimens were prepared from rock blocks. All of the cores had a nominal diameter, D, of approximately 42 mm. The actual specimen diameter ranged from 42.2 to 44.2 mm. The specimen is cut to a nominal length of $1.5 \times B$ using a standard water cooled rock cut-off saw. The ends are made parallel by proper adjustment of the core guide prior to cutting;

2 The rig used for holding SR specimens is setup to an angle of 27.3 degrees as shown in Figure 4.8(a);

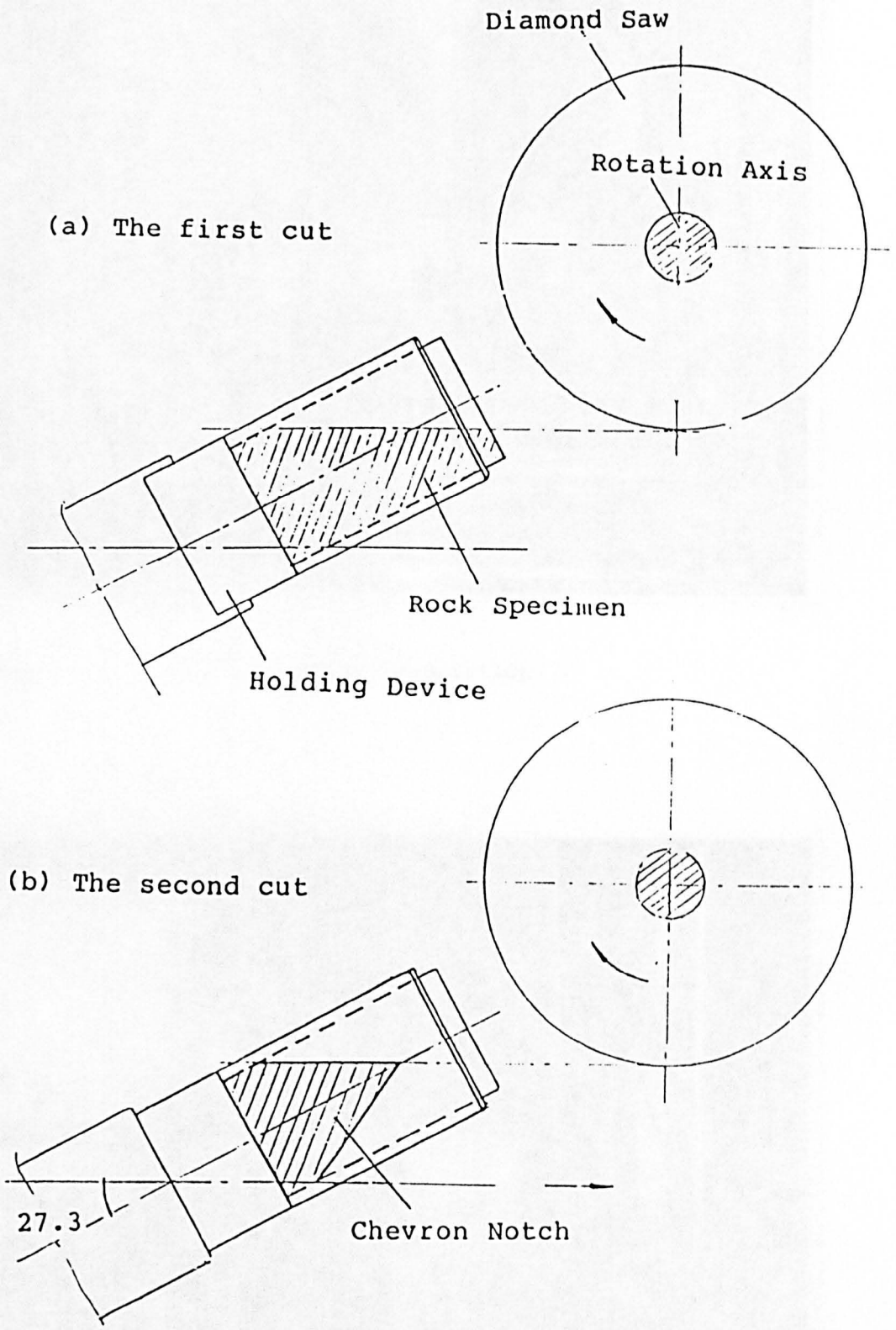


**Figure 4.8 — The Short Rod Specimen Preparation Diagram**

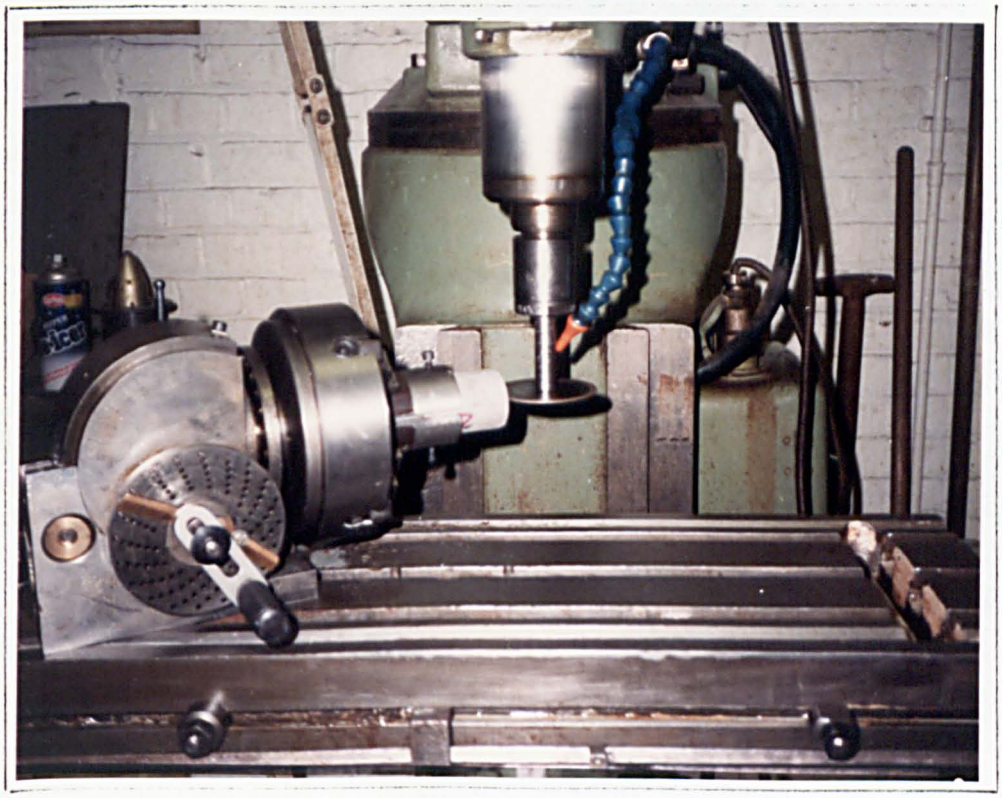

Photo 4.3 - The SR Specimen Preparation

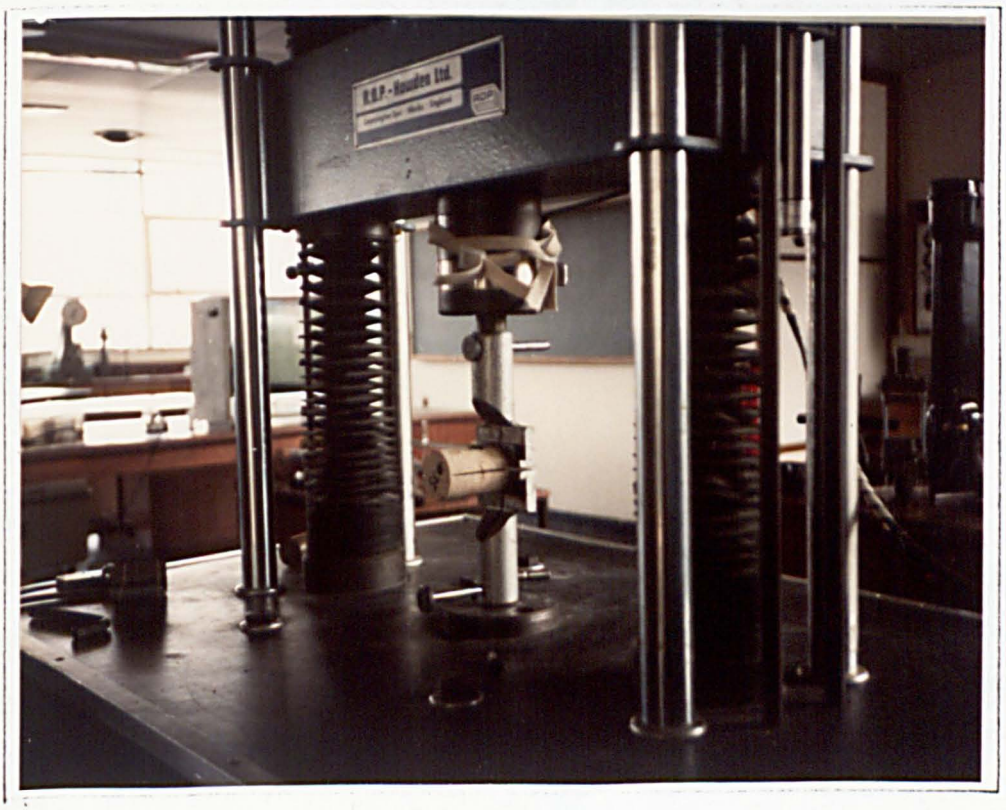


Photo 4.4 - Experimental Apparatus of Rock Testing Using the SR Method

3 The first slot is cut by moving the rig leftward and forward to the required cutting depth as shown in Figure 4.8(a).

4 Then the specimen is rotated 180 degrees by adjusting the holding rig, the second slot is cut by moving the rig leftward and forward to the required cutting depth as shown Figure 4.8(b), so far the SR specimen is prepared;

5 Lastly, two aluminum end plates, of approximately 50 by 15 by 4 mm, are glued to the top surface to act as loading lines for the splitting force. The end plates must be parallel and equi-distant from the central crack. This was accomplished with a parallel-sided spacer bar which has a central stem which rests in the saw cut. After 24 hours, the specimen is ready for testing. Preparation time is such that a technican with minimal training could prepare 20 specimens a day from rock cores.

### 4.5.4 Calculation of $K_{IC}$ using the SR method

The standard geometry short rod specimen is used. The following formula is used for the calculation of $K_{IC}$:

$$K_{IC} = 24.0 \times \frac{P_{max}}{D^{1.5}} \tag{4.4}$$

Where:

$K_{IC}$ – Mode I rock fracture toughness ($MN/m^{1.5}$);

$P_{max}$ – Maximum failure load (kN);

D – The SR specimen diameter (cm).

### 4.5.5 Experimental Procedures of the SR Method

The procedures as suggested for Level I of the SR method were used. The fixtures as shown in Figure 4.9 are used to part the crack by tensile loading. If necessary a sling is used to balance at the end of the SR specimen. The load is applied through the loading bar at a constant displacement rate 0.08 mm/minute.

The maximum failure load is recorded. The rock fracture toughness is calculated using Equation (4.5).

The experimental apparatus is shown in Figure 4.9 and Photo 4.4.

### 4.5.6 Presentation of Experimental Results

All the rock fracture toughness testing results using the Short Rod method are presented in Table 4.5.

### 4.5.7 Comment for the SR Method

The SR method requires a tensile load. Each time, two aluminum end plates have to be glued to the surface of the SR specimen, therefore it is quite time-consumming. The magnitude of the failure load is quite small, therefore great care must be taken in order to make sure that any contact between loading fixture and the SR specimen does not fail the specimen. Transverse tensile failure exists.

## 4.6 Rock Fracture Toughness Testing by the CCNBD Method

### 4.6.1 Introduction

The CCNBD method for rock fracture toughness measurement was proposed and developed by Chen (1989). In this method, a compressive load is applied along the slot direction to part the crack. As analysed in Chapter 3, the CCNBD specimen ID Db01 is used for the experimental validation of the CCNBD method.

### 4.6.2 Dimensions of the CCNBD Specimen Used Here

The geometry of the CCNBD specimen Db01 is shown in Figure 4.10. Its dimensions are listed in Table 4.4.

### 4.6.3 Calculation Formula for $K_{IC}$ Using the CCNBD Method

The disc Db01 is used for the validation experiment. The following formula is used for the calculation of $K_{IC}$:

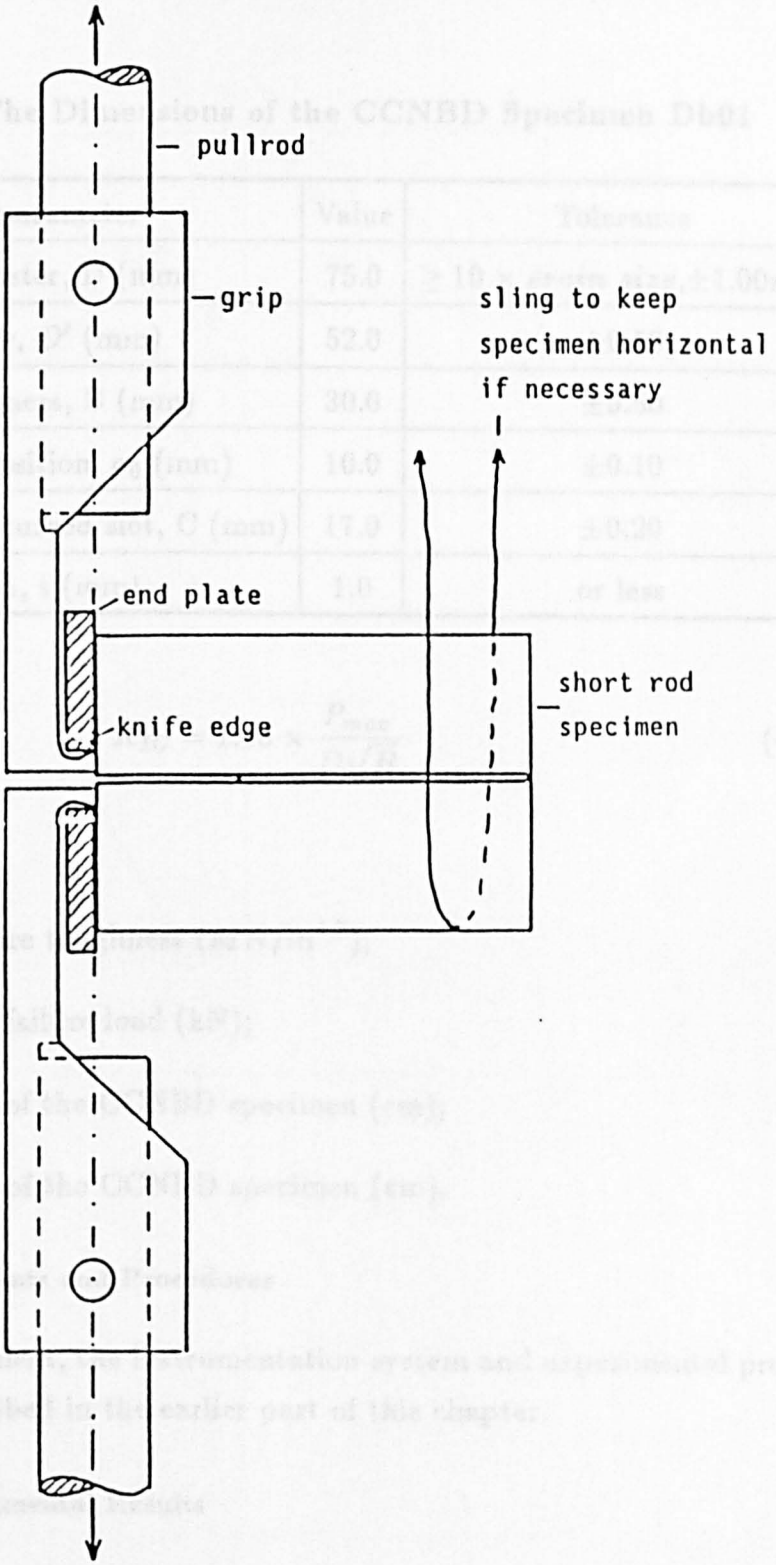


**Figure 4.9 — Experimental Diagram of $K_{IC}$ Testing Using the SR Method**

Table 4.4 — The Dimensions of the CCNBD Specimen Db01

| Geometry parameter | Value | Tolerance |
|---|---|---|
| Specimen diameter, D (mm) | 75.0 | $\geq 10 \times grain\ size$,$\pm 1.00mm$ |
| Saw diameter, $D'$ (mm) | 52.0 | $\pm 0.50$ |
| Specimen thickness, B (mm) | 30.0 | $\pm 0.50$ |
| Chevron V tip position, $a_0$ (mm) | 10.0 | $\pm 0.10$ |
| Cutting depth of the curved slot, C (mm) | 17.0 | $\pm 0.20$ |
| Notch width, t (mm) | 1.0 | or less |

$$K_{IC} = 1.18 \times \frac{P_{max}}{D\sqrt{B}} \tag{4.3}$$

Where:

$K_{IC}$ – Rock fracture toughness ($MN/m^{1.5}$);

$P_{max}$ – Maximum failure load (kN);

D – The diameter of the CCNBD specimen (cm);

B – The thickness of the CCNBD specimen (cm).

### 4.6.4 Experimental Equipments and Procedures

The testing equipment, the instrumentation system and experimental procedures have been described in the earlier part of this chapter.

### 4.6.5 Presentation of Experimental Results

After the test, the maximum failure load is recorded. The rock fracture toughness value is calculated using Equation (4.3) for each rock sample. The results are presented in Table 4.5.

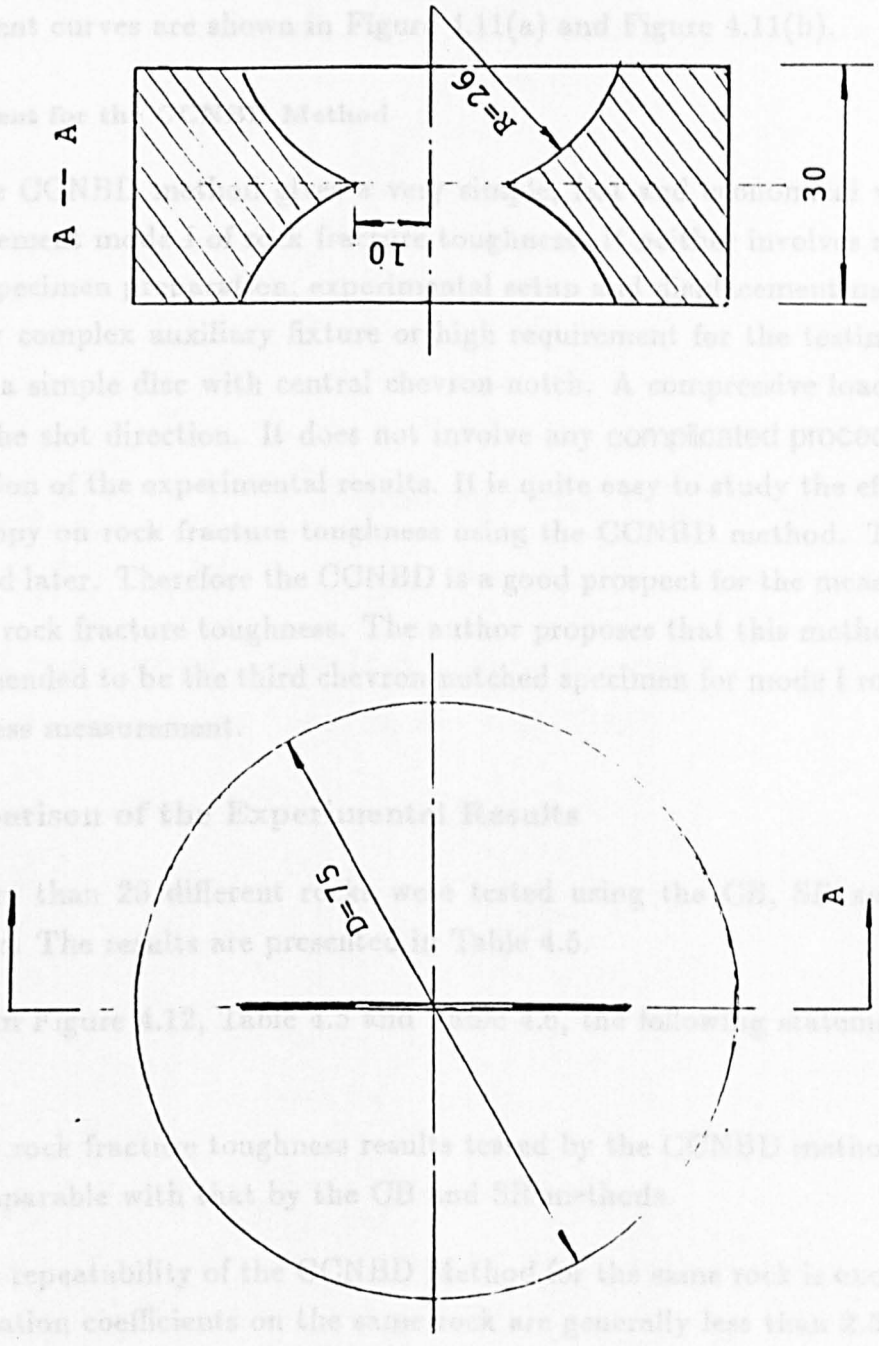


**Figure 4.10 — Disc Db01 Used for Experimental Validation of the CCNBD Method**

A typical load vs loading line displacement and crack mouth opening displacement curves are shown in Figure 4.11(a) and Figure 4.11(b).

#### 4.6.6 Comment for the CCNBD Method

The CCNBD method gives a very simple, fast and economical way for the measurement mode I of rock fracture toughness. It neither involves any complicated specimen preparation, experimental setup and displacement measurement nor any complex auxiliary fixture or high requirement for the testing machine. It uses a simple disc with central chevron-notch. A compressive load is applied along the slot direction. It does not involve any complicated procedures for the evaluation of the experimental results. It is quite easy to study the effect of rock anisotropy on rock fracture toughness using the CCNBD method. This will be analysed later. Therefore the CCNBD is a good prospect for the measurement of mode I rock fracture toughness. The author proposes that this method could be recommended to be the third chevron-notched specimen for mode I rock fracture toughness measurement.

### 4.7 Comparison of the Experimental Results

More than 20 different rocks were tested using the CB, SR and CCNBD methods. The results are presented in Table 4.5.

From Figure 4.12, Table 4.5 and Table 4.6, the following statements can be made:

1 The rock fracture toughness results tested by the CCNBD method are quite comparable with that by the CB and SR methods.

2 The repeatability of the CCNBD Method for the same rock is excellent. The variation coefficients on the same rock are generally less than 2.5 %. Of the three chevron-notched $K_{IC}$ testing methods, the variation coefficient is the lowest using the CCNBD method. For sandstone, 12 CCNBD specimens, 10 CB specimens and 10 SR specimens were tested. The variation coefficients of $K_{IC}$ using the CCNBD method is 2.2 %. Whilst for the CB method, it is 6.4 %; for the SR method, it is 4.9 %.

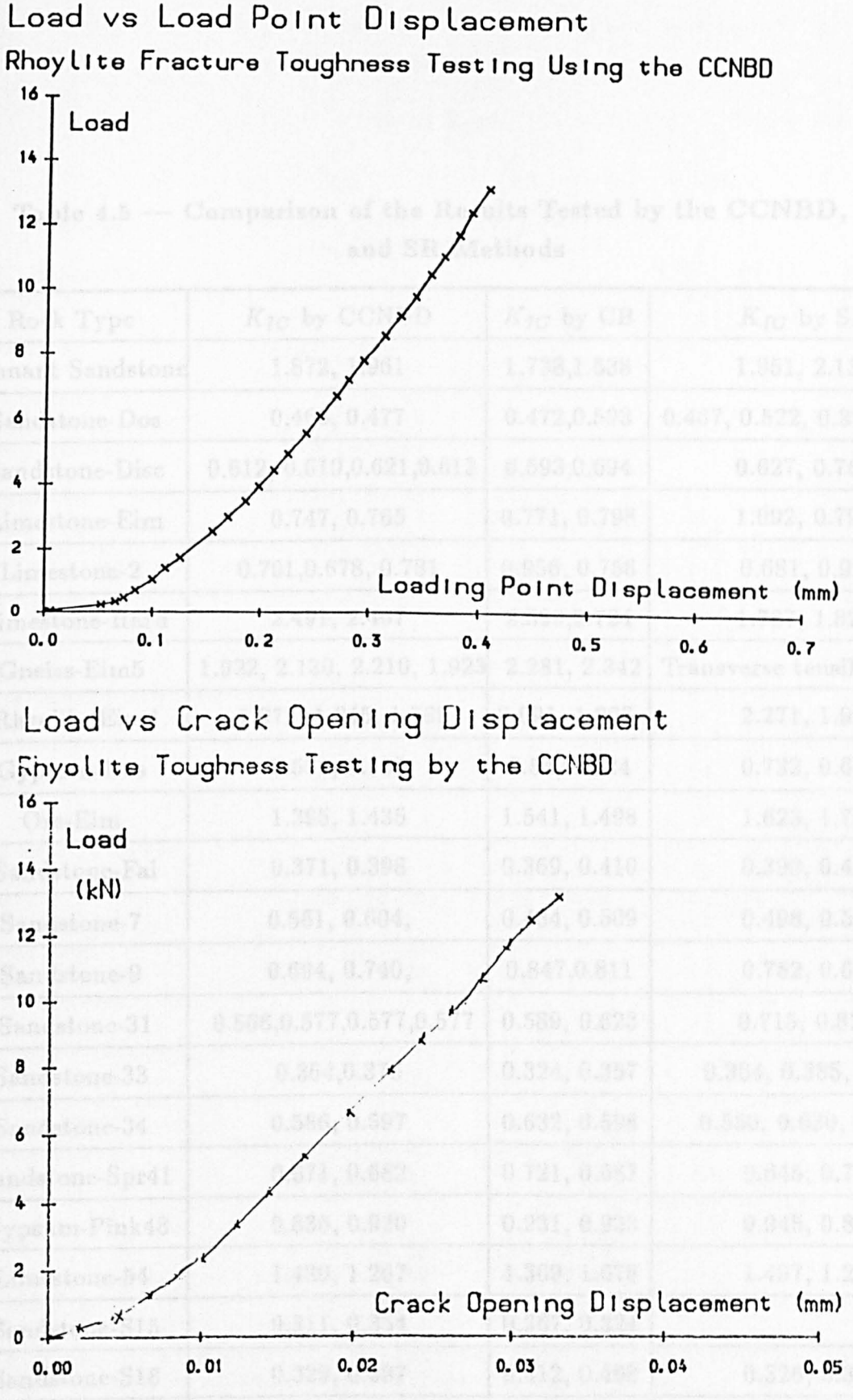


**Figure 4.11 — Load vs LPD or CMOD for Rhoylite**

**Table 4.5 — Comparison of the Results Tested by the CCNBD, CB and SR Methods**

| Rock Type | $K_{IC}$ by CCNBD | $K_{IC}$ by CB | $K_{IC}$ by SR |
|---|---|---|---|
| Pennant Sandstone | 1.872, 1.961 | 1.738,1.538 | 1.951, 2.131 |
| Sandstone-Dos | 0.466, 0.477 | 0.472,0.593 | 0.467, 0.522, 0.385, 0.467 |
| Sandstone-Disc | 0.612, 0.610,0.621,0.613 | 0.593,0.694 | 0.627, 0.760 |
| Limestone-Eim | 0.747, 0.765 | 0.771, 0.798 | 1.092, 0.798 |
| Limestone-2 | 0.701,0.678, 0.781 | 0.956, 0.756 | 0.681, 0.921 |
| Limestone-Hard | 2.491, 2.467 | 2.399,2.724 | 1.787, 1.829 |
| Gneiss-Eim5 | 1.922, 2.130, 2.210, 1.923 | 2.281, 2.342 | Transverse tensile failure |
| Rhyolite-Eim4 | 1.971, 1.845, 1.769 | 2.091, 1.967, | 2.271, 1.968 |
| Gypsum-Dos | 0.551, 0.565 | 0.54, 0.624 | 0.732, 0.657 |
| Ore-Eim | 1.395, 1.435 | 1.541, 1.498 | 1.623, 1.734 |
| Sandstone-Fai | 0.371, 0.398 | 0.369, 0.410 | 0.398, 0.423 |
| Sandstone-7 | 0.561, 0.604, | 0.484, 0.509 | 0.498, 0.512 |
| Sandstone-9 | 0.694, 0.740, | 0.847,0.811 | 0.752, 0.698 |
| Sandstone-31 | 0.566,0.577,0.577,0.577 | 0.589, 0.623 | 0.715, 0.822 |
| Sandstone-33 | 0.364,0.376 | 0.324, 0.357 | 0.364, 0.385, 0.330 |
| Sandstone-34 | 0.586, 0.597 | 0.632, 0.598 | 0.550, 0.630, 0.630 |
| Sandstone-Spr41 | 0.671, 0.682 | 0.721, 0.687 | 0.645, 0.714 |
| Gypsum-Pink48 | 0.836, 0.920 | 0.931, 0.923 | 0.945, 0.834 |
| Limestone-54 | 1.480, 1.267 | 1.369, 1.678 | 1.497, 1.298 |
| Sandstone-S15 | 0.311, 0.354 | 0.367, 0.324 | |
| Sandstone-S18 | 0.329, 0.387 | 0.412, 0.498 | 0.326, 0.398 |
| Sandstone-S25 | 0.324, 0.345 | 0.310, 0.365 | |
| Sandstone-S26 | 0.307, 0.324 | 0.345, 0.312 | |

Fracture toughness values obtained from core specimens, given as $mean_{no.tests} \pm$ std.dev. in $MN/m^{1.5}$.

| Rocks: | Chevron Bend $K_{CB}$ | Chevron Bend $K^c_{CB}$ | Short Rod $K_{SR}$ | Short Rod $K^c_{SR}$ |
|---|---|---|---|---|
| Tampomas andesite | $1.50_7 \pm 0.12$ | $1.68_7 \pm 0.15$ | - | - |
| " " | $1.26_5 \pm 0.10$ | $1.26_5 \pm 0.26$ | - | - |
| Whin Sill dolerite | - | - | $2.86_6 \pm 0.12$ | $3.26_6 \pm 0.09$ |
| Kallax gabbro | - | - | $2.22_{13} \pm 0.11$ | $2.58_{18} \pm 0.22$ |
| " " | - | - | $2.86_{10} \pm 0.14$ | $3.23_{13} \pm 0.34$ |
| Bohus granite | $1.46_5 \pm 0.07$ | - | $1.8_3$ | $2.4_3$ |
| " " | $1.69_4 \pm 0.04$ | $1.42_4 \pm 0.14$ | - | - |
| Cornwall granite | $1.32_4 \pm 0.10$ | - | - | - |
| Epprechtstein granite | $1.74_8 \pm 0.18$ | - | - | - |
| Falkenberg granite | $0.65_4 \pm 0.14$ | - | - | - |
| " " | - | $1.52_5 \pm 0.20$ | - | - |
| Iidate granite | $1.09_5 \pm 0.13$ | $1.73_5 \pm 0.21$ | - | - |
| " " | $1.37_3 \pm 0.13$ | $2.26_3 \pm 0.65$ | $1.01_4 \pm 0.18$ | $1.12_4 \pm 0.35$ |
| " " D,A | $1.43_3 \pm 0.01$ | $0.83_3 \pm 0.13$ | $1.58_3 \pm 0.08$ | $1.85_3 \pm 0.06$ |
| " " ST | - | - | $1.11_3 \pm 0.12$ | $1.26_3 \pm 0.18$ |
| Kråkemåla granite | $1.64_3 \pm 0.04$ | $2.16_3 \pm 0.23$ | $1.69_6 \pm 0.17$ | $2.22_5 \pm 0.24$ |
| Merrivale granite | - | - | $1.50_{24} \pm 0.10$ | $1.80_{24} \pm 0.13$ |
| Pink granite | - | - | $1.58_4 \pm 0.04$ | $2.03_4 \pm 0.08$ |
| Råsjö granite | - | - | $2.37_6 \pm 0.32$ | $2.80_6 \pm 0.33$ |
| Strath Halladale granite | - | - | $1.80_{11} \pm 0.10$ | $2.19_{11} \pm 0.11$ |
| Stripa granite | | - | $2.01_5 \pm 0.14$ | $2.36_{11} \pm 0.13$ |
| " " | - | - | $2.37_9 \pm 0.15$ | $2.70_9 \pm 0.27$ |
| Westerly granite | - | - | $1.64_9 \pm 0.03$ | $1.82_9 \pm 0.07$ |
| " " | - | - | $2.28_{17} \pm 0.19$ | - |
| " " | - | - | $2.04_4 \pm 0.05$ | $2.27_4 \pm 0.03$ |
| Finnsjön granodiorite | - | - | $2.95_3 \pm 0.11$ | $3.35_3 \pm 0.08$ |
| Grey norite | - | - | $2.23_{11} \pm 0.11$ | $2.69_6 \pm 0.16$ |
| Ogino tuff | $1.05_{17} \pm 0.11$ | $1.08_9 \pm 0.10$ | $1.02_{11} \pm 0.05$ | $1.06_{19} \pm 0.05$ |
| Pennant sandstone | - | - | $1.98_6 \pm 0.06$ | $2.56_6 \pm 0.07$ |
| Ruhr sandstone | $1.03_{10} \pm 0.04$ | - | - | - |
| Älvdalen sandstone | $1.51_6 \pm 0.08$ | $0.73_6 \pm 0.08$ | $1.54_{11} \pm 0.08$ | $1.91_{11} \pm 0.14$ |
| Indiana limestone | - | - | $0.90_7 \pm 0.11$ | $1.13_7 \pm 0.09$ |
| " " | - | - | $1.05_9 \pm 0.06$ | - |
| Klinthagen limestone | $1.31_2$ | - | $1.41_8 \pm 0.19$ | $1.87_8 \pm 0.25$ |
| Shelly limestone | - | - | $1.40_5 \pm 0.03$ | $1.44_5 \pm 0.04$ |
| Anvil Points oil shale D | - | - | $0.56_5 \pm 0.09$ | $1.02_3 \pm 0.14$ |
| " " " " ST | - | - | $0.25_4 \pm 0.04$ | $0.47_2 \pm 0.07$ |
| Carrara marble | $1.26_5 \pm 0.08$ | $1.38_5 \pm 0.09$ | - | - |
| Ekeberg marble | $1.89_{16} \pm 0.12$ | - | $1.83_9 \pm 0.35$ | $2.25_9 \pm 0.36$ |
| " " ST | - | - | $1.48_3 \pm 0.16$ | $1.82_3 \pm 0.10$ |
| " " D | - | - | $2.28_2 \pm 0.01$ | $2.62_2 \pm 0.05$ |
| " " | $1.79_4 \pm 0.07$ | $1.76_4 \pm 0.21$ | - | - |
| Treuchtlingen marble | $1.26_6 \pm 0.07$ | $1.70_6 \pm 0.09$ | - | - |
| Yizhang marble | $1.49_7 \pm 0.09$ | $1.83_7 \pm 0.18$ | - | - |

Notes: A, D and ST mean arrester, divider and short transverse orientations of crack with respect to discernible structure in rock

Table 4.6 — $K_{IC}$ Tested by the SR, CB Methods from Ouchterlony

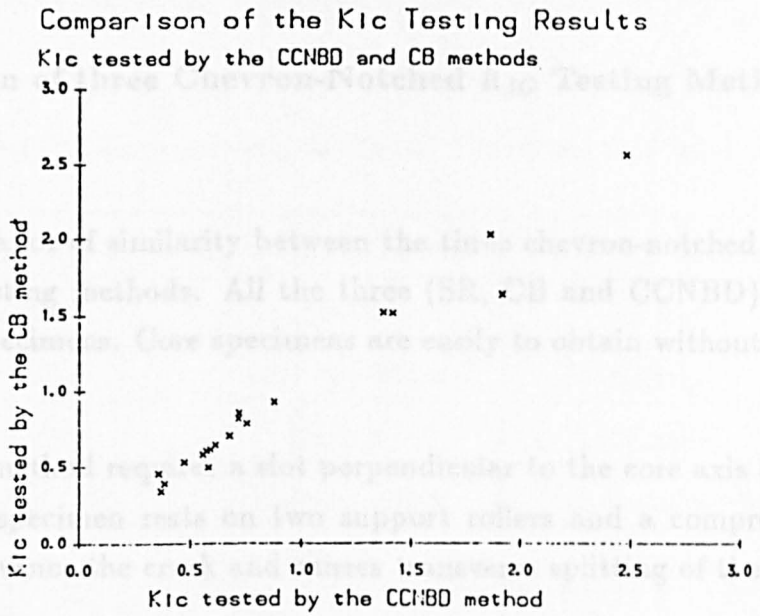


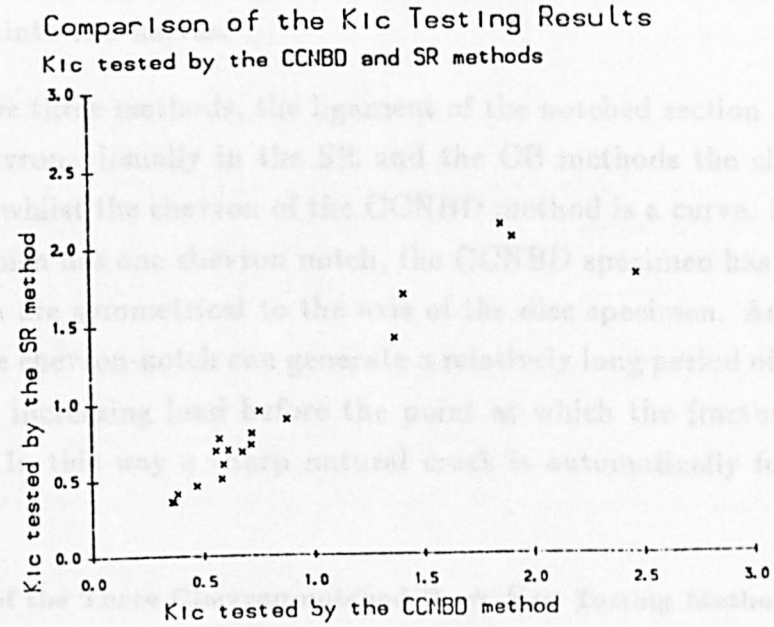


**Figure 4.12 — Comparison of the $K_{IC}$ Results by the CB, SR and CCNBD Methods**

## 4.8 Comparison of three Chevron-Notched $K_{IC}$ Testing Methods

### 4.8.1 Introduction

There is a lot of similarity between the three chevron-notched rock fracture toughness testing methods. All the three (SR, CB and CCNBD) methods use core-based specimens. Core specimens are easily to obtain without any complex machining.

The CB method requires a slot perpendicular to the core axis (Ouchterlony, 1980). The specimen rests on two support rollers and a compressive load is applied to advance the crack and causes transverse splitting of the specimen.

The SR method requires a slot parallel to the core axis. A tensile load is applied to the specimen to pull apart the notch sides.

The CCNBD method requires a slot perpendicular to the cores axis. A compressive load is appled along the slot direction to advance the crack and split the specimen into two halves.

In all these three methods, the ligament of the notched section has the form of a V or chevron. Usually in the SR and the CB methods the chevron has a straight side, whilst the chevron of the CCNBD method is a curve. Both the CB and SR specimen has one chevron notch, the CCNBD specimen has two chevron notches which are symmetrical to the axis of the disc specimen. As analysed in Chapter 1, the chevron-notch can generate a relatively long period of stable crack growth under increasing load before the point at which the fracture toughness is evaluated. In this way a sharp natural crack is automatically formed in the specimens.

### 4.8.2 Comparison of the Three Chevron-notched Rock $K_{IC}$ Testing Methods

The overall comparison for the three chevron-notched rock fracture toughness testing methods are presented in Table 4.7.

### 4.8.3 Analysis of Table 4.7

The advantages of the CCNBD method over the CB and SR methods can be

**Table 4.7 — Comparison of Three Chevron-Notched Methods**

| Item of Comparison | The CCNBD Method | The CB Method | The SR Method |
|---|---|---|---|
| Size of specimen | Small | Long | Small |
| Source of sample | Easy to obtain | difficult | easy |
| Preparation apparatus | Simple | Simple | Complex |
| Specimen preparation time | 30 samples/day | 20 samples/day | 20 samples/day |
| Setup of testing rig | Simple | Complex | Complex |
| Loading machines | Compressive | Compressive | Tensile |
| Preload Requirement | Less than 2 kN | Zero | Zero |
| Auxiliary apparatus | Simple | Complex | Complex |
| Displacement measurement | Simple | Complex | Complex |
| Loading method | Compressive Loading | Three Point Bending | Tensile Loading |
| Failure load range (usually) | $\geq 1kN$ | $\leq 1kN$ | $\leq 1kN$ |
| Experimental time (usually) | 5 minutes | 10 minutes | 5 minutes |
| Repeatability of results | Excellent | Reasonable | Reasonable |
| Requirement of Testing Machine | Ordinary | High | High |
| Study of Rock Anisotropy | Easy | Difficult | Middle |
| Transverse Tensile Failure | No | No | Yes |
| Availability | Easy | Difficult | Difficult |

summarized as following:

1 The CCNBD method requires a relative small specimen. A set of the CB, SR and CCNBD (CD) specimens are shown in Figure 4.13 and Photo 4.5.

As seen from Photo 4.5 and Figure 4.13, that the CB specimen requires a relatively long core specimen, which is usually not easy to obtain, due to the discontinuites inside the rock body making it impossible to obtain such long core

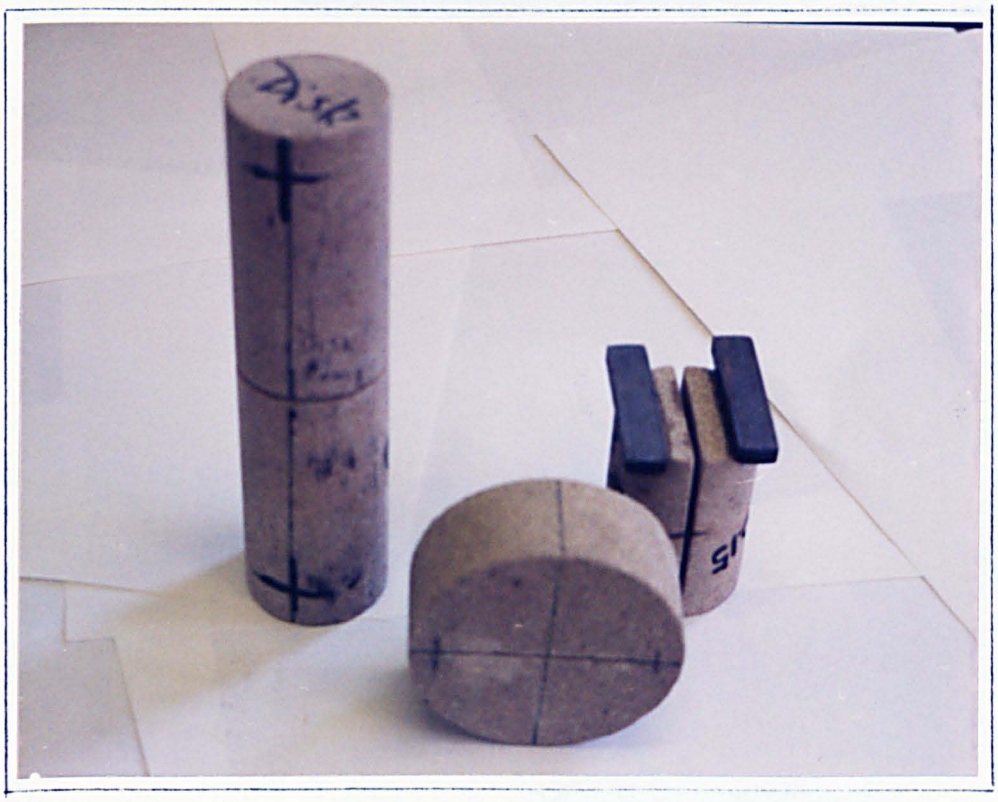

Photo 4.5 - A Set of the CB, SR and CCNBD Specimens

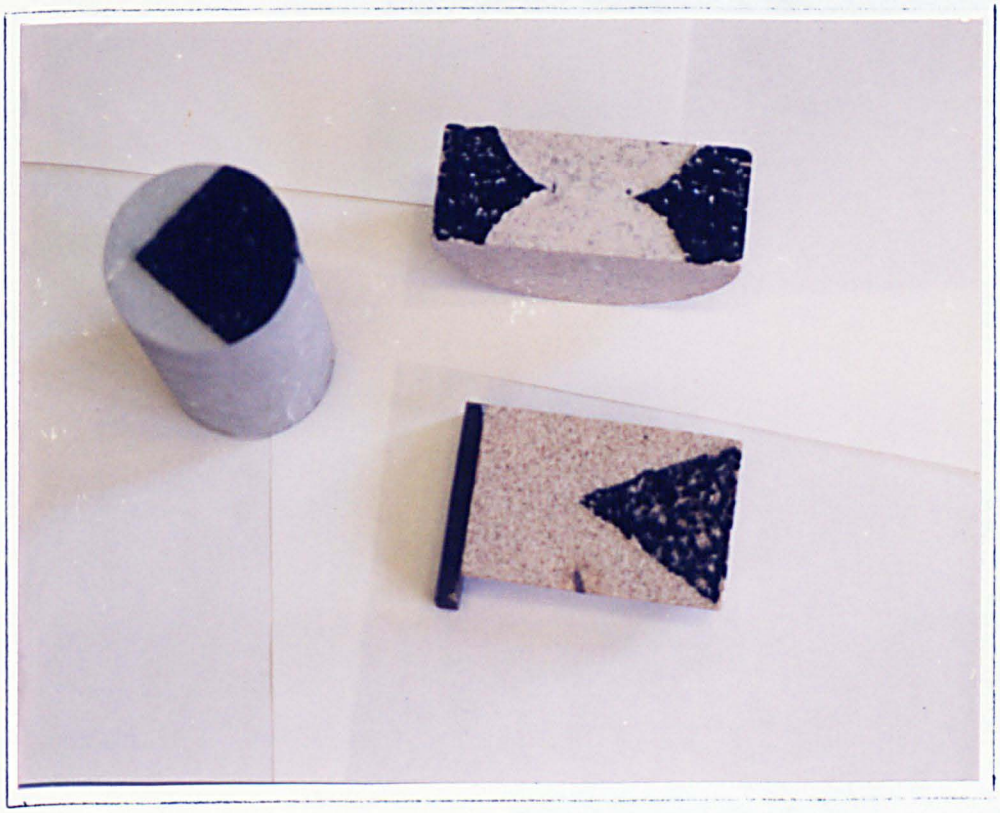

Photo 4.6 - A Set of the Failure Surface CB, SR and CCNBD Specimens

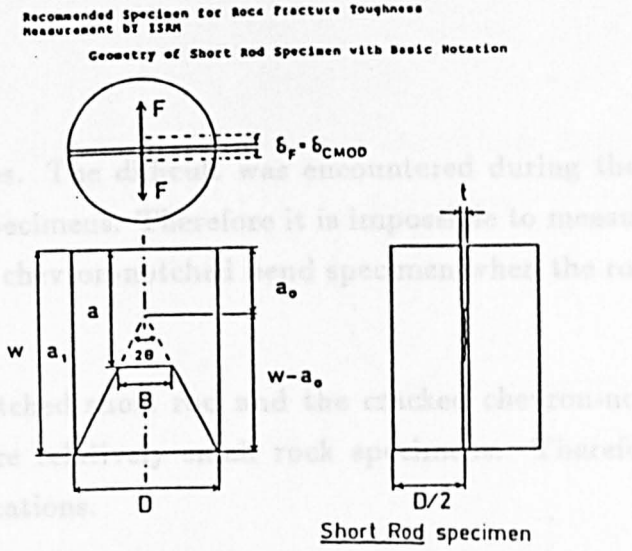


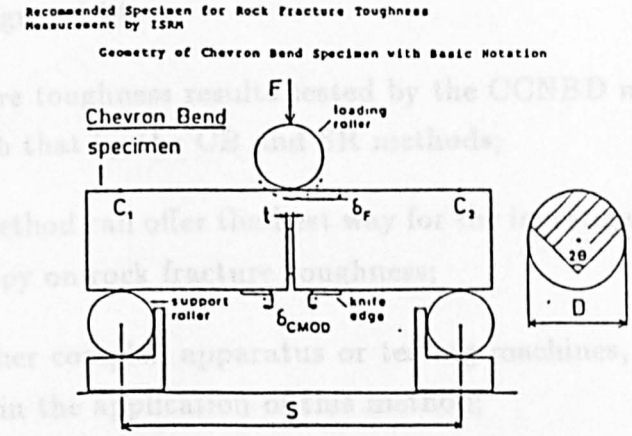


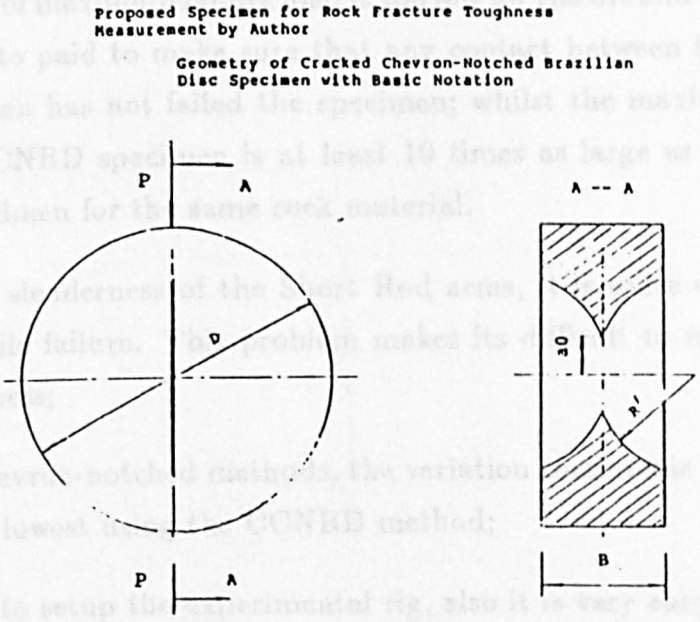


**Figure 4.13 — A Set of the CB, SR and CCNBD Specimens**

specimens sometimes. The difficult was encountered during the research when preparing the CB specimens. Therefore it is impossible to measure rock fracture toughness using the chevron-notched bend specimen when the rock block or core is small.

The chevron-notched short rod and the cracked chevron-notched Brazilian disc methods require relatively small rock specimens. Therefore they have a wide range of applications.

The failure surfaces of the CB, SR and CCNBD fracture specimens are shown in Photo 4.6 and Figure 4.14.

1 The rock fracture toughness results tested by the CCNBD method are quite comparable with that by the CB and SR methods;

2 The CCNBD method can offer the best way for the investigation of the effect of rock anisotropy on rock fracture toughness;

3 It requires neither complex apparatus or testing machines, which shows its great potential in the application of this method;

4 The magnitude of maximum failure load is too low for the SR and CB method, great care has to paid to make sure that any contact between the load bar and the specimen has not failed the specimen; whilst the maximum failure load for the CCNBD specimen is at least 10 times as large as that by the Short Rod specimen for the same rock material.

5 Because of the slenderness of the Short Rod arms, it is quite easy to have transverse tensile failure. This problem makes its difficult to measure rock fracture toughness;

4 Of the three chevron-notched methods, the variation coefficients for the same material is the lowest using the CCNBD method;

5 It is very easy to setup the experimental rig, also it is very easy to measure the loading line displacement and the crack opening displacement. Therefore it is a fast, efficient and economical method;

(a) Failure Surface of Chevron Bending Specimen

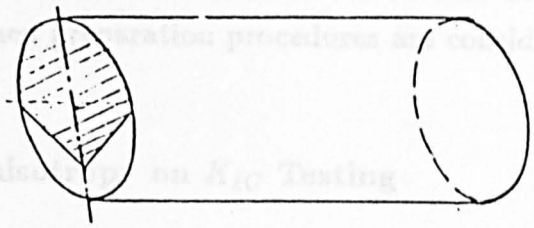

(b) Failure Surface of Short Rod Specimen

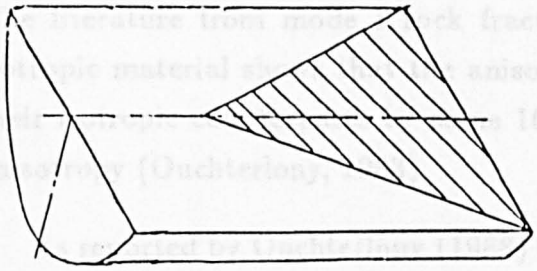

(c) Failure Surface of the CCNBD Specimen

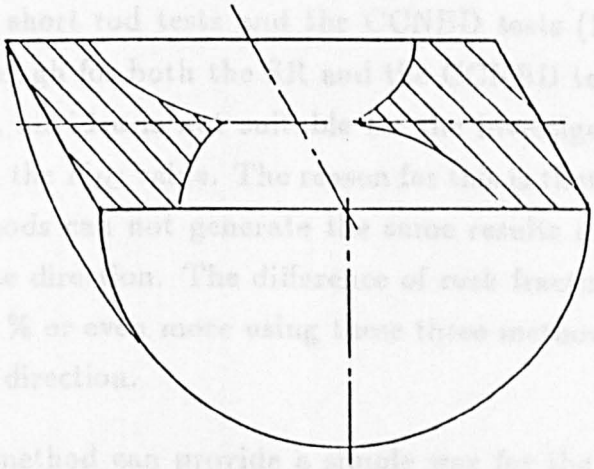

**Figure 4.14 — The Geometry of Failure Surface of the Chevron-Notched Specimens**

6 The CCNBD specimen preparation takes about two thirds the CB and SR specimen preparation if all the specimen preparation procedures are considered.

## 4.9 The Study of the Effect of Rock Anisotropy on $K_{IC}$ Testing

The prevalent anisotropy of rock material could be important in the fracture toughness testing of rock (Barton, 1982; Ouchterlony, 1983). The anisotropy of elastic constants is seldom fully considered in fracture toughness testing, not even when the measured fracture properties are shown to be anisotropic. The literature from mode I rock fracture toughness testing of a transversely isotropic material shows that the anisotropic stress intensity factors differ from their isotropic counterparts by some 10 percent or less for moderate degrees of anisotropy (Ouchterlony, 1983).

As reported by Ouchterlony (1988) the CB, SR and the third method (which author here refers it to the CCNBD method developed by Chen in 1989) can study the effect of rock anisotropy on $K_{IC}$ testing, as shown in Figure 4.15. As designed by Ouchterlony (1988), the direction of the crack propagation of the three chevron notched testing methods is perpendicular to each other, so only one core is used since the CB specimen is long enough for the remaining halves to be used in the short rod tests and the CCNBD tests (Note: the remaining halves are long enough for both the SR and the CCNBD tests, Chen, 1989). In the author's view, his idea is not suitable for the investigation of the effect of rock anisotropy on the $K_{IC}$ value. The reason for this is that the SR, the CB and the CCNBD methods can not generate the same results even when their slots are cut in the same direction. The difference of rock fracture toughness testing results is up to 10 % or even more using these three methods even for the same crack propagation direction.

The CCNBD method can provide a simple way for the investigation of the effect of rock anisotropy on the rock fracture toughness value. As shown in Figure 4.16, rock fracture toughness values can be tested using three CCNBD specimens from relatively small blocks. If a 75 mm diameter and 30 mm thickness CCNBD specimen is used for $K_{IC}$ testing, a rock block with dimension $120mm \times 120mm \times$

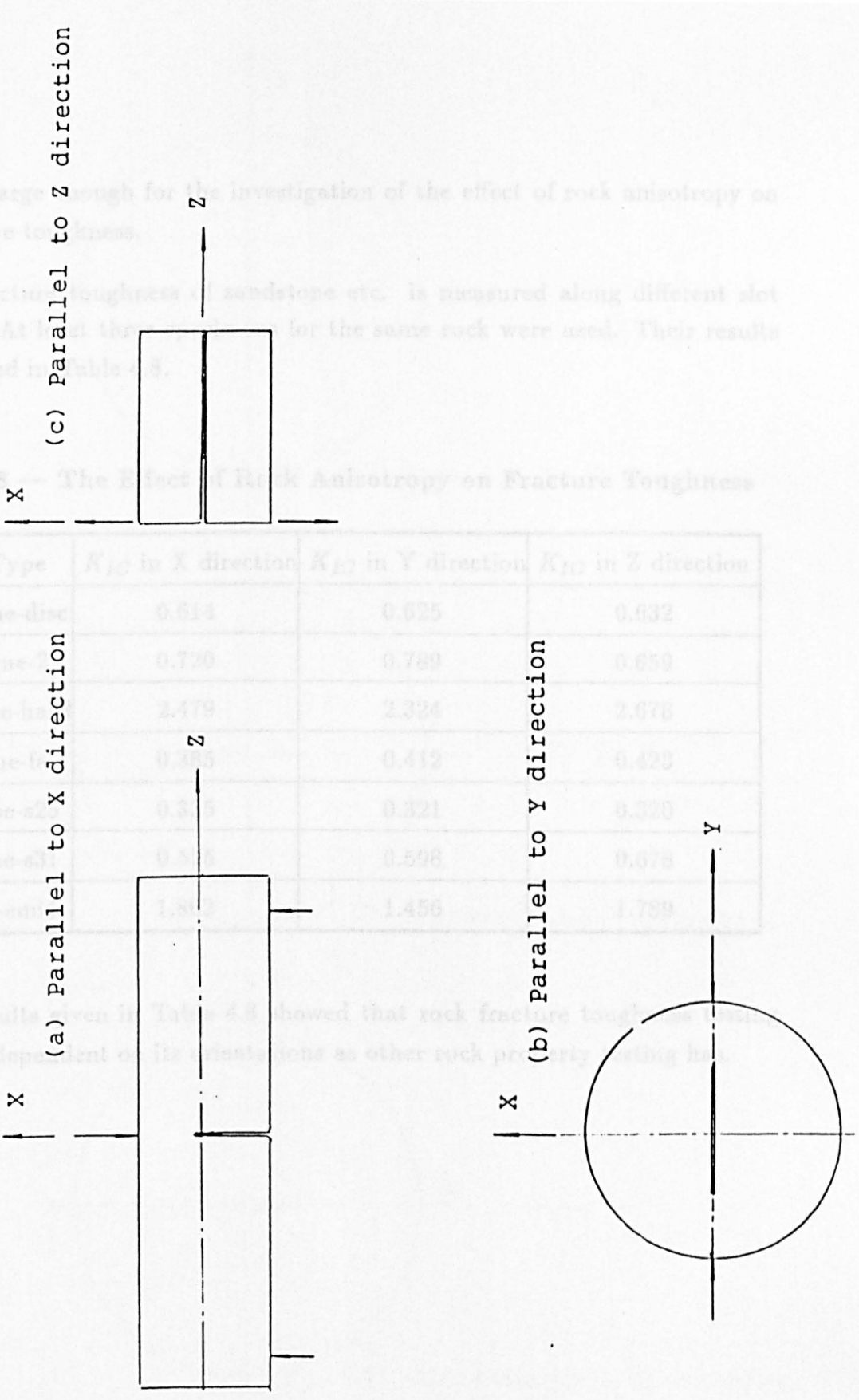


**Figure 4.15 — The Study of Rock Anisotropy on $K_{IC}$, Idea from Ouchterlony, 1988**

$120mm$ is large enough for the investigation of the effect of rock anisotropy on rock fracture toughness.

The fracture toughness of sandstone etc. is measured along different slot directions. At least three specimens for the same rock were used. Their results are presented in Table 4.8.

**Table 4.8 — The Effect of Rock Anisotropy on Fracture Toughness**

| Rock Type | $K_{IC}$ in X direction | $K_{IC}$ in Y direction | $K_{IC}$ in Z direction |
|---|---|---|---|
| Sandstone-disc | 0.614 | 0.625 | 0.632 |
| Limestone-2 | 0.720 | 0.789 | 0.659 |
| Limestone-hard | 2.479 | 2.324 | 2.678 |
| Sandstone-fai | 0.385 | 0.412 | 0.423 |
| Sandstone-s25 | 0.335 | 0.321 | 0.320 |
| Sandstone-s31 | 0.575 | 0.598 | 0.678 |
| Rhyolite-emi4 | 1.862 | 1.456 | 1.789 |

The results given in Table 4.8 showed that rock fracture toughness testing results are dependent on its orientations as other rock property testing has.

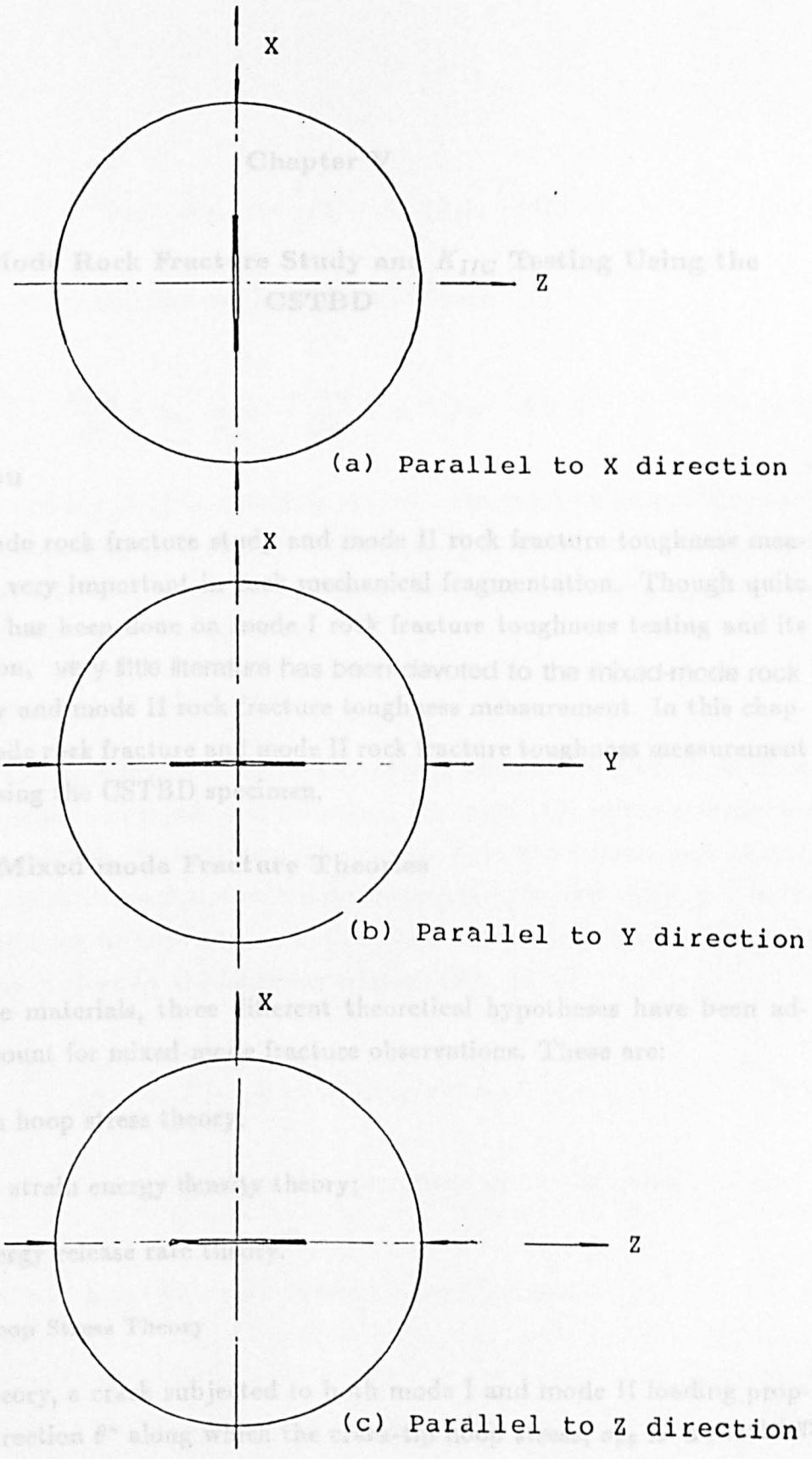


**Figure 4.16 — The Effect of Rock Anisotropy on $K_{IC}$ Study by Chen**

# Chapter V

# Mixed-Mode Rock Fracture Study and $K_{IIC}$ Testing Using the CSTBD

## 5.1 Introduction

Mixed-mode rock fracture study and mode II rock fracture toughness measurement are very important in rock mechanical fragmentation. Though quite a lot of work has been done on mode I rock fracture toughness testing and its standardization, very little literature has been devoted to the mixed-mode rock fracture study and mode II rock fracture toughness measurement. In this chapter, mixed-mode rock fracture and mode II rock fracture toughness measurement are studied using the CSTBD specimen.

## 5.2 Review of Mixed-mode Fracture Theories

### 5.2.1 Introducton

For brittle materials, three different theoretical hypotheses have been advanced to account for mixed-mode fracture observations. These are:

1 Maximum hoop stress theory;

2 Minimum strain energy density theory;

3 Strain energy release rate theory.

### 5.2.2 Maximum Hoop Stress Theory

In this theory, a crack subjected to both mode I and mode II loading propagates in a direction $\theta^*$ along which the crack-tip hoop stress, $\sigma_{\theta\theta}$ is a maximum and fracture occurs when the hoop stress attains a material-characteristic critical value $\sigma^*$. In the vicinity of the crack tip subjected to both mode I and mode II loading the hoop stress is given by the following relation (J. L. Swedlow, 1976):

$$\sigma_{\theta\theta} = K_I(3\cos\frac{\theta}{2}/4) - K_{II}(3\sin\frac{\theta}{2}/4) \tag{5.1}$$

The hoop stress criterion can be stated as follows:

$$\frac{d\sigma_{\theta\theta}}{d\theta} = 0, \quad and \quad \frac{d^2\sigma_{\theta\theta}}{d^2\theta} < 0, \quad for \quad \theta = \theta^* \tag{5.2}$$

Substition of eqn.(5.1) in eqn.(5.2) provides the crack-extension direction, $\theta^*$, which can then be substituted back in eqn.(5.1) to calculate the mode I and mode II stress intensity factors that generate the same crack-tip hoop stress as in the case of pure open mode loading.

### 5.2.3 Minimum Strain Energy Density Theory

Sih G. C (1974) proposed a criterion for mixed-mode fracture which, in effect, states that a crack subjected to both mode I and mode II loading extends in a direction along which the strain energy density, $\psi$, is a minimum and fracture occurs when its value reaches a material-characteristic critical value, $\psi^*$. In the vicinity of the crack tip subjected to both mode I and mode II loading the strain energy density is given by the following relation (Sih, 1974):

$$\psi = a_{11}K_I^2/r + 2a_{12}K_IK_{II}/r + a_{22}K_{II}^2/r \tag{5.3}$$

where the coefficients $a_{11}, a_{12}$ *and* $a_{22}$ are given by the following relations:

$$a_{11} = [(3 - 4\nu - \cos\theta)(1 + cos\theta)]/(16\pi G) \tag{5.4}$$

$$a_{12} = [(\cos\theta - 1 + 2\nu)]\sin\theta/(8\pi G) \tag{5.5}$$

$$a_{22} = [(1-\nu)(1 - \cos\theta + (1 + \cos\theta)(3\cos\theta - 1)]/(16\pi G) \tag{5.6}$$

Where G is the shear modulus and $\nu$ is the Poisson's ratio. The maximum strain energy criterion is stated as:

$$\frac{d\psi(\theta)}{d\theta} = 0 \quad and \quad \frac{d^2\psi}{d\theta^2} > 0 \quad for \quad \theta = \theta^* \tag{5.7}$$

The strain energy density criterion was applied to the CSTBD test results in a manner similar to the hoop stress criterion.

The crack propagation angle calculated from eqn.(5.7) was substituted back in eqn.(5.3)–eqn.(5.6) to predict the $K_I - -K_{II}$ combinations that produce the same strain energy density as in open mode loading.

#### 5.2.4 Strain Energy Release Rate Theory

Griffith's energy balance analyses of nonplanar extension of inclined cracks have been reported by several investigators (M. A. Hussain, K. Palaniswamy etc.) The analysis of Palaniswamy and Knauss appears to be most rigorous and their results can be fitted to a simple empirical mixed-mode fracture criterion:

$$\frac{K_I}{K_{IC}} + 1.5(\frac{K_{II}}{K_{IIC}})^2 = 1 \tag{5.8}$$

### 5.3 Review of Mixed-mode Rock Fracture Study

#### 5.3.1 Introduction

A lot of analytical and experimental data exist with respect to the fracture mechanics in brittle materials such as ceramics under mixed-mode. (Brace and Bombolakis, 1963; Hoek and Bieniawski, 1965; Ingraffea and Heuze, 1980; Nemat-Nasser and Horii, 1982; Vallejo and Pramono, 1987 etc). The following are simple review for some methods used for mixed-mode rock fracture investigations.

#### 5.3.2 Semi-circular Specimen Proposed by Chong and Kuruppu

Chong K. P. proposed a semi-circular specimen with an edge crack subjected to three-point bending. For mode I fracture, the edge crack is cut perpendicular

to the bottom edge, for mixed mode rock fracture investigations, the edge crack is to be cut at an angle (other than 90 degrees) with the bottom edge.

The geometry of the semi-circular specimen is shown in Figure 5.1(a).

### 5.3.3 Sample with Inclined Crack under Compression

This specimen geometry was used by Vallejo L. etc. (1987). It is shown in Figure 5.1(b).

### 5.3.4 Plate with a Slant Edge Crack Subjected to Uniform Tension

Lavery P. L., Chong K. P., etc. used a plate with a slant edge subjected to uniform tension for mixed-mode rock fracture investigation. The geometry of the specimen is shown in Figure 5.1(c).

### 5.3.5 Four Point Bending Specimens Used by Huang and Wang

Huang and Wang (1985) used a set of bending specimen for rock fracture studies. As shown in Figure 5.2, a symmetrical three point bending specimen is used to measure mode I rock fracture toughness, axisymmetrical four point bending specimens are used for mixed-mode rock fracture investigations, the symmetrical four point shearing specimen is used for mode II rock fracture toughness measurement.

### 5.3.6 Cracked-Straight-Through Brazilian Disc (CSTBD) Specimen

The center-cracked diametral-compression disc (Cracked-Straight-Through Brazilian Disc) specimen provides a simple method for mixed-mode rock fracture study and mode-II rock fracture toughness measurement by selecting the angle of inclination of the center-through-crack relative to the diametral line of compression loading. A set of the CSTBD specimens for rock fracture study is shown in Figure 5.3. Rock fractures in mode I, mixed mode and mode II in the following case:

1 When the angle of inclination $\theta$ of the center-through-crack relative to the diametral line of compression loading is zero degree, rock fractures under pure mode I (tensile mode);

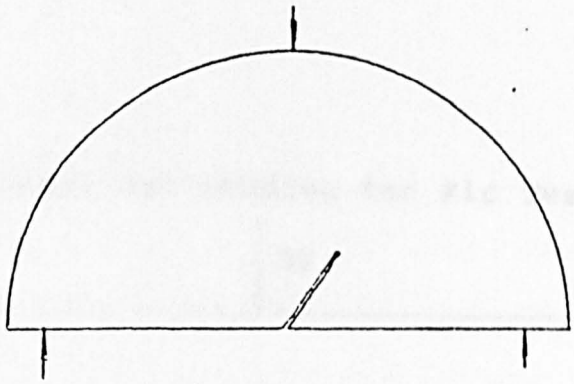

(a) Semi-Circular Fracture Specimen

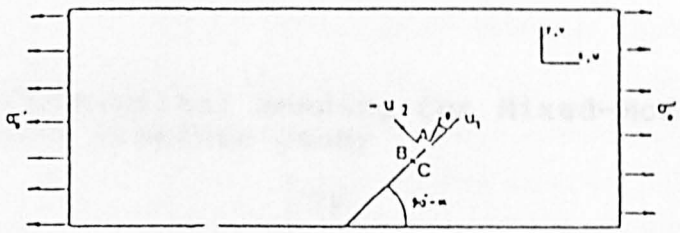


(b) Plate with a Slant Edge Crack
Subjected to Uniform Tension

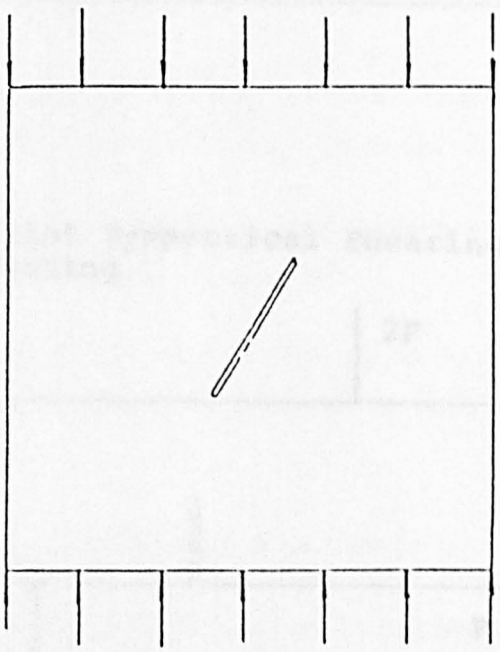

(c) Sample with Inclined Crack under Compression

**Figure 5.1 — The Geometry of Mixed-mode Rock Fracture Specimens**

(a) Symmetrical Bending for Kic Testing

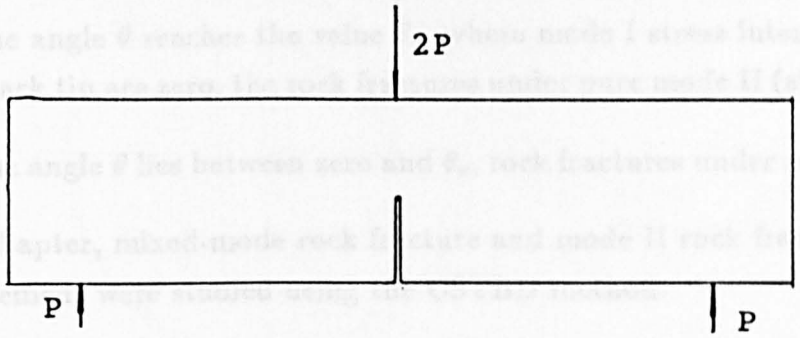


(b) Asymmetrical Bending for Mixed-Mode Rock Fracture Study

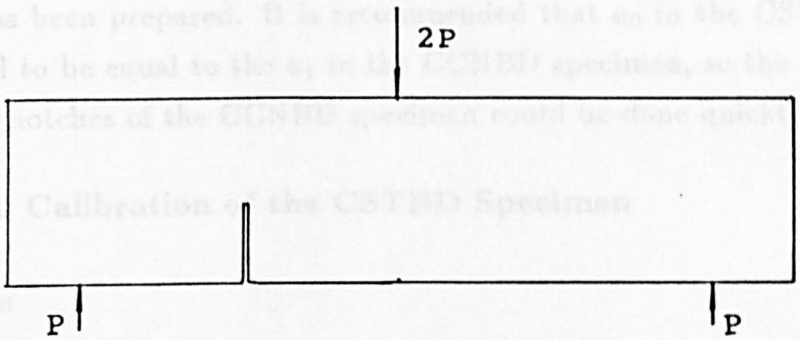


(c) Four-Point Symmetrical Shearing for Kiic Testing

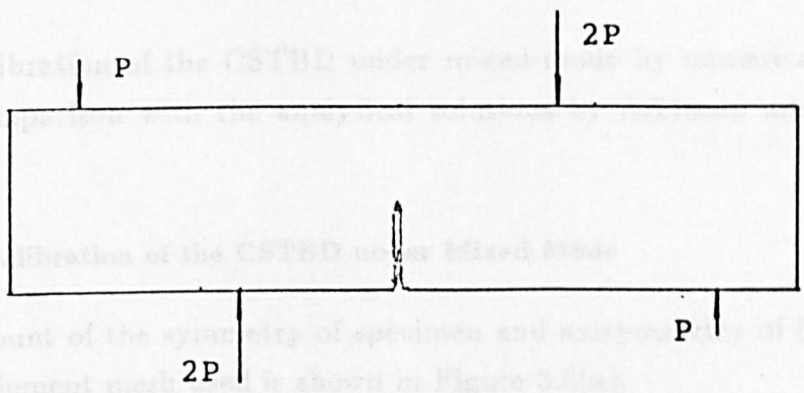


**Figure 5.2 — A Set of Specimens for Rock Fracture Study by Huang and Wang**

2 When the angle $\theta$ reaches the value $\theta_c$, where mode I stress intensity factors at the crack tip are zero, the rock fractures under pure mode II (shear mode);

3 When the angle $\theta$ lies between zero and $\theta_c$, rock fractures under mixed-mode.

In this chapter, mixed-mode rock fracture and mode II rock fracture toughness measurement were studied using the CSTBD method.

## 5.4 The CSTBD Specimen Preparation Method

As shown in Figure 5.4, the CSTBD specimen could be machined directly from the Cracked-Chevron-Notched Brazilian disc specimen. After the chevron-notched sections of the CCNBD specimens are cut off by a hand saw, the CSTBD specimen has been prepared. It is recommended that $a_0$ in the CSTBD should be machined to be equal to the $a_1$ in the CCNBD specimen, so the cuting off of the chevron-notches of the CCNBD specimen could be done quickly and easily.

## 5.5 Numerical Calibration of the CSTBD Specimen

### 5.5.1 Introduction

As described before, when load is applied at an angle $\theta$ relative the slot direction, the rock fractures under mixed mode or mode II (pure shear mode).

The 2D FEM and BEM are used for the calculation of the stress intensity factors at the crack tip of the CSTBD specimen.

The calibration of the CSTBD under mixed-mode by numerical method is only for comparison with the analytical solutions by Atkinson and co-workers (1980).

### 5.5.2 2D BEM Calibration of the CSTBD under Mixed-Mode

On account of the symmetry of specimen and axisymmetry of loading. The boundary element mesh used is shown in Figure 5.5(a).

It is modelled as a two-zone problem. A central through crack is represented by line CD. Loading is applied along the direction as shown in Figure 5.5. Lines

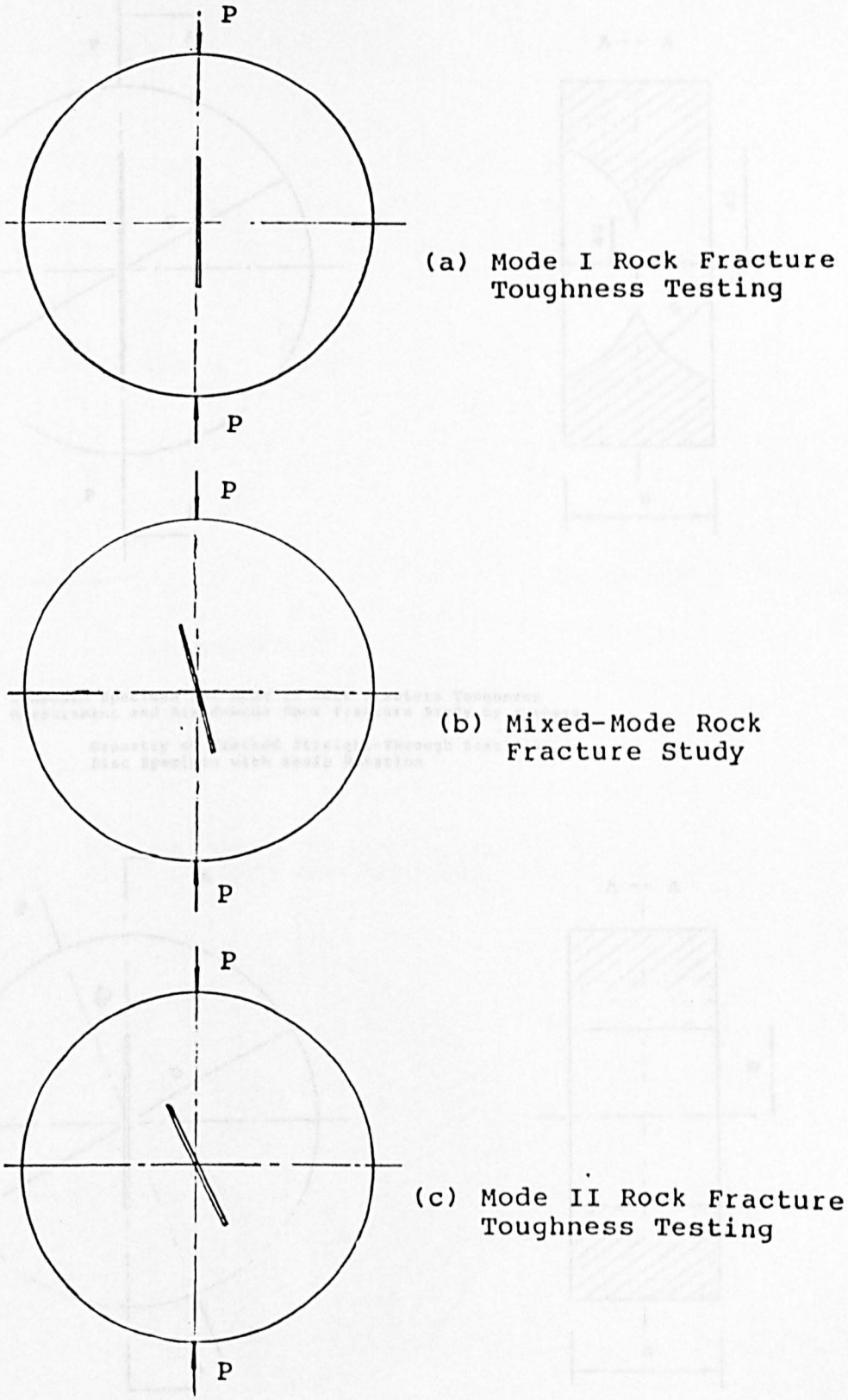


**Figure 5.3 — A Set of the CSTBD Specimens for Rock Fracture Study**

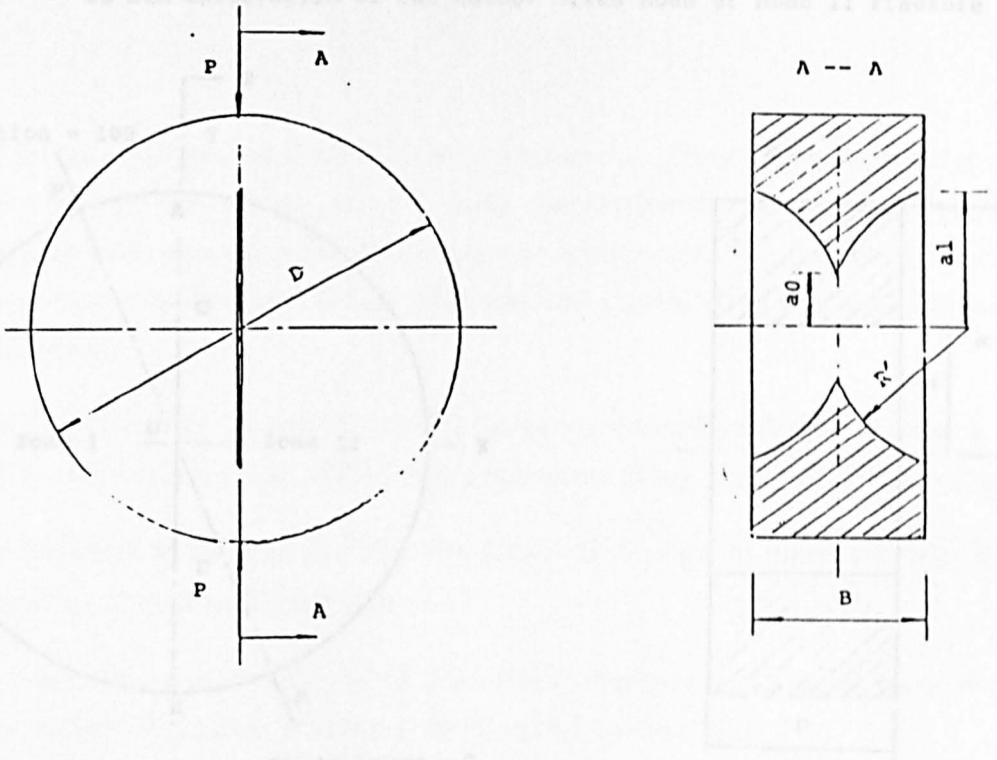


Proposed Specimen for Mode II Rock Fracture Toughness Measurement and Mixed-mode Rock Fracture Study by Authors

Geometry of Cracked Straight-Through Brazilian Disc Specimen with Basic Notation

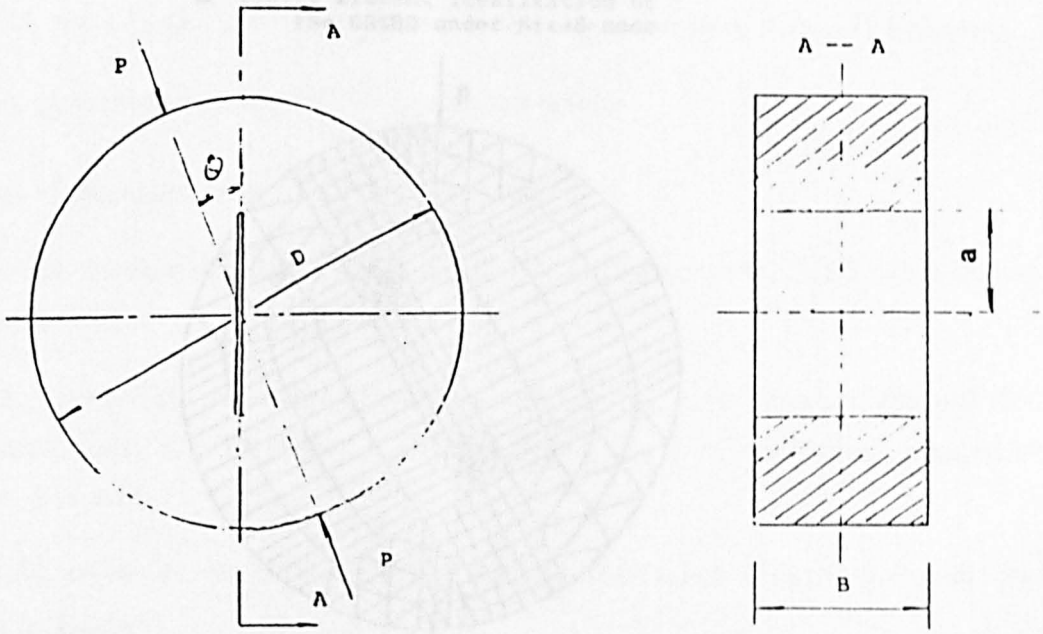


**Figure 5.4 — The CSTBD Specimen Preparation**

a. 2D BEM Calibration of the CSTBD, Mixed Mode or Mode II Fracture

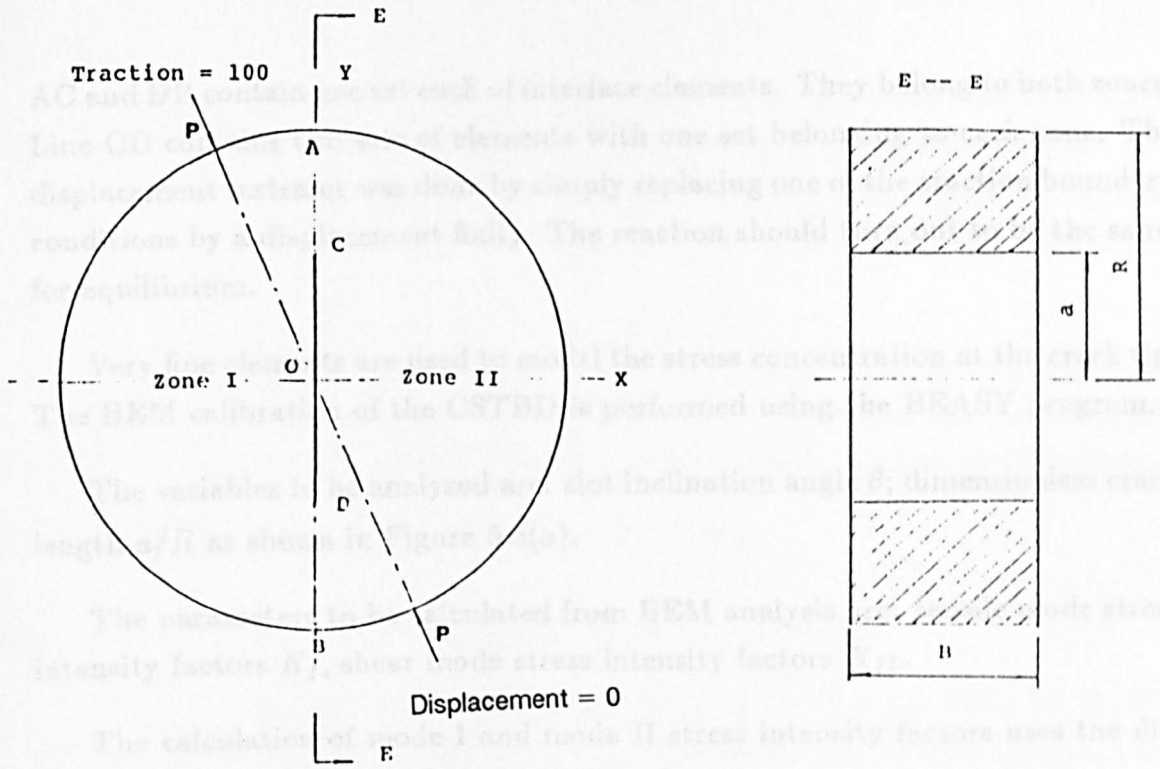


b. Finite Element Idealization of the CSTBD under Mixed-mode

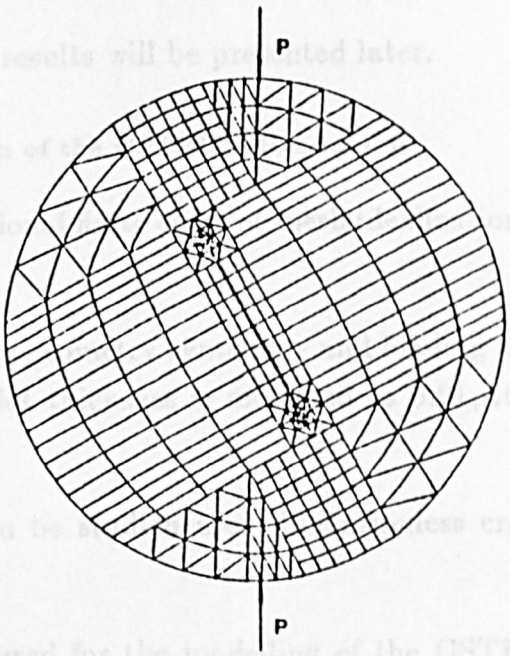


**Figure 5.5 — Numerical Calibration of the CSTBD under Mixed-mode**

AC and DB contain one set each of interface elements. They belong to both zones. Line CD contains two sets of elements with one set belonging to each zone. The displacement restraint was done by simply replacing one of the traction boundary conditions by a displacement fixity. The reaction should turn out to be the same for equilibrium.

Very fine elements are used to model the stress concentration at the crack tip. The BEM calibration of the CSTBD is performed using the BEASY program.

The variables to be analysed are: slot inclination angle $\theta$; dimensionless crack length $a/R$ as shown in Figure 5.5(a).

The parameters to be calculated from BEM analysis are: tensile mode stress intensity factors $K_I$, shear mode stress intensity factors $K_{II}$.

The calculation of mode I and mode II stress intensity factors uses the displacement method as described in Chapter 2.

By changing the loading angle $\theta$ for the dimensionless crack length $a/R$, $N_I$, $F_I$, $N_{II}$ and $F_{II}$ could be calculated in the same way as described in Chapter 2. If $N_I = 0$, $F_I = 0$, the loading angle $\theta_c$ is the angle for pure mode II behavior.

The calibration results will be presented later.

### 5.5.3 2D FEM Calibration of the CSTBD, Mixed-mode

The two dimensional finite element mesh idealization of the CSTBD is shown in Figure 5.5(b).

On account of its geometry symmetry and loading axisymmetry, the full disc is modelled. The slot thickness is modelled as 0.01, it is very small compared with the disc size.

The variables to be studied are: dimensionless crack length $a/R$ and slot inclination angle $\theta$.

The program used for the modelling of the CSTBD under mixed-mode is PAFEC. As described in Chapter 2, 4-noded isoparametric solid elements are used everywhere, if needed, except around the crack tip. The elements around

the crack tip are modelled by type 9 blocks. All elements around the crack tip are 36110 to represent the crack tip elastic singularity. The mesh close to the crack tip is made finer than the rest of the body to cater for the high stress gradient close to the crack tip. Mode I and mode II stress intensity factors results are calculated in the program.

By changing the loading angle $\theta$ for the dimensionless crack length $a/R$, $N_I$, $F_I$, $N_{II}$ and $F_{II}$ could be calculated in the same way as described in Chapter 2. If $N_I = 0$, $F_I = 0$, the loading angle $\theta_C$ is the angle for pure mode II behavior.

The calibration results will be presented later.

## 5.6 Analytical Solutions for the CSTBD by Atkinson

Atkinson and co-workers (1980) developed a series of solutions for stress intensity factor calculations (mode I and mode II) for the CSTBD specimen by a method that involves representing the crack by a continuous distribution of edge dislocations.

They used the following equations to calculate the stress intensity factors at the crack tip for the CSTBD specimen.

$$K_I = N_I \times \frac{P}{\pi BR} \times \sqrt{\pi a} \tag{5.9}$$

$$K_{II} = N_{II} \times \frac{P}{\pi BR} \times \sqrt{\pi a} \tag{5.10}$$

$$N_I = \sum_{i=1}^{n} T_i (\frac{a}{R})^{2i-2} A_i(\theta) \tag{5.11}$$

$$N_{II} = 2 \sin 2\theta \sum_{i=1}^{n} S_i (\frac{a}{R})^{2i-2} B_i(\theta) \tag{5.12}$$

Where:

$N_I$, $N_{II}$ are normalized stress intensities;

P — Load applied on disc;

R — The radius of the disc;

a — The crack length;

$\theta$ – The loading inclination angle relative to slot direction;

$T_i$ and $S_i$ are the first five coefficients as listed in Table 5.1;

$A_i$ and $B_i$ are the first five angular constants as listed in Table 5.2.

**Table 5.1 — First Five Coefficients for Equation (5.11) and (5.12)**

| $\frac{a}{R}$ | $T_1$ | $T_2$ | $T_3$ | $T_4$ | $T_5$ |
|---|---|---|---|---|---|
| | $S_1$ | $S_2$ | $S_3$ | $S_4$ | $S_5$ |
| 0.1 | 1.014998 | 0.503597 | 0.376991 | 0.376991 | 0.314159 |
| | 1.009987 | 0.502341 | 0.376363 | 0.376363 | 0.314159 |
| 0.2 | 1.060049 | 0.514907 | 0.382430 | 0.383392 | 0.318086 |
| | 1.039894 | 0.509959 | 0.379956 | 0.380584 | 0.316245 |
| 0.3 | 1.135551 | 0.533477 | 0.391640 | 0.393835 | 0.325033 |
| | 1.089702 | 0.522272 | 0.386086 | 0.387518 | 0.320834 |
| 0.4 | 1.243134 | 0.559734 | 0.404603 | 0.408597 | 0.334831 |
| | 1.160796 | 0.539824 | 0.394822 | 0.397403 | 0.327411 |
| 0.5 | 1.387239 | 0.594892 | 0.421949 | 0.428533 | 0.347941 |
| | 1.257488 | 0.563966 | 0.406869 | 0.410966 | 0.336447 |
| 0.6 | 1.578258 | 0.642124 | 0.445387 | 0.454861 | 0.365559 |
| | 1.390654 | 0.597985 | 0.424037 | 0.430072 | 0.349219 |

Figure 5.6 (from Atkison, 1980) shows that as the crack changes its orientation from the vertical to the horizontal when the normalized stress intensity factor Ni

Table 5.2 — The First Five Angular Constants for Eqn.(5.11) and (5.12)

| | |
|---|---|
| $A_1$ | $1-4S^2$ |
| $A_2$ | $8S^2(1-4C^2)$ |
| $A_3$ | $-4S^2(3-36C^2+48C^4)$ |
| $A_4$ | $-16S^2(-1+24C^2-80C^4+64C^6)$ |
| $A_5$ | $-20S^2(1-40C^2+240C^4-448C^6+256C^8)$ |
| $B_1$ | $1$ |
| $B_2$ | $-5+8C^2$ |
| $B_3$ | $-3+8(1-2C^2)(2-3C^2)$ |
| $B_4$ | $3+16(1-2C^2)-12(1-2C^2)^2-32(1-2C^2)^3$ |
| $B_5$ | $5-16(1-2C^2)-60(1-2C^2)^2+32(1-2C^2)^3+80(1-2C^2)^4$ |

Note: $s=\sin\theta$, $c=\cos\theta$

changes from positive to negative indicating the crack closure. At the point of crack closure, it is pure mode II (shear mode) behavior.

If the crack length is relatively short compared with the radius of the disc, Atkinson (1980) proposed the following equations for the calculation of $N_I$ and $N_{II}$.

$$N_I = A_1 + \frac{A_2}{2}(\frac{a}{R})^2 \tag{5.13}$$

$$N_{II} = [B_1 + \frac{B_2}{2}(\frac{a}{R})^2]2\sin 2\theta \tag{5.14}$$

From equation (5.13), an explicit equation for the angle $\theta_c$, at which the crack just begins to close ($K_I = 0$), is obtained:

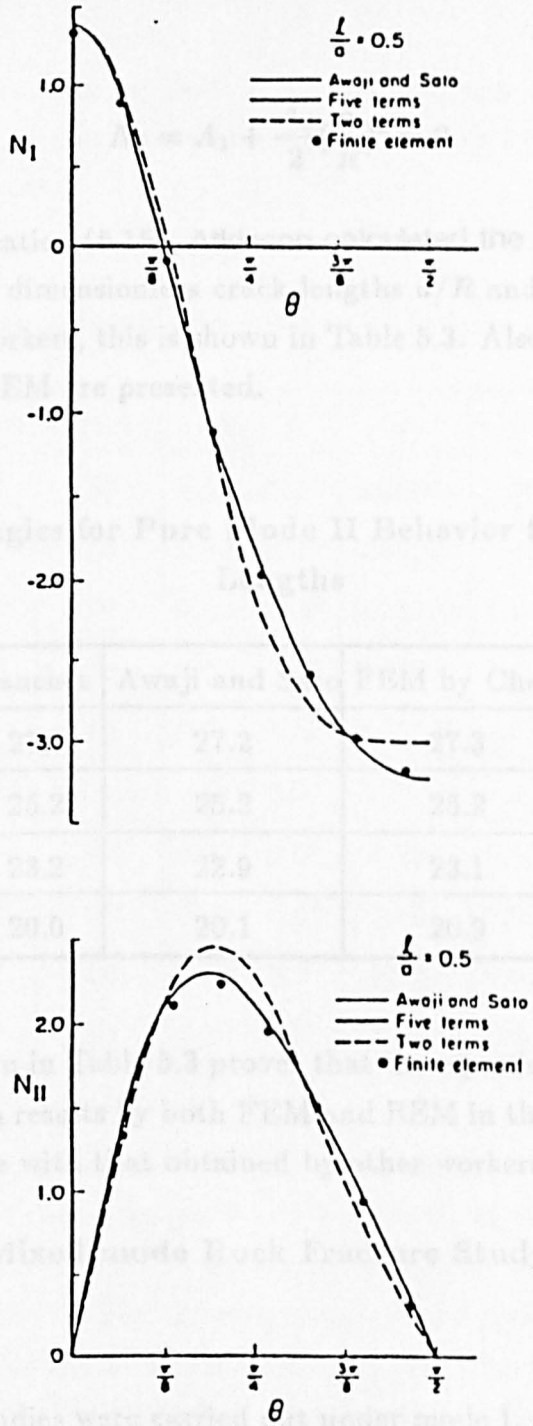


**Figure 5.6 — The Normalized SIFs vs $\theta$ for $a/R = 0.5$ by Atkinson**

$$N_I = A_1 + \frac{A_2}{2}(\frac{a}{R})^2 = 0 \qquad (5.15)$$

By using the equation (5.15), Atkinson calculated the angles for pure mode II behavior for various dimensionless crack lengths $a/R$ and compared the results obtained by other workers, this is shown in Table 5.3. Also the results calibrated by both FEM and BEM are presented.

Table 5.3 — Angles for Pure Mode II Behavior for Various Crack Lengths

| $l/a$ | Atkinson | Sanchez | Awaji and Sato | FEM by Chen | BEM by Chen |
|---|---|---|---|---|---|
| 0.3 | 27.2 | 27.7 | 27.2 | 27.3 | 27.4 |
| 0.4 | 25.4 | 25.2 | 25.2 | 25.2 | 25.3 |
| 0.5 | 23.3 | 23.2 | 22.9 | 23.1 | 23.4 |
| 0.6 | 21.3 | 20.0 | 20.1 | 20.9 | 20.5 |

The results shown in Table 5.3 proves that the equation (5.15) is quite accurate. The calibration results by both FEM and BEM in this research programme are quite comparable with that obtained by other workers.

## 5.7 Experiment for Mixed-mode Rock Fracture Study using the CSTBD

### 5.7.1 Introduction

Rock fracture studies were carried out under mode I, mixed mode and mode II. Mode I and mode II rock fracture toughness were tested using the CSTBD. On account of the time limit and samples available, only a small scale investigation was carried out. More extensive research is recommended.

### 5.7.2 The CSTBD Specimen Dimensions

The dimensions of the specimens, their normalized stress intensity factors

$N_I$ and $N_{II}$ are presented in Table 5.4. The samples come from the rest of the samples for the development the CCNBD method for mode I rock fracture toughness measurement.

Table 5.4 — Specimen Dimensions and their $N_I$, $N_{II}$, $F_I$, $F_{II}$

| Disc ID | D (mm) | B (mm) | $a/R$ | $\theta$ | $N_I$ | $N_{II}$ | Comment |
|---|---|---|---|---|---|---|---|
| Ma01 | 100 | 30 | 0.50 | 23.1° | 0.00000 | 1.7626 | Mode II |
| Ma02 | 100 | 30 | 0.60 | 20.5° | 0.00000 | 1.7889 | Mode II |
| Ma03 | 100 | 30 | 0.60 | 18.0° | 0.25803 | 1.6487 | Mixed mode |
| Ma04 | 100 | 30 | 0.60 | 15.0° | 0.46851 | 1.4435 | Mixed mode |
| Ma05 | 100 | 30 | 0.60 | 10.0° | 0.75436 | 1.0237 | Mixed mode |
| Disc ID | D (mm) | B (mm) | $a/R$ | 0.0° | $F_I$ | $F_{II}$ | Comment |
| Ma11 | 75 | 30 | 0.67 | 0.0° | 1.284 | 0.0000 | Mode I |
| Ma12 | 75 | 30 | 0.70 | 0.0° | 1.363 | 0.0000 | Mode I |
| Ma13 | 75 | 30 | 0.75 | 0.0° | 1.544 | 0.0000 | Mode I |
| Ma14 | 75 | 30 | 0.80 | 0.0° | 1.798 | 0.0000 | Mode I |

As shown in Table 5.4, diameter 100 mm and thickness 30 mm specimens were used for mixed-mode rock fracture study and mode II rock fracture toughness testing. 100 mm diameter and 30 mm thick specimens were originally from the CCNBD specimen Da01. The dimensionless crack length $a/R$ for Disc Ma02, Ma03, Ma04and, Ma05 is 0.6. In these samples, the $\theta$ varies from 20.5° to 10.0°. For specimen Ma01, the dimensionless crack length $a/R$ is 0.50, its corresponding inclination angle $\theta_c$ for pure mode II behavior is 23.1°. It is used for comparison with Disc Ma02 to study the effect of dimensionless crack length on mode II rock fracture toughness testing results.

75 mm diameter and 30 mm thick specimens were used to measure mode I rock fracture toughness as described in Chapter 4. These specimen were originally machined from the CCNBD specimen Db01. In these specimens, the di-

mensionless crack length varies from 0.67 to 0.80 so as to investigate the effect of dimensionless crack length $a/R$ on mode I rock fracture toughness testing results using the CSTBD specimen. The inclination angle $\theta$ is zero.

### 5.7.3 Calculation of the Stress Intensity Factors $K_I$ and $K_{II}$

The stress intensity factors $K_I$ and $K_{II}$ at the crack tip can be calculated using Equation (5.9) and Equation (5.10). When $N_I = 0$, it means that rock fractures under pure shear mode (mode II); when $N_{II} = 0$, it means that rock fractures under pure tensile mode (mode I); otherwise the rock fractures under mixed mode.

### 5.7.4 Experimental Procedures

As shown in Figure 5.7 and Photo 5.1, load is applied at an angle of $\theta$ with the slot direction. Load is applied at a constant displacement rate of 0.08 mm/minute. The loading inclination angle is maintained by two plates similar to those used in the CCNBD method. The fixture, instrumentation system and experimental procedures are basically the same as those in the CCNBD method for mode I rock fracture toughness testing.

At least three identical samples were tested. Average results are presented.

### 5.7.5 Presentation of Experimental Results

Experimental Results are presented in Table 5.5.

### 5.7.6 Analysis of the Experimental Results

As shown in Table 5.5, mode II rock fracture toughness testing results using the CSTBD method depend on its dimensionless crack length. This can be seen from the testing results by Disc Ma01 and Ma02.

The mode I rock fracture toughness testing results using the CSTBD method also showed its dependence on the dimensionless crack length. The lesser the dimensionless crack length, the larger the mode I critical stress intensity factors. The minimum dimensionless crack length used here is 0.67, generating the largest critical mode I stress intensity factor 0.538 $MN/m^{1.5}$. It is about 11% less than

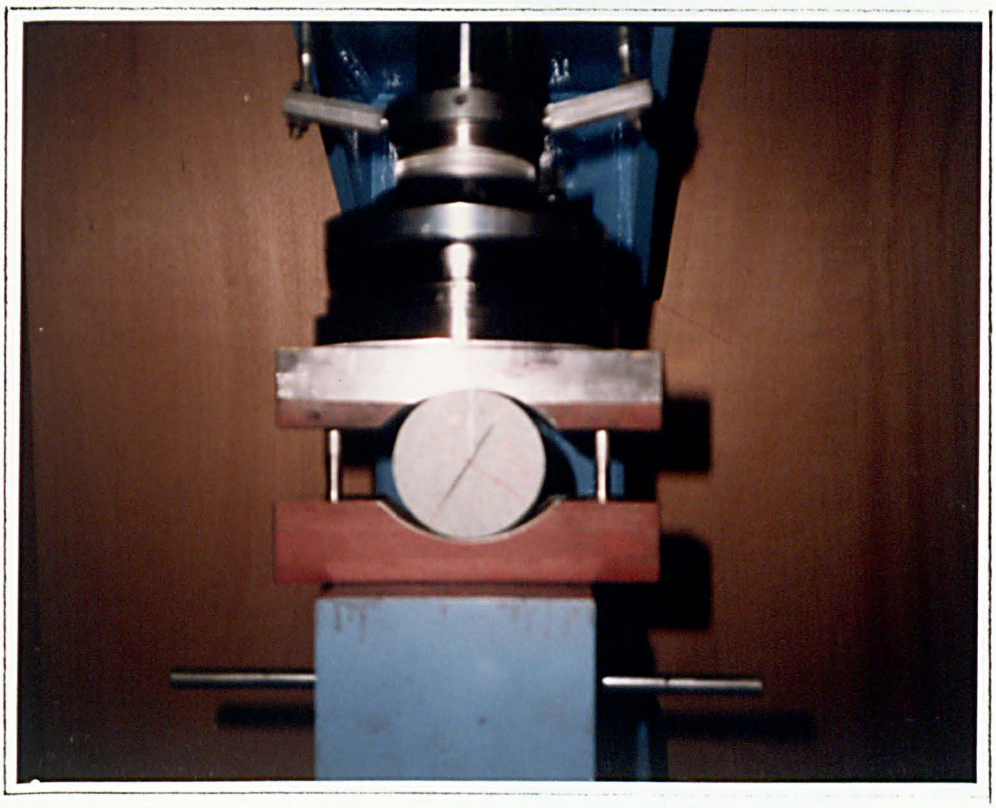

Photo 5.1 - The Apparatus for Mixed-Mode Rock Fracture Study


Photo 5.2 - The Specimens for Mixed-Mode Rock Fracture Study

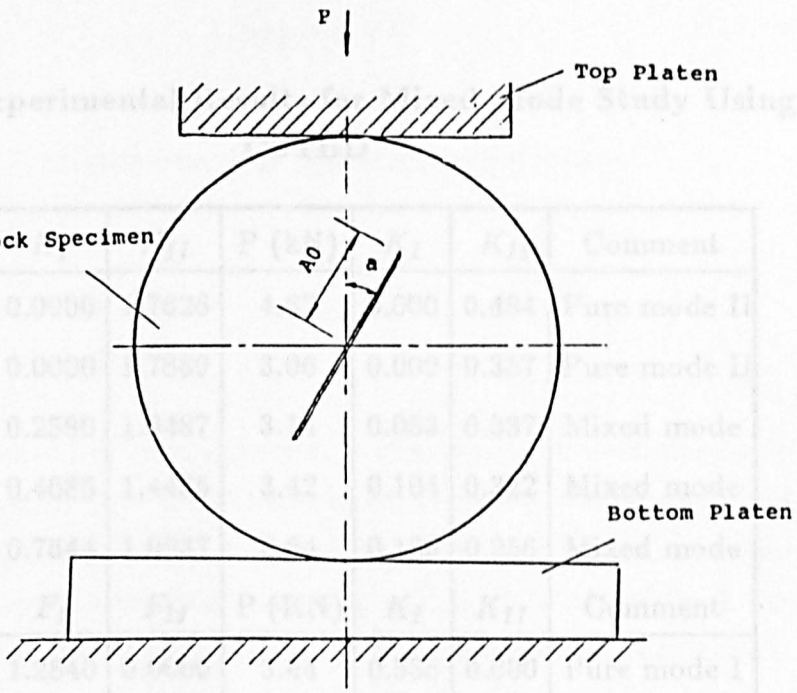


**Figure 5.7 — The Apparatus for Mixed-mode Rock Fracture Study and $K_{IIC}$ Testing using the CSTBD**

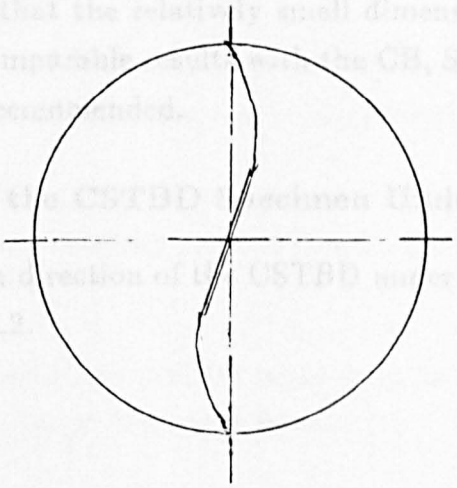

Figure 5.8 Mixed-mode Rock Fracture Crack Pattern

Table 5.5 — Experimental Results for Mixed Mode Study Using the CSTBD

| Disc ID | $N_I$ | $N_{II}$ | P (kN) | $K_I$ | $K_{II}$ | Comment |
|---|---|---|---|---|---|---|
| Ma01 | 0.0000 | 1.7626 | 4.62 | 0.000 | 0.484 | Pure mode II |
| Ma02 | 0.0000 | 1.7889 | 3.06 | 0.000 | 0.357 | Pure mode II |
| Ma03 | 0.2580 | 1.6487 | 3.14 | 0.053 | 0.337 | Mixed mode |
| Ma04 | 0.4685 | 1.4435 | 3.42 | 0.104 | 0.322 | Mixed mode |
| Ma05 | 0.7544 | 1.0237 | 3.84 | 0.189 | 0.256 | Mixed mode |
| Disc ID | $F_I$ | $F_{II}$ | P (KN) | $K_I$ | $K_{II}$ | Comment |
| Ma11 | 1.2840 | 0.0000 | 3.44 | 0.538 | 0.000 | Pure mode I |
| Ma12 | 1.3630 | 0.0000 | 2.95 | 0.489 | 0.000 | Pure mode I |
| Ma13 | 1.5440 | 0.0000 | 2.60 | 0.489 | 0.000 | Pure mode I |
| Ma14 | 1.7980 | 0.0000 | 2.22 | 0.486 | 0.000 | Pure mode I |

that tested by the CCNBD, CB and SR methods. Therefore we can see that long crack CSTBD specimen is not suitable for mode I rock fracture toughness measurement. It is expected that the relatively small dimensionless crack CSTBD specimen may generate comparable results with the CB, SR and CCNBD methods. Further research is recommended.

## 5.8 Crack Propagation of the CSTBD Specimen Under Mixed-mode

The crack propagation direction of the CSTBD under mixed-mode is shown in Figure 5.8 and Photo 5.2.

# Chapter VI

# Conclusions and Recommendations

## 6.1 Conclusions

The following work has been reported in this thesis: three-dimensional FEM and BEM calibration of the CCNBD specimen; two-dimensional FEM and BEM calibration of the CSTBD specimen under open mode; the size requirement investigation, experimental validation testing of the CCNBD method for mode I rock fracture toughness measurement by comparison with that by the standard methods for mode I rock fracture toughness measurement, recommended by the testing commission of the ISRM; a detailed comparison among the three chevron-notched rock fracture toughness testing methods; two-dimensional BEM and FEM calibration under mixed mode and mode II (pure shear mode); mixed-mode rock fracture study and mode II rock fracture toughness measurement using the CSTBD method. Based on this work, the following statements can be made:

1. The CCNBD method can generate comparable results to those using the Chevron-notched Short Rod and the Chevron-notched Bend methods;

2. The CCNBD method has many advantages over the chevron-notched short rod method and chevron notched bend method. These can summarized as follows:

   * Easy specimen preparation, 20 percent more samples can be prepared than for the CB or SR methods in the same time;

   * Easy to set up, easy to measure load line displacement and crack opening displacement. It uses compressive loading rather than tensile loading as used in the SR method. It does not require any complex apparatus for loading line displacment or crack mouth opening displacement measurements as used in

the CB or SR methods. Therefore the CCNBD method is much more efficient and economical than the CB and SR methods;

* There is no restriction for zero pre-load requirement of testing machine. The magnitude of failed load is quite large compared with that of the CB and SR methods;

* Easy to obtain samples for rock fracture toughness testing. It requires a relative small rock block. This method has a wider range application than the CB method;

* Easy to study the effect of rock anisotropy on rock fracture toughness testing results;

3. The formula used for mode I rock fracture toughness measurement using the CCNBD method is listed as equation (6.1).

$$K_{IC} = F_{IC} \times \frac{P}{D^{0.5}B} \tag{6.1}$$

Where:

$K_{IC}$ – Mode I rock fracture toughness, $MN/m^{1.5}$;

$F_{IC}$ – Dimensionless stress intensity factors;

D – Diameter of the CCNBD specimen, cm;

B – Thickness of the CCNBD specimen, cm;

P – Maximum failure load, kN.

4. Dimensionless stress intensity factors can be obtained from three-dimensional BEM and FEM calibration or compliance calibration using aluminum as an experimental material. Dimensionless stress intensity factors calibrated by three dimensional BEM for the CCNBD specimen are presented in Table 2.2 of Chapter II.

5. For short crack specimen ($a_1/R \leq 0.3$), the CCNBD specimen could be treated as the CSTBD specimen without losing its accuracy. The minimum stress intensity factor will be reached at $a/R = a_1/R$. This statement is from both 2D and 3D BEM stress intensity factors calculated for the cracked Brazilian disc specimen. For a long crack specimen, critical (minimum) dimensionless stress intensity factors will be reached at $a/R < a_1/R$, it can only be assessed by three dimensional BEM and FEM calibration or compliance calibration using aluminum as an experimental material;

6. The curved loading contact angle has no influence on rock fracture toughness testing results when the arc angle is less than 10 degrees for $a_1/R \leq 0.8$. This gives strong support to the recommendation that the rig used for indirect tensile strength testing by Brazil test could be used for rock fracture toughness testing by the CCNBD method;

7. Rock fracture toughness testing using the CCNBD method shows its independence of the specimen thickness, initial crack length, radius of curved slot within the size range tested. The minimum size criterion using the CCNBD method for mode I rock fracture toughness testing is that specimen diameter should be larger than 50 mm. If a 50 mm specimen or even a smaller dimension specimen is used, a geometry correction factor should be used. It is required that $a_1/R \leq 0.85$ so that no stress concentration are generated around the intersection of the loading line and the chevron notches;

8. Three dimensional BEM calibration for the CCNBD specimen using the BEASY programme shows that even a relative coarse mesh can generate very accurate results. BEM is preferable to the FEM in the modelling of the crack tip in terms of easy data preparation, computer time saving etc.;

9. The variation coefficients of the testing results for the same material is generally smaller than 3%. From the results obtained in this research programme, for the three chevron-notched mode I rock fracture toughness testing methods, the variation coefficients are the lowest using the CCNBD method;

10. Transverse tensile failure does not exist in the CCNBD testing. It makes this method more attractive than the SR method which sometimes has transverse

tensile failure;

11. The standard geometry specimen recommended for mode I rock fracture toughness measurement using the CCNBD method is disc Db01. Its dimensions are: diameter, $75 \pm 1.0mm$; thickness, $30 \pm 0.5mm$; initial crack length: $10 \pm 0.2mm$; radius of the curved slot: $52 \pm 1.0mm$. The other discs used in this research programme such as Da11 etc. could also be used for rock fracture toughness testing;

12. There are quite a lot of similarities between the testing methods for rock tensile strength and rock fracture toughness testing. The three point bend and Brazilian disc test can be used for rock tensile strength testing. The chevron-notched three point bend and the chevron-notched Brazilian disc could be used for mode I rock fracture toughness testing. The only difference is that a slot is cut in the rock fracture toughness testing specimen;

13. A number of semi-circular specimens such as a chevron-notched semi-circular three point bend specimen, chevron-notched compact tension, semi-circular three point bend specimen etc. could be used for mode I rock fracture toughness measurement;

14. Rock fracture toughness (mode I) could be measured using the CSTBD method. The results obtained in this research programme show its dependence on dimensionless crack length. The short crack CSTBD specimen presumbly could generate comparable results with that by the CCNBD, SR and CB methods;

15. The effect of rock anisotropy on rock fracture toughness measurement (mode I) can be easily studied using a small block of rock by the CCNBD method. A group of fracture specimens such as the CB, SR and the CCNBD tested for the effect of rock anisotropy on mode I rock fracture toughness study proposed by Ouchterlony (1988) can not be used. The results measured for the three chevron-notched rock fracture specimens can not be the same, even for perfectly homogeneous material;

16. Mode II rock fracture toughness can be measured by the CSTBD specimen with an inclined angle of loading relative to slot direction. The CSTBD specimen could be prepared directly from the CCNBD specimen. The only extra procedure required is that the chevron notches of the CCNBD specimen should be cut-off by a hand saw. The cracked Brazilian disc used in this research programme for mode II rock fracture toughness testing has a long crack. The results obtained show that the mode II rock fracture toughness testing results depend on dimensionless crack length. The short crack Brazilian disc specimen could presumedly generate ideal $K_{IIC}$ testing results.

## 6.2 Recommendations

The work done so far proves that the CCNBD method has many advantages over the recommended chevron-notched specimens, i.e., the Chevron-notched Bend specimen and the Chevron-notched Short Rod specimen. Comparable results can be generated with the two recommended methods, therefore it has good prospects for being adopted as one of the rock fracture toughness testing methods. There is still a lot of work to be done before the CCNBD method is recommended as the third chevron-notched specimen for mode I rock fracture toughness measurement. A comprehensive further investigation is recommended. This should consist of the following aspects.

1. Round-robin numerical calibration of the CCNBD and CSTBD specimen is recommended. It is recommended that disc Db01 etc. should be calibrated at different research sites using both the BEM and FEM;

2. Compliance calibration of the CCNBD specimen using aluminum as an experimental material should be done. A round-robin calibration is also recommended;

3. Effect of loading rate or loading line displacement rate on $K_{IC}$ testing results should be performed in the future;

4. Level II testing of the CCNBD method should be developed for rock plasticity correction. This could be done by a graphical construction method

suggested in the recommended standards for mode I rock fracture toughness measurement by the testing commission of the ISRM;

5. A round-robin testing using the CB, SR and CCNBD methods is also recommended. Samples from different sources should be tested by these three chevron-notched methods, the results should be evaluated;

6. Mixed-mode rock fracture theories should be studied using the CSTBD specimen.

7. The effect of specimen thickness, diameter, initial crack length etc. on mode II rock fracture toughness value should be studied further. A short crack length CSTBD specimen should be tested for mode II rock fracture toughness measurement;

8. A comparison between mode II rock fracture toughness testing results by both symmetrical four point shear testing proposed by Wang and Huang (1985) and the CSTBD specimen should be performed.

9. The detailed numerical calibration should be performed. A round robin numerical calibration for the CSTBD specimen under mixed-mode or pure shear mode should be performed. An accurate value of the inclination angle $\theta_c$ for pure mode II rock fracture behavior should be calculated using FEM and BEM;

10. The application of mode II rock fracture toughness and mixed-mode rock fracture theories should be studied. Drag tool rock cutting mechanism analysis could be based on mixed-mode rock fracture theories;

11. More rock samples should be measured. The relationship between mode II rock fracture toughness and rock mechanical properties, rock textural properties, acoustic testing etc. should be investigated.

12. A draft for a recommended standard for mode I rock fracture toughness measurement using the CCNBD is being prepared.

# Part II

# Tunnelling Machine Performance Prediction

# Chapter VII

## The Review of Tunnelling Machine Performance Prediction

### 7.1 Introduction

The research program for the prediction of tunnelling machine performance consists of two parts: (1) the comprehensive review for existing methods for the prediction of tunnelling machine performance, especially the evaluation of intact rock cuttability. (2) the step-wise curvilinear regression analysis of intact rock cuttability based on a large database including rock physical, mechanical, energy and fracture properties etc.

The Prediction of tunnelling machine performance has previousely been conducted by many workers (Fowell R.J., 1976, 1982, 1983; Nelson, 1985, 1986; McFeat-Smith, 1976, 1979, 1983, 1985; Xu X. H., 1984; Howarth, 1983; Tarkoy 1976; Bauman, Aleman, 1981; et al).

Due to the complicated interaction between rock and cutting tool, the prediction of tunnelling machine performance is influenced by many factors.

In order to have a complete understanding of drag tool rock cutting machine performance, rock cutting theories are presented here.

### 7.2 Drag Tool Rock Cutting Mechanism Analysis

The rock cutting process is very complicated. At present, the failure mechanisms of rock cutting are not well understood. A number of mechanical models based on different failure mechanisms have been proposed.

Models of rock cutting usually try to explain the underlying phenomena. This may be very difficult in an inhomogeneous rock because of large grains, pores, cracks, fissures and discontinuities.

Most rock cutting models are purely analytical. Such models based on different rock strength theories are very important for the understanding of the rock cutting process. They often describe reality quite well, although they contain some simplifications and assumptions. The models are often based on empirical results and observations.

To account for the behaviour during the cutting process and chip formation, various models have required various assumptions concerning the stress field beneath the indentor, geometry of the tool and chip (debris) and the material failure or yield criterion.

Statistical models require a lot of experiments (both observation and measured results) before any conclusions can be drawn. It does not try to explain any of the underlying processes. The model simply describes any observed phenomena, usually in statistical terms.

The use of numerical methods has increased rapidly with the development of cheaper and more powerful computers. The development of FEM and BEM provides a way of simulating the rock cutting processes based on the accurate calculation of mode I and mode II stress intensity factors of the crack tip.

### 7.2.1 Merchant's Theory Based on Shear Strength Theory

Merchant (1945) derived an expression for the cutting force required in metal cutting by considering the equilibrium of the "chip" of the material lying against the tool and used the hypothesis of minimum force to determine the orientation of the plane of shear and the corresponding cutting force. The model for cutting force calculation is shown in Figure 7.1.

In his theory, the cutting force is calculated by the formula:

$$F_c = \frac{cd\sin(\beta+\phi)}{\sin\theta\sin(\beta+\phi+\theta)} \tag{7.1}$$

Where:

c = shear strength of the material ($N/m^2$);

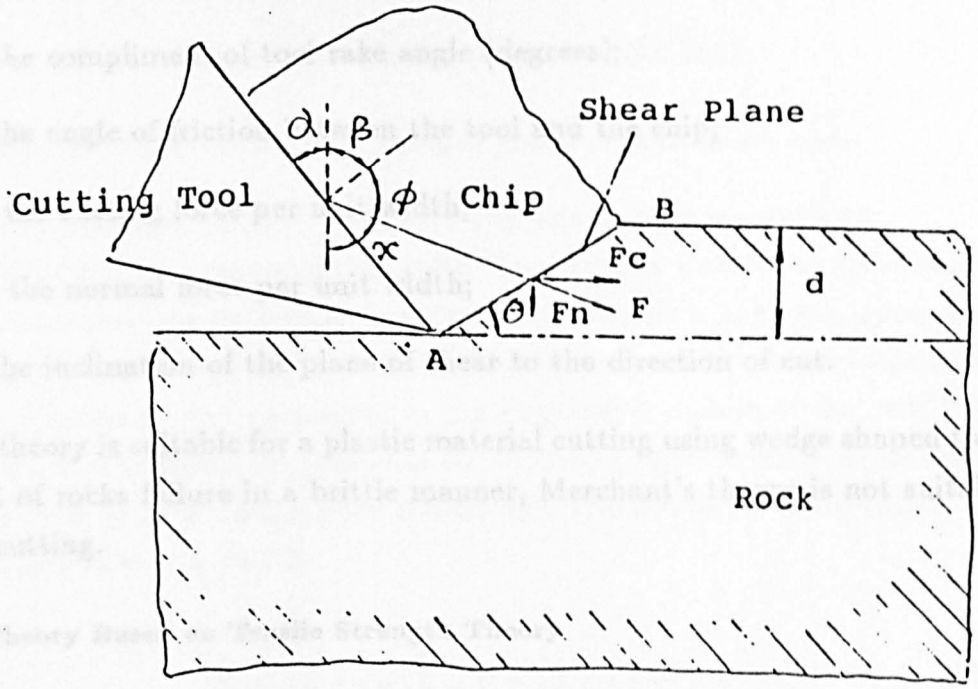


**Figure 7.1 — Merchant's Theory: Shear Strength Failure Criterion**

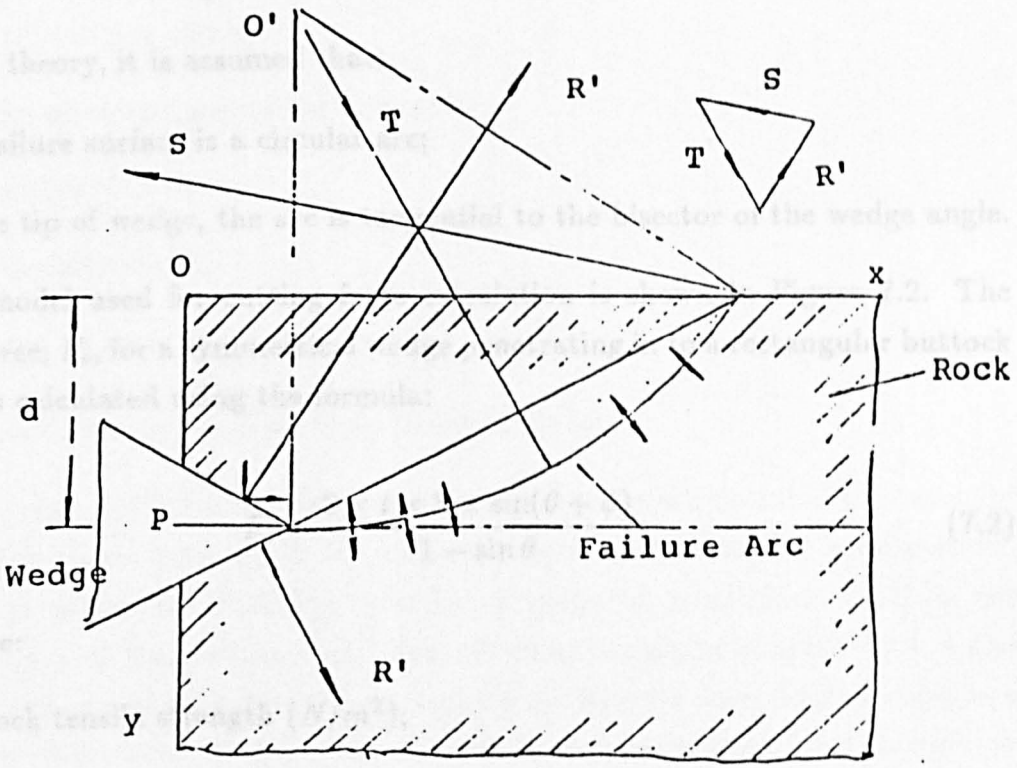


**Figure 7.2 — Evans' Theory: Tensile Strength Failure Criterion**

d = the depth of cut (m);

$\beta$ = the compliment of tool rake angle (degrees);

$\phi$ = the angle of friction between the tool and the chip;

$F_c$ = the cutting force per unit width;

$F_n$ = the normal force per unit width;

$\theta$ = the inclination of the plane of shear to the direction of cut.

This theory is suitable for a plastic material cutting using wedge shaped tool. But most of rocks failure in a brittle manner, Merchant's theory is not suitable for rock cutting.

### 7.2.2 Evans' Theory Based on Tensile Strength Theory

Based on the observations during the penetration of wedge to coal, Evans (1962) proposed that the breaking of coal is essentially tensile failure and suggested a tensile breaking theory for rock cutting.

In his theory, it is assumed that:

1 The failure surface is a circular arc;

2 At the tip of wedge, the arc is tangential to the bisector of the wedge angle.

The model used for cutting force calculation is shown in Figure 7.2. The cutting force, $F_c$, for a symmetrical wedge penetrating in to a rectangular buttock of rock, is calculated using the formula:

$$F_c = \frac{2 \times t \times h \times \sin(\theta + \phi)}{1 - \sin\theta} \tag{7.2}$$

Where:

t = rock tensile strength ($N/m^2$);

h = cutting depth (m);

$\theta$ = the half wedge angle;

$\phi$ = the angle of friction between the wedge and the rock.

### 7.2.3 Evans' Theory for point-attack; Rock Cutting Based on Tensile Strength

Evans I. (1984) proposed a model for the rock cutting mechanism point-attack tools. It is assumed that radial compressive stresses are produced in the rock, accompanied by tensile hoop stresses. Tensile cracks will open up at the interface between tool and rock when the stress equals the tensile strength of the rock. The cracks will propagate to the unstressed surface of the rock if the conditions are propitious. He proposed the following formula for the calculation of cutting force exerted on the point-attack tool. The model for point-attack tool cutting is shown in Figure 7.3.

$$P_c = 16 \times \cos^2\theta \times [t \times u] \times t \times d^2 \tag{7.3}$$

Where:

$P_c$ = the cutting force;

u = the unaxial compressive strength;

d = cutting depth;

t = tensile strength;

$\theta$ = semi-angle of cone.

### 7.2.4 Nishimatsu's Theory based on Mohr Strength Theory

Nishimatsu (1971) proposed a rock cutting theory which takes into account compressive stress induced by the cutting forces, as well as the tensile stress. The theory is thus based on the criterion of failure dependent on depth of cut and geometry of the cutting tool. The criterion of failure is given by a set of principal stresses which define the state of stress. Results were shown to compare favourably with experimental work. The model for the cutting force calculation is shown in Figure 7.4.

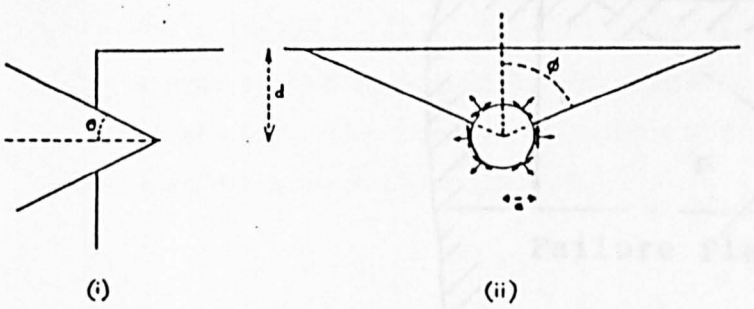


1 (i) Point attack pick acting on buttock of mineral
(ii) Equivalent hole under internal pressure

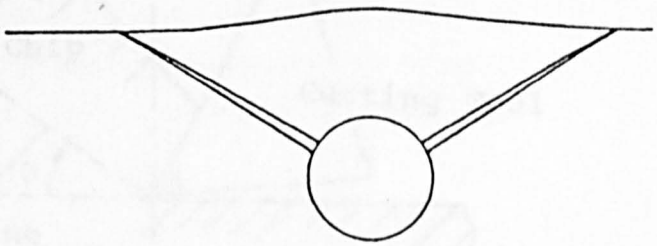

2 Pattern of breakout

3 Forces acting on half-segment

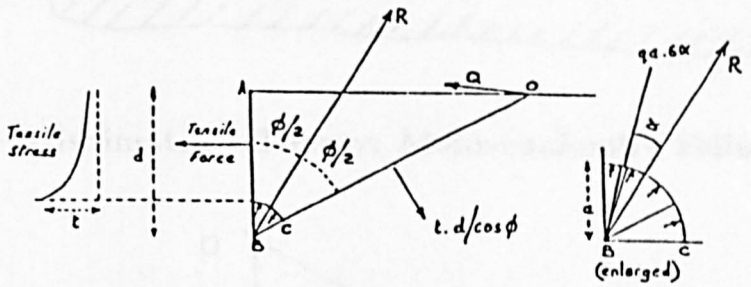


4 Angle of a V-notch variation

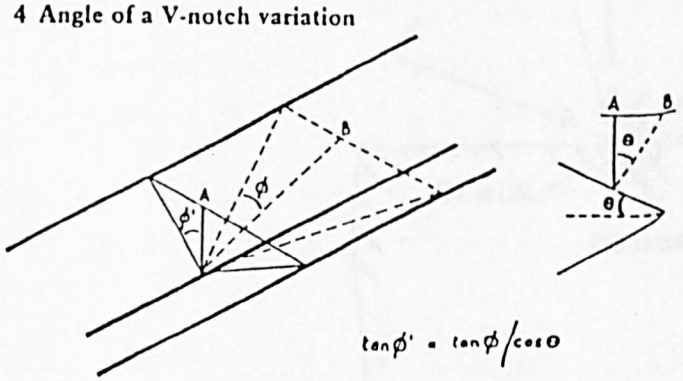


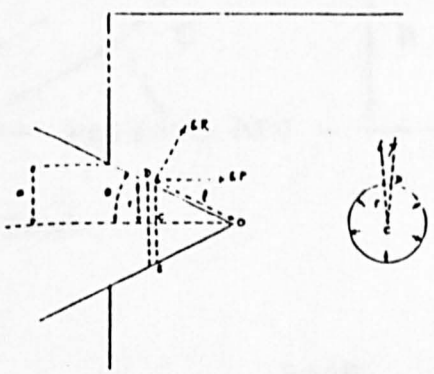

5 Range of perspective when looking at point-attck from side

Figure 7.3 — Evans' Model for Point-attck Tool Rock Cutting

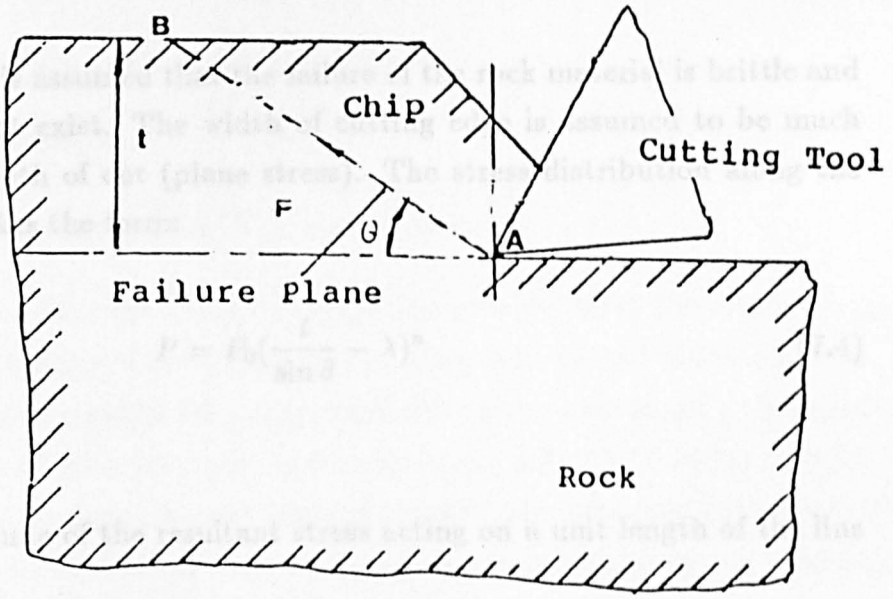


**Figure 7.4 — Nishimatsu's Theory: Mohr-coulomb's Failure Criterion**

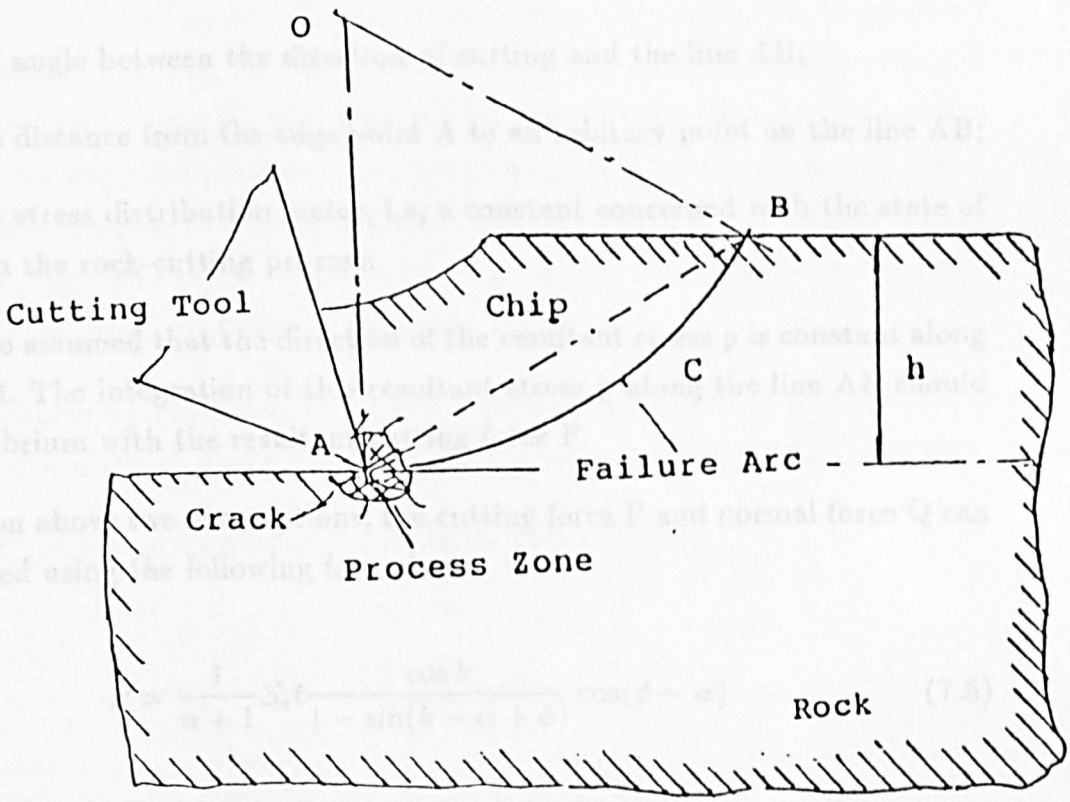


**Figure 7.5 — Deliac's Theory: Mode I Rock Fracture Toughness Failure Criterion**

In his theory, it is assumed that the failure of the rock material is brittle and plastic zone does not exist. The width of cutting edge is assumed to be much greater than the depth of cut (plane stress). The stress distribution along the failure plane AB takes the form:

$$P = P_0(\frac{t}{\sin\theta} - \lambda)^n \tag{7.4}$$

Where:

P = the magnitude of the resultant stress acting on a unit length of the line AB;

$P_0$ = a constant determined from the equilibrium of forces;

t = the depth of cut;

$\theta$ = the angle between the direction of cutting and the line AB;

$\lambda$ = the distance from the edge point A to an arbitary point on the line AB;

n = the stress distribution factor, i.e, a constant concerned with the state of stress in the rock-cutting process.

It is also assumed that the direction of the resultant stress p is constant along the line AB. The integration of this resultant stress p along the line AB should be in equilibrium with the resultant cutting force F.

Based on above two assumptions, the cutting force P and normal force Q can be calculated using the following formulae.

$$P = \frac{1}{n+1} S_s t \frac{\cos k}{1 - \sin(k - \alpha + \phi)} \cos(\phi - \alpha) \tag{7.5}$$

$$Q = \frac{1}{n+1} S_s t \frac{\cos k}{1 - \sin(k - \alpha + \phi)} \sin(\phi - \alpha) \tag{7.6}$$

where:

k = a constant of the angle of internal friction;

$S_s$ = the shear strength.

### 7.2.5 Rock Cutting Mechanism Based on $K_{IC}$ etc. by Deliac

Rock cutting process is an energy propagation process, when the stored energy exceeds the critical energy of rock, new cracks are produced and if the external energy is continually applied to the rock, crack will extend continuouly. Because of the development of rock fracture mechanics, especially the development of rock fracture toughness measurement techniques and the numerical calculation of stress intensity factors of the crack tip, it makes it possible to study the breaking model of rock cutting from the energy point of view. Deliac (1986) suggested that there are, in fact, two fundamental chipping modes, which he called mode A and Mode B. Mode A is typical of shear failure of the rock. Assuming that the chip has a three-dimensional prismatic shape and that chip formation is governed by the Coulomb criterion, he has obtained good agreement with experimental values of maximum forces for radial drag bits. Mode B is a fracture propagation mode, using a simplified fracture mechanics approach, and assuming the rock chip surface to be part of a sphere. Deliac has developed the equations for the maximum cutting and thrust force exerted by the tool. The model for drag tool rock cutting proposed by Deliac is shown in Figure 7.5.

The formulae proposed by Deliac are based on the formulae for rock fracture toughness measurement using the direct indentation method given by Atkinson (1980).

Table 7.1 summarizes the dual modes by Deliac (1986).

Table 7.1 — Rock Cutting Modes by Deliac

| Chipping Mode | Mean Rock Parameters | Maximum Cutting Force | Comments |
|---|---|---|---|
| A | $\sigma_c, \theta$ | $A \times h + B \times h^2$ | A and B $\propto sigma_c$, $B \ll A$ |
| B | $K_{IC}, a_c$ | $C \times h^{3/2}$ | C $\propto K_{IC}$ |

When the pick is wide, the rock is not very brittle, or the depth of cut is high, mode A is predominant;

When the pick is sharp and rigid, rock is brittle, mode B is predominant.

### 7.2.6 Rock Cutting Model Based on Mixed-mode Fracture Theory

The cutting model proposed by Deliac is based on mode I rock fracture toughness and rock shear strength. The mode II (shear mode) rock fracture toughness could be measured by CSTBD method analysed in part I, therefore it is possible to study drag tool rock cutting mechanism based on mixed-mode (tensile and shear fracture mode) crack propagation theories. There are three existing mixed-mode crack propagation theories, such as:

1 Maximum hoop stress theory;

2 Minimum strain energy density theory;

3 Strain energy release rate theory.

Future research could be done based on numerical analysis and experimental observations so as to develop the mixed-mode drag tool rock cutting model.

### 7.2.7 Finite Element Modelling of Rock Cutting

The finite element method has been used by some workers to model the rock cutting processes (Swenson, Ingraffea, Saouma etc).

Hardy (1973) in his Ph.D thesis used the finite element method to model rock cutting based on the fracture mechanics method. The model for the stress intensity factor of crack tip is shown in Figure 7.6. The finite element method was used to determine the energy release rate for assumed crack directions. The direction that maximizes the energy release rate in the direction, in which the crack will grow at the lowest applied load, and is thus the direction of crack growth.

Ingraffea used the finite element method to model the crack propagation during rock cutting based on rock fracture mechanics approach. The finite element mesh used is shown in Figure 7.7.

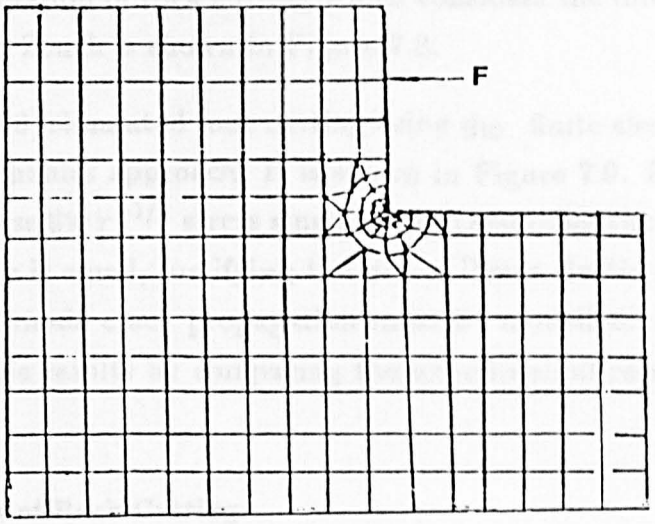


**Figure 7.6 — Hardy's Finite Element Simulation of Rock Cutting**

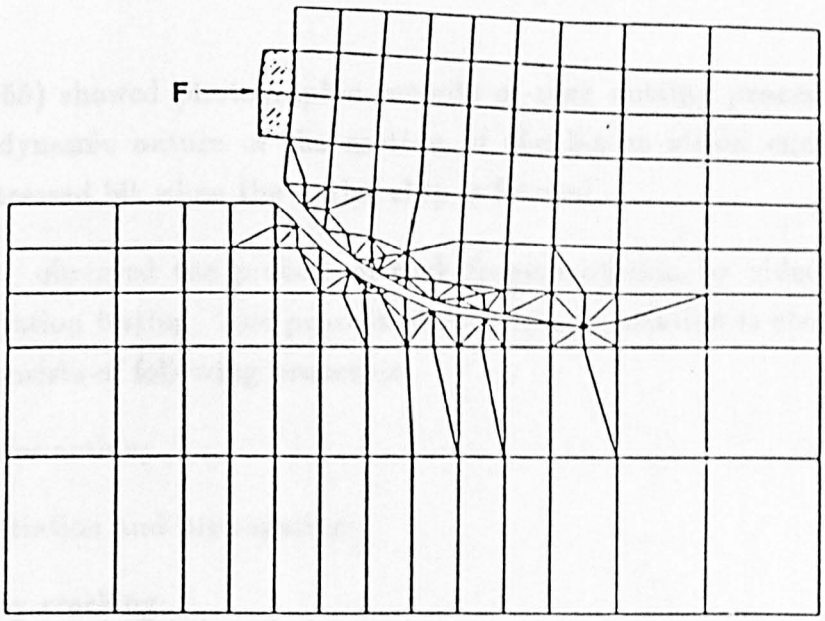


**Figure 7.7 — Ingraffea's Finite Element Simulation of the Rock Cutting Process**

The finite element simulation of rock cutting which considers the interaction of rock and cutting tool by Zeuch is shown in Figure 7.8.

Saouma V. E. et al.(1986) simulated rock cutting using the finite element method based on the fracture mechanics approach. It is shown in Figure 7.9. For the simulation of rock cutting process,the $r^{-1/2}$ stress singularities (assuming the process zone ahead of the crack tip is small, justifying the use of linear elastic fracture mechanics) and the mixed-mode crack propagation must be modelled. He validated his numerical analysis results by comparing the experimental results and obtained some success.

### 7.2.8 Experimental Observations of Rock Cutting

Nguyen Mink (1974) based on experimental observations and proposed three stages for rock cutting. It is shown in Figure 7.10.

Three cyclic stages were defined by Goodrich (1956) in the development of chips by drag bits; these are crushing, crushing-chipping and major chip formation.

Fairhurst (1955) showed photographic records of rock cutting process and emphasized the dynamic nature of the motion of the bit as strain energy is released by the stressed bit when the major chip is formed.

Lindqvist etc. observed the process of rock fragementation by video tape recorder in indentation testing. The process of rock fragementation is shown in Figure 7.11. It consists of following processes:

1 A: contact deformation;

2 B-C: crack initiation and propagation;

3 D-E: secondary cracking;

4 F: chipping.

### 7.2.9 Comment on Drag Tool Rock Cutting Models

From the analysis of rock cutting models above, we can see that the process

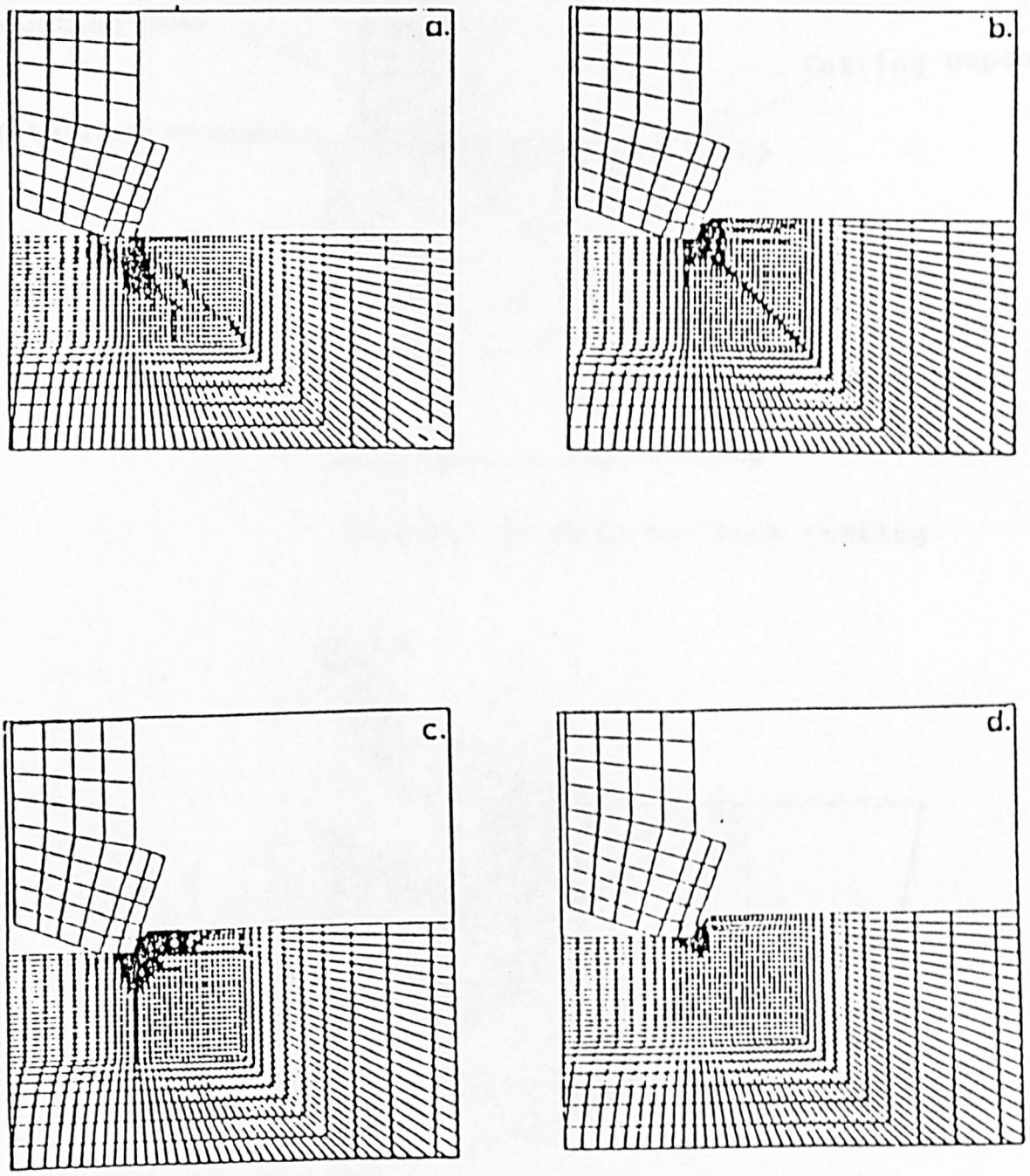


**Figure 7.8 — Zeuch's Finite Element Modelling; Fractures and Crushing Zones are Indicated by Shaded Regions**

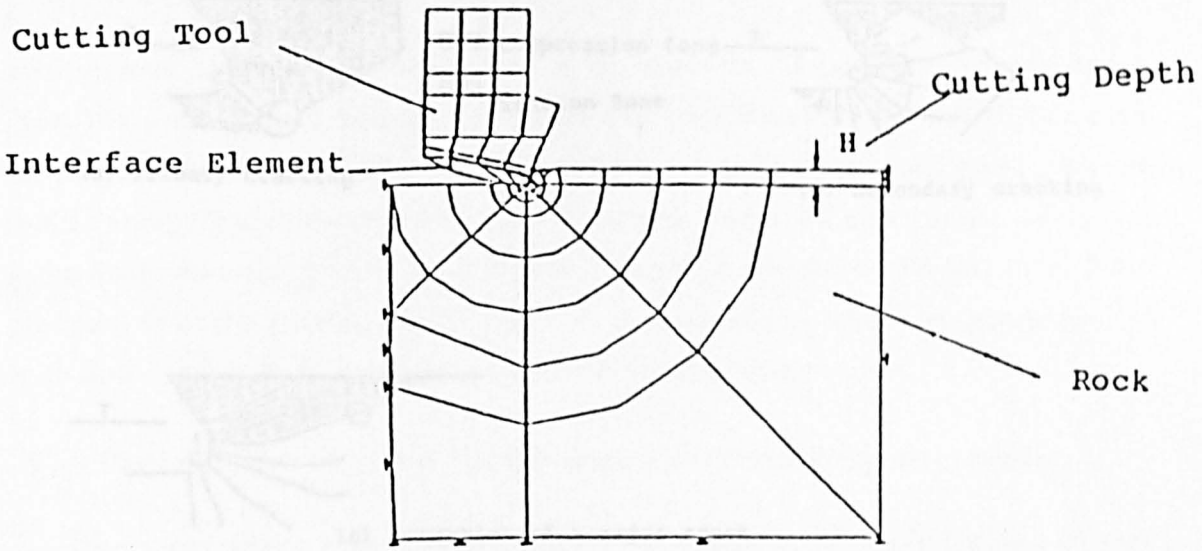


Initial FE Mesh for Rock Cutting

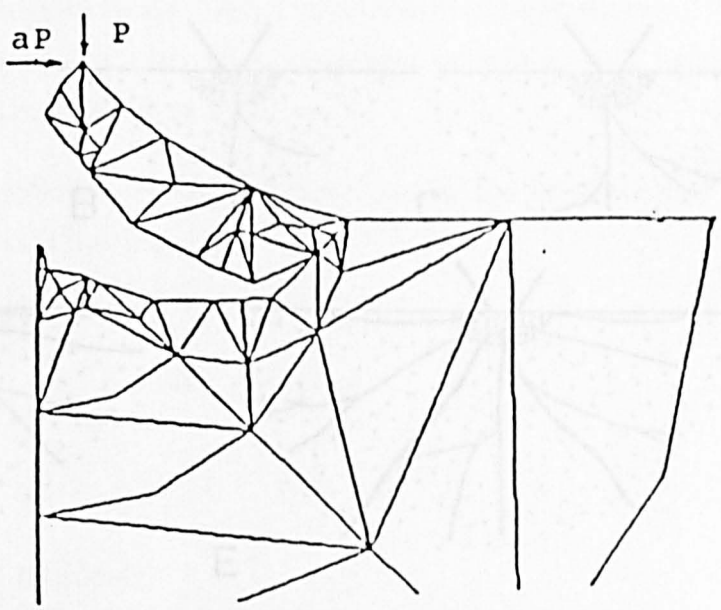


Deformed FE Mesh, Line Load

**Figure 7.9 — Saouma's Finite Element Simulation for Rock Cutting**

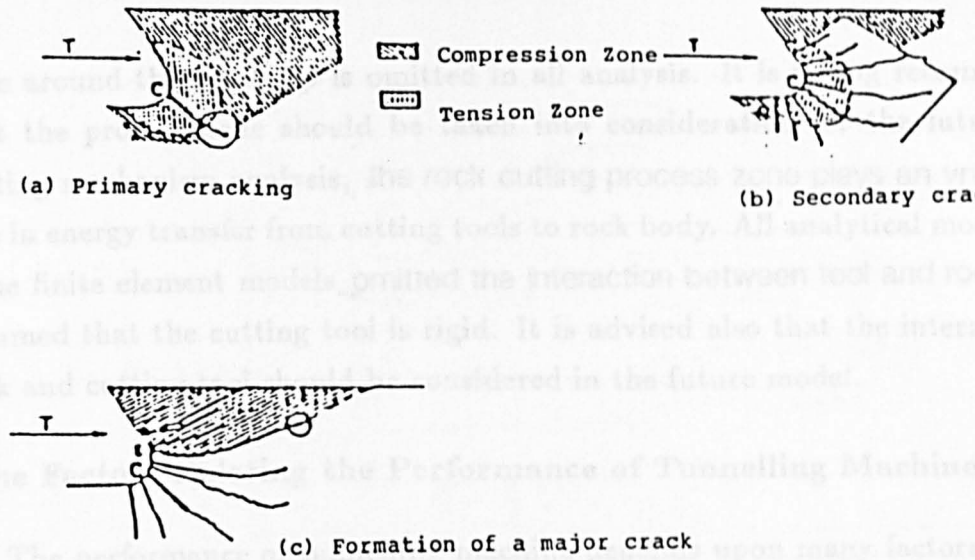


**Figure 7.10 — Crack Propagation Process by Nguyen Mink**

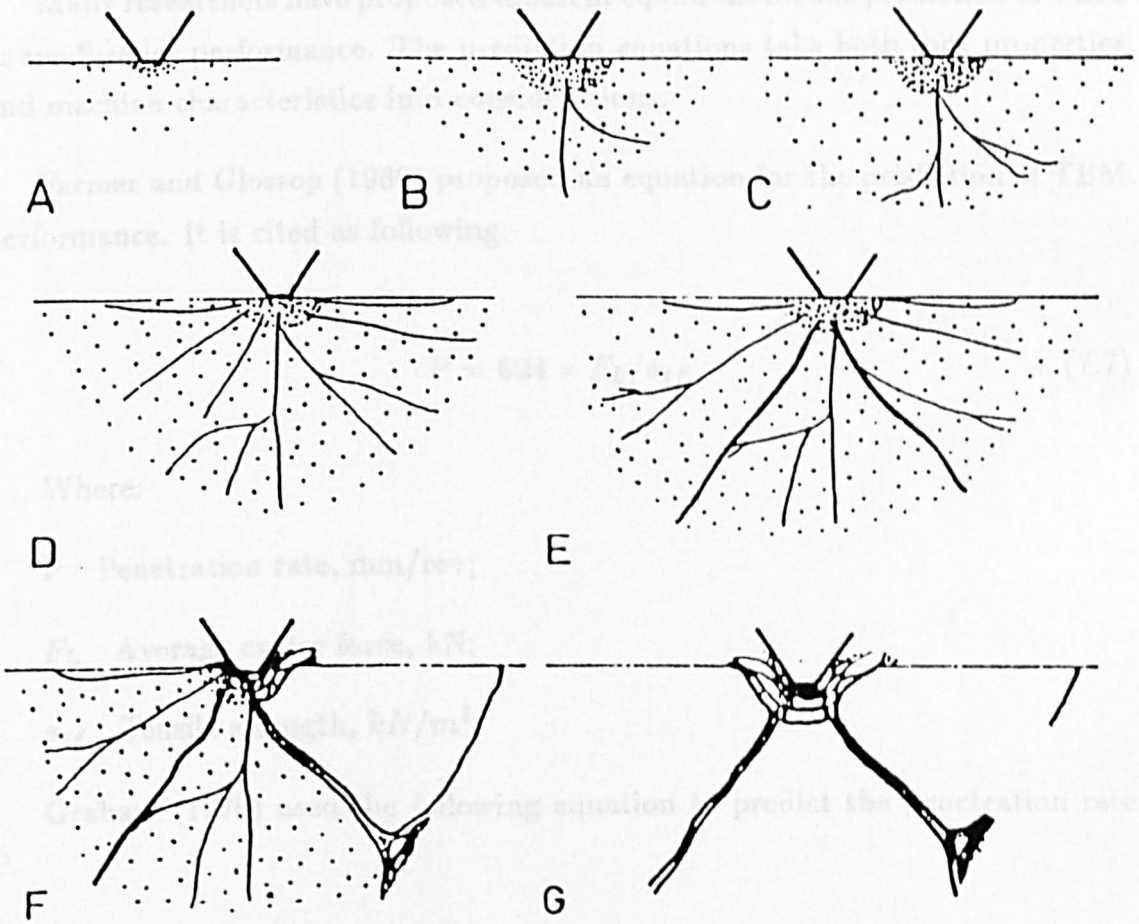


**Figure 7.11 — Rock Fragementation Process under Indentation by Linaqvist**

zone around the crack tip is omitted in all analysis. It is strong recommended that the process zone should be taken into consideration for the future rock cutting mechanism analysis, the rock cutting process zone plays an vry important role in energy transfer from cutting tools to rock body. All analytical models and some finite element models omitted the interaction between tool and rock, they assumed that the cutting tool is rigid. It is advised also that the interaction of rock and cutting tool should be considered in the future model.

## 7.3 The Factors Relating the Performance of Tunnelling Machines

The performance of tunnelling machine depends upon many factors. Fowell and Johnson (1982) have done extensive research on the factors affecting the performance of tunnelling machine. It was summarized in Table 7.2.

Many researchers have proposed different equations for the prediction of TBM or roadheader performance. The prediction equations take both rock properties and machine characteristics into considerations.

Farmer and Glossop (1980) proposed an equation for the prediction of TBM performance. It is cited as following:

$$P = 624 \times F_L/\sigma_{tf} \tag{7.7}$$

Where:

P Penetration rate, mm/rev;

$F_L$ Average cutter force, kN;

$\sigma_{tf}$ Tensile strength, $kN/m^2$.

Graham (1976) used the following equation to predict the penetration rate P.

$$P = 3940F_L/UCS \tag{7.8}$$

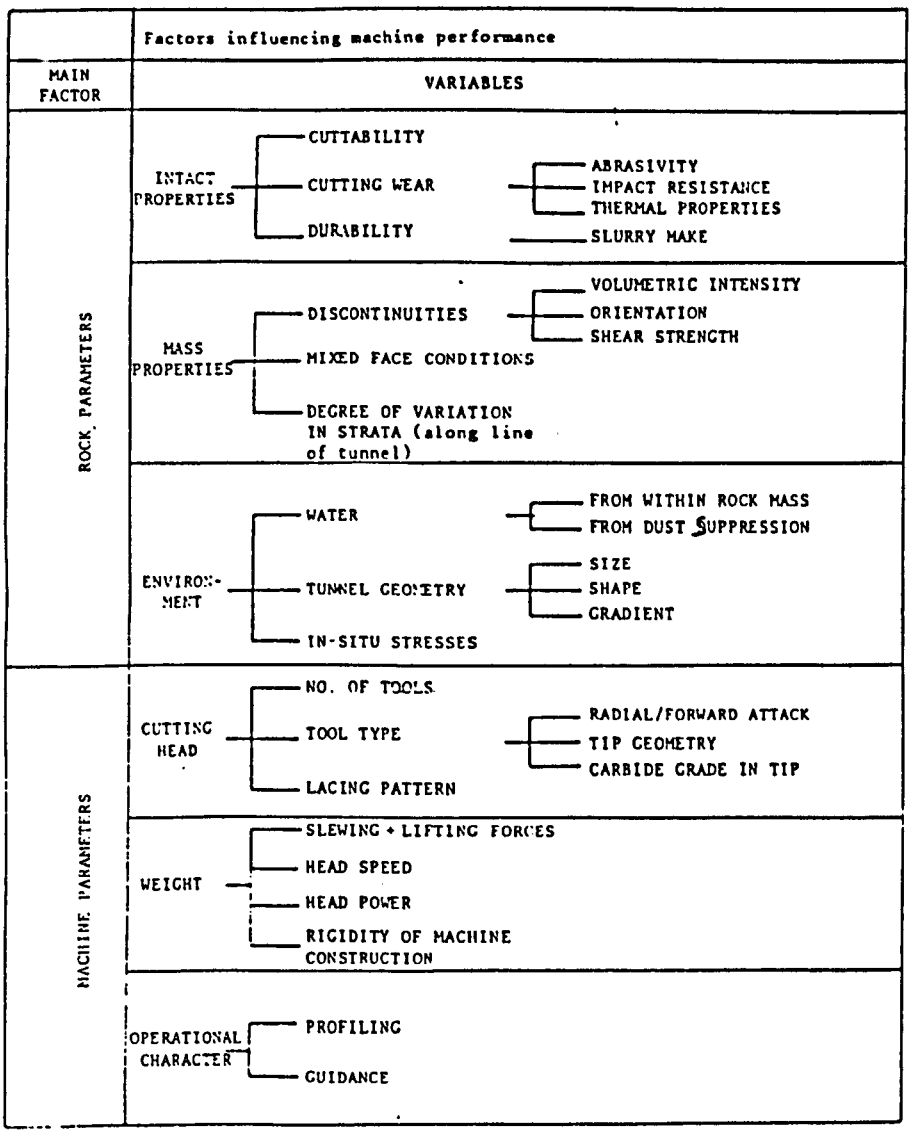


Table 7.2 — Factors Influencing Tunnelling Machine Performance by Fowell

Where:

UCS Rock uniaxial compressive strength, MPa;

$F_L$ Average cutter force, kN;

P Penetration per revolution, mm/rev.

Bamford (1984) proposed the following equation for the prediction of penetration rate of TBMs.

$$P = 0.535Sch - 8.49 - 0.00344T - 0.000823CI + 0.0137\theta \tag{7.9}$$

Where:

P Penetration rate, m/h;

T Machine propel thrust force, t;

$\theta$ Angle of shearing resistance, degrees;

Sch Schmidt hammer hardness;

CI NCB cone indenter hardness, N/mm.

Hughes (1986) used the following equation to predict the penetration rate of TBM.

$$V = \frac{6 \times Th^{1.2} \times N \times n}{UCS^{1.2} \times r^{0.6}} \tag{7.10}$$

Where:

V Rate of advance, m/h;

Th Thrust per disk periphery, kN;

N Speed of cutting head, rev/s;

r Average radius of disks, m;

UCS Uniaxial compressive strength, MPa.

## 7.4 Rock Mass Properties

All existing rock mass classification systems considered the following factors:

1 Strength of intact rock;

2 Frequency of jointing;

3 Joint strength;

4 Confining stress;

5 Water presence.

It is well known that increases in joint frequency and aperture can influence tunnelling machine performance. Rock cuttability with the use of a roadheader in heavily fractured ground was found to be a function more of rock fracture spacing than of rock strength (Douglas W., 1985). Blindheim O. T. (1986) reported that weakness planes (parallel to tunnel axis) have a significant effect on TBM penetration rates, especially when the distance between the planes is of the same order as that between cutter grooves.

Aleman (1982) in his Ph.D thesis analysised and reviewed many methods for deriving a rock mass classification index which was proposed for roadway support or other purposes. He tried to relate these rock mass classification index to tunnelling machine performance and obtained some success.

Vasek (1978) used the four indices: workability, abrasivity, degree of fissuration of strata and indentation strength. Workability is assessed by standard instrumented cutting tests; abrasivity is determined by the weight loss measured on a standard steel pin which has been drawn across the rock surface under a given load. Degrees of fissuration are calculated from measurements of discontinuity spacings either from borehole cores. Indentation strength is measured by indentation testing. Then he used the following formula to predict the machine performance:

$$NS = \frac{1}{R_C \times SP} \times K \tag{7.11}$$

Where

NS = cutting rate, $m^3/h$;

$R_c$ = workability;

SP = degree of fissuration;

K = constant depending on machine and cutting head type.

Jenni and Balissat (1972) proposed an equation for the prediction of tunnelling machine performance based on boreability index and rock masses evaluation index, i.e., the number of discontuities per linear meter. The equation is shown here:

$$PenetrationRate = ThrustForce \times \frac{K}{b_q} \tag{7.12}$$

Where:

k = discontinuity per meter;

$b_q$ = boreability index.

Poole (1978) has successfuly correlated RQD with machine cutting performance data.

Sandbak compared in-situ GRCS (Geomechanical rock classification systems) of rock mass with TBM and roadheader performance data and demonstrated a moderately good correlation as shown in Figure 7.12(a). A similar result has been reported by Cassinelli et al.(1982) who used the rock support rating (RSR) geomechanics classification system for correlation with TBM performance as shown in Figure 7.12(b).

Fowell and Johnson has done extensive research on the effect of rock mass rating on tunnelling machine advance rate. It is shown in figure 7.12(c).

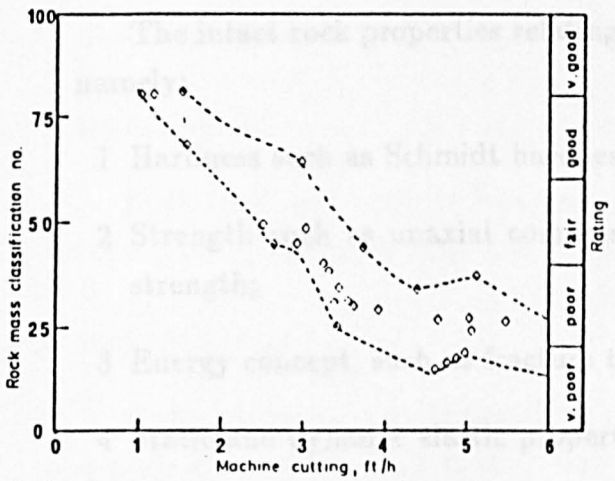


(a) Roadheader performance versus rock classification number

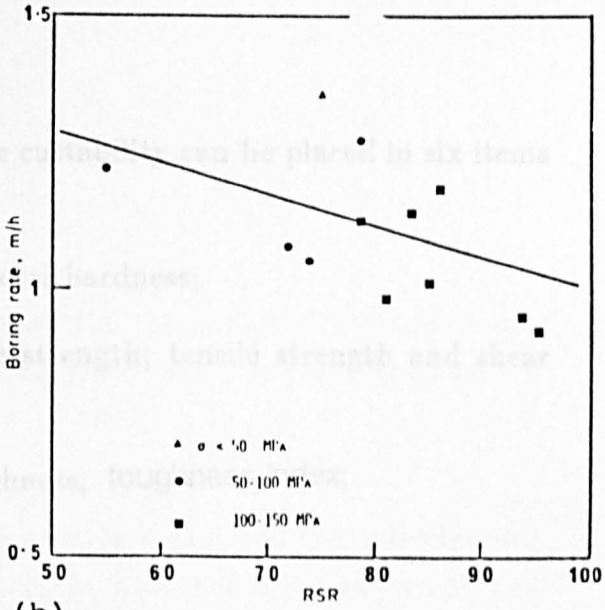


(b) Regression line for correlation of TBM advance rate with rock support rating (RSR) factor

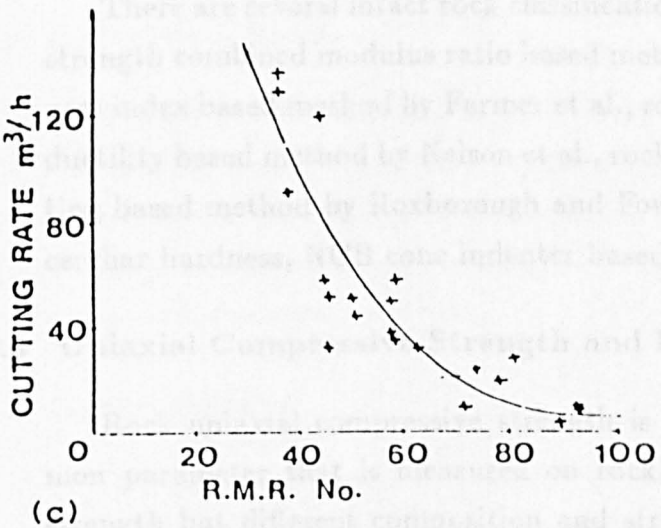


(c)

**Figure 7.12 — Tunnelling Machine Performance vs Rock Mass Classification Index**

## 7.5 Intact Rock Properties

The intact rock properties relating the cuttability can be placed in six items namely:

1 Hardness such as Schmidt hardness, total hardness;

2 Strength such as unaxial compressive strength; tensile strength and shear strength;

3 Energy concept, such as fracture toughness, toughness index;

4 Static and dynamic elastic properties;

5 Rock internal texture properties: grain shape, grain size, cementation and orientation of grains etc.;

6 Physical properties.

There are several intact rock classifications listed such as unaxial compressive strength combined modulus ratio based method by Deere and Miller, rock toughness index based method by Farmer et al., rock fracture toughness combined with ductility based method by Nelson et al., rock specific energy by instrumented cutting based method by Roxborough and Fowell et al. Rock index testing such as cerchar hardness, NCB cone indenter based method etc.

## 7.6 Uniaxial Compressive Strength and Moduli Ratio

Rock uniaxial compressive strength is the first, and by far the most common parameter that is measured on rock. However rocks of similar uniaxial strength but different composition and structure show significant variations in cuttability. To a large extent these can be revealed by differences in the results of indentation tests. Differences in composition and structure can be obtained from petrographic analysis; rocks with a closely intergrown fabric are much more difficult to break than those in which the mineral grains are separated by a weak matrix.

Rock moduli ratio is an very important rock properties which relates rock cuttability, it has been proven by the analysis of step-wise curvilinear regression

in chapter 8.

## 7.7 Rock Hardness

### 7.7.1 Introduction

Rock hardness property has been used for the prediction of tunnelling machine performane for a long time. A comprehensive review is presented here.

### 7.7.2 Mohr Hardness

Mohs hardness scale is preferred by geologists because it is relatively easy to perform in the field, but it is very imprecise, mistakes are easily made and the standard minerals do not advance in definite or regular ratio of hardness (Atkinson T., 1984). The Mohrs' scale is still a useful guide once a constituent mineral has been indentified but a more precise form of measurement for rock cuttability and rock abrasivity evaluation is required.

### 7.7.3 Rosiwal Rock Hardness

Rosiwal (1981) proposed another method on the base of Mohr's hardness. This method called Rosiwal hardness offered a method for composite materials, and relates the proportions of each material and its known hardness. The obvious drawback of this hardness method lies in its neglecting the cementing strength of the grain-pore-crack matrix.

### 7.7.4 Cerchar Hardness

This method has some similarity with the Rosiwal hardness. The original of this method measure the mineral hardness by cerchar hardness testing and account the proportion of each mineral in rock composition and then calculating the total hardness of rock.

There are different mechanical methods of measuring rock hardness. They are reviewed here.

### 7.7.5 The Schmidt Hammer Method

This method was originally designed for non-destructive, in-situ testing of the quality of concrete. The device is small and light and also used to estimate the uniaxial compressive strength of rocks.

The schimdt hammer rebound height depend upon rock elastic properties. Haramy K. Y. and DeMARCO M. J. (1984) reported that a variety of additional factors may affect laboratory and field-determined index values, including the following:

1 Varying degrees of surface irregularity;

2 Impact surface moisture content;

3 Inhomogeneities in the rock fabric;

4 Presence of cleavage, slips, bedding planes, porous cavities etc.;

5 Orientation and size of test surface;

6 Duration and degree of test surface weathering;

7 Rock mass confinement; in place versus unconfined laboratory setting.

### 7.7.6 The Shore Scleroscope

This instrument originally used to determine the hardness of metals, is designed to measure the rebound height of a small, round edged, diamond hammer which falls from a fixed height and rebounds freely from a specially prepared surface of the rock specimen.

The Shore Scleroscope has been proven to be a valuable laboratory tool for the determination of rock hardness with good correlation with uniaxial compressive strength.

McFeat-Smith proposed a plasticity index using Shore Scleroscope hardness testing and obtained good success for weak, friable rock cuttability evaluations.

### 7.7.7 Abrasion Hardness, $H_A$

Two measures of abrasion hardness and strength were used. They are determined by the inverse of the weight loss of the rock disc or the inverse of the weight loss of the abrasive wheel which abrades the rock.

A case history by Nelson and co-workers showed that, of various rock property indices, Taber abrasion hardness provided the most significant correlation with TBM penetration rates.

### 7.7.8 Total Hardness, $H_T$

This index was proposed by Tarkoy. It is a combination of rebound or mass hardness $H_R$, and abrasion hardness or small scale hardness, and is defined as:

$$H_T = H_R \times \sqrt{H_A} \tag{7.13}$$

Tarkoy reported that both mass sample hardness and small scale properties effectively controlled rock disintegration. Therefore, it was obviously desirable to combine two indices which measured distinctly different physical properties. For example, a quartzite may be resistant to abrasion but rebound hardness may nevertheless be low because of inherent fracturing in brittle quartzite. Similarly, a massive intact limestone, although hard in terms of rebound, is soft in terms of mineral hardness.

Tarkoy has successfully used total hardness for the prediction of tunnelling machine performance.

### 7.7.9 NCB Indenter Hardness Tests

The NCB cone indenter, designed by MRDE is used to determine rock hardness, it measures penetration of a tungsten carbide cone under normal forces of 14, 40 and 110 N, according to the descriptive hardness of the rock material, i.e. weak, strong or very strong. Atkinson reported that NCB cone indenter met difficulties with weak, friable rock materials in the G4 (Cemented soil) - R1 (weak rock) range on the GS scale, e.g. Cuddalore Sandstone. Fowell et al. has

analysed the relationship between NCB cone indenter and tunnelling machine performance and cutting pick performance. It is shown in Figure 7.13.

The step-wise regression analysis in Chapter 8 also concludes that NCB cone indenter is an very important rock property index for the determination of rock cuttability.

### 7.7.10 Cerchar Hardness Testing

The test is extensively used by the French coal mining industry and by tunnelling machinery manufactures. The abrasiveness of the rock is determined by measuring the resulting flat worn on the stylus.

Atkinson (1984) reported that the cerchar test experienced the difficulties with weak, friable rocks because the stylus tends to dig in, particularly if the matrix material is soft and penetrates easily. The conical stylus sinks deeper into the specimen re-distributing the normal load onto the sides of the cone and away from the point, thus indicating an abrasive index lower than the true index. He suggested that when weak rocks are tested, the cerchar abrasive indices must be viewed with a healthy scepticism and other methods also considered.

Cerchar hardness testing permits a certain degree of strength classification of rocks but CERCHAR holds that it is not enough in itself, because drill tests carried out on rocks with similar hardness values can produce very different rates of wear at the cutting-tip of the tool, other things being equal.

### 7.7.11 Conclusions for Hardness Testing

From the analysis above, we know that all mechanical or geological hardness classification systems are statistical results with the testing methods subject to observational errors, being testing equipment dependent. For weak, friable rocks or very strong rock, all experienced difficulties with the anomolous results. All mechanical methods are based on the old principle: energy principle. The higher the mass rebounds, the harder the rocks is. The fact is that the interaction of drop mass and rock mass is very complicated. The energy transfer (from potential energy to moving energy) is not as simple as the energy balanced theory would suggests. Rock may absorb the energy because of its un-recoverable ductile

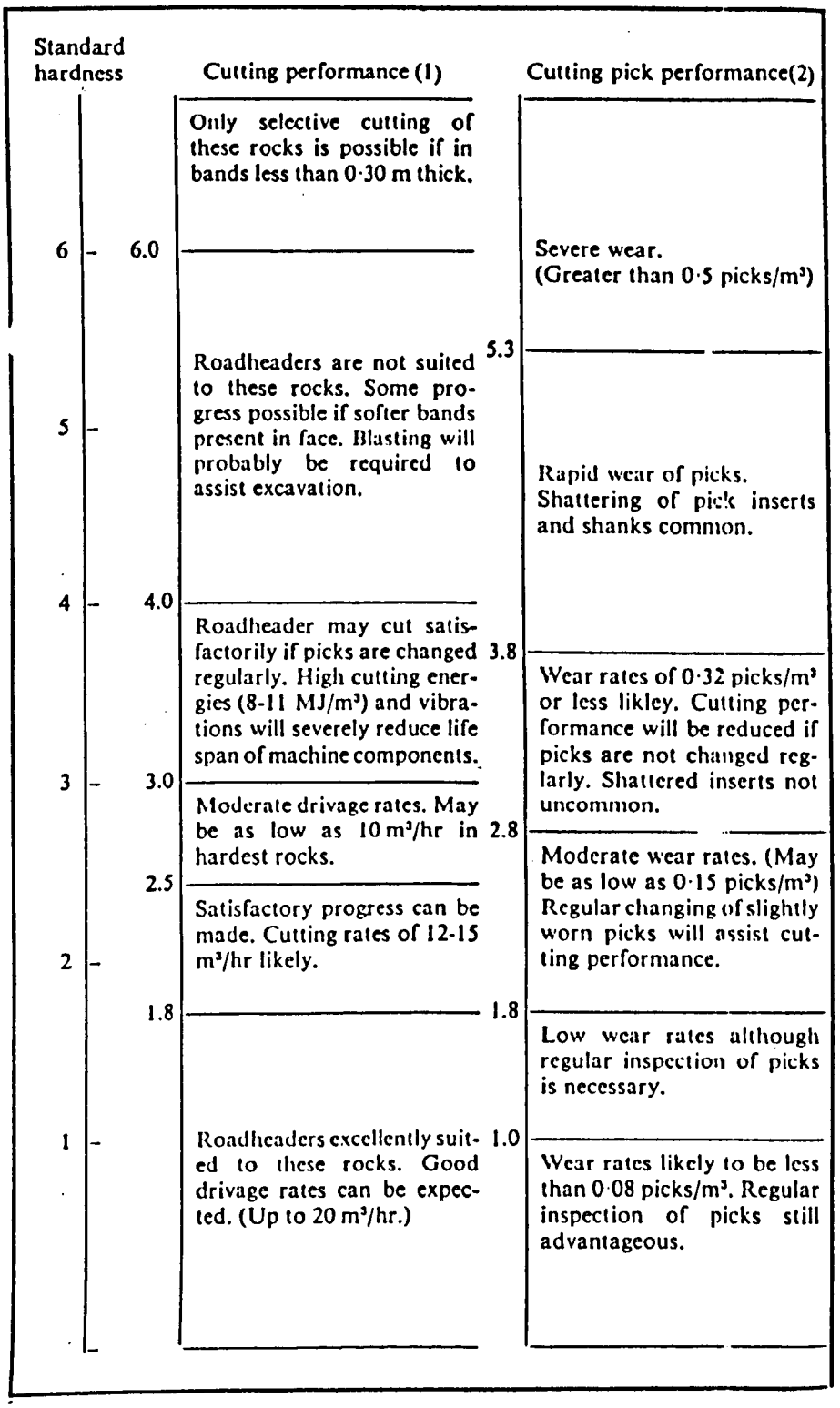


Figure 7.13 — NCB Cone Indenter vs Tunnelling Machine Performance by MacFeat-Smith

deformation and the magnitude of energy absorbed by the rock specimen is very factor dependent. Though the rebound height can simply reflect the hardness of rocks and it is based on character and statical experience. The cementation un-uniformity of rock grains, mineralogy variation, grain shape and size, pore shape and size variation gives a wide scatter of results and makes accuracy of results to some extent unbelievable.

All rebound hardness testing assumes that rock which at low stresses behaves totally elastic and at the yield stress becomes plastic.

Cerchar hardness testing has some difference with Schmidt hammer or Scleroscope its tip hardness dependent, rock texture variation, cementation change, and for weak, friable, or quartz content very high strength rock will give incredible results.

### 7.7.12 Abrasiveness

Abrasiveness of rock describes the ability of rock fragements to wear away the drilling or cutting tool and polish its cutting edges.

Various factors affect the abrasiveness of rock. The most important factors are:

1 Mineral Composition;

2 The hardness of mineral constituents;

3 Grain shape and size;

4 The type of matrix material;

5 Rock strength, hardness and toughness etc.

Rock abrasiveness strongly affects a tunnelling machine's advance rate. Fowell et al. has successfully correlated the rock abrasiveness with tunnelling machine advance rate.

## 7.8 Energy Concept for the Evaluation of Rock Cuttability

### 7.8.1 Introduction to Energy Concept for Rock Cuttability Prediction

An alternative approach to tunnelling machine performance prediction is that using energy concept. Rock specific energy is normally defined as the energy required to cut unit volume of rock. The toughness index is defined as the strain energy stored in a unit volume of rock just before failure, and therefore can be seen as the amount of energy required to cause fracture, hence breakage. Rock fracture toughness is measured in terms of either the stress intensity factor, K, or the energy release rate (also known as the crack driving force), G.

Many workers (Ian Farmer Associates, 1986; Nelson, 1986; Fowell, 1973; Poole et al. 1987 etc. ) tried to use the energy concept for the evaluation of tunneling machine performance.

Hughes H. M. (1972) stated that as a general statement, tools applied to rock do work in two basic models:

1 The preparatory work of breaking into the rock;

2 The productive work of breaking off the rock.

Using drag picks, the greater part of the preparatory work goes in friction. Once the tools have broken into the rock, they proceed to elastically strain it. When the strain energy become excessive, the rock fractures by propagating pre-existing cracks. The strain energy is thereby released and can be converted into the following:

1 The surface energy of the fresh faces (the only ultimately useful quantity);

2 Work of plastic deformation in zones adjacent to the running cracks;

3 The kinetic energy of the fragements;

4 Chemical reactions in thermally unstable materials.

However, in practice, the energy of most rock cutting and comminution processes converted into surface energy is only of the order of 10th of 1 percent. It

is proportional to the area of the new surfaces created.

In ductile materials, a large proportion of the strain energy is absorbed in plastic deformation (strain-soften) in mi -ocrack (or process) zones adjacent to the running crack.

In the case of brittle materials such as rock, fragments can burst from the work place with high velocity. Obviously, they have kinetic energy. Possibly, the lower the strain energy absorbed in plastic deformation, the greater the proportion that goes into the kinetic energy of the fragments. It may be considered that such energy is proportional to the mass of the fragements – and thus to the volume of the unfractured piece (rock density is supposed constant).

Some of the strain energy released by fracture could be used in promoting chemical reactions in thermally unstable materials such as Carbonates. These reactions are limited to a zone around the crack tip as it progresses, so that this quantity of energy would be proportional to the area of the new surfaces created.

Hughes H. M. (1972) reported that the tunnelling machine at Cloud Hill Quarry, Breedon-on the hill showed that about one half of the energy of the machine went into raising the air temperature and evaporating moisture and about 1/3 into heating the debris. Moreover, as indicated above, the proportion of the energy of comminution ultimately utilized in the creation of new surfaces in only about one tenth of 1 percent.

### 7.8.2 Specific Energy

Rock specific energy could be said to be the first energy index for the evaluation of rock cuttability. Specific energy is defined as the energy required to excavate unit volume of rock. It is therefore a direct measurement of the rock strength in relation to the effectiveness of any rock-cutting process. For example, it can be used to establish the relative efficiency of various tools, machines, or cutting process in a given rock material. Conversely it can establish the relative order of resistance of various rock materials to given machine, or to a specific mode of excavation.

This index has a direct relationship with the rock cuttability. It reflects the energy for breaking the rock during the drilling process. The University of Newcastle has standardized the measurement of rock specfic energy in the laboratory using an instrumented shaping machine.

MacFeat and Fowell have successfully correlated the rock specific energy and tunnelling machine advancing rate. It is shown in Figure 7.14.

### 7.8.3 Rock Fracture Properties

Rock fracture toughness describes the resistance to fracture that comes essentially from the tensile strength of rock. Many mining tools (drilling or boring) are designed to induce local tensile failure within rock, as rock is much weaker in tension than it is in compression. Interlocking of mineral grains and strong mineral content affect toughness.

Thimons E. D. (1986) used rock fracture mechanics concept to explain the mechanism of rock mechanical cutting assisted by high pressure water jets. As is well known, the energy release rate is energy per unit crack extension, therefore the energy consumed in fracture, U, can be found by multiplying the critical energy release rate by the area of new surfaces, A, created during fracture,

$$U = \frac{K_{IC}^2(1-\nu^2)}{E} \times A \tag{7.14}$$

In applying this equation to rock cutting it is necessary to determine the area of the new surfaces created during cutting. This was achieved by analyzing the rock chips collected during cutting to determine a shape factor for each of the size fraction. The shape factor relates the surface area of a particle to its volume, hence knowing the rock density, weight, and shape factor for each size fraction, it is possible to obtain an estimate of the total surface area in a chip sample.

In his research, the total specific energy calculated from the water jet energy and the forces measured during the traverse speed tests showed an inverse relationship with the advance rate. At the same time, the specific energy has also been calculated theoretically using the area of new surfaces produced and the

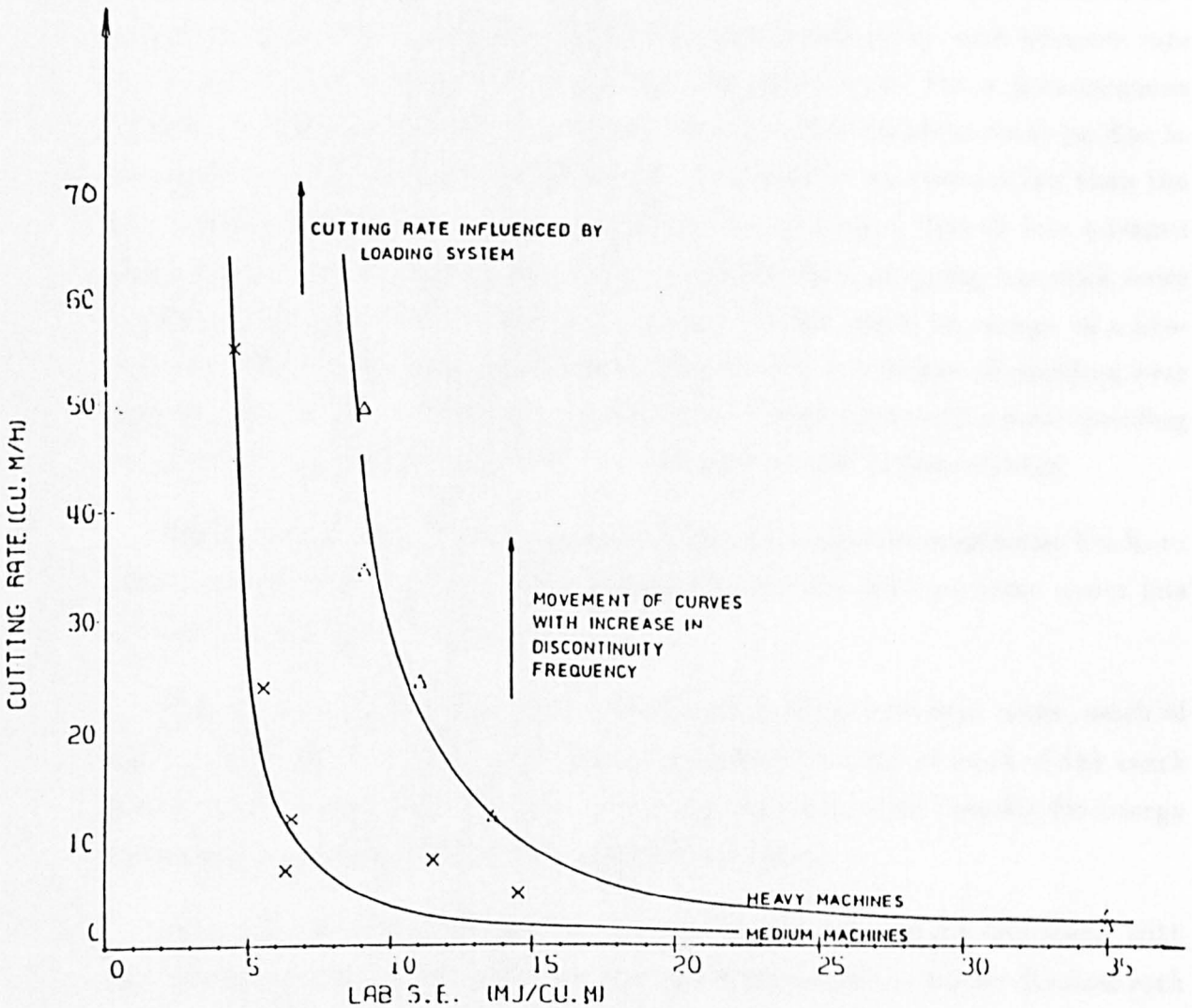


**Figure 7.14 — In-situ Cutting Rate vs Lab Specific Energy by Fowell**

critical energy release rate (fracture toughness). He found that the theoretically calculated specific energy showed no correlation with the advance rate or with any other variables. He also reported that the energy consumed per unit area of new surface decreases with increasing advance rates. It is generally accepted that increase in cutting efficiency with advanc rate is due to the creation of a coarse product. This indicates that the increase in efficiency with advance rate is not completely attributable to produce size differences. For a homogeneous rock the critical energy rate is constant, therefore the variation must be due to the existence of a plastic zone and energy consumed in processes other than the fracture propagation. From above analysis, he concluded that at low advance rates increases as a result of the water jet application, chipping becomes more dominant and the cutting efficiency increases. As the water jet energy as a proportion of the total energy is increased, the relative dominance of profiling over chipping increases. This leads to a reduction in energy losses and a corresponding reduction in the energy consumed per unit area of new surface created.

Matthias Hessling (1988) has reported that rock fracture toughnesss has been correlated successfully with cutting depth for abrasive high pressure water jets cutting. This is shown in Figure 7.15.

Prior to crack advancement in a ductile material, as well as in rocks, much of the crack driving energy is absorbed in a localized volume in front of the crack tip, referred to as the plasticity or microcracking zone. This capacity for energy absorption substantially increases material resistance.

Nelson (1987) reported that toughness or strength can be combined with ductility for a new rock classification system with pertinence for mechanical rock cutting studies. The ratio between R-curve and plain strain toughness is defined as the ductility ratio of the rock material, a ratio which reflects the ability of the rock materials to sustain prolonged and stable crack growth during fragementation. The value of ductility varies from 1.19 to 1.60 reported by Nelson. The higher the ductility ratio, the more ductile the material. According to her system there are three basic groups of rock:

1 Rocks which are ductile and strong in compression, such as Granite;

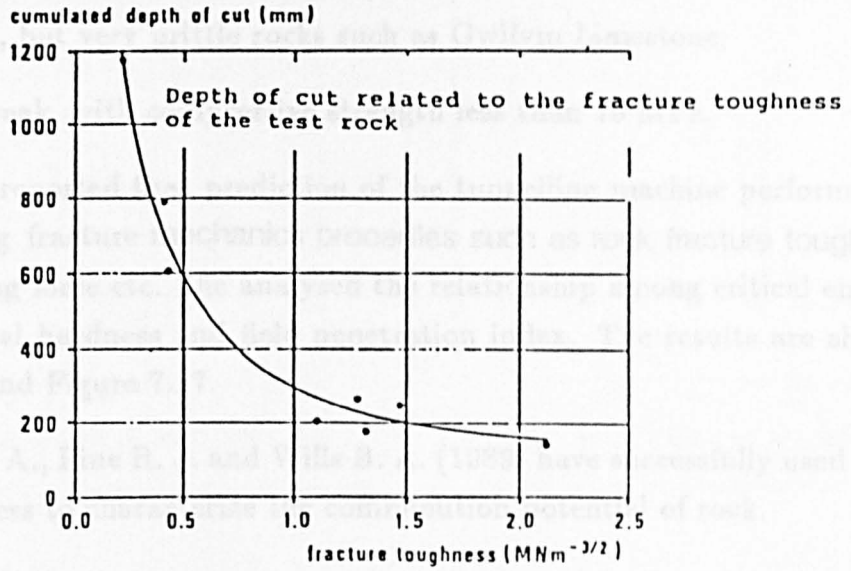


**Figure 7.15 — Rock Cutting Depth vs $K_{IC}$ by Matthias Hessling**

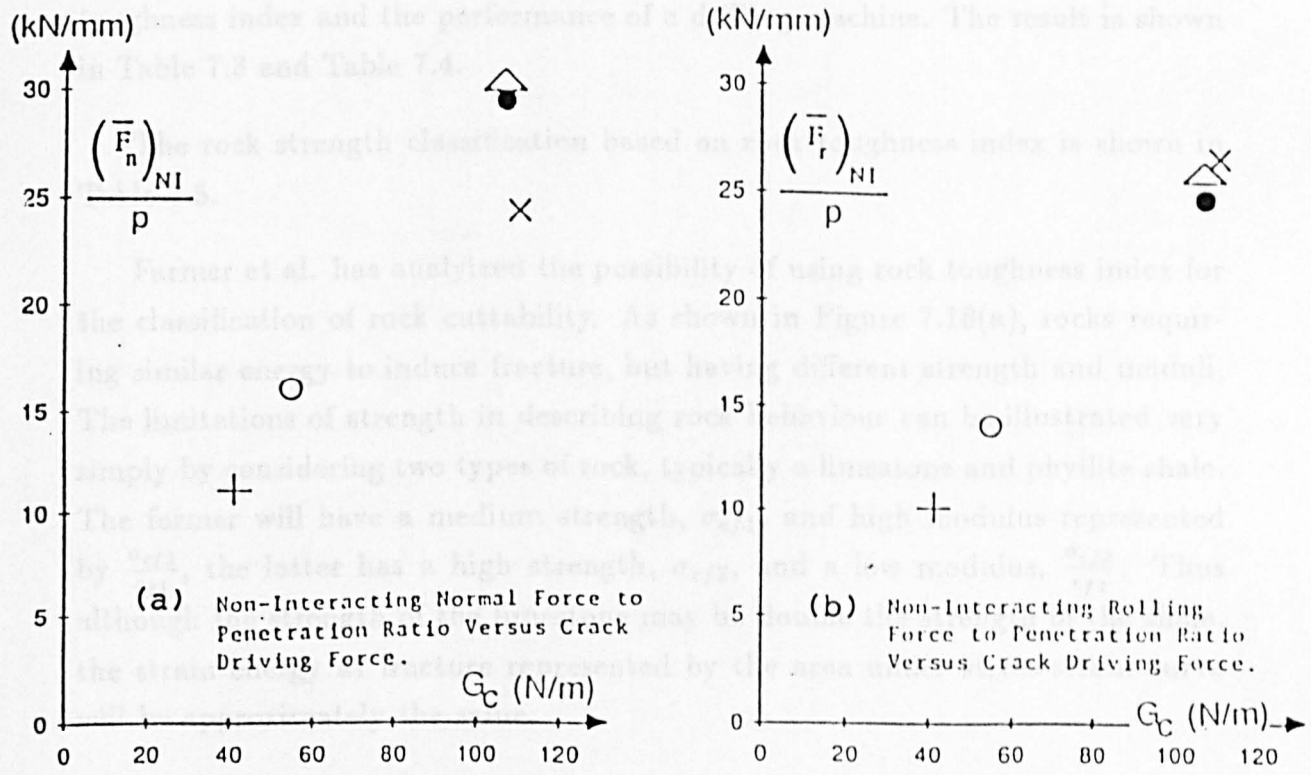


**Figure 7.16 — Nelson's Experimental Results for Non-interactive Disc Cutting**

2 Very Strong, but very brittle rocks such as Gwilym Limestone;

3 Relatively weak, with compressive strength less than 70 MPa.

Nelson also reported that prediction of the tunnelling machine performance is possible using fracture mechanics properties such as rock fracture toughness and crack driving force etc. She analysed the relationship among critical energy release rate, total hardness and field penetration index. The results are shown in Figure 7.16 and Figure 7.17.

Bearman R. A., Pine R. J. and Wills B. A. (1989) have successfully used rock fracture toughness to characterize the comminution potential of rock.

### 7.8.4 Rock Toughness Index

Rock toughness index is a derived parameter from the stress/strain curve, and is a measure of elastic energy requirements for deforming the rock with a cutting tool

Adler L. and Krishnan G. V. (1983) analysised the relationship between rock toughness index and the performance of a drilling machine. The result is shown in Table 7.3 and Table 7.4.

The rock strength classification based on rock toughness index is shown in Table 7.5.

Farmer et al. has analyzed the possibility of using rock toughness index for the classification of rock cuttability. As shown in Figure 7.18(a), rocks requiring similar energy to induce fracture, but having different strength and moduli. The limitations of strength in describing rock behaviour can be illustrated very simply by considering two types of rock, typically a limestone and phyllite shale. The former will have a medium strength, $\sigma_{cf1}$, and high modulus represented by $\frac{\sigma_{cf1}}{\epsilon_{f1}}$, the latter has a high strength, $\sigma_{cf2}$, and a low modulus, $\frac{\sigma_{cf2}}{\epsilon_{f2}}$. Thus although the strength of the limestone may be double the strength of the shale, the strain energy at fracture represented by the area under stress-strain curve will be approximately the same.

$$\frac{1}{2}\sigma_{cf1}\epsilon_{f1} = \frac{1}{2}\sigma_{cf2}\epsilon_{f2} \tag{7.15}$$

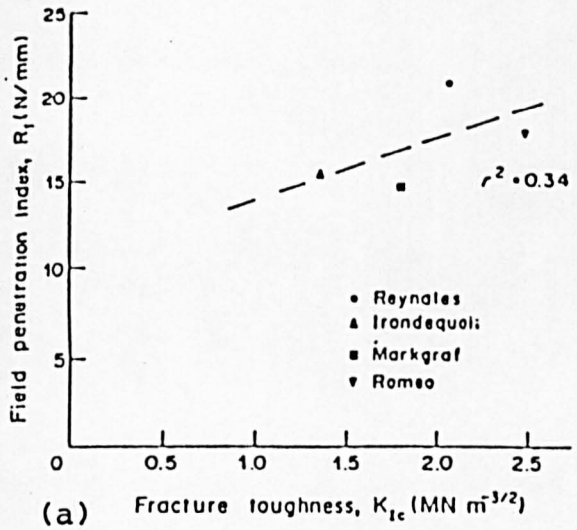


Plot of field penetration index data vs fracture toughness.

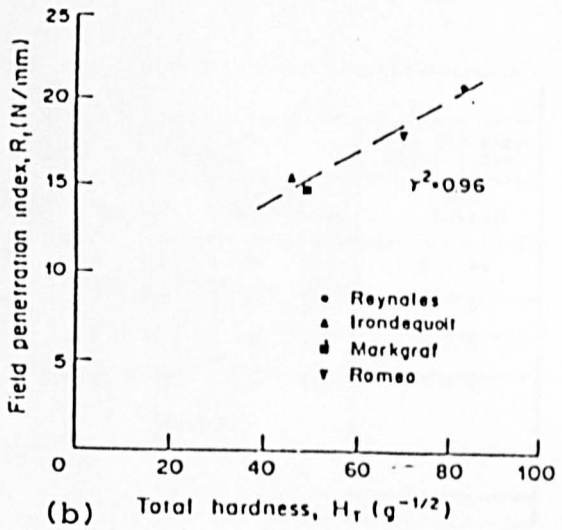


Plot of field penetration index data vs total hardness.

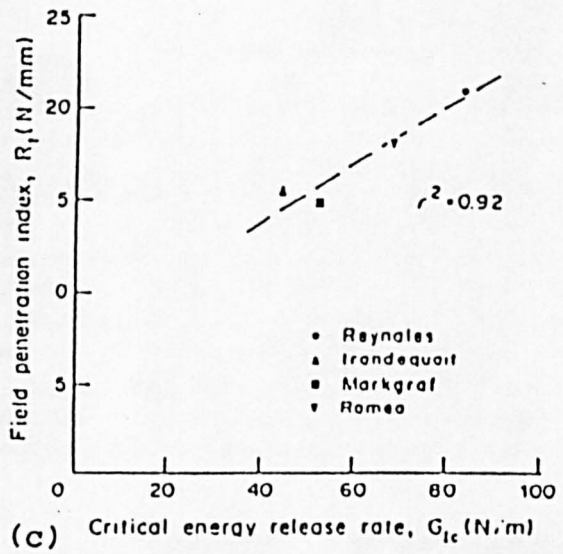


Plot of field penetration index data vs critical energy release rate.

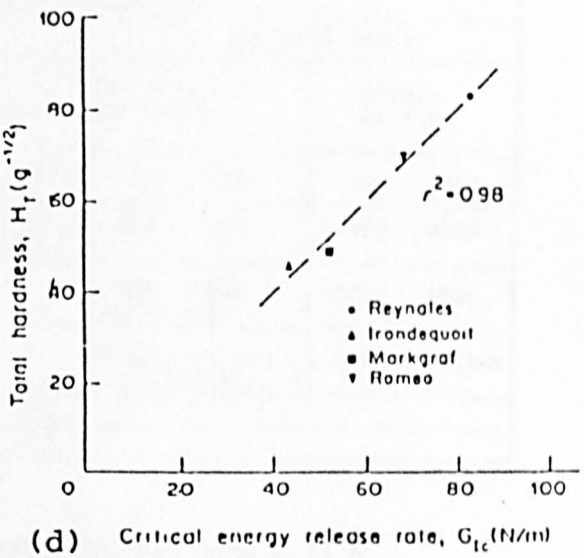


Plot of total hardness data vs critical energy release rate

**Figure 7.17 — $K_{IC}$ vs Field Penetration Index etc. by Nelson, 1985**

## Table 7.3 — Operation Parameters vs Rock Toughness Index by Adler

| Rock Toughness Class | Drill Operational Parameters | | | | | | |
|---|---|---|---|---|---|---|---|
| | Thrust (lb./in. diam) | | | Rotation or Frequency (rpm) (bpm) | | | Air Velocity (fps) x $10^3$ |
| | Percussive or Rotary | D-H-D | Rotary-Percussive | Percussive & D-H-D | Rotary | Rotary-Percussive | All Drills[1] |
| Very High | 3000 - 8000[2] | 3000 - 8000 | 500 - 1000 | 1500 | 20 - 60 | 20 - 50 | 6 - 10 |
| High | 3000 - 6000 | 2000 - 5000 | 500 - 1000 | 2300 | 40 - 60 | 30 - 50 | 5 - 6 |
| Medium | 2000 - 5000 | 1500 - 4000 | - | 2300 | 60 - 140 | 60 - 130 | 4 - 5 |
| Low | 1000 - 4000 | 1000 - 3000 | - | 4000 | 140 - 300<br>15 - 50 (clay) | 130 - 280 | 3 - 4 |
| Very Low | ← Auger, dig, rip, cave, etc. → | | | | | | |

## Table 7.4 — Performance Parameters vs Rock Toughness Index by Adler

| Rock Toughness Class | Drill Performance Parameters | | | | | |
|---|---|---|---|---|---|---|
| | Penetration Rate (fph) | | | | Bit Life (ft.) | |
| | Percussive | Rotary | Rotary-Percussive | D-H-D | Percussive or D-H-D | Rotary or R-P |
| Very High | 20 - 40 | 10 - 30 | 15 - 30 | 15 - 30 | 500 - 1500 | 500 - 1500 |
| High | 30 - 50 | 20 - 30 | 15 - 50 | 15 - 30 (60) | 500 - 1500 | 500 - 2000 |
| Medium | 30 - 60 | 30 - 70 | 40 - 80 | - | 1500 - 4000 (No D-H-D) | 2000 - 5000 |
| Low | 85 - 120 | 70 - 150 (300 - 600) | 70 - 160 | - | 4000 - 18,000 (No D-H-D) | 5000 - 20,000 |
| Very Low | ← Auger, dig, rip, cave, etc. → | | | | | |

## Table 7.5 — *Rock Toughness, Specific Energy and C.R.S.*

| Rock Strength & Toughness Class | Toughness (psi) | Coefficient of Rock Strength (C.R.S.) | Specific Energy (ft lb/$in^3$) |
|---|---|---|---|
| Very High | > 59 | >2.8 | > 6700 |
| High | 59 - 16 | 1.8 - 2.8 | 5500 - 6700 |
| Medium | 16 - 4 | 1.0 - 1.8 | 3860 - 5500 |
| Low | 4 - .75 | 0.5 - 1 | 2000 - 3860 |
| Very Low | < 0.75 | < 0.5 | <2000 |

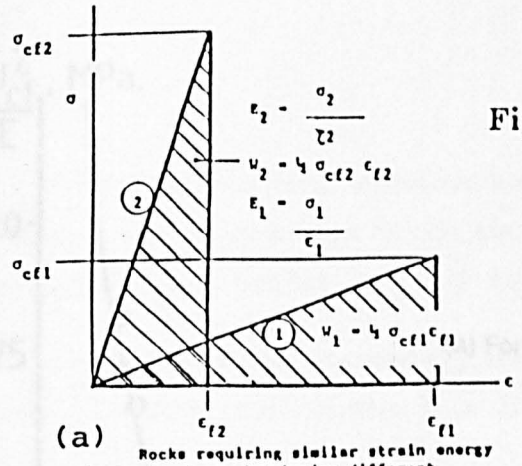


(a) Rocks requiring similar strain energy to induce fracture, but having different strength and modulus

**Figure 7.18 — Rock Toughness Used for Rock Cuttability Classification by Farmer**

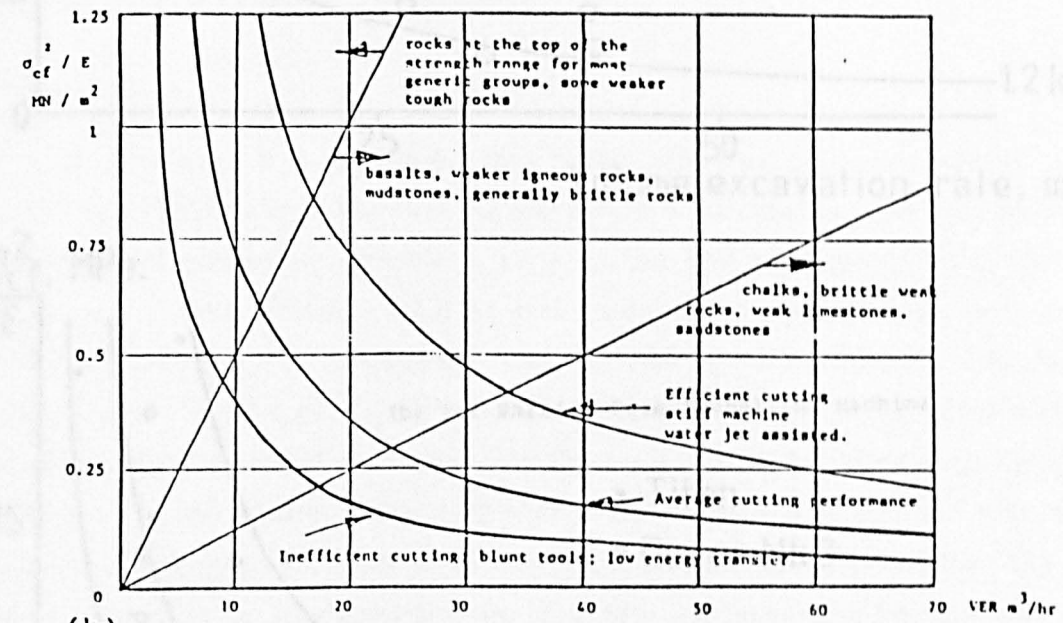


(b) A suggested scheme for assessing cuttability of rocks based on fracture toughness of the rock, volume excavation rate and machine-rock energy transfer.

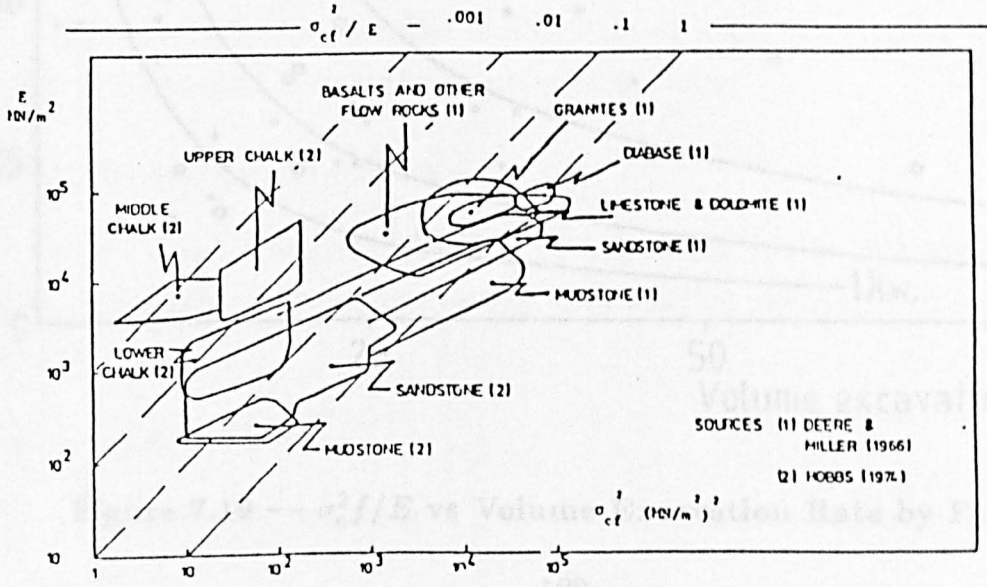


(c) Fracture toughness (x2) bands, superimposed on strength/modulus ranges proposed by Hobbs (1974) and Deere & Miller (1966) for various rock types.

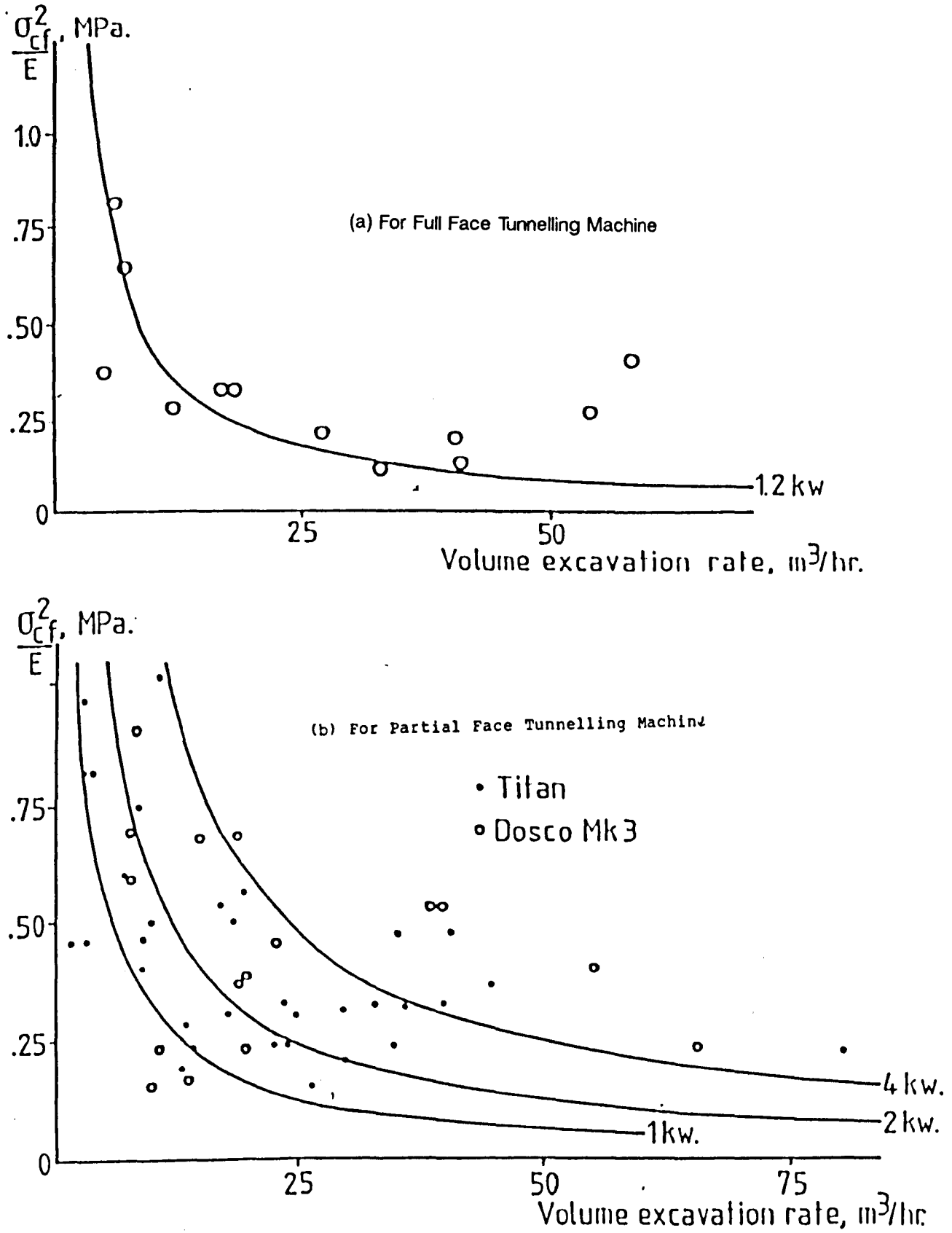


**Figure 7.19 — $\sigma_c^2 f/E$ vs Volume Excavation Rate by Farmer**

Thus in simple ultimate stress term, moduli terms the resistance of the limestone would be presumed double the resistance of the shale. In terms of energy required to fracture the rock they have equal resistance.

Farmer et al. has successfully correlated the rock toughness index with tunneling machine performance. It is shown in Figure 7.19(a) and Figure 7.19(b).

In chapter 8, a step-wise regression analysis also concluded that toughness index is very important index relating the cuttability of intact rock.

## 7.9 Rock Micro-texture Coefficients

### 7.9.1 Introduction

Rock texture is a very important factor affecting rock cuttability. Olsson and Peng (1976) suggested that rock fracture is associated with four sequential events-crack nucleation, initiation, propagation and coalescence. It is obviously that rock texture features such as grain size, shape, interlocking and orientation will influence the propagation and networking of cracks and, thus the rock cuttability. Sangha et al. (1974) did experimental studies of microfracturing and concluded that failure occurred in the cement matrix rather than the quartz grains. The indentation testing by sharp and truncated wedge and observed in a scanning electron microscope (Lindqvist et al. 1984) indicated that the influence of texture on fracture patterns. Fracture patterns of a fine-grained, dense limestone were straight with few crack interactions, whereas cracks in a medium-grained, weakly grained-bonded marble showed many interactions and forking, which, presumably, followed weak grain boundaries.

### 7.9.2 Rock Grain Shape and Grain Size

Grain shape and grain size play an important role in rock crack propagation, rock mechanical property testing, rock fracture mechanics testing, and rock engineering.

### 7.9.3 Rock Grain Cementation

The degree of cementation of grains is very difficult to describle quantitately.

It deals with a lot of factors including the factors of cementing material and cemented material.

### 7.9.4 Rock Porosity

The porosity of rock is defined as the ratio of the volume of internal open spaces to the bulk volume of the rock. It depends on the following factors:

1 Size distribution;

2 Shape of grains;

3 Degree of interlocking of grains;

4 Orientation of grains;

5 Degree of Compaction;

6 Amount of non-granular materials (colloids or cement) in pores or coating the grains.

There are two kinds of pore: open pore (inter-connected with each other and linked to the external surfaces); closed pore (no connection with the external surfaces or open pores).

Studies using ion thining of polished surfaces of rock and surface electron microscopy (Sprunt and Brace, 1974) have revealed that cavities present in rocks are of different shapes:

1 Some are long and crack-like;

2 Some are slot-like with rounded and blunted ends;

3 Some are circular or triangular and some are simply irregular.

The low aspect ratio cavities ($a \ll 0.1$) in unstressed samples have blunt, circular or square terminations. The long narrow, sharp ended cracks typical of brittle fracture were rarely observed in the rocks. The number of these low aspect ratio cavities sharing a common point of interaction varied from 2 to 6 depending on the rock type.

The high aspect ratio cavities ($a \gg 0.1$) appear scattered or are jointed by low aspect ratio cavities and are found concentrated in certain mineral grains while the other mineral grains may be free of these.

In mechanically stressed rocks, the low aspect ratio cavities tend to increase and there seems to be a strong preferred orientation and the bridges formed between them tend to break under mechanical and thermal stresses.

All strength properties of rocks fall with increase in porosity (Price, 1960; Kowalski, 1966; Smorodinov, 1970). The reasons for this are:

1 Stress concentration caused on the boundary of the pores reduces the strength;

2 Decrease in the bearing area of the rock causes decrease in strength;

3 The pores may be filled with water or some other liquid which may help in crack propagation by reacting at the points of stress concentration or reducing its surface energy (pore water pressure).

### 7.9.5 Rock Texture Coefficient by Howarth

The quantitative assessment of rock texture consists of four parts:

1 Measurement and analysis of grain circularity;

2 Measurement and analysis of grain elongation;

3 Measurement and quantification of grain orientation;

4 Weighting of results based upon degree of grain packing.

The formula used for the calculation by Howarth is given below:

$$TC = AW\left(\frac{N_0}{N_0 + N_1} \times \frac{1}{FF_0} + \frac{N_1}{N_0 + N_1} \times AR_1 \times AF_1\right) \qquad (7.16)$$

Where:

TC = texture coefficient;

AW = grain packing weighting;

$N_0$ = number of grains whose aspect ratio is below a pre-set discrimination level;

$N_1$ = Number of grains whose aspect ratio is above a pre-set discrimination level;

$FF_0$ = Arithmetic mean of discriminated form factors;

$AR_1$ = Arithmetic mean of discriminated aspects ratios;

$AF_1$ = Angle factor, quantifying grain orientation.

Rock texture was assessed using microscopic image analysis of thin sections. Image processing was performed using a DAPPLE systems, IMAGE PLUS TM, automatic image analysis, with video camera input of thin section photographic prints.

In his experimental analysis, he concluded that:

1 The texture coefficient describes grain-shape, orientation, degree of grain interlock and relative proportions of grains and matrix (packing density), there is significant correlations between rock texture coefficent and rock strength and penetration rates;

2 Texture coefficent is a measure of the resistance of the microstructure of a rock to crack propagation;

3 The prediction of rock cuttability by texture coefficent is superior to the Schmidt hammer rebound hardness.

Rock texture coefficients against penetration rate, uniaxial compressive strength, dynamic Young's modulus, Brazilian disc tensile strength, P wave velocity and static tangent Young's modulus are shown in Figure 7.20.

## 7.10 In-situ Determination of Rock Cuttability

Hudson and Drew (1976) developed an impact penetrometer for assessing the cuttability of rock. It is reported that the impact penetration technique

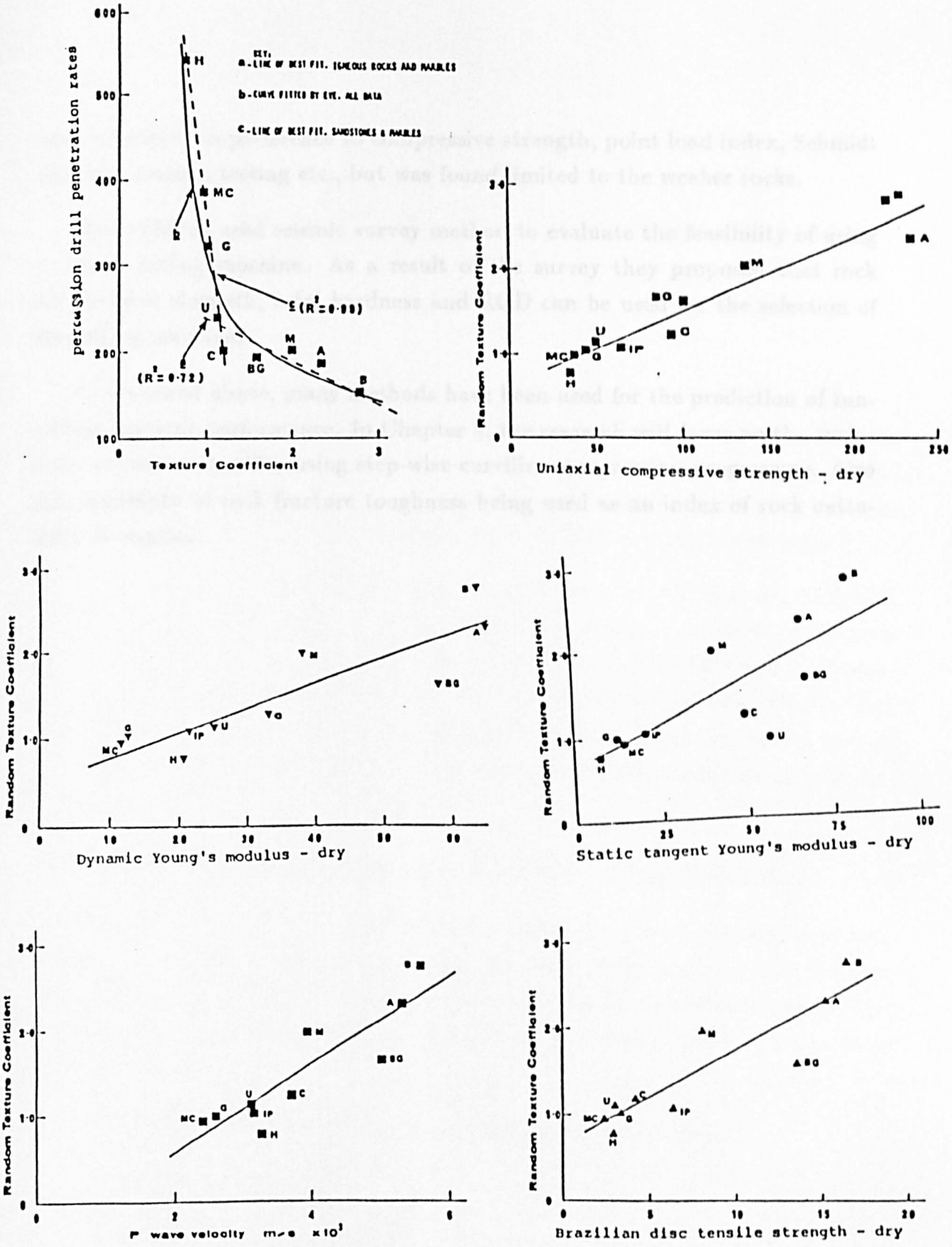


Figure 7.20 — Rock Texture Coefficents vs Penetration Rate etc. by Howarth

was considered in preference to compressive strength, point load index, Schmidt hammer, seismic testing etc., but was found limited to the weaker rocks.

Desai (1976) used seismic survey method to evaluate the feasibility of using a tunnel boring machine. As a result of the survey they proposed that rock compressive strength, total hardness and RQD can be used for the selection of tunnelling machine.

As reviewed above, many methods have been used for the prediction of tunnelling machine performance. In Chapter 8, the research will focus on the evaluation of rock cuttability using step-wise curvilinear regression programme. Also the possibility of rock fracture toughness being used as an index of rock cuttability is studied.

# Chapter VIII

# Rock Cuttability Prediction Using Stepwise Regression Method

## 8.1 Background

In the Department of Mining Engineering at University of Newcastle upon Tyne, a wide series of research programmes have been undertaken to predict the performance of tunnelling machine accurately using rock property, machine characteristic and geological parameters gained from in-situ monitoring.

The purpose of this research lies in setting up a rock property and rock cuttability database, then using a stepwise curvilinear regression programme *MINITAB to analysis the relationship between rock cuttability and rock properties, and identifying the important rock properties for the evaluation of rock cuttability. Some important rock properties such as toughness index, moduli ratio and rock fracture toughness were evaluated for the prediction of rock cuttability.

## 8.2 Introduction to the Database for Rock Cuttability Prediction

Many rocks were tested and formed a sedimentary rock property and rock cuttabilty parameters database. Some new rock properties and rock fracture properties were input into the database. Therefore, it is possible to analysis the potential relationship between rock properties and rock cuttability parameters on a large scale.

The rock properties tested in this research program include:

1 Rock physical properties;

2 Rock mechanical properties;

3 Rock textural properties;

4 Rock index properties such as cone indenter index;

5 Rock energy properties such as toughness index, specific energy;

6 Rock fracture properties such as fracture toughness.

The measurement of the first five groups of rock properties has been described by I.McF Smith in his Ph.D thesis, therefore it is not my intention to repeat it here. The measurement of rock fracture properties has been described in part I: "The Development of Cracked-Chevron-Notched Brazilian Disc Specimen for Rock Fracture Toughness Measurement".

The rock properties vs rock cuttability database is presented in Appendix No.11 to Appendix No.15.

## 8.3 Data Analysis Method

### 8.3.1 Outline of Statistical Method

The multiple regression programe is used for selecting the important rock properties which relate to rock cuttability. The equation used for the regression is as the following:

$$y = b_0 + b_1 x^1 + b_2 x^2 + ..... + B_k x^k \tag{8.1}$$

Where:

y ..... Variable called the response (dependent variable);

$x^i$ .... the predictors variables;

$b_i$ .... the regression coefficients.

This regression procedure can be used to study the relationship between a dependent variable and a set of independent variables. Regression coefficient (R-squared) can be calculated, along with a variety of statistics which evaluate how well the model fits and what each of the individual variables contributes. Forward-inclusion, backward-elimination and step-wise selection algorithms are used for selecting the independent variables to be included in the equation.

A stepwise regression procedure is the basic method used. Forward selection, backwards elimination, and user intervention are special cases. At each step, the procedure first calculates an F-statistic for each variable already in the model. If the F-statistic for any variable is less than FREEMOVE, then the variable with the smallest F-statistic is removed from the model. The regression equation is calculated for this smaller model, the results are printed, and the procedure goes on to a new step. At each stage, *MINITAB prints out the coefficient and t-statistic for each variable in the model.

If no variable can be removed, the procedure tries to add a new variable. A F-statistic is calculated for each variable not yet in the model. The above procedures are repeated. If no variable enters, STEPWISE ends.

In this study, the maximum number of independent variables inputed into the equation is 20. By the transformation such as $x_i^{1/3}$, $x_i^{1/2}$, $x_i$, $x_i^2$ and $x_i^3$, all the independent variables are related to the dependent variable by the statistical programe *MINITAB. There are several considerations to be made when using this programe *MINITAB. These are:

1 The programme can use the dependent variables, which is very important for this project. Because many rock property parameters are dependent on each, other. *MINITAB statistical package uses t-testing (importance factors) for evaluating the relative importance in the regression procedure when the variables entered the equation in STEPWISE. This is the major difference between the statistical method used by I.McFeat-Smith in 1975. In his analysis, the importance of entered prediction variables is judged by the fall in standard error and rise of R-Squared.

2 The prediction equation can use the sum of variables (inclusive of the transformation of each variable) and also the products of each variable. Two variables (toughness index and moduli ratio, if transformed, they will give 10), these are from the products of the former variables and are added into the database for the prediction of rock cuttability.

In order to compare the relative importance of toughness index and moduli ratio for the evaluation of rock cuttability, a simple programme was designed. It

Table 8.1 — Analysis Structure for Curvilinear Regression

| Dependent variables | Datatypes | Prediction variables |
|---|---|---|
| Rock specific energy | 87 Case of rocks | $C_4 - C_{20}$ |
| Rock cutting tool wear | 20 case of rocks | $C_4 - C_{20} + C_{101}$ |
| Coarseness index | Sandstone group | $C_4 - C_{20} + C_{106}$ |
| | | $C_4 - C_{20} + C_{101} + C_{106}$ |

(Note: $C_{101}$ toughness index; $C_{106}$ moduli ratio)

is listed in Table 8.1.

An example of the datafile for the rock cuttability prediction using *MINITAB programme is presented in Appendix No.10.

### 8.3.2 The Interpretation of Results by *MINITAB

In I.McFeat-Smith's research, the success of each programme is judged by the fall in the standard error (S.E.) of the prediction equation (i.e. its proximity to zero), the rise in the multiple correlation coefficient (m.c.) (i.e. its nearness to 100 percent), and the number of 'steps' or independent variables in the selected equation. In this research programe the prediction variable is input into the equation and has t-statistical testing carried out for evaluating the importance of inputed prediction variables in stepwise programe.

The following will present the analysis results by the *MINITAB.

## 8.4 Rock Specific Energy Prediction

As shown in Table 8.1, the research programme consists of different datatypes: all sedimentary rocks, sandstone group and small number group.

Another topic investigated is to find whether some very important rock properties such as rock toughness index and rock moduli ratio are suitable for the prediction of rock cuttability.

The results analysed by curvilinear regression for the prediction of rock specific energy are shown in Table 8.2.

**Table 8.2 — The Prediction of Rock Specific Energy**

The most important prediction Variables are:

$C_4$ To $C_{20}$

87 sets of data

$CI^{1/3}$; $ES^3$; (Important rock properties)

($S.E.$ 4.73 – –4.41; $R - Sq$ 85.35 – –87.71)

$SE = -14.8 + 18.4CI^{1/3} + 0.000024ES^3$ (*The prediction equation*)

20 sets of data

$GS$; $CI^{1/3}$; $Lst^2$; $Ls^{1/3}$; $BD^3$; $TI^{1/3}$; $GR^3$; $TS^{1/3}$; $ES$; $A^3$

$SE = 26.3 - 0.02GS - 11.6CI^{1/3} + 10^{-3}Lst^2 - 0.7Ls^{1/3} - 0.8BD^3 + 0.8TI^{1/3} + 0.7TS^{1/3} + 0.02ES$

For sandstone group

CI

($S.E.$4.04; $R - Sq$91.27)

$$SE = -14.0 + 19.0CI^{1/3} \tag{8.4}$$

$C_4$ To $C_{20} + C_{101}$

87 sets of data

$CI^{1/3}$; $ES^3$

($S.E.$ 4.73 – –3.34; $R - Sq$ 85.35 – –93.46)

$SE = -2.2 + 18.4CI^{1/3} + 0.000025ES^3$

20 sets of data

$GS;\ CI^{1/3};\ Lst^2;\ CS^3;\ Ls^{1/3};\ BD^3;\ TI^{1/3};\ TI^2;\ TS^{1/3};\ ES$

$(S.E.\ 2.98 - -0.0000;\ R - Sq34.06 - -100.00)$

$SE = -23.3 - 0.008GS - 0.7CI^{1/3} + 0.002Lst^2 + 2 \times 10^{-6}CS^3 - 0.3Ls^{1/3} + 0.24BD^3 + 0.16TI^{1/3} - 2 \times 10^{-5}TI^2 + 17.8TS^{1/3} - 0.5ES$

For sandstone group

CI

$(S.E.\ 4.04 - -3.73;\ R - Sq\ 91.27 - -92.91)$

$SE = -13.6 + 17.9CI^{1/3}$

$C_4$ To $C_{20} + C_{101} + c_{106}$

87 sets of data

$CI^{1/3};\ MR;\ BD^{1/3};\ GR^{1/3}$

$(S.E.\ 4.73 - -3.47;\ R - Sq\ 85.35 - -92.92)$

$SE = -49.4 + 21.2CI^{1/3} + 0.317MR + 26.7BD^{1/3} - 3.82GR^{1/3}$

20 sets of data

$GS;\ CI^{1/3};\ Lst^2;\ Ls^{1/3};\ BD^3;\ C101^{1/3};\ TS^{1/3}$

$(S.E.\ 2.98 - 0.0205;\ R - Sq\ 34.06 - -100.00)$

$SE = -23.3 - 0.008GS - 0.7CI^{1/3} + 0.002Lst^2 - 0.3Ls^{1/3} + 1.2BD^3 + 0.16TI^{1/3} - 0.00002TI^2 + 17.8TS^{1/3} - 0.5ES$

For sandstone group

$CI;\ MR^{1/3};\ MR^3$

$(S.E.\ 4.04 - -3.02;\ R - Sq\ 91.27 - -95.62)$

$SE = -17.1 + 19.5CI^{1/3} + 1.1MR^{1/3} - 0.001MR^3$

$C_4$ To $C_{20} + C_{106}$

87 sets of data

$CI^{1/3}$; $C106$; $B.D^{1/3}$; $G.R^{1/3}$

($S.E.$ 4.73 – –3.47; $R - Sq$ 85.35 – –92.92)

$SE = -49.4 + 21.2CI^{1/3} + 0.317MR + 26.7BD^{1/3} - 3.82GR^{1/3}$

20 sets of data

$GS$; $CI^{1/3}$; $Lst^2$; $Ls^{1/3}$; $BD^3$; $GR^3$; $TS^{1/3}$; $A^3$

($S.E.$ 2.98 – –0.0627; $R - Sq$ 34.06 – –99.99)

$SE = 34.4 - 0.04GS + 3CI^{1/3} + 0.007Lst^2 - 2.3Ls^{1/3} - 1.3BD^3 - 0.04GR^3 - TS^{1/3} - 0.04A^3$

For sandstone group

$CI$; $MR^{1/3}$; $MR^3$

($S.E.$ 4.04 – –3.02; $R - SQ$ 91.27 – –95.62)

$SE = -17.1 + 19.5CI^{1/3} + 1.1MR^{1/3} - 0.001MR^3$

The results for the prediction of rock specific energy are summarized in Table 8.3.

**Table 8.3 — Best Prediction Equations for Rock Specific Energy**

For any types of sedimentary rock

(Sandstone, limestone and mudstone)

$SE = -49.4 + 21.2CI^{1/3} + 0.32MR + 26.7BD^{1/3} - 3.82GR^{1/3}$

($S.E.$ 3.47; $R - Sq$ 92.92)

For sandstone group

$$SE = -17.1 + 19.5CI^{1/3} + 1.1MR^{1/3} - 0.001MR^3$$

($S.E.$ 3.02; $R - Sq$ 95.62) (Note: $C_{101}$, toughness index; $C_{106}$, moduli ratio)

From the Table 8.2 and Table 8.3, the following conclusions are drawn:

1 From the regression using 95 prediction variables ($C_4$ $TO$ $C_{20} + C_{101} + C_{106}$). It is easy to see that rock moduli ratio is very important prediction variable, it is only less important than the NCB cone indenter. If the rock moduli ratio is not input into the prediction equation, rock toughness index is also a very important variable for the prediction of rock specific energy, it is only less important than cone indenter and static elastic moduli;

2 The most important prediction variables are cone indenter, rock moduli ratio, static elastic moduli, bulk density, grain roundness, rock toughness index and grain density;

3 Rock lithology is very important for the prediction of rock cuttability. The more accurate the determination of rock lithology, the greater the accuracy in the prediction of rock cuttability;

4 For sandstones, the most important rock properties for the evaluation of rock cuttability are listed as follows:

- Cone indenter;
- Moduli ratio.

5 There are some differences for the important prediction variables for different data type. It is obviously that prediction equations are rock lithology dependent. The prediction equation for sandstone group uses only 2 variables and a total of 3 steps compared with 4 variables and 4 steps in the prediction equation for all sedimenary rocks, but the standard error of the prediction equation for sandstone data type is 3.02 and R-Sq is 95.62 compared with standard error is 3.47 and R-Sq is 92.92 for sedimentary rocks (sandstone, limestone and mudstone). It is obviously that the prediction equation of sandstone group gives much more reliable results than that by

all-type sedimentary rock cutting database. This enhances the need for a detailed petrographic assessment of rock samples for the accurate determination of rock cuttability;

6 The data type ($C_4 - C_{20}$ + toughness index and rock moduli ratio) gives the best results for sedimentary rock type. The standard error in last step is 3.34, R-squared is 92.92 and takes totally 4 steps. The data type ($C_4 - C_{20}$ + moduli ratio + toughness index) also gives the best results for sandstone group;

If 20 sets of data selected from 87 sets of data is used, the following conclusions can be drawn from the analysis:

1 The most important rock properties for the prediction of rock specific energy are: GS; CI; Lst; Ls; BD; TI; Ts and ES;

2 8 prediction variables are required and the first few steps give a not ideal R-sq. and Standard error. In this respect, it is refered to Professor J. Abel's opinion that equation giving M.C. values greater than 85 percent in the first few steps are highly significant. Therefore we think that only 20 sets of data is not enough for concluding the most important variables for the prediction of rock cuttability;

3 Rock toughness index and rock moduli ratio are also important prediction variables for the evaluation of rock cuttability;

4 The greater the data on rock properties available, the greater the reliability of the results generated.

In a word, rock moduli ratio and rock toughness index are very important prediction variables for all datatypes. The prediction equations have strong dependence on rock lithology. The prediction equation for sandstone group gives the most reliable results compared with the prediction equations for other datasets.

## 8.5 The Prediction of Rock Cutting Tool Wear

The same procedures used for the prediction of rock specific energy were used for the prediction of rock cutting tool wear. The importance of toughness index

and moduli ratio for the prediction of rock cutting tool wear was also investigated. The lithology dependence of rock cutting wear prediction was studied.

The results analysed by curvilinear regression method for the prediction of rock cutting tool is listed in Table 8.4.

**Table 8.4 — Rock Properties Controlling Cutting Tool Wear**

$C_1$ To $C_{20}$

87 sets of data

$GR^3$; $A$; $Ss^{1/3}$; $A^3$

($S.E.$ 0.737 – –0.375; $R - Sq$ 97.15 – –99.31)

$$CW = 0.94 + 0.000001GR^3 + 0.146A + 0.17Ss^{1/3} + 0.019A^3$$

20 sets of data

$SH^{1/3}$; $Ls^{0.5}$

($S.E.$ 0.321 – –0.200; $R - Sq$ 41.81 – –82.51)

$$CW = -4.386 + 1.30SH^{1/3} - 0.059Ls^{0.5}$$

For sandstone group

$CI$; $A^3$; $GR^2$;

($S.E.$ 0.659 – –0.382; $R - Sq$98.37 – –99.51)

$$CW = -1.89 - 0.014CI + 0.0248A^3 + 0.000347GR^2$$

$C_4$ To $C_{20} + C_{101}$

87 sets of data

$GR^3$; $A$; $Ss^{1/3}$; $A^3$

($S.E.$ 0.737 – –0.375; $R - Sq$ 97.15 – –99.31)

$CW = 0.94 + 0.000001GR^3 + 0.146A + 0.17Ss^{1/3} + 0.02A^3$

20 sets of data

$GS^3;\ SH^{1/3};\ Ls^{0.5}$

$(S.E.\ 0.321 - -0.200;\ R - Sq41.81 - -82.51)$

$CW = -4.5 + 1.93SH^{1/3} - 0.0341Ls^{0.5}$

For sandstone group

$CI;\ A^3;\ GR^2$

$(S.E.\ 0.659 - -0.382;\ R - Sq\ 98.37 - -99.51)$

$CW = -1.89 - 0.014CI + 0.0248A^3 + 0.000347GR^2$

$C_4$ To $C_{20} + C_{101} + C_{106}$

87 sets of data

$GR^3;\ A; Ss^{1/3};\ A^3$

$(S.E.\ 0.737 - -0.375;\ R - Sq\ 97.15 - -99.31)$

$CW = 0.94 + 0.000001GR^3 + 0.146A + 0.17Ss^{1/3} + 0.019A^3$

20 sets of data

$SH^{1/3};\ Ls^{0.5}$

$(S.E.\ 0.321 - -0.200;\ R - Sq\ 41.81 - -82.51)$

$CW = -4.5 + 1.93SH^{1/3} - 0.034Ls^{0.5}$

For sandstone group

$CI;\ A^3;\ GR^2$

$(S.E.\ 0.659 - -0.382;\ R - Sq\ 98.37 - -99.51)$

$CW = -1.89 - 0.014CI + 0.0248A^3 + 0.000347GR^2$

$C_4$ To $C_{20} + C_{106}$

87 sets of data

$GR^3$; $A$; $Ss^{1/3}$; $A^3$

($S.E.$ 0.737 – –0.375; $R - Sq$ 97.15 – –99.31)

$CW = 0.94 + 0.000001GR^3 + 0.146A + 0.17Ss^{1/3} + 0.0189A^3$

20 sets of data

$SH^{1/3}$; $Ls^{0.5}$

($S.E.$ 0.321 – –0.200; $R - Sq$ 41.81 – –82.51

$CW = -4.50 + 1.93SH^{1/3} - 0.0341Ls^{0.5}$

For sandstone group

$CI$; $A^3$; $GR^2$

($S.E.$ 0.659 – –0.382; $R - Sq$ 98.37 – –99.51)

$CW = -1.89 - 0.014CI + 0.0248A^3 + 0.000347GR^2$

The results for the prediction of rock cutting wear can be summarized in Table 8.5.

**Table 8.5 — Best Prediction Equations for Cutting Tool Wear**

For any types of sedimentary rocks

(sandstone, limestone and mudstone)

$CW = 0.94 + 0.000001GR^3 + 0.146A + 0.17Ss^{1/3} + 0.019A^3$

($S.E.$ 0.375; $R - Sq$ 99.31)

For sandstone group

$$CW = -1.89 - 0.014CI + 0.025A^3 + 0.00035GR^2$$

($S.E.$ 0.659 – –0.382; $R - Sq$ 98.37 – –99.51)

(Note: $C_{101}$ toughness index; $C_{106}$ moduli ratio)

The following conclusions can be drawn from the analysis:

1 Rock toughness index and moduli raio are not suitable for the prediction of rock cutting tool wear;

2 The prediction equations have stong dependence on rock lithology. It is easy to see that the most important variables for the prediction of rock cutting wear are different in different datatypes. For any sedimentary rocks (sandstone, mudstone and limestone etc.) the important variables for the prediction of cutting wear are:

- Grain roundness;
- Abrasivity index;
- Sandstone content.

The standard error is 0.375 and R-Sq is 99.31.

For the sandstone group, the most important rock properties controlling the rock cutting tool wear are:

- Cone indenter;
- Abrasivity index;
- Grain roundness;
- Grain size.

The standard error is 0.382 and R-Sq is 99.51.

3 The most important rock properties controlling the rock cutting tool wear are rock rock textural coefficient. Therefore, the textural coefficient proposed by Howarth, which considers both grain shape factor and cementation between

grains, hopefully could be a very important rock property for the prediction of cutting tool wear.

## 8.6 The Prediction of Coarseness Index

The coarseness index is of lesser importance than rock specific energy and cutter wear in the prediction of rock cuttability. But it is very important parameter for evaluating the energy transfer ratio from mechanical tool or water jet to rock body and the formation of dust during rock cutting. Both field and laboratory investigations of coarseness index are very useful to determine the requirements of a mucking systems for different rock and machine types.

Table 8.5 shows that the significant rock properties controlling rock coarseness index.

**Table 8.6 — The Prediction of Rock Coarseness Index**

$C_4$ To $C_{20}$

87 sets of data

$ISI^3$; $A^{1/3}$; $TS^{1/3}$; $GD^3$

($S.E.$ 14.1 – –10.5; $R-Sq$ 50.92 – –75.81)

$$CoI = 423 + 0.00006ISI^3 - 27.8A^{1/3} + 40.8TS^{1/3} - 4.93GD^3$$

20 sets of data

CS

($S.E.$ 8.28; $R-Sq$ 79.52)

$$CoI = 393.9 + 0.376CS$$

For sandstone group (30 sets of data)

$ES^2$; $ISI^3$; $GD^3$; $A^{0.5}$; $CC$

$(S.E.\ 20.0 - -10.1;\ R - Sq\ 96.29 - -99.28)$

$CoI = 385 - 0.022ES^2 + 0.00008ISI^3 - 0.42GD^3 - 40A^{0.5} + 3.34CC$

$C_4$ To $C_{20} + C_{101}$

87 sets of data

$ISI^3;\ A^0.33;\ TI^{1/3};\ P^3;\ CS^3;\ GR^3$

$(S.E.\ 14.1 - -6.29;\ R - Sq\ 50.92 - -91.65)$

$CoI = 371 + 6 \times 10^{-6}ISI^3 - 15.2A^{1/3} + 7.9TI^{1/3} - 0.004P^3 - 10^{-6}CS^3 + 0.03GR^3 + 0.03GD^3$

20 sets of data

CS

$(S.E.\ 8.28;\ R - Sq\ 79.52)$

$Co.I = 401 + 0.262CS$

For sandstone group (30 sets of data)

$ES^2;\ C101^{0.5};\ GD^3;\ CC$

$(S.E.\ 20.0 - -7.24;\ R - Sq\ 96.29 - -99.66)$

$CoI = 295 - 0.022ES^2 + 4.1TI^{0.5} - 0.41GD^3 + 4.6CC + 6.21Ms^{0.5}$

$C_1$ To $C_{20} + C_{101} + C_{106}$

87 sets of data

$ISI^3;\ A^{1/3};\ TI^{1/3};\ P^3;\ CS^3;\ GR^3;\ GD^3$

$(S.E.\ 14.1 - -6.29;\ R - Sq\ 50.92 - -91.65)$

$CoI = 371 + 6 \times 10^{-6}ISI^3 - 15.2A^{1/3} + 7.9TI^{1/3} - 0.004P^3 - 10^{-6}CS^3 + 0.03GR^3 + 0.03GD^3$

20 sets of data

CS

$(S.E.\ 8.28;\ R-Sq\ 79.52)$

$CoI = 401 + 0.262CS$

For sandstone group (30 sets of data)

$ES^2;\ TI^{0.5};\ GD^3;\ CC;\ Ms^{0.5};\ Lst^3$

$(S.E.\ 20.0 - -7.24;\ R-Sq\ 96.29 - -99.66)$

$CoI = 295 - 0.0217ES^2 + 4.1TI^{0.5} - 0.41GD^3 + 4.6CC$

$C_4$ To $C_{20} + C_{106}$

87 sets of data

$ISI^3;\ A^{1/3};\ TS^{1/3};\ GD^3$

$(S.E.\ 14.1 - -10.5;\ R-Sq\ 50.92 - -75.81)$

$CoI = 423 + 0.00006ISI^3 - 27.8A^{1/3} + 40.8TS^{1/3} - 4.93GD^3$

20 sets of data

CS

$(S.E.\ 8.28;\ R-Sq\ 79.52)$

$CoI = 401 + 0.262CS$

For sandstone group

$ES^2;\ ISI^3;\ GD^3;\ A^{0.5};\ CC$

$(S.E.\ 20.0 - -7.24;\ R-Sq\ 96.29 - -99.66)$

$CoI = 295 - 0.02ES^2 + 4.1TI^{0.5} - 0.4GD^3 + 4.6CC + 6.2Ms^{0.5} - 0.00003Lst^3$

The analysis results for the prediction of coarseness index can be summarized in Table 8.7.

Table 8.7 — Best Prediction Equations of Rock Coarseness Index

For all sedimentary rocks

(Sandstone, limestone, mudstone)

$CoI = 371 + 6 \times 10^{-6} ISI^3 - 15.2A^{1/3} + 7.9TI^{1/3} - 0.004P^3 - 10^{-6} CS^3 + 0.03GR^3 + 0.03GD^3$

($S.E.$ 36.29; $R - Sq$ 91.65)

For sandstone group

$CoI = 295 - 0.02ES^2 + 4.1TI^{0.5} - 0.4GD^3 + 4.6CC + 6.2Ms^{0.5} - 0.00003Lst^3$

($S.E.$ 20.0 – –7.24; $R - Sq$ 96.29 – –99.66)

(Note: $C_{101}$ toughness index; $C_{106}$ moduli ratio)

From Table 8.6 and Table 8.7, the following conclusions can be drawn:

1 Rock toughness index is very important property for the prediction of rock coarseness index;

2 For all sedimentary rocks type, the most important variables for the prediction of coarseness index are: SI; A and TI;

3 For sandstone group, the most important variables for the prediction of coarseness index are: ES; TI and GD;

4 The accurate determination of rock lithology is very important for accurate prediction of rock coarseness index.

## 8.7 Comparison of Analysis Results with that by McFeat-Smith

As analysed above, the most important prediction variables for the prediction of rock specific energy, cutting tool wear and coarseness index are listed in Table 8.8.

Table 8.8 — For any types of sedimentary rocks

| | Specific Energy | Cutter Wear | Coarseness Index |
|---|---|---|---|
| Highly important | CI, MR | GR, A | ISI, A, TI |
| Important | BD, GR | Ss | P, CS, GR, GD |

Table 8.9 — For Sandstone Group

| | Specific Energy | Cutter Wear | Coarseness Index |
|---|---|---|---|
| Highly important | CI, MR | CI, A | TI, GD, ES |
| Important | GR, GS | CC, MS, LST | |

The most important variables by I.McF. Smith in 1975

Table 8.10 — Rock Properties Controlling Rock Cuttability

| | Specific energy | Cutter Wear | Coarseness Index |
|---|---|---|---|
| Highly significant | CI, GD | AW,SE, MI, GD | SP, P |
| Significant | TS, SH, P. | Sst, SH | Sst, ISI |
| Lesser important | BD, ES, ScH, ISI | CI, P | ScH, TS |

By comparing Table 8.8 and Table 8.9, these following conclusions can be reached:

1 The difference in the methods of judging the importance of input variables result in completely different results. It is easy to say that the results by t-testing in regression analysis in STEPWISE is much better than that by the fall in standard error and increase in R-Sq. According to statistical theory, the t-testing for evaluating the importance of inputed variables is very important for accurate prediction;

2 It is obviously that the prediction equations have strong dependence on the rock lithology;

3 The Prediction equations by *Minitab analysis can be classified into two groups:

- Sedimentary rocks;
- Sandstone.

4 Cutting tool wear is controlled by rock texture properties to some extent;

5 Rock toughness index and rock moduli ratio are very important rock properties for the prediction of rock cuttability.

## 8.8 The Summary of the Prediction Equations for Rock Cuttability

The prediction equations for rock cuttability evaluation are summarized in Table 8.11:

**Table 8.11 — The Summary of Rock Cuttability Prediction Equations**

For any type sedimentary rock

(sandstone, limestone and mudstone etc.)

Specific Energy Prediction Equation:

$$SE = -69.4 + 21.2CI^{1/3} + 0.317MR + 26.7BD^{1/3} - 3.82GR^{1/3}$$

(*Standard error* 2.47; $R - Sq$ 92.92)

Cutter Wear Prediction Equation:

$$CW = 0.94 + 0.000001GR^3 + 0.146A + 0.17Ss^{1/3} + 0.019A^3$$

(*Standard error* 0.375; $R - Sq$ 99.31)

Coarseness Index Prediction Equation:

$$CoI = 371 + 6 \times 10^{-6} ISI^3 - 15.2A^{1/3} + 7.9TI^{1/3} - 0.004P^3 - 10^{-6} CS^3 + 0.03GR^3 + 0.03GD^3$$

For sandstone group:

Specific Energy Prediction Equation:

$$SE = -17.1 + 19.5CI^{1/3} + 1.09MR^{1/3} + 0.0011MR^3$$

(*Standard error* : 3.02; $R - Sq$ 95.62)

Cutter Wear Prediction Equation:

$$CW = -1.89 - 0.014A^3 + 0.00035GR^2$$

(*Stanard error* 0.382; $R - Sq$ 99.51)

Coarseness Index Prediction Equation:

$$CoI = 385 - 0.022ES^2 + 8 \times 10^{-5} ISI^3 - 0.4BD^3 - 40.9A^{0.5}$$

(Standard error 10.1; R-Sq 99.28)

## 8.9 The Evaluation of the Prediction Equations for Specific Energy

In order to prove the reliability of prediction equation for rock cuttability, Specimen 8 in Appendix No.15 as an example.

### 8.9.1 The Evaluation of the Prediction Equation for All-type Rock Database

For any type of sedimentary rocks, the following rock properties parameters must be measured for the prediction of rock cuttability:

1 Cone Indenter testing using NCB device;

2 Rock moduli ratio;

3 Bulk density;

4 Grain roundness.

By using prediction equation for rock specific energy analysed from all-type rock cutting database, the results are obtained by either:

1 Inserting the measured value of each property in prediction equation or by;

2 Reading the partial specific energy from the corresponding rock property on Table 8.10 and adding this to the equation constant.

For example, specimen 13 in Appendix No.15 has a specific energy of $22.9 MJ/m^3$ The rock properties and corresponding partial specific energy as read from Table 8.12.

**Table 8.12 — The Prediction of Rock Specific Energy**

| Factor | Value | Partial specific energy |
|---|---|---|
| B | -49.4 | -49.4 |
| CI | 7.0 | 40.554 |
| MR | 7.25 | 3.056 |
| BD | 2.71 | 37.225 |
| GR | 3.50 | -5.800 |
| | | 25.635 |

The predicted value of a rock with a specific energy of 22.90 $MJ/m^3$ is $25.635 \pm 2.735 MJ/m^3$, therefore, this equation is satisfactory for the prediction of rock specific energy.

In 1975, I.McFeat-Smith gave the following prediction equation for rock specific energy evaluation.

$$SE = -8.4 + 0.14CI^2 + 2.61CS^{1/3} + 1.6 \times 10^{-5} SII^3 + 0.007CC$$

For this prediction equation, the following rock properties should be measured:

1 The cone indenter;

2 Compressive strength;

3 Shore hardness;

4 Cementation coefficients.

The same procedure used above is used for the prediction equation proposed by Smith, the predicted specific energy of specimen 13 is 14.79 $MJ/m^3$ compared with a specific energy of 22.90 $MJ/m^3$ by the instrummented cutting testing. It is obviously that the prediction equation proposed in this research gives much better results and higher reliability for the prediction of rock specific energy.

### 8.9.2 The Evaluation of the Prediction Equation for Sandstone

Because of the dependence of rock cuttability prediction on rock lithology, accurate determination of rock lithology is very important for reliable prediction. As shown in Table 8.10, for the prediction of sandstone group rock specific energy, the following rock properties should be measured:

1 Cone indenter;

2 Moduli ratio.

In order to compare the predicted value of sandstone specific energy, specimen 6 in Appendix No.11 is used as a example. In this research, the predicted value of rock specific energy is calculated as the following:

Table 8.13 — Rock Specific Energy Calculation

| Factor | Value | Partial specific energy |
|---|---|---|
| C | -17.10 | -17.100 |
| CI | 3.500 | 29.607 |
| MR | 6.692 | 2.054 |
| MR | 6.692 | 0.330 |
| - | - | 14.880 |

While Using the prediction equation by Smith in 1975, the predictied value is 8.631 compared with a rock specific energy of 11.7 $MJ/m^3$. Both prediction equations seems to have the same reliability.

The same procedures are performed for another three sandstone specimens.

For specimen 5 in Appendix No.11, the predicted value calculated using the prediction equation proposed in this research programe is 12.37 $MJ/m^3$, while the predicted value calculated using the prediction equation proposed by Smith is 4.14 $MJ/m^3$, the specific energy obtained from the laboratory instrumented cutting testing is 13.90 $MJ/m^3$. It is obvious that the prediction equation proposed in this research programme gives much accurate results.

For sandstone specimen 19 in Appendix No.11, the predicted value calculated from the equation proposed in this research programe is 16.1 $MJ/m^3$, while the predicted value calculated from the equation proposed by Smith is 6.96 $MJ/m^3$, the specific energy for this rock sample obtained from the laboratory instrumented cutting testing is 11.6 $MJ/m^3$, we can see that the new prediction equation proposed in this research programe gives more reliability for the prediction of rock cuttability. It also further indicated that the importance of rock lithology accurate determination.

For rock specimen 20 in Appendix No.11, the predicted value of specific energy for this rock calculated from the equation proposed in this research, is 12.0 $MJ/m^3$; while the predicted value calculated from the equation proposed by Smith is 18.0 $MJ/m^3$; the rock specific energy for obtained from the laboratory instrumented cutting testing is 14.7 $MJ/m^3$. When the equation for all rock types proposed in this research is used, the predicted value of this rock is 12.726 $MJ/m^3$. It shows that both prediction equations proposed in this research programe for specific energy evaluation have the same reliability.

For rock specimen 13 in Appendix No.11, the predicted value of this rock using the equation proposed for sandstone group in this research programe is 14.2 $MJ/m^3$. while the predicted value by Smith's equation is 5.59 $MJ/m^3$, the predicted value of rock specific energy by the prediction equation analysed from all-type rock cutting database is 13.45 $MJ/m^3$. The specific energy of this

specimen by the instrummented cutting testing is 16.6 $MJ/m^3$. It is very easy to see that two new prediction equations proposed in this research give much reliable prediction for rock specific energy. It also concludes that the prediction equations analysed from sandstone group rock cutting database give a bit better reliability than the prediction equation analysed from all-type sedimentary rock cutting database.

From the analysis above, it is easy to reach the following statements:

1 The accurate determination of lithology is very necessary for reliable rock specific energy evaluation;

2 The prediction equations analysed from sandstone group cutting database give much reliable results for the evaluation of rock cuttability than other prediction equations. Only a few rock properties testing were required for the prediction of rock specific energy compared with the former research conducted by Smith in 1975.

## 8.10 The Evaluation of the Prediction Equations for Cutting Tool Wear

Similar procedures as above are performed for the evaluation of the prediction equations for rock cutting wear.

### 8.10.1 The Evaluation for the Prediction Equation for all Rocks

The prediction equation for all-type sedimentary rock cutting tool wear is shown in Table 8.11, after four steps, the standard error fell from 0.737 to 0.375 and R-Sq rose from 97.15 to 99.31. In order to check the reliability of the prediction equations for rock cutter wear, rock specimen 22 in Appendix No.12. By using this equation, the predicted value of rock cutting tool wear is 1.76 mg/m compared with 3.60 mg/m in I.McFeat-Smith's equation, while specimen 22 cutter wear is 1.89 mg/m. Other similar procedures also prove that the equation for cutter wear prediction proposed in this research gives much better reliability than the former equation proposed by I.McFeat-Smith.

In order to predict the rock cutter wear, the following rock properties should be measured:

1 Grain roundness by petrographic analysis;

2 Abrasivity index;

3 Sandstone content.

### 8.10.2 Evaluation of the Prediction Equations for Sandstone

The similar procedures as above are run for the evaluation of the reliabilty of rock cutting wear prediction equation. The same rock specimen, sandstone 22 in Appendix No.12 is used for this purpose and also for the the evaluation of the importance of rock lithology.

For sandstone rock cutting tool wear prediction, the following rock properties should be measured:

1 Cone indenter;

2 Abrasivity index;

3 Grain roundness;

4 Grain size.

In 4 steps of regression of the prediction equation, the Standard error fell from 0.659 to 0.382 and R-Sq rose from 98.37 to 99.51. The cutter wear of specimen 22 in Appendix No.12, calculated using sandstone group cutter wear prediction equation, the cutter wear for this specimen is 1.7859 compared with the predicted value of rock cutter wear, calculated from the prediction equation for sedimentary rock proposed in this research programme and the prediction equation proposed by I.McFeat-Smith, the result obtained by the prediction equation for sandstone group is the best, the worst result is obtained by the prediction equation proposed by I.McFeat-Smith. In fact, the prediction equation proposed by I.McFeat-Smith can not used for the evaluation of rock cutting tool wear, the difference between the predicted value and the real value is too large.

The same procedure was performed for the other specimens, the similar conclusions were reached. This indicates that t-statistical analysis in the regression procedure is very important for accurate prediction of rock cutting tool wear, and

the accurate rock lithology determination is very necessary for the prediction of rock cutting wear.

## 8.11 Fracture Toughness for the Prediction of Rock Cuttability

### 8.11.1 Introduction

As analysed in Chapter 7, rock fracture toughness has been used by some researchers (Nelson P. P. et al.) for the prediction of TBM performance etc. Here the possibility of rock fracture toughness is used for the evaluation of intact rock cuttability.

The specific energy and rock fracture toughness (Mode I) of rock samples from different tunnelling projects have been tested. The strength of rock samples varies from soft to strong. Rock fracture toughness is tested by chevron-notched three-point bending method. Rock specific energy is tested by the instrummented cutting testing. It was found that rock fracture toughness has a strong relationship with rock specific energy. It is shown in Figure 8.1 the relation between these two variables can be described using the following equation:

$$SE = 2.9698 + 9.70K_{IC} \tag{8.2}$$

Where:

SE – Rock specific energy ($MJ/m^3$);

$K_{IC}$ – Rock fracture toughness ($MN/m^{1.5}$);

The index of determination is 0.955.

## 8.12 Recommendations and Conclusions

As analysed in chapter 7 and chapter 8, the following important conclusions could be reached:

1 Rock moduli ratio is a very important rock property controlling the rock specific energy index;

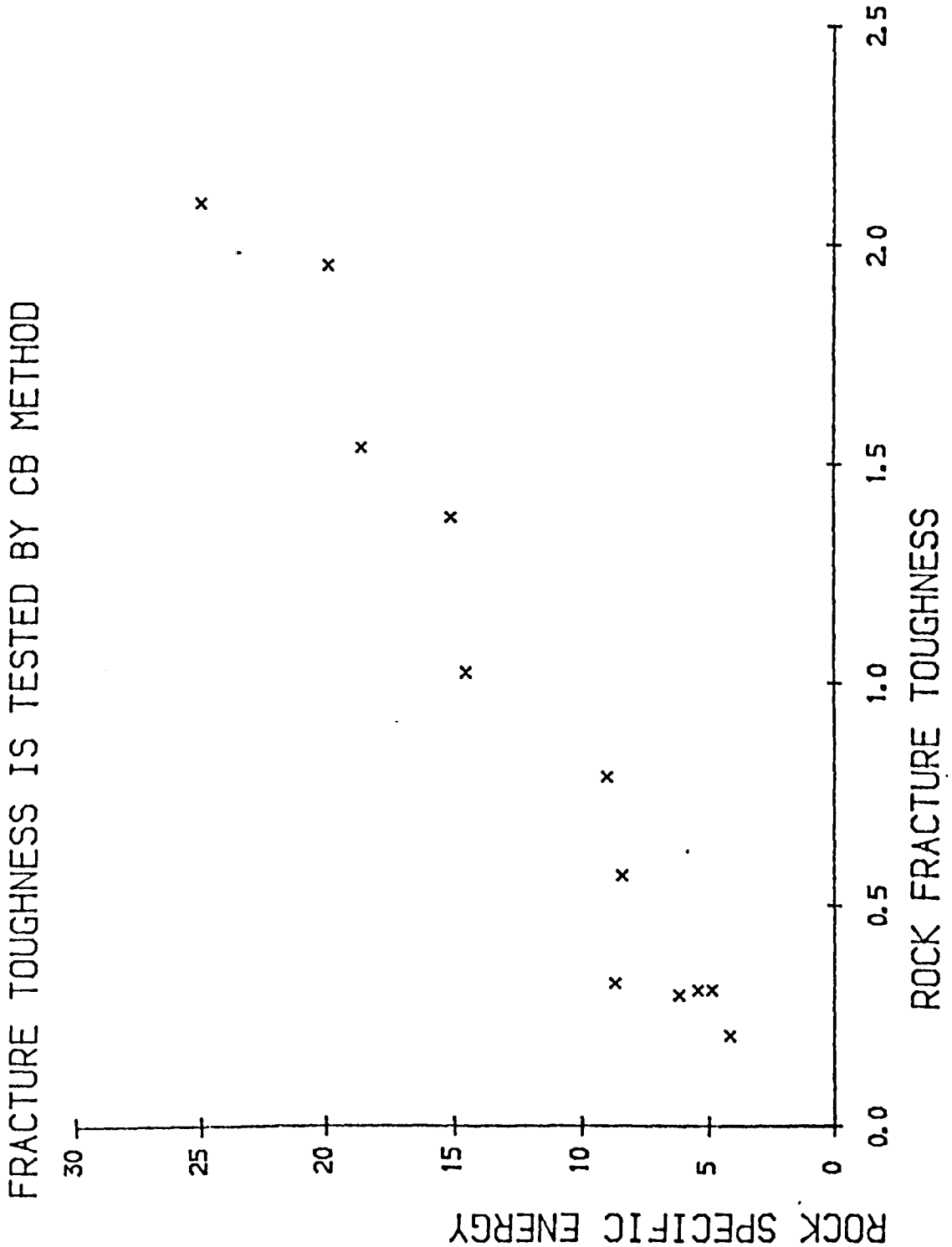


**Figure 8.1 — $K_{IC}$ vs Rock Specific Energy**

2 Rock toughness is a very important rock property for the prediction of rock specific energy, cutter tool wear and coarseness index;

3 Rock cuttability prediction equations have a very strong dependence on rock lithology. Accurate rock lithology determination is necessary for accuracte prediction of rock cuttability;

4 The prediction equations reached in this research programme give much more reliable results than former equations proposed by I.McFeat Smith;

5 The most important rock properties for the prediction of rock specific energy are: cone indenter, toughness index, moduli ratio. For sandstone group, the most important prediction variables are: cone indenter, moduli ratio and toughness index;

6 The most important rock properties for the prediction of rock cutting tool wear are: grain roundness and lathe abrasivity index. For sandstone group, the most important prediction variables are: toughness index and grain density;

7 The most important variables for coarseness index prediction are: impact strength index, lathe abrasivity index and toughness index. For sandstone group, the most important prediction variables are: toughness index and grain density;

8 Rock fracture toughness has strong correlation with rock specific energy;

9 Drag tool cutting mechanism should be investigated based on mixed-mode rock fracture theories and numerical calculation of stress intensity factors (Mode I and Mode II) of crack tip.

The further research could be focused on the following fields:

1 Expanding the existing rock cutting database, some new rock properties variables such as mode I and mode II rock fracture toughness, mode I and Mode II critical energy release rate, rock ductility coefficient proposed by Nelson P. P. and dynamic rock fracture toughness etc. should be included in the future database.

2 New methods for classifing rock mass should be investigated. Quantity description of rock mass should be performed so as to expand the existing database from intact rock to rock mass;

3 Machine specification quantity index should be determined by the accurate analysis of machine performance, so for a specific tunnelling machine and rock mass condition in situ, the performance of the tunnelling machine can be assessed accurately;

4 Rock breaking mechanism analysis could be based on mixed-mode rock fracture theories. The rock-tool interaction, the effect of process zone ahead of cutting tool etc. should be considered in future drag tool rock cutting mechanism analysis;

5 The combination of rock properties variables by their products etc. should be studied so that new indices, which gives better prediction, could be developed based on curvilinear regression analysis. The products of $K_{IC}$, $K_{IIC}$, Toughness index and rock mass classification index Q or RMR could be very important rock mass cuttability indices;

6 Finite element method and boundary element method are very useful tool for the analysis of rock-tool interaction and the stress intensity factors (Mode I and Mode II). More research should be done in these fields.

## Bibliography


1. Adler, L. & Krishnan, G. V. *"A Unified Rock Classification for Drilling and Boring"*, Proceedings of 1983 Rapid Excavation and Tunnelling Conference, AIME and Canadian Institute of Mining and Metallurgy, Engineering Institute of Canada, Vol. 1, New York, pp. 157-174, 1983

2. Aleman, V. P. *"Characterization of Strata with Particular Reference to the Performance of Roadway Drivage Machines"*, Ph.D Thesis, University of Nottingham, 1982

3. Atkinson T. & Cassapi V. B. *"The Prediction and Reduction of Abrasive Wear in Mine Excavating Machinery"*, Tribology in Mineral Extraction, War on Wear, 1984

4. Atkinson B. K. *"Fracture Toughness of Tennessee Sandstone and Carrara Marble"*, Int. J. Rock Mech. Min. Sci. & Geomech. Abstr. Vol.16, pp.151-163, 1979

5. Atkinson C. & R. E. Smelser & J. Sanchez *"Combined Mode Fracture via the Cracked Brazilian Disk Test"*, International Journal of Fracture, Vol. 18, No. 4, April 1982

6. ASTM E399 *"Standard Test Methods for Plane-Strain Fracture Toughness of Metal"*, ASTM Testing Standard, 1978

7. Bamford W. E. *"Rock Test Indices are Being Successfully Correlated with Tunnel Boring Machine Performance"*, Fifth Australian Tunnelling Conference, sydney, Australia. 1984.

8. Bamford W. E. *"Cuttability and Drillability of Rock"*, Civil College Technical Report, Engineers, Australia, July 11 1986.

9. Banks-Sills L. & Arcan M. & Bortman Y. *"A Mixed-Mode Fracture Specimen for Mode II dominate deformation"*, Engineering Fracture Mechanics 20, pp. 145-157, 1984.

10. Barker L. M. *"Theory for Determining Kic from Small, Non-Linear Specimens"*, Int. J. of Fracture 15, pp.513-536, 1979.

11. Barker L. M. *"Specimen Size Effects in Short Rod Fracture Toughness Measurements"*, Chevron-Notched Specimens: Testing and Stress analysis, ASTM STP 855, pp.117-133, Philadelphia PA, 1984.

12. Barton C. C. *"Variables in Fracture Energy and Toughness Testing of Rock"*, 26th US Symposium on Rock Mechanics, USA, 1985.

13. Bearman R. A. & Pine R. J. & Wills B. A. *"Use of Fracture Toughness Testing in Characterizing the Comminution Potential of Rock"* Today's Technology for the Mining and Metallurgical Industries, MMIJ/IMM Joint Symposium, Shigaku-Kaikan, Kyoto, Japan, Oct. 1989.

14. Beech J. F. *"Three-Dimensional Finite Element Calibration of the Short Rod Specimen"*, Engineering Fracture Mechanics, 1981.

15. Brown E. T. *"Rock Characterization Testing and Monitoring. ISRM Suggested Methods"*, Published for the Commision on Testing Methods, International Society for Rock Mechanics, 1981.

16. Chiang W. T. *"Fracture Criteria for Combined Mode Cracks"*. Fracture 4, pp.135–154, 1977.

17. Chen Jun Fang *"Review of Existing Rock Fracture Toughness Testing Methods"*. Progress report, 1987.

18. Chen Jun Fang *"Numerical Calibration of the Cracked Brazilian Disc Specimen"*. Progress report, 1988.

19. Chen Jun Fang *"Size Requirement Study of the CCNBD Method"*. Progress report, 1988.

20. Chen Jun Fang *"Experimental Validation of the CCNBD Method"*. Progress report, 1989.

21. Conca J. L. & Cubba R. *"Abrasion Resistance Hardness Testing of Rock Materials"*, Int. J. Rock Mech. Min. Sci. & Geomech. Abstr., Technical Note, 1986.

22. Cook N.G. W. & Hood M. & Tsai F. *"Observation of Crack Growth in Hard Rock Loaded by an Indenter"*, Int. J. Rock Mech. Min. Sci. & Geomech. Abstr., Vol.21, pp.91–107, 1984.

23. Crouch S. L *"Solution of Plane Elasticity Problems by the Displacement Discontinuous Method"*, Int. J. Num. Meth. Engineering, Vol.10, pp.301–343, 1976

24. Deliac Eric P. *"Optimization of Rock Breaking Machine"*, Ph.D thesis, Mining Tech. and Econ. Dept., Ecole des Mines de Paris, Fontainebleau, France, 1988.

25. Ewing P. D. & Swedlow J. L. & Williams J. Q. *"Further Results on the Angled Crack Problems"*, Int. J. Fracture 18, pp.19-28, 1976.

26. Evans I. & Pomeroy C. D. *"The Strength, Fracture and Workability of Coal"*, Published by the Authors, 1973.

27. Evans I. *"A Theory of the Cutting Force for Point-attack Picks"*, Int. J. Min. Eng., Vol.2, pp.63-67, 1984.

28. Evenden M. P. & Edwards J. S. *"Cutting Theory and Coal Seam Assessment Techniques and Their Application to Shearer Design"*, Min. Sci. and Tech., vol.2, pp.253-270, 1985.

29. Farmer I. W. *"Energy Based Rock Characterization"*, Proceedings of the Symp. Held at the SME-AIME Annual Meeting, New Orleans, Louisiana, USA, 1986.

30. Farmer I. W. & Garritty P. *"Prediction of Roadheader Cutting Performance from Fracture Toughness Considerations"*, 6th International Rock Mechanics Conference, Canada, 1987.

31. Fong F. L.C; Nelson P. P. *"R-Curve Fracture Toughness Measurement: Testing Procedures, Correlation with Other Rock Properties and Applications in Rock Breakage Studies"*, Proceedings of the 1986 SEM Spring Conference on Experimental Mechanic Published by the Society of Experimental Mechanics, 1986.

32. Fowell R. J.; McFeat-Smith I. *"Factors Influencing the Cutting Performance of a Selective Tunnelling Machines"*, Proc. First Int. Symp. Tunnelling 76 (London) IMM. 1-5 March, 1976.

33. Fowell R. J.; Pycroft S. *"Rock Machineability Studies for the Assesement of Selective Tunnelling Machine Performance"*, Proc. 21st Rock Mechanics Symp. Rolla, USA, 1980.

34. Fowell R. J.; Johnson S. T. *"Rock Classification and Assessment for Rapid Excavation"*, Proc. Symp. Strata Mechanics, University of Newcastle upon Tyne, 1982.

35. Friedman M.; Ford L. M. *"Analysis of Rock Deformation and Fractures Induced by Rock Cutting Tool Used in Coal Mining"*, Proceedings of 24th U.S. Symposium on Rock Mechanics: Theory - Experiment - Practice, Texas A & M University, USA, 1983.

36. Gill D. E. & Pichette C. & Rochon P. & Dube B. *"Relation Between Some of the Methods for Predicting the Penetration Rate of Full Face Boring Machines"*, Underground Rock Engineering. 13th Canadian Rock Mechanics Symposium (The H. R. Rice Memorial Symposium), 1980.

37. Griffith A. A. *"The Theory of Rupture"*, Proceedings of 1st Int. Congress of Applied Mechanics. PP. 55-63, Delf, 1924.

38. Gunsallus K. L. & Kulhawy F. H. *"A Comparative Evaluation of Rock Strength Measurements"*, Int. J. Rock Mech. Min. Sci. & Geomech. Abstr. Vol. 16, pp. 293-302 1984

39. Hideo Awaji & Sennosuke Sato+ *"Combined Mode Fracture Toughness Measurement by the Disc Test"*, J. of Eng. Materials and Technology, 1978

40. Hoagland R. G. & Hahn G. T. & Rosenfield A. R. *"Influence of Microstructure on Fracture Propagation in Rock"*, Rock Mechanics 5, pp.77-106, 1973.

41. Howarth D. F. & Adamson W. R. & Berndt J. R. *"Correlation of Model Tunnelling Boring and Drilling Machine Performances with Rock Properties"*, Int. J. Rock Mech. Min. Sci. & Geomech. Abstr., Vol.23, No. 2, pp.171-175, 1986.

42. Howarth D. F. *"Mechanical Rock Excavation - Assessment of Cuttability and Boreability"*, Proceedings of 1987 Rapid Excavation and Tunnelling Conference, New Oreleans, Louisiana, June 14-17 1987.

43. Huang J. A. & Wang S. *"An Experimental Investigation Concerning the Compressive Fracture Toughness of Some Brittle Rocks"*, Int. J. Rock Mech. Min. Sci. & Geomech. Abstr. Vol. 22, pp. 99-104, 1985.

44. Hughes H. M. *"Some Aspects of Rock Machining"*, Int. J. Rock Mech. Min. Sci. & Geomech. Abstr., Vol. 9, pp. 205-211, 1972.

45. Inazaki T. & Takahashi Y. *"Evaluation of Rock Mass Quality Utilizing Seismic Tomography"*, 6th International Rock Mechanics Conference, Canada, 1987

46. Ingraffea A. R. & Gunsallus J. F. & Nelson P. P. *"A Fracture Toughness Testing System for Prediction of Tunnelling Boring Machine Performance"*, 27th U.S. Rock Mechanical Symposium, 1986

47. Isida Makoto *"Arbitrary Loading Problems of Doubly Symmetric Regions Containing a Central Crack"*, Engineeing Fracture Mechanics, Vol.7, pp. 505-514, 1975.

48. Janach W. & Merinod A. *"Rock Abrasivity Tests with a Modified Schmidt Hammer"*, Int. J. Rock Mech. Min. Sci. & Geomech. Abstr., 1982.

49. Kenner V. H. & Advani H. & Richard T. G. *"A Study of Fracture Toughness for an Anoisotropic Shale"*, Int. J. Rock Mech. Min. Sci. & Geomech. Abstr., 1986.

50. Kenny P. & Johnson S. N. *"The Effect of Wear on the Performance of Mineral Cutting Tools"*, Wear Conference, 1983.

51. Khalaf F. & Abdel-Zaher M. *"Analogy Between Indentation and Blasting Tests on Brittle Rocks"*, Rock Mechanics 13, 99-117, 1980.

52. Kuruppu M. D. & Chong K. P. *"New Specimens for Modes I and II Fracture Investigations of Geomaterials"*, Proceedings of the 1986 SEM Spring Conference on Experimental Mechanics, Published by the Society of Experimental Mechanics, 1986.

53. Laqueche H. & Rousseau A. & Valentin G. *"Crack Propagation Under Modes I and II Loading in Slate Schist"*, Int. J. Rock Mech. Min. Sci. & Geomech. Abstr., 1986.

54. Lavery P. L. & Chong K. P. & Kuruppu M. D. *"Mixed Mode Fracture Mechanics with Emphasis on Transversely Isotropic Rocks"*, Rock Mechanics in Productivity, Protection, 1985.

55. Lindqvist P. A. *"Energy Consumption in Disc Cutting of Hard Rock"*, Tunnelling 82, PP. 189-196, London, 1982.

56. Maki K. *"On the Applicability of the Tensile Strength as an Index to Rock Fragementation"*, First Int. Symp. on Rock Fragementation by Blasting, 1983.

57. Marion R. H. *"Use of Indentation Fracture to Determine Fracture Toughness"*, Fracture Mechanics Applied to Brittle Materials, ASTM STP 678, pp.103-111, 1979.

58. McFeat-Smith I. *"Correlation of Rock Properties and Tunnel Machine Performance in Selected Sedimentary Rocks"*, Ph.D Thesis, University of Newcastle upon Tyne, 1975.

59. Meredith P. G. *"A Fracture Mechanics Study of Experimentally Deformed Crustal Rocks"*, Unpublished Ph.D Thesis, University of London, 1983.

60. MRDE Handbook No.5 *" NCB Cone Indenter"*, Mining Research and Development Establishment, 1977.

61. Nelson P. P. & Fong L. C. *"Characterization of Rock for Boreability Evaluation Using Fracture Material Properties"*, 27th U.S. Rock Mechanics Symposium, 1986.

62. Nelson P. P. *"Soft Rock Tunnelling: Equipment Selection Concepts and Performance Case Histories"*, Proceedings of 1987 Rapid Excavation and Tunnelling Conference. New Orleans, Louisiana, June 14-17, 1987.

63. Nishimatsu Y. *"The Mechanics of Rock Cutting"*, Int. J. Rock Mech. Min. Sci. & Geomech. Abstr. Vol. 9, pp. 261-270, 1972.

64. Ostojic P. & McPHERSON C. *"A Review of Indentation Fracture Theory: Its Development, Principles and Limitations"*, International Journal of Fracture, 1987.

65. Ouchterlony F. *"Review of Fracture Toughness Testing of Rock"*, SM Archivet No.7, pp.131-211, 1982.

66. Ouchterlony F. *"Suggested Methods for Determining Fracture Toughness of Rock Material. International Society for Rock Mechanics Commission on Testing Method "*, J. A. Franklin (Canda); Sun Zongqi (China); B. K. Atkinson and P. Mere (England); W. Muller (Germany); Y. Nishimatsu and H. Takahashi (Japan), 1987.

67. Palaniswamy K. & Knauss W. G. *" On the Problem of Crack Extension in Brittle Solids under General Loading"*, Mechanics Today, Vol.4, pp.87-148, 1978.

68. Panasyuk V. V. & Berezhnitskiy L. T. *"Propagation of an Arbitarily Oriented Rectilinear Crack during the Extension of a Plate"*, Prikladnaya Mekhanike 1, pp.48-55, 1965.

69. John J. Petrovic *"Mixed-Mode Fracture of Hot-Pressed $Si_3N_4$"*, J. Am. Ceram. Soc., 68[6] 348-55, 1985.

70. Per-Arne Lindqvist & Lai Hai-Hui & Dve Alm *"Indentation Fracture in Rocks Observed in-Situ in a Scanning Electron Microscope"*, Rock Mechanics and Rock Engineering, 1984.

71. Phillips H. R. & Bilgin N. *"Correlation of Rock Properties with the Measured Performance of Disc Cutting"*, Proceedings of a Conference on Rock Engineering The University of Newcastle Upon Type, 1977.

72. Pook l. P. & Smith R. A. *"Theoretical Background to Elastic Fracture Mechanics"*, A Conference, 1977.

73. Poole D. *"The Effectiveness of Tunnelling Machines"*, Tunnels & Tunnelling, 1987.

74. Protodyakonov M. M. *"Mechanical Properties and Driabilities of Rock"*, 5th U.S. Rock Mech. Conference, USA, 1963.

75. Raju Ivatury S. & Newman.Jr J. C. *"Three-Dimensional Finite-Element Analysis of Chevron-Notched Fracture Specimens"*, Chevron-Notched Specimens: Testing and Stress Analysis, 1984.

76. Rummel F. *"A Review of Fracture Criteria of Brittle Rock"*, Int. Center for Mech. Sci., Rock Mechanics Courses and Lectures - No. 165, Edited by L. Muller, 1974.

77. Sandbak L. A. *"Roadheader Drift Excavation and Geotechnical Rock Classification at San Manuel, Arozina, USA"*, Proceedings of 1985 Rapid Excavation and Tunnelling Conference. New York, USA. Vol.II, 1985.

78. Saouma V. E. & Kleinosky M. J. *"Finite Element Simulation of Rock Cutting, Fracture Mechanics Approach"*, Rock Mechanics in Productivity, Protection, 1985.

79. Schmidt R. A. & Huddle C. W. *"Effects of Confining Pressure on Fracture Toughness of Indian Limestone"*, Int. J. Rock Mech. Min. Sci. & Geomech. Abstr. Vol.14, pp. 289-293, 1977.

80. Schmidt R. A. & Lutz T. J. *"Kic and Jic of Westerly Granite - Effects of Thickness and in-plane Dimension"*, Fracture Mechanics Applied to Brittle Materials, Part 2, 1978.

81. Shetty D. K. & Alan R. Rosenfield & Winston II. Duchworth *"Fracture Toughness of Ceramics Measured by Chevron-Notch Diametral-Compression Test"*, J. Am. Ceram. Soc., 68[12] C-325-C-327, 1985.

82. Shetty D. K. & Rosenfield A. R.& Duckworth W. H. *"Mixed-Mode Fracture in Biaxial Stress State: Application of the Diametrical-Compression (Brazilian Disk) Test"* Engineering Fracture Mechanics Vol 26, No. 6, pp 825-840, 1987.

83. Sih G. C. *"Strain-Energy Density Factor Applied Mixed-Mode Crack Problems"*, Int. J. Fracture 10, pp.305-320, 1974.

84. Singh R. N. & Pathan A. G. *"Fracture Toughness of Some British Rocks by Diametral Loading of Discs"*, Mining Science and Technology, 6(1988) 179-190 Elsevier Science Publishers B.V. Amsterdam, 1987.

85. Singh S. P. *"Criterion for the Assessment of the Cuttability of Coal"*, Underground Mining Methods and Technology, edited by A. B. SzwilskiA Conf. Held in Dept. of Mining Eng., University of Nottingham, 1986.

86. Smith R.N. L. & Crook S. H. *"Cracks at Stress Concentors"*, Betch 86: Proceedings of the 2nd Boundary Element Technology Conference, Massachusetts Institute of Technology USA,, 1986.

87. Strauss A. M. *"The Microcracking of Rock and the Prediction of Fracture and Failure"*, Rock Mechanics in Productivity, Protection. 1985

88. Suana M. & peters Tj *"The Cerchar Abrasivity Index and Its relation to Rock Mineralogy and Petrograph"*, Int. J. Rock Mech. & Min. Sci., Vol. 15, pp. 1-7, 1982.

89. Sun Zong Qi & Ouchterlony Finn *"Fracture Toughness of Round Specimens of Strpa Granite"*, Int. J. Rock Mechanics Min. Sci. & Geomech, Abstr. Vol.23, pp.399-409, 1986.

90. Swedlow J. L. *"Criteria for Growth of the Angled Crack"*, Cracks and Fracture, ASTM STP 601, pp.506-521, 1976.

91. Tarkoy P. J. *"Predicting Raise and Tunnel Boring Machine Performance: State of the Art"*, Proceedings of 1979 Rapid Excavation and Tunnelling Conference. Vol.1, PP.33-334, 1979.

92. Tsur-Lavie Y. & Denekamp S. A. *"Comparison of Size Effect for Different Types of Strength Tests"*, Rock Mechanics 15, pp.243-254, 1982.

93. Udd J. E. & Wang H. *"A Comparison of Some Approaches to the Classification of Rock Masses for Geotechnical Purposes"*, 26th U.S. Symposium on Rock Mechanics, 1985.

94. West G. A. *"A Review of Rock Abrasiveness Testing for Tunnelling"*, Proceedings of the Int. Symp. on Weak Rock, 1981.

95. Yokobori T. & Mackawa. I. & Sato Jr. K. & Ishizaki Y. *"A New Methodology for the Study on Fracture Criterion for the Notched or Cracked Specimen under Mixed Modes I and II"*, Proc. Symp. Absorbed Energy Strain Energy Density, Edited by Sih C.G. , Czoboly E., Gillemot F., 1980.

96. Zipf. Jnr. Karl and Bieniawski Z. T. *"Mixed-mode Testing for Fracture Toughness of Coal Based on Critical Density"*, Proc. 27th U.S. Symp. on Rock Mechanics, Tuscaloosa, Alabama, pp.16-23, 1986.

## @.1 Datafile for the CSTBD Calibration by 2D BEM, Open mode

```
BE2DTE   0   0
TITLE D = 100, a = 30, Plane stress, Poisson's ratio ν = 0.3
*DEFINE BOUNDARY POINT COORDINATES
BP 1 0 0
BP 2 30 0
BP 3 50 0
BP 4 49.9695 1.745
BP 5 0 50
*DEFINE CURVE LINE
BC 1 3 4 1 3
BC 2 4 5 1 -905
*DEFINE STRAIGHT LINE
BL 3 1 2 909
BL 4 2 3 -405
*DEFINE ZONE INFORMATION
ZN 1
*DEFINE AXIS SYMMETRY INFORMATION
ZX 1
*DEFINE PATCHES NUMBER
ZB 1-4
*DEFINE DISPLACEMENT CONDITION
PD 4 2 0 0 0
*DEFINE LOADING INFORMATION
PP 1 -1 -100 -100 -100
END
```

## @.2 Data File for the CCNBD Calibration by 3D BEM, Open Mode

BE3DTE 0 0

TITLE: $D = 50$, $R = 26$, $B = 15$, $a_0 = 10$, $a_1 = 20.094$, $a = 15.0$, $b = 2.763$

*BOUNDARY POINTS COORDINATE

BP 1 0 0 0

BP 2 0 0 15.0

BP 3 0 0 25

BP 4 7.5 0 0

BP 5 7.5 0 20.094

BP 6 7.5 0 25

BP 7 2.763 0 0

BP 8 2.763 0 15.0

BP 9 2.763 0 25

BP 10 7.5 25 0

BP 11 0 25 0

BP 12 0 0.8725 24.9848

BP 13 7.5 0.8725 24.9848

BP 14 2.763 0 20.094

BP 20 24 0 0

* DEFINE CURVE LINE

BC 1 11 12 1 1

BC 2 12 3 1 1

BC 3 10 13 4 1

BC 4 13 6 4 1

BC 5 8 5 20 1

* DEFINE PATCHES

BR 1 1 2 8 7 409 2

BR 2 7 8 5 4 409 4

BR 3 2 3 9 8 -405 2

BR 4 14 9 6 5 4 4

BD 5 8 14 5 3 3

BR 6 10 13 12 11 4 2

```
BR 7 13 6 3 12 1 4
BD 8 4 6 10 3 3
* DEFINE ZONE INFORMATION
ZN 1
* DEFINE SYMMETRY IMFORMATION
ZX 1
ZZ 1
* DEFINE PATCHES NUMBER USED IN THIS ANALYSIS
ZB 1-8
* DEFINE YOUNG'S MODULI
ZE 10000
* DEFINE INTERFACE DISPLACEMENT CONDITION
PD 3 2 0 0 0 0
PD 2 2 0 0 0 0
PD 5 2 0 0 0
* DEFINE PRESSURE APPLIED
PP 7 -1 -100 -100 -100 -100
END
```

## @.3 Datafile for the CCNBD Calibration by 3D BEM

Disc ID: , Date of Calibration:

D = , D1 = , B = , A0 =

A = , b = , $\alpha$ = degree, C =

Young Moduli = 10000, $P/B = 100 \times B \times \sin.\alpha =$

Poisson's ratio = 0.3, Plane Stress/ Plain Strain:

$\lambda$ $COD(x = 0, y = 0, z = 0)$ =

$\lambda$ $COD$ $EB$ =

$\lambda$ $LPD$ $(x = 0, y = 0, z = D/2)$ =

$\lambda$ $LPD$ $EB$ =

### Dimensionless Stress Intensity Factors Calculation

| x coordinate | $2x/b$ | $Dis(y) \times 10$ | $K_1$ | $F_1$ | $F_a$ |
|---|---|---|---|---|---|
| | | | | | |
| | | | | | |
| | | | | | |
| | | | | | |
| | | | | | |
| | | | | | |
| | | | | | |
| | | | | | |

### Critical Dimensionless Stress Intensity Factors:

## @.4 Effect of Element Mesh on the Calibration Results

### 2D BEM

| Element Number | Dimensionless SIFs $F_1$ | $C_1EB$ | $C_2EB$ |
|---|---|---|---|
| 42 | 0.870 | 3.575 | 0.912 |
| 47 | 0.870 | 3.525 | 0.912 |
| 55 | 0.877 | 3.576 | 0.912 |
| 62 | 0.881 | 3.575 | 0.913 |
| 82 | 0.895 | 3.627 | 0.916 |
| 98 | 0.896 | 3.523 | 0.911 |
| 130 | 0.892 | 3.562 | 0.911 |
| 182 | 0.879 | 3.577 | 0.912 |
| 212 | 0.887 | 3.626 | 0.918 |
| 260 | 0.886 | 3.622 | 0.913 |
| 301 | 0.886 | 3.622 | 0.913 |

### 3D BEM

| Element Number | Critical Dimensionless SIFs $F_{IC}$ | $F_0$ | $C_1EB$ | $C_2EB$ |
|---|---|---|---|---|
| 64 | 1.09 | 1.03 | 2.41 | 0.92 |
| 68 | 1.09 | 1.03 | 2.50 | 0.92 |
| 70 | 1.08 | 1.03 | 2.41 | 0.94 |
| 72 | 1.07 | 1.02 | 2.47 | 0.93 |
| 76 | 1.06 | 1.02 | 2.41 | 0.92 |
| 85 | 1.06 | 1.01 | 2.48 | 0.92 |
| 104 | 1.05 | 1.01 | 2.35 | 0.93 |
| 149 | 1.08 | 1.01 | 2.38 | 0.92 |
| 155 | 1.07 | 1.01 | 2.42 | 0.92 |
| 168 | 1.05 | 1.01 | 2.45 | 0.92 |

## @.5 Effect of Loading Contact Angle on $F_1$, $C_1EB$ and $C_2EB$

### Effect of Loading Angle on F

| Loading Contact Angle | $a/R = 0.9$ | 0.8 | 0.7 | 0.6 | 0.5 |
|---|---|---|---|---|---|
| 0.500 | 2.630 | 1.779 | 1.358 | 1.097 | 0.896 |
| 1.000 | 2.620 | 1.778 | 1.363 | 1.096 | 0.895 |
| 2.000 | 2.620 | 1.774 | 1.363 | 1.095 | 0.895 |
| 4.000 | 2.610 | 1.763 | 1.355 | 1.093 | 0.894 |
| 6.000 | 2.560 | 1.718 | 1.342 | 1.087 | 0.891 |
| 14.000 | 1.500 | 1.483 | 1.245 | 1.038 | 0.863 |

### Effect of Loading Contact Angle on $C_1EB$

| Loading Contact Angle | $a/R = 0.9$ | 0.8 | 0.7 | 0.6 | 0.5 |
|---|---|---|---|---|---|
| 0.500 | 3.916 | 2.599 | 1.815 | 1.289 | 0.911 |
| 1.000 | 3.898 | 2.596 | 1.814 | 1.286 | 0.911 |
| 2.000 | 3.897 | 2.594 | 1.814 | 1.285 | 0.910 |
| 4.000 | 3.892 | 2.568 | 1.809 | 1.284 | 0.909 |
| 6.000 | 3.888 | 2.543 | 1.801 | 1.284 | 0.908 |
| 10.000 | 3.831 | 2.505 | 1.801 | 1.270 | 0.907 |
| 14.000 | 3.377 | 2.423 | 1.801 | 1.251 | 0.896 |

### Effect of Loading Contact Angle on $C_2EB$

| Loading Contact Angle | $a/R = 0.9$ | 0.8 | 0.7 | 0.6 | 0.5 |
|---|---|---|---|---|---|
| 0.500 | 5.178 | 4.457 | 4.234 | 4.024 | 3.731 |
| 1.000 | 4.783 | 3.999 | 3.879 | 3.769 | 3.531 |
| 2.000 | 4.356 | 3.534 | 3.349 | 3.239 | 3.176 |
| 4.000 | 3.894 | 3.246 | 2.895 | 2.779 | 2.707 |
| 6.000 | 3.292 | 2.828 | 2.637 | 2.519 | 2.444 |
| 10.000 | 2.970 | 2.495 | 2.350 | 2.196 | 2.121 |
| 14.000 | 2.331 | 2.221 | 2.021 | 1.984 | 1.911 |

## @.6 Effect of Poisson's Ratio on the Calibration Results

### Effect of Poisson's Ratio on the CSTBD Calibration by 2D BEM

| Poisson's Ratio | Dimensionless SIFs, F1 | C1EB | C2EB |
|---|---|---|---|
| 0.00 | 0.79 | 3.36 | 0.91 |
| 0.17 | 0.82 | 3.43 | 0.91 |
| 0.30 | 0.90 | 3.49 | 0.91 |
| 0.40 | 0.90 | 3.50 | 0.91 |

### Effect of Poisson's Ratio on the CCNBD Calibration by 3D BEM

| Poisson's Ratio | Dimensionless Stress Intensity Factors $F_I$ |
|---|---|
| 0.00 | 1.173 |
| 0.17 | 1.185 |
| 0.30 | 1.195 |
| 0.40 | 1.209 |
| 0.49 | 1.223 |

## @.7 Results of the CSTBD Calibration by 2D BEM, Open Mode

Variation of $F_1$, $C_1EB$ and $C_2EB$ with $a/R$

| Dimensionless Crack Length, $a/R$ | $F_{IC}$ | $C_1EB$ | $C_2EB$ |
|---|---|---|---|
| 0.05000 | 0.205 | 3.15 | 0.06 |
| 0.10000 | 0.288 | 3.36 | 0.13 |
| 0.15000 | 0.342 | 3.44 | 0.19 |
| 0.20000 | 0.440 | 3.52 | 0.27 |
| 0.25000 | 0.511 | 3.52 | 0.38 |
| 0.27500 | 0.547 | 3.53 | 0.39 |
| 0.30000 | 0.570 | 3.53 | 0.43 |
| 0.35000 | 0.631 | 3.53 | 0.53 |
| 0.40000 | 0.715 | 3.54 | 0.64 |
| 0.50000 | 0.896 | 3.63 | 0.91 |
| 0.55000 | 0.992 | 3.65 | 1.09 |
| 0.61688 | 1.154 | 3.74 | 1.36 |
| 0.65000 | 1.212 | 3.76 | 1.56 |
| 0.70000 | 1.363 | 3.84 | 1.81 |
| 0.75000 | 1.544 | 3.88 | 2.15 |
| 0.80374 | 1.802 | 4.03 | 2.63 |
| 0.85000 | 2.063 | 4.17 | 3.15 |
| 0.85766 | 2.139 | 4.17 | 3.25 |
| 0.87636 | 2.289 | 4.25 | 3.52 |
| 0.89312 | 2.411 | 4.32 | 3.79 |
| 0.90000 | 2.533 | 4.36 | 3.92 |

## @.8 Results for the CCNBD Calibration by 3D BEM, Open Mode

### Variation of $F_1$ along the Crack Front

| $2x/b$ | 0.00 | 0.10 | 0.20 | 0.30 | 0.40 | 0.50 | 0.60 | 0.70 | 0.80 | 0.90 | 1.00 |
|---|---|---|---|---|---|---|---|---|---|---|---|
| $F_1$ | 1.184 | 1.186 | 1.190 | 1.197 | 1.206 | 1.217 | 1.232 | 1.250 | 1.274 | 1.310 | 1.379 |

**Da01, Dimension:** $D = 100$, $D_1 = 100$, $B = 40$, $a_0 = 15$, $C = 22.30$

| $a/R$ | $F_{IC}$(average) | $F_0(x = 0)$ | $C_1EB$ | $C_2EB$ |
|---|---|---|---|---|
| 0.4000 | 1.934 | 1.835 | 2.437 | 1.438 |
| 0.5500 | 1.819 | 1.645 | 2.439 | 1.671 |
| 0.6000 | 1.629 | 1.539 | 2.630 | 2.016 |
| 0.6569 | 1.706 | 1.583 | 3.044 | 2.316 |
| 0.7565 | 1.862 | 1.709 | 3.201 | 3.017 |
| 0.8326 | 2.151 | 1.991 | 3.723 | 3.938 |

**DA02, Dimension:** $D = 100$, $D_1 = 100$, $B = 35$, $a_0 = 15$, $C = 19.80$

| $a/R$ | $F_{IC}$(average) | $F_0(x = 0)$ | $C_1EB$ | $C_2EB$ |
|---|---|---|---|---|
| 0.4000 | 2.035 | 1.821 | 2.191 | 1.366 |
| 0.5000 | 1.699 | 1.560 | 2.479 | 1.611 |
| 0.6000 | 1.573 | 1.547 | 2.595 | 1.977 |
| 0.6565 | 1.660 | 1.549 | 3.154 | 2.284 |
| 0.7565 | 1.804 | 1.712 | 3.550 | 3.047 |
| 0.7970 | 1.937 | 1.853 | 3.665 | 3.509 |

**DA03, Dimension:** $D = 100$, $D_1 = 100$, $B = 30$, $a_0 = 15$, $C = 17.30$

| $a/R$ | $F_{IC}$ | $F_0$ | $C_1EB$ | $C_2EB$ |
|---|---|---|---|---|
| 0.4000 | 2.039 | 1.704 | 2.441 | 1.296 |
| 0.5000 | 1.618 | 1.488 | 2.500 | 1.550 |
| 0.5947 | 1.519 | 1.469 | 3.293 | 1.921 |
| 0.6400 | 1.600 | 1.517 | 3.240 | 2.170 |
| 0.7565 | 1.835 | 1.832 | 3.562 | 3.110 |

**DA04, Dimension:** $D = 100$, $D_1 = 100$, $B = 25$, $a_0 = 15$, $C = 14.80$

| $a/R$ | $F_{IC}$ | $F_0$ | $C_1EB$ | $C_2EB$ |
|---|---|---|---|---|
| 0.400 | 1.905 | 1.734 | 3.220 | 1.220 |
| 0.450 | 1.518 | 1.419 | 3.23 | 1.340 |
| 0.500 | 1.494 | 1.386 | 3.26 | 1.490 |
| 0.590 | 1.336 | 1.328 | 3.32 | 1.860 |
| 0.640 | 1.533 | 1.459 | 3.38 | 2.150 |
| 0.710 | 1.697 | 1.658 | 3.55 | 2.730 |

**DA05, Dimension:** $D = 100$, $D_1 = 100$, $B = 35$, $a_0 = 20$, $C = 21.67$

| $a/R$ | $F_{IC}$ | $F_0$ | $C_1EB$ | $C_2EB$ |
|---|---|---|---|---|
| 0.5000 | 2.042 | 1.917 | 3.253 | 1.794 |
| 0.5593 | 1.856 | 1.726 | 3.296 | 1.963 |
| 0.6709 | 1.782 | 1.666 | 3.420 | 2.470 |
| 0.7000 | 1.787 | 1.672 | 3.459 | 2.644 |
| 0.8241 | 2.188 | 2.093 | 3.747 | 3.967 |

**DA11, Dimension:** $D = 100$, $D_1 = 52$, $B = 30$, $a_0 = 10$, $C = 17.00$

| $a/R$ | $F_{IC}$ | $F_0$ | $C_1EB$ | $C_2EB$ |
|---|---|---|---|---|
| 0.3262 | 1.101 | 1.048 | 2.15 | 0.770 |
| 0.3600 | 0.987 | 0.929 | 2.36 | 0.823 |
| 0.4019 | 0.955 | 0.899 | 2.68 | 0.900 |
| 0.4532 | 0.958 | 0.930 | 2.96 | 1.040 |
| 0.4879 | 0.971 | 0.996 | 3.17 | 1.160 |

**DA12, Dimension:** $D = 100$, $D_1 = 52$, $B = 25$, $a_0 = 10$, $C = 14.50$

| $a/R$ | $F_{IC}$ | $F_0$ | $C_1EB$ | $C_2EB$ |
|---|---|---|---|---|
| 0.3000 | 1.037 | 0.953 | 2.417 | 0.715 |
| 0.3600 | 0.954 | 0.909 | 2.390 | 0.813 |
| 0.4299 | 0.940 | 0.912 | 3.152 | 0.978 |
| 0.4664 | 0.959 | 0.979 | 3.196 | 1.114 |

**DA13, Dimension:** $D = 100$, $D_1 = 52$, $B = 20$, $a_0 = 10$, $C = 12.00$

| $a/R$ | $F_{IC}$ | $F_0$ | $C_1EB$ | $C_2EB$ |
|---|---|---|---|---|
| 0.2924 | 0.995 | 0.935 | 3.03 | 0.670 |
| 0.3200 | 0.883 | 0.840 | 3.08 | 0.717 |
| 0.3550 | 0.869 | 0.833 | 3.15 | 0.777 |
| 0.4019 | 0.902 | 0.876 | 3.24 | 0.899 |
| 0.4382 | 0.921 | 0.910 | 3.32 | 1.030 |

DA14, Dimension: $D = 100$, $D_1 = 52$, $B = 30$, $a_0 = 8$, $C = 16.26$

| $a/R$ | $F_{IC}$ | $F_0$ | $C_1EB$ | $C_2EB$ |
|---|---|---|---|---|
| 0.3069 | 0.933 | 0.879 | 3.057 | 0.720 |
| 0.3893 | 0.929 | 0.881 | 3.071 | 0.864 |
| 0.4100 | 0.932 | 0.889 | 3.090 | 0.911 |
| 0.4445 | 0.960 | 0.932 | 3.108 | 1.005 |
| 0.4821 | 0.972 | 0.971 | 3.130 | 1.139 |

DB01, Dimension: $D = 75$, $D_1 = 52$, $B = 30$, $a_0 = 10$, $C = 17.00$

| $a/R$ | $F_{IC}$ | $F_0$ | $C_1EB$ | $C_2EB$ |
|---|---|---|---|---|
| 0.4000 | 1.303 | 1.226 | 3.075 | 1.121 |
| 0.4800 | 1.238 | 1.159 | 3.100 | 1.281 |
| 0.5200 | 1.195 | 1.121 | 3.140 | 1.390 |
| 0.5600 | 1.181 | 1.144 | 3.180 | 1.510 |
| 0.6218 | 1.239 | 1.184 | 3.270 | 1.790 |
| 0.6505 | 1.344 | 1.274 | 3.310 | 1.959 |

DB02, Dimension: $D = 75$, $D_1 = 52$, $B = 25$, $a_0 = 10$, $C = 14.50$

| $a/R$ | $F_{IC}$ | $F_0$ | $C_1EB$ | $C_2EB$ |
|---|---|---|---|---|
| 0.4000 | 1.295 | 1.204 | 2.970 | 1.090 |
| 0.4800 | 1.207 | 1.136 | 3.080 | 1.259 |
| 0.5200 | 1.141 | 1.111 | 3.180 | 1.376 |
| 0.5600 | 1.206 | 1.150 | 3.260 | 1.523 |
| 0.6218 | 1.277 | 1.257 | 3.380 | 1.839 |

**DB03, Dimension:** $D = 75$, $D_1 = 52$, $B = 20$, $a_0 = 10$, $C = 12.00$

| $a/R$ | $F_{IC}$ | $F_0$ | $C_1EB$ | $C_2EB$ |
|---|---|---|---|---|
| 0.4000 | 1.187 | 1.119 | 3.154 | 0.779 |
| 0.4267 | 1.135 | 1.076 | 3.162 | 1.094 |
| 0.4533 | 1.134 | 1.074 | 3.174 | 1.163 |
| 0.4867 | 1.182 | 1.117 | 3.190 | 1.260 |
| 0.5200 | 1.205 | 1.156 | 3.210 | 1.380 |
| 0.5842 | 1.253 | 1.220 | 3.270 | 1.678 |

**DB04, Dimension:** $D = 75$, $D_1 = 52$, $B = 30$, $a_0 = 8$, $C = 16.26$

| $a/R$ | $F_{IC}$ | $F_0$ | $C_1EB$ | $C_2EB$ |
|---|---|---|---|---|
| 0.4092 | 1.194 | 1.123 | 3.065 | 1.093 |
| 0.5190 | 1.156 | 1.092 | 3.110 | 1.360 |
| 0.5467 | 1.194 | 1.124 | 3.120 | 1.450 |
| 0.5927 | 1.244 | 1.182 | 3.163 | 1.627 |
| 0.6429 | 1.506 | 1.433 | 3.160 | 1.950 |

**DB11, Dimension:** $D = 75$, $D_1 = 100$, $B = 25$, $a_0 = 7.05$, $C = 13.00$

| $a/R$ | $F_{IC}$ | $F_0$ | $C_1EB$ | $C_2EB$ |
|---|---|---|---|---|
| 0.3733 | 2.160 | 2.062 | 3.070 | 1.430 |
| 0.4984 | 1.865 | 1.703 | 3.250 | 1.710 |
| 0.6915 | 2.109 | 1.943 | 3.487 | 2.774 |
| 0.7955 | 2.143 | 1.969 | 3.730 | 3.680 |
| 0.8968 | 2.863 | 2.601 | 3.900 | 5.430 |

**DB12, Dimension:** $D = 88$, $D_1 = 52$, $B = 30$, $a_0 = 10$, $C = 17.00$

| $a/R$ | $F_{IC}$ | $F_0$ | $C_1EB$ | $C_2EB$ |
|---|---|---|---|---|
| 0.3710 | 1.062 | 1.004 | 3.065 | 0.921 |
| 0.4567 | 1.046 | 0.990 | 3.100 | 1.090 |
| 0.5150 | 1.062 | 1.023 | 3.123 | 1.267 |
| 0.5544 | 1.146 | 1.086 | 3.153 | 1.437 |

**DC01, Dimension:** $D = 50$, $D_1 = 52$, $B = 20$, $a_0 = 10$, $C = 12.00$

| $a/R$ | $F_{IC}$ | $F_0$ | $C_1EB$ | $C_2EB$ |
|---|---|---|---|---|
| 0.5000 | 2.351 | 2.247 | 3.181 | 1.950 |
| 0.5848 | 1.926 | 1.814 | 3.310 | 2.160 |
| 0.7099 | 2.024 | 1.875 | 3.460 | 2.829 |
| 0.7600 | 2.062 | 1.904 | 3.548 | 3.210 |
| 0.8038 | 2.150 | 1.979 | 3.043 | 3.642 |
| 0.8764 | 2.626 | 2.372 | 4.010 | 4.751 |

**DC02, Dimension:** $D = 50$, $D_1 = 52$, $B = 15$, $a_0 = 10$, $C = 9.50$

| $a/R$ | $F_{IC}$ | $F_0$ | $C_1EB$ | $C_2EB$ |
|---|---|---|---|---|
| 0.5000 | 2.245 | 1.886 | 3.270 | 1.750 |
| 0.5463 | 1.821 | 1.698 | 3.290 | 1.871 |
| 0.6523 | 1.716 | 1.592 | 3.340 | 2.345 |
| 0.7200 | 1.824 | 1.717 | 3.530 | 2.830 |
| 0.8037 | 2.114 | 2.049 | 3.760 | 3.760 |

## @.9 Comparison of the Calibration Results by BEM and FEM

### Comparison of the CSTBD Calibration by 2D FEM and BEM, Open Mode

| $a/R$ | $F_1$-BE | $C_1EB$-BE | $C_2EB$-BE | $F_1$-FE | $C_1EB$-FE | $C_2EB$-FE |
|---|---|---|---|---|---|---|
| 0.10000 | 0.288 | 3.36 | 0.13 | 0.280 | 3.25 | 0.109 |
| 0.12500 | 0.307 | 3.43 | 0.16 | 0.300 | 3.31 | 0.138 |
| 0.20000 | 0.440 | 3.52 | 0.27 | 0.430 | 3.41 | 0.261 |
| 0.25000 | 0.511 | 3.52 | 0.38 | 0.501 | 3.42 | 0.328 |
| 0.32500 | 0.607 | 3.53 | 0.48 | 0.589 | 3.44 | 0.448 |
| 0.37500 | 0.663 | 3.54 | 0.58 | 0.651 | 3.50 | 0.546 |
| 0.50000 | 0.896 | 3.63 | 0.91 | 0.881 | 3.60 | 0.902 |
| 0.55000 | 0.992 | 3.65 | 1.09 | 0.980 | 3.60 | 1.027 |
| 0.65000 | 1.212 | 3.76 | 1.56 | 1.200 | 3.70 | 1.526 |
| 0.70000 | 1.363 | 3.84 | 1.81 | 1.350 | 3.80 | 1.787 |
| 0.75000 | 1.544 | 3.88 | 2.15 | 1.532 | 3.80 | 2.134 |
| 0.85000 | 2.063 | 4.17 | 3.15 | 2.050 | 4.10 | 3.134 |

### Comparison of the CCNBD Calibration by 3D FEM and BEM

| $a/R$ | $F_1$-BE | $C_1EB$-BE | $C_2EB$-BE | $F_1$-FE | $C_1EB$-FE | $C_2EB$-FE |
|---|---|---|---|---|---|---|
| 0.4000 | 1.304 | 3.08 | 1.12 | 1.298 | 2.98 | 1.02 |
| 0.4800 | 1.238 | 3.10 | 1.28 | 1.210 | 3.00 | 1.18 |
| 0.5200 | 1.195 | 3.14 | 1.39 | 1.156 | 3.04 | 1.29 |
| 0.5600 | 1.209 | 3.18 | 1.51 | 1.200 | 3.10 | 1.41 |
| 0.6218 | 1.279 | 3.27 | 1.79 | 1.270 | 3.17 | 1.69 |
| 0.6505 | 1.345 | 3.31 | 1.97 | 1.335 | 3.21 | 1.87 |

## @.10 Datafile for Curvilinear Regression Analysis Using *MINITAB

```
read test.sand(1,98) C1 - -C20;
format (3x,10f7.2/3x,10f7.2).
oh = 0
name C1 = SE, C2 = CW, C3 = CoI, C4 = CS, C5 = TS
name C6 = ES, C7 = WV, C8 = BD, C9 = GD, C10 = P.
name C11 = SH, C12 = CI, C13 = GS, C14 = GR
name C15 = CC, C16 = Sst, C17 = Lst, C18 = Mst
name C19 = A, C20 = ISI, C24 = CS^2, C25 = TS^2
name C26 = ES^2, C27 = WV^2, C28 = BD^2, C29 = GD^2
name C30 = P^2 , C31 = SH^2, C32 = CI^2, C33 = GS^2
name C34 = GR^2, C35 = CC^2, C36 = Sst^2, C37 = Lst^2
name C38 = Mst^2, C39 = A^2, C40 = ISI^2, C44 = CS^3
name C45 = TS^3, C46 = ES^3, C47 = WV^3, C48 = BD^3
name C49 = GD^3, C50 = P^3, C51 = SH^3, C52 = CI^3
name C53 = GS^3, C54 = GR^3, C55 = CC^3, C56 = Sst^3
name C57 = Lst^3, C58 = Mst^3, C59 = A^3, C60 = ISI^3
name C64 = CS^1/2, C65 = TS^1/2, C66 = ES^1/2
name C67 = WV^1/2, C68 = BD^1/2, C69 = GD^1/2
name C70 = P.^1/2, C71 = SH^1/2, C72 = CI^1/2
name C73 = GS^1/2, C74 = GR^1/2, C75 = CC^1/2
name C76 = St^1/2, C77 = Ls^1/2, C78 = Ms^1/2
name C79 = A^1/2, C80 = ISI^1/2, C84 = CS^1/3
name C85 = TS^1/3, C86 = ES^1/3, C87 = WV^1/3
name C88 = BD^1/3, C89 = GD^1/3, C90 = P^1/3
name C91 = SH^1/3, C92 = CI^1/3, C93 = GS^1/3
name C94 = GR^1/3, C95 = CC^1/3, C96 = Ss^1/3
name C97 = Ls^1/3, C98 = Ms^1/3, C99 = A^1/3
name C100 = ISI^1/3, C101 = TI, C102 = TI^2, C103 = TI^3
name C104 = TI^1/2, C105 = TI^1/3, C106 = MR
name C107 = MR^2, C108 = MR^3, C109 = MR^1/2, C110 = MR^1/3
let C101 = C4^2 / C6
let C102 = C101^2
```

let $C_{103} = C_{101}^3$

let $C_{104} = C_{101}^{1/2}$

let $C_{105} = C_{101}^{1/3}$

let $C_{106} = C_4 \ / \ C_6$

let $C_{107} = C_{106}^2$

let $C_{101} = C_4^2 \ / \ C6$

let $C_{102} = C_{101}^2$

let $C_{103} = C_{101}^3$

let $C_{104} = C_{101}^{1/2}$

let $C_{105} = C_{101}^{1/3}$

let $C_{106} = C_4 \ / \ C_6$

let $C_{107} = C_{106}^2$

let $C_{108} = C_{106}^3$

let $C_{109} = C_{106}^{1/2}$

let $C_{110} = C_{106}^{1/3}$

store

print $K_1$

let $K_2 = K_1 + 20$

let $K_3 = K_1 + 40$

let $K_4 = K_1 + 60$

let $K_5 = K_1 + 80$

let $CK_2 = CK_1^2$

let $CK_3 = CK_1^3$

let $CK_4 = CK_1^{1/2}$

let $CK_5 = CK_1^{1/3}$

let $K_1 = K_1 + 1$

end

let $K_1 = 4$

exec stored commands 17 times

stepwise $C_1$ on 95 predictors in $C_4 - -C_{20}, C_{24} - -C_{40}$
$C_{44} - -C_{60}, C_{64} - -C_{80}, C_{84} - -C_{110}$

## @.11 Rapid Transit Tunnel

| | 1 | 2 | 3 | 4 | 5 | 6 | 7 | 8 | 9 | 10 |
|---|---|---|---|---|---|---|---|---|---|---|
| | S | S | S | M | S | S | M | S | L | M |
| SE | 10.70 | 12.70 | 9.60 | 7.10 | 13.90 | 11.70 | 22.40 | 21.30 | 11.20 | 7.50 |
| CW | 2.76 | 2.12 | 1.68 | 1.65 | 1.40 | 2.09 | 2.10 | 1.16 | 1.76 | 1.54 |
| CoI | 404.0 | 421.0 | 434.0 | 451.0 | 412.0 | 433.0 | 381.0 | 408.0 | 464.0 | 443.0 |
| CS | 80.00 | 74.00 | 83.00 | | 76.00 | 99.00 | | | 188.00 | |
| TS | 6.20 | 4.50 | 6.00 | 4.90 | 5.40 | 5.60 | 6.30 | 5.90 | 15.60 | 6.10 |
| ES | 9.90 | 14.40 | 12.80 | | 9.90 | 14.80 | | | 22.70 | |
| WV | 2.50 | 2.90 | 2.70 | | 2.40 | 3.00 | | | 3.50 | |
| BD | 2.25 | 2.36 | 2.35 | 2.55 | 2.33 | 2.31 | 2.50 | 2.39 | 2.49 | 2.44 |
| GD | 2.61 | 2.61 | 2.57 | 2.65 | 2.64 | 2.51 | 2.66 | 2.64 | 2.75 | 2.75 |
| P. | 13.80 | 9.70 | 8.80 | 2.80 | 11.50 | 8.00 | 6.20 | 9.40 | 9.40 | 11.20 |
| SH | 30.00 | 32.00 | 33.00 | 25.00 | 27.00 | 36.00 | 33.00 | 31.00 | 41.00 | 28.00 |
| CI | 2.70 | 2.80 | 3.70 | 1.50 | 2.60 | 3.50 | 2.20 | 2.20 | 7.10 | 1.40 |
| GS | 150.00 | 100.00 | 200.0 | 3.00 | 100.00 | 100.00 | 40.00 | 30.00 | 30.00 | 3.00 |
| GR | 2.50 | 3.50 | 2.00 | 6.00 | 2.50 | 2.50 | 2.00 | 2.50 | 4.00 | 6.00 |
| CC | 8.00 | 9.00 | 9.00 | 8.00 | 3.00 | 7.00 | 2.00 | 6.00 | 6.00 | 3.00 |
| Sst | 82.00 | 94.00 | 99.00 | 1.00 | 90.00 | 95.00 | 35.00 | 71.00 | 19.00 | 1.00 |
| Lst | 18.00 | 0.00 | 0.00 | 0.00 | 0.00 | 0.00 | 0.00 | 29.00 | 81.00 | 0.00 |
| Mst | 0.00 | 6.00 | 1.00 | 99.00 | 10.00 | 5.00 | 65.00 | 0.00 | 0.00 | 99.00 |
| A | | 0.24 | 0.18 | | 0.13 | 0.29 | | | 0.04 | |
| ISI | 78.00 | 80.00 | 82.00 | 78.00 | 80.00 | 83.00 | 78.00 | 77.00 | 91.00 | 78.00 |
| MI | | | | | | | | | | |
| SS | | | | | | | | | | |
| SP | 5.70 | 6.90 | 7.20 | 4.40 | 4.80 | 2.60 | 4.30 | 4.30 | 1.40 | 2.60 |
| IBI | | | | | | | | | | |
| ScH | | | | | | | | | | |
| K | | | | | | | | | | |

Continue

| | 11 | 12 | 13 | 14 | 15 | 16 | 17 | 18 | 19 | 20 |
|---|---|---|---|---|---|---|---|---|---|---|
| | M | M | S | S | L | S | S | L | S | S |
| SE | 8.50 | 9.40 | 16.60 | 7.60 | 23.10 | 8.20 | 10.30 | 20.50 | 11.60 | 14.70 |
| CW | 0.00 | 0.00 | 1.47 | 1.46 | 1.44 | 2.61 | 1.52 | 1.32 | 1.53 | 1.40 |
| CoI | 430.0 | 448.0 | 420.0 | 422.0 | 433.0 | 423.0 | 396.0 | 436.0 | 431.0 | 413.0 |
| CS | | | 56.00 | 53.00 | 188.0 | 45.0 | 38.00 | 118.0 | 82.0 | 71.0 |
| TS | 5.90 | 6.80 | 4.70 | 3.10 | 14.80 | 3.50 | 3.40 | 7.00 | 5.90 | 7.40 |
| ES | | | 5.90 | 6.10 | 29.30 | 7.10 | 7.70 | 18.80 | 9.80 | 10.60 |
| WV | | | 1.90 | 1.90 | 3.90 | 2.10 | 2.20 | 3.20 | 2.40 | 2.60 |
| BD | 2.50 | 2.55 | 2.33 | 2.28 | 2.62 | 2.15 | 2.18 | 2.47 | 2.29 | 2.19 |
| GD | 2.64 | 2.67 | 2.57 | 2.58 | 2.75 | 2.59 | 2.59 | 2.73 | 2.62 | 2.64 |
| P. | 5.20 | 4.50 | 9.50 | 8.40 | 4.60 | 17.10 | 15.60 | 9.60 | 12.80 | 17.00 |
| SH | 27.00 | 28.00 | 30.00 | 25.00 | 37.00 | 24.00 | 21.00 | 33.00 | 30.00 | 32.00 |
| CI | 1.90 | 1.90 | 2.90 | 2.20 | 3.80 | 2.60 | 2.50 | 3.00 | 3.80 | 2.60 |
| GS | 50.00 | 3.00 | 50.00 | 50.00 | 200.0 | 400.0 | 300.0 | 100.0 | 100.0 | 100.0 |
| GR | 3.50 | 6.00 | 3.50 | 3.50 | 2.50 | 2.00 | 3.50 | 3.00 | 1.00 | 1.00 |
| CC | 7.00 | 5.00 | 5.00 | 7.00 | 6.00 | 8.00 | 8.00 | 6.00 | 6.00 | 7.00 |
| Sst | 10.00 | 1.00 | 90.00 | 90.00 | 33.00 | 96.00 | 96.00 | 38.00 | 70.00 | 70.00 |
| Lst | 0.00 | 0.00 | 0.00 | 0.00 | 67.00 | 0.00 | 0.00 | 62.00 | 20.00 | 24.00 |
| Mst | 90.00 | 99.00 | 10.00 | 10.00 | 0.00 | 4.00 | 4.00 | 0.00 | 10.00 | 6.00 |
| A | | | 0.09 | | | 0.40 | 0.75 | 0.06 | 0.14 | 0.14 |
| ISI | 81.00 | 79.00 | 77.00 | 77.00 | 91.00 | 68.00 | 73.00 | 87.00 | 79.00 | 81.00 |
| MI | | | | | | | | | | |
| SS | | | | | | | | | | |
| SP | 4.40 | 5.10 | 7.50 | 2.60 | 1.50 | 12.80 | 12.60 | 3.70 | 7.40 | 7.80 |
| ScH | | | | | | | | | | |
| IBI | | | | | | | | | | |
| K | | | | | | | | | | |

Continue

| | 21 | 22 | 23 | 24 | 25 | 26 | 27 | 28 | 29 |
|---|---|---|---|---|---|---|---|---|---|
| | M | S | S | S | S | M | S | S | M |
| SE | 8.20 | 14.20 | 11.70 | 12.30 | 11.10 | 13.10 | 4.90 | 12.50 | 15.30 |
| CW | 0.55 | 0.39 | 1.67 | 1.57 | 0.98 | 1.24 | 0.00 | 1.63 | 0.91 |
| CoI | 444.00 | 466.00 | 381.00 | 387.00 | 401.00 | 414.00 | 443.00 | 366.00 | 396.00 |
| CS | | 86.00 | 44.00 | 43.00 | 51.00 | | | 39.00 | |
| TS | 4.90 | 6.50 | 2.90 | 3.10 | 3.50 | | | 2.20 | 3.60 |
| ES | | 10.00 | 9.80 | 9.90 | 9.60 | | | 10.10 | |
| WV | | 2.40 | 2.50 | 2.50 | 2.40 | | | 2.50 | |
| BD | 2.47 | 2.31 | 2.14 | 2.15 | 2.23 | 2.71 | 2.39 | 2.16 | 2.45 |
| GD | 2.65 | 2.87 | 2.57 | 2.57 | 2.60 | 2.71 | 2.60 | 2.61 | 2.64 |
| P. | 6.80 | 19.50 | 16.70 | 16.50 | 14.30 | 0.00 | 8.30 | 17.10 | 7.00 |
| SH | 25.00 | 33.00 | 29.00 | 25.00 | 28.00 | 24.00 | 21.00 | 22.00 | 27.00 |
| CI | 1.70 | 2.20 | 2.30 | 2.40 | 2.50 | 1.40 | 1.60 | 2.90 | 1.70 |
| GS | 50.00 | 50.00 | 500.00 | 800.00 | 990.00 | 10.00 | 100.00 | 100.00 | 80.00 |
| GR | 2.50 | 2.50 | 3.00 | 2.00 | 1.50 | 6.00 | 3.00 | 1.50 | 3.00 |
| CC | 5.00 | 5.00 | 8.00 | 8.00 | 8.00 | 3.00 | 7.00 | 8.00 | 9.00 |
| Sst | 25.00 | 66.00 | 98.00 | 90.00 | 94.00 | 2.00 | 85.00 | 99.00 | 89.00 |
| Lst | 5.00 | 24.00 | 2.00 | 7.00 | 6.00 | 0.00 | 0.00 | 1.00 | 0.00 |
| Mst | 70.00 | 10.00 | 0.00 | 3.00 | 0.00 | 98.00 | 15.00 | 0.00 | 11.00 |
| A | | | 0.68 | 0.69 | 0.39 | | | 1.04 | |
| ISI | 80.00 | 84.00 | 60.00 | 61.00 | 76.00 | 81.00 | 79.00 | 48.00 | 80.00 |
| MI | | | | | | | | | |
| SS | | | | | | | | | |
| SP | 8.50 | 4.50 | 14.20 | 11.90 | 10.90 | 7.80 | 3.00 | 12.20 | 5.80 |
| ScH | | | | | | | | | |
| IBI | | | | | | | | | |
| K | | | | | | | | | |

## @.12 Type Tees Aqueduct Matrix

| | 1 | 2 | 3 | 4 | 5 | 6 | 7 | 8 | 9 | 10 | 11 | 12 |
|---|---|---|---|---|---|---|---|---|---|---|---|---|
| | S | S | S | M | S | S | M | L | S | S | L | D |
| SE | 17.60 | 18.50 | 14.40 | | 20.10 | | 32.30 | 26.40 | 22.10 | 38.90 | 24.10 | 38.90 |
| CW | 1.93 | 1.95 | 1.84 | 1.00 | 2.80 | 1.57 | | 1.13 | 4.61 | 2.04 | 1.61 | 1.70 |
| CoI | 400.0 | 366.0 | 389.0 | | 408.0 | 394.0 | | 414.0 | 407.0 | 407.0 | 436.0 | 418.0 |
| CS | 50.00 | 58.00 | 37.00 | 41.00 | 72.00 | 74.00 | 32.00 | 144.0 | 156.0 | 117.0 | 92 | 314.0 |
| TS | 3.30 | 4.20 | 2.50 | | 4.60 | 5.20 | 6.70 | 7.90 | 7.30 | 8.90 | 10.0 | 21.30 |
| ES | 12.50 | 18.70 | 9.30 | | 21.40 | 22.50 | | 56.60 | 39.80 | 38.80 | 50.70 | 80.60 |
| WV | 2.70 | 3.30 | 2.50 | | 3.50 | 3.50 | | 5.60 | 4.80 | 4.90 | 5.20 | 6.20 |
| BD | 2.31 | 2.40 | 2.10 | | 2.35 | 2.48 | | 2.59 | 2.38 | 2.26 | 2.58 | 2.89 |
| GD | 2.58 | 2.59 | 2.57 | | 2.60 | 2.75 | | 2.67 | 2.59 | 2.59 | 2.71 | 2.96 |
| P. | 10.80 | 18.40 | 18.40 | | 9.80 | 15.20 | | 5.30 | 8.10 | 12.90 | 7.90 | 10.40 |
| SH | 29.00 | 28.00 | 27.00 | | 38.00 | 19.00 | | 35.00 | 47.00 | 36.00 | 41.00 | 54.00 |
| CI | 4.10 | 2.50 | 4.60 | 1.70 | 2.90 | 4.20 | 1.70 | 12.00 | 8.90 | 7.10 | 8.00 | 9.90 |
| GS | 20.00 | 220.0 | 375.0 | 30.00 | 170.0 | 180.0 | 30.00 | 20.00 | 118.0 | 118.0 | 7.00 | 800.0 |
| GR | 4.00 | 2.00 | 3.00 | 6.00 | 1.50 | 2.50 | 6.00 | 6.00 | 2.50 | 1.00 | 6.00 | 6.00 |
| CC | 8.00 | 8.00 | 7.00 | 4.00 | 8.00 | 8.00 | 3.00 | 6.00 | 9.00 | 8.00 | 6.00 | 6.00 |
| Sst | 65.00 | 79.00 | 78.00 | 4.00 | 81.00 | 85.00 | 5.00 | 8.00 | 91.00 | 99.00 | 1.00 | 55.00 |
| Lst | 14.00 | 20.00 | 1.00 | 96.00 | 12.00 | 12.00 | 0.00 | 80.00 | 1.00 | 0.00 | 96.00 | 8.00 |
| Mst | 21.00 | 1.00 | 21.00 | 0.00 | 7.00 | 8.00 | 95.00 | 12.00 | 8.00 | 1.00 | 3.00 | 37.00 |
| A | 0.79 | 1.50 | | | 1.09 | 0.58 | | 0.06 | 4.86 | 1.46 | 0.05 | |
| ISI | 81.00 | 66.00 | 68.00 | | 80.00 | 73.00 | | 83.00 | 82.00 | 61.00 | 78.00 | 81.00 |
| MI | 25.00 | 17.00 | 28.00 | | 13.00 | 32.00 | | 77.00 | 4.00 | 5.00 | 60.00 | 4.00 |
| SS | 7.50 | 8.00 | 9.50 | 8.00 | 11.50 | 11.50 | 9.00 | 28.00 | 18.50 | 17.50 | 21.50 | 50.00 |
| SP | 6.40 | 10.30 | 6.70 | | 2.90 | 13.20 | | 3.40 | 4.10 | 4.30 | 0.00 | 0.00 |
| ScH | 51.00 | 52.00 | 37.00 | | 51.00 | 52.00 | | 54.00 | 59.00 | 53.00 | 58.00 | 62.00 |
| IBI | | | | | | | | | | | | |
| K | | | | | | | | | | | | |

Continue

| | 13 | 14 | 15 | 16 | 17 | 18 | 19 | 20 | 21 | 22 | 23 | 24 |
|---|---|---|---|---|---|---|---|---|---|---|---|---|
| | L | S | S | L | S | L | S | S | L | S | S | S |
| SE | 25.80 | 25.60 | 20.90 | 23.10 | 23.80 | 28.10 | 32.70 | 21.70 | 22.40 | 30.30 | 28.20 | 16.50 |
| CW | 0.74 | 1.80 | 1.58 | 1.06 | 2.70 | 0.78 | 1.74 | 2.32 | 0.81 | 1.89 | 1.82 | 1.89 |
| CoI | 17.0 | 399.0 | 409.0 | 428.0 | 426.0 | 428.0 | 408.0 | 413.0 | 444.0 | 412.0 | 401.0 | 391.0 |
| CS | 34.00 | 53.00 | 72.00 | 147.0 | 123.0 | 133.0 | 84.00 | 158.0 | 193.0 | 146.0 | 150.0 | 46.0 |
| TS | 8.60 | 5.80 | 8.70 | 10.10 | 6.20 | 6.40 | 6.60 | 11.10 | 9.70 | 7.20 | 10.30 | |
| ES | 48.00 | 16.50 | 18.70 | 43.20 | 33.10 | 62.30 | 31.20 | 50.00 | 65.10 | 38.90 | 44.80 | |
| WV | 5.20 | 3.10 | 3.30 | 4.80 | 4.40 | 5.80 | 4.20 | 5.40 | 6.00 | 4.70 | 4.90 | |
| BD | 2.41 | 2.31 | 2.35 | 2.56 | 2.39 | 2.58 | 2.43 | 2.34 | 2.50 | 2.46 | 2.58 | 2.41 |
| GD | 2.70 | 2.62 | 2.60 | 2.71 | 2.60 | 2.71 | 2.60 | 2.61 | 2.72 | 2.67 | 2.64 | 2.60 |
| P. | 10.50 | 11.90 | 9.70 | 5.50 | 8.30 | 4.70 | 7.90 | 10.40 | 8.20 | 7.90 | 5.70 | 7.50 |
| SH | 37.00 | 52.00 | 43.00 | 35.00 | 38.00 | 38.00 | 42.00 | 55.00 | 39.00 | 47.00 | 44.00 | 34.00 |
| CI | 7.60 | 9.90 | 7.20 | 6.30 | 9.90 | 8.00 | 7.60 | 7.40 | 7.40 | 7.60 | 6.90 | 4.90 |
| GS | 00.00 | 50.00 | 62.00 | 999.0 | 115.0 | 400.0 | 200.0 | 100.0 | 80.00 | 160.0 | 66.00 | 120.0 |
| GR | 6.00 | 4.50 | 2.00 | 6.00 | 1.00 | 6.00 | 1.00 | 2.50 | 6.00 | 1.50 | 2.00 | 4.00 |
| CC | 6.00 | 6.00 | 8.00 | 6.00 | 8.00 | 6.00 | 10.00 | 8.00 | 6.00 | 10.00 | 3.00 | 7.00 |
| Sst | 0.00 | 65.00 | 62.00 | 0.00 | 93.00 | 0.00 | 84.00 | 81.00 | 0.00 | 88.00 | 83.00 | 70.00 |
| Lst | 99.00 | 6.00 | 5.00 | 80.00 | 4.00 | 95.00 | 2.00 | 0.00 | 9.00 | 4.00 | 2.00 | 9.00 |
| Mst | 1.00 | 29.00 | 33.00 | 20.00 | 3.00 | 5.00 | 14.00 | 19.00 | 91.00 | 8.00 | 15.00 | 21.00 |
| A | | 0.06 | | 0.07 | 1.97 | 2.68 | 0.08 | 0.37 | 0.08 | 0.37 | | 0.67 |
| ISI | 83.00 | 85.00 | 91.00 | 76.00 | 85.00 | 86.00 | 77.00 | 78.00 | 82.00 | 84.00 | 74.00 | |
| MI | 83.00 | 2.00 | 15.00 | 90.00 | 21.00 | 60.00 | 6.00 | 3.00 | | 8.00 | 7.00 | 32.00 |
| SS | 23.00 | 20.50 | 20.00 | 23.30 | 18.00 | 18.00 | 14.30 | 24.00 | 30.50 | 0.00 | 22.00 | |
| SP | 5.20 | 3.00 | 4.90 | 0.00 | 5.10 | 0.00 | 4.50 | 4.20 | 0.80 | 3.10 | 3.20 | 5.10 |
| ScH | 53.00 | 58.00 | 54.00 | 55.00 | 54.00 | 56.00 | 54.00 | 58.00 | 55.00 | 54.00 | 60.00 | 44.00 |
| IBI | | | | | | | | | | | | |
| K | | | | | | | | | | | | |

## @.13 Livepool Loop Matrix

| | 1 | 2 | 3 | 4 | 5 | 6 | 7 |
|---|---|---|---|---|---|---|---|
| | S | S | S | S | S | S | S |
| SE | 14.70 | 11.50 | 6.10 | 9.40 | 15.40 | 5.60 | 7.70 |
| CW | 1.63 | 1.48 | 0.43 | 1.44 | 1.98 | 0.57 | 1.54 |
| Col | | | | | | | |
| CS | 36.00 | 48.00 | 7.00 | 18.00 | 23.00 | 8.00 | 41.00 |
| TS | 5.80 | 2.70 | 1.00 | 2.40 | 3.90 | 1.10 | 1.80 |
| ES | 10.70 | 6.70 | 5.90 | 6.30 | 9.40 | 5.60 | 7.90 |
| WV | 2.50 | 2.10 | 2.00 | 2.00 | 2.40 | 1.90 | 2.30 |
| BD | 2.38 | 2.12 | 2.03 | 2.12 | 2.34 | 2.05 | 2.13 |
| GD | 2.62 | 2.62 | 2.61 | 2.62 | 2.58 | 2.62 | 2.63 |
| P. | 0.92 | 11.00 | 22.20 | 19.00 | 9.30 | 21.80 | 19.00 |
| SH | 54.00 | 37.00 | 26.00 | 36.00 | 47.00 | 19.00 | 37.00 |
| CI | 4.60 | 2.30 | 1.70 | 3.00 | 3.50 | 1.30 | 2.10 |
| GS | 520.00 | 130.0 | 120.0 | 280.0 | 450.0 | 350.0 | 320.0 |
| GR | 4.20 | 2.80 | 4.00 | 3.00 | 3.00 | 4.50 | 3.70 |
| CC | 7.00 | 5.00 | 1.00 | 5.00 | 7.00 | 1.00 | 4.00 |
| Sst | 89.00 | 62.00 | 80.00 | 78.00 | 88.00 | 84.00 | 95.00 |
| Lst | 0.00 | 0.00 | 0.00 | 0.00 | 0.00 | 0.00 | 0.00 |
| Mst | 11.00 | 38.00 | 20.00 | 22.00 | 12.00 | 16.00 | 5.00 |
| A | | | | | | | |
| ISI | | | | | | | |
| MI | | | | | | | |
| SS | | | | | | | |
| SP | | | | | | | |
| ScH | 24.00 | 33.00 | 53.00 | 39.00 | 38.00 | 63.00 | 33.00 |
| IBI | 13.00 | 42.00 | 48.00 | 45.00 | 19.00 | 58.00 | 44.00 |
| K | | | | | | | |

## @.14 Coal Measure Matrix

| | 1 | 2 | 3 | 4 | 5 | 6 | 7 | 8 | 9 | 10 | 11 | 12 | 13 |
|---|---|---|---|---|---|---|---|---|---|---|---|---|---|
| | S | M | M | C | C | M | M | M | M | M | M | S | M |
| SE | | | | | | | | | | | | 9.30 | 6.90 |
| CW | 1.64 | 0.16 | 0.94 | 0.00 | 0.14 | 0.30 | 0.80 | 0.56 | 0.76 | | | 1.09 | 0.05 |
| CoI | | | | | | | | | | | | | |
| CS | 37.00 | 18.00 | 32.00 | 16.00 | 4.00 | 23.00 | 47.00 | 27.00 | 24.00 | 71.00 | 71.00 | 36.0 | 26.0 |
| TS | 7.80 | 5.10 | 3.70 | 0.30 | 0.30 | 7.40 | 6.90 | 6.60 | 6.60 | 3.80 | 2.80 | 6.10 | 3.40 |
| ES | 23.80 | 15.70 | 25.20 | 2.20 | 2.70 | 19.10 | 23.90 | 27.10 | 13.60 | 22.30 | 28.80 | 18.50 | 15.20 |
| WV | 3.60 | 2.90 | 3.60 | 1.50 | 1.70 | 3.20 | 3.50 | 3.70 | 2.60 | 3.40 | 3.90 | 3.10 | 2.90 |
| BD | 2.47 | 2.57 | 2.75 | 1.26 | 1.30 | 2.50 | 2.65 | 2.75 | 2.77 | 2.65 | 2.61 | 2.64 | 2.50 |
| GD | 2.62 | 2.62 | 2.75 | 1.26 | 1.30 | 2.52 | 2.67 | 2.75 | 2.77 | 2.65 | 2.61 | 2.64 | 2.50 |
| P. | 5.60 | 1.90 | 0.00 | 0.00 | 0.00 | 1.20 | 0.70 | 0.00 | 0.00 | 0.00 | 0.00 | 0.15 | 0.80 |
| SH | 57.00 | 31.00 | 42.00 | 15.00 | 15.00 | 32.00 | 45.00 | 42.00 | 36.00 | 46.00 | 34.00 | 45.00 | 22.00 |
| CI | 6.90 | 2.70 | 3.00 | 2.50 | 1.90 | 2.60 | 3.40 | 3.50 | 1.80 | 4.90 | 2.80 | 4.70 | 1.80 |
| GS | 110.0 | 5.00 | 5.00 | 0.00 | 0.00 | 40.00 | 34.00 | 50.00 | 2.00 | 70.00 | 2.00 | 90.00 | 2.00 |
| GR | 2.00 | 6.00 | 6.00 | 6.00 | 6.00 | 2.50 | 2.50 | 3.00 | 6.00 | 2.50 | 6.00 | 1.50 | 6.00 |
| CC | 7.00 | 4.00 | 4.00 | 4.00 | 4.00 | 4.00 | 4.00 | 4.00 | 4.00 | 7.00 | 4.00 | 7.00 | 4.00 |
| Sst | 65.00 | 1.00 | 4.00 | 0.00 | 0.00 | 11.00 | 4.00 | 7.00 | 8.00 | 30.00 | 4.00 | 60.00 | 3.00 |
| Lst | 20.00 | 0.00 | 0.00 | 99.00 | 99.00 | 0.00 | 0.00 | 0.00 | 0.00 | 0.00 | 0.00 | 0.00 | 0.00 |
| Mst | 15.00 | 99.00 | 96.00 | 1.00 | 1.00 | 89.00 | 96.00 | 93.00 | 92.00 | 70.00 | 96.00 | 40.00 | 97.00 |
| ISI | | | | | | | | | | | | | |
| A | | | | | | | | | | | | | |
| MI | | | | | | | | | | | | | |
| SS | | | | | | | | | | | | | |
| ScH | | | | | | | | | | | | | |
| SP | 5.70 | 6.90 | 7.20 | 4.20 | 4.80 | 2.60 | 4.30 | 4.30 | 1.40 | 2.60 | | | |
| IBI | 10.00 | 6.00 | 6.00 | 15.00 | 14.00 | 6.00 | 10.00 | 7.00 | 7.00 | 7.00 | 7.00 | 7.00 | 9.00 |
| K | 22.00 | 26.00 | 17.00 | 0.00 | 3.00 | 23.00 | 18.00 | 25.00 | 28.00 | 18.00 | | | |

## @.15 Miscellaneous Sedimentary Rocks

| | 1 | 2 | 3 | 4 | 5 | 6 | 7 | 8 | 9 | 10 | 11 | 12 | 13 | 14 |
|---|---|---|---|---|---|---|---|---|---|---|---|---|---|---|
| | S | S | L | L | L | L | L | S | S | S | S | S | L | L |
| SE | 9.50 | 7.30 | 19.30 | 2.60 | 21.90 | 9.60 | 13.80 | 2.80 | 40.00 | 4.30 | 71.00 | 10.40 | 22.90 | 30.30 |
| CW | 2.03 | 2.33 | 0.40 | 0.27 | 0.75 | 0.36 | 0.17 | 1.10 | 15.30 | 2.30 | 25.30 | 0.17 | 0.00 | 0.00 |
| CoI | | | | | | | | | | | | | | |
| CS | 73.00 | 46.00 | 117.00 | 35.00 | 113.00 | 40.00 | 45.00 | 25.00 | 145.00 | 120.00 | 218.00 | 51.00 | 135.00 | 170.00 |
| TS | 3.80 | 1.70 | 9.50 | 1.60 | 5.50 | 1.40 | 2.80 | 1.30 | 5.80 | 7.70 | 16.20 | 4.30 | 7.80 | 9.20 |
| ES | 14.40 | 12.70 | 38.30 | 7.50 | 56.50 | 23.10 | 23.70 | 3.70 | 20.00 | 29.60 | 59.30 | 12.00 | 14.00 | 62.00 |
| WV | 2.20 | 2.80 | 5.00 | 2.70 | 2.46 | 2.92 | 2.20 | 2.33 | 2.63 | 2.60 | 5.40 | 3.10 | 6.50 | 5.60 |
| BD | 14.20 | 15.80 | 2.50 | 24.60 | 0.50 | 0.00 | 3.15 | 20.80 | 0.00 | 16.50 | 2.63 | 2.25 | 2.75 | 2.71 |
| GD | 2.60 | 2.59 | 2.70 | 2.46 | 2.92 | 2.20 | 2.33 | 2.63 | 2.63 | 2.60 | 2.66 | 2.64 | 2.77 | 2.71 |
| P. | 14.20 | 15.80 | 2.50 | 24.60 | 0.50 | 0.00 | 3.10 | 20.80 | 0.00 | 16.50 | 1.00 | 14.60 | 0.80 | 0.00 |
| SH | 47.00 | 36.00 | 51.00 | 15.00 | 36.00 | 14.00 | 26.00 | 52.00 | 71.00 | 27.00 | 99.00 | 41.00 | 44.00 | 41.00 |
| CI | 4.50 | 3.00 | 6.10 | 1.40 | 4.10 | 3.60 | 4.50 | 0.60 | 10.80 | 2.10 | 15.00 | 3.00 | 7.00 | 7.50 |
| GS | 140.00 | 500.0 | 70.00 | 9.00 | 600.0 | 120.0 | 24.00 | 210.0 | 132.0 | 230.0 | 250.0 | 230.0 | 300.0 | 100.0 |
| GR | 2.50 | 1.50 | 6.00 | 6.00 | 6.00 | 6.00 | 6.00 | 4.30 | 2.00 | 4.00 | 2.00 | 3.50 | 3.50 | 6.00 |
| CC | 7.00 | 7.00 | 6.00 | 6.00 | 6.00 | 6.00 | 6.00 | 1.00 | 10.00 | 5.00 | 10.00 | 7.00 | 6.00 | 6.00 |
| Sst | 88.00 | 90.00 | 0.00 | 2.00 | 0.00 | 0.00 | 0.00 | 99.00 | 99.00 | 85.00 | 85.00 | 82.00 | 31.00 | 0.00 |
| Lst | 0.00 | 0.00 | 95.00 | 60.00 | 99.00 | 90.00 | 70.00 | 0.00 | 0.00 | 0.00 | 10.00 | 18.00 | 58.00 | 90.00 |
| Mst | 22.00 | 10.00 | 5.00 | 38.00 | 1.00 | 10.00 | 30.00 | 1.00 | 1.00 | 15.00 | 88.00 | 59.00 | 83.00 | 81.00 |
| ISI | 52.00 | 40.00 | 87.00 | 68.00 | 76.00 | 59.00 | 80.00 | 30.00 | 10.00 | 41.00 | 1.00 | 65.00 | 37.30 | 4.00 |
| MI | 37.00 | 45.00 | 13.00 | 96.00 | 19.00 | 83.00 | 100.00 | 75.00 | 2.00 | | 1.00 | 65.00 | 37.00 | 4.00 |
| SS | | | | | | | | | | | | | | |
| SP | 13.60 | 15.60 | 0.20 | 23.00 | 0.20 | 0.00 | 0.00 | 16.20 | 0.00 | 1.20 | 13.50 | 15.60 | 0.20 | 23.00 |
| ScH | | | | | | | | | | | | | | |
| IBI | | | | | | | | | | | | | | 12.00 |
| K | 27.00 | 7.00 | 25.00 | 62.00 | 31.00 | 46.00 | 33.00 | 2.00 | 8.00 | 45.00 | 0.00 | 32.00 | 64.00 | 22.00 |